From Department of Cell and Molecular Biology
Karolinska Institutet, Stockholm, Sweden

IMPLEMENTING NEW GENOMIC TOOLS TO STUDY VENTRAL MIDBRAIN DEVELOPMENT AND INJURY RESPONSE IN THE NEWT *PLEURODELES WALTL*

Zeyu Yao

Karolinska Institutet

Stockholm 2023

All previously published papers were reproduced with permission from the publisher.
Published by Karolinska Institutet.
Printed by Universitetsservice US-AB, 2023

ISBN 978-91-8017-217 -2
Cover illustration: Immunohistochemical analysis of ventral midbrain in a larval Nucbow/Cytbow transgenic newt after transient expression of cre-recombinase. Red, green, and blue represent cells with color transformation after the *Cre* expression, white represents tyrosine hydroxylase-expressing neurons.

Implementing new genomic tools to study ventral midbrain development and injury response in the newt *Pleurodeles waltl*

Thesis for Doctoral Degree (Ph.D.)

By

Zeyu Yao

The thesis will be defended in public at Ragnar Granit, Biomedicum, Solnavägen 9, Solna, on Friday the 15th of December 2023 at 09:30.

Principal Supervisor:
András Simon
Karolinska Institutet
Department of Cell and Molecular Biology

Co-supervisor(s):
Alberto Joven Araus
Karolinska Institutet
Department of Cell and Molecular Biology

Ahmed Elewa
Karolinska Institutet
Department of Cell and Molecular Biology

Per Svenningsson
Karolinska Institutet
Department of Clinical Neuroscience

Opponent:
Jan Kaslin
Australian Regenerative Medicine Institute

Examination Board:
Lena Gunhaga
Umeå Universitet
Umeå Centre for Molecular Medicine (UCMM)

Jonas Muhr
Karolinska Institutet
Department of Cell and Molecular Biology

Qiaolin Deng
Karolinska Institute
Department of Physiology and Pharmacology

Dedicated to my parents and grandparents

ABSTRACT

Mammals have a poor ability to regenerate organs or tissues. In particular, brain neurons do not regenerate after damage. A good example of this limitation is the irreversible degeneration of midbrain dopaminergic neurons in Parkinson's disease (PD).

Several strategies are being developed to treat PD. The proposed treatments include transplantations and local reprogramming of brain cells. Transplantation approaches involve different sources of dopaminergic progenitors or neurons which can be sourced either *in vivo* from fetal ventral midbrain tissues, or *in vitro* from either embryonic stem cells or induced pluripotent stem cells. Reprogramming approaches try to directly convert local glial cells into dopaminergic neurons *in vivo*. While clinical progress has been made in trials, several issues need to be addressed, such as the safety of the techniques, and ethical considerations.

In this thesis I explored how dopaminergic neurons could be generated locally in the ventral midbrain from the endogenous neural stem cells. I used newts as the animal model, which have an extraordinary ability to regenerate organs and tissues including limb, tail, heart, lens, spinal cord, and the brain. Previous studies showed that newts functionally recovered after mesencephalic and diencephalic ablation of dopaminergic neurons by a process which is fueled by regenerative neurogenesis. However, the cellular and molecular mechanisms after dopaminergic lesion have remained largely unrevealed, mostly because of the paucity of available molecular tools. In addition to the regeneration studies, studying newts broadens our understanding of the function and the shaping of the midbrain from a developmental and evolutionary perspective.

The work in this thesis made use of recent technological advances, such as a newly assembled genomic resource, single-cell RNAseq (scRNAseq) and single-nucleus RNAseq (snRNAseq) methods, and genomic modification techniques. I implemented and refined those tools in the following projects.

In Project I, I made use of new genomic and transcriptomic resources for the Iberian ribbed newt, *Pleurodeles waltl*. I identified gene orthologues of key dopaminergic determinants and other genes expressed in vertebrate ventral midbrain. I found examples of both evolutionary conservation and divergence. I designed and produced plasmids and gRNAs which were used to generate transgenic and mutant newts. I predicted reactivities of multiple commercially available antibodies that I tested in *Pleurodeles waltl* tissues. I also designed probes for single and multiplexed *in situ* hybridizations.

In Project II, I studied the development of the *Pleurodeles waltl* ventral midbrain. Using scRNAseq/snRNAseq analyses in combination with immunohistochemical and functional analyses I focused on two aspects: (i) cellular heterogeneity, and (ii) transition of neural stem/progenitor cells from active proliferation to quiescence. Based on marker gene expression, I found high degree of conservations of major cell types between *Pleurodeles waltl* and mammals. I then studied in detail the development of the ventral midbrain with emphasis on the dopaminergic system. I uncovered that the cellular diversity observed in the adult ventral midbrain is established at the late larval stage, though the proportions of cell types change as

development proceeds. I used the snRNAseq data to detect changes in gene expression from development to adulthood. The *in silico* data were confirmed by validating protein expression in the midbrain, by which I could observe defined subpopulations in their spatial distribution. Furthermore, I found that overexpression of the transcription factor NFI *in vivo* promotes the natural transition of stem/progenitor cells into quiescence.

In Project III, I explored the cellular and molecular responses to dopaminergic injury in the *Pleurodeles waltl* ventral midbrain. I found, in accordance with the results of Project II, a downregulation of NFI correlating with the reactivation of ependymolial cells, which are neural stem cells in the newt brain. Overexpression of NFI after dopaminergic ablation inhibited the activation of ependymoglia. Bulk RNAseq analyses revealed sets of up- and downregulated genes which I explored further in the snRNAseq datasets. Furthermore, using the transgenic line mpeg1:GFP and PLX3397-mediated depletion, I revealed a role for microglia/macrophages in the reactivation of ependymolia after the ablation of dopaminergic neurons.

In sum, the work provides new resources and entry points in how to consider the development and evolution of the newt ventral midbrain, and its ability to recover following loss of dopaminergic neurons.

LIST OF PROJECTS

This thesis is divided into the following projects:

I. Implementing and refining the molecular toolkit for *Pleurodeles waltl*.

II. Molecular categorization of cell populations with temporal resolution in the developing *Pleurodeles waltl* ventral midbrain.

III. Response to dopaminergic neuron ablation with special focus on the interplay between microglia/macrophages and ependymoglia.

Published scientific papers not attached in this thesis are:

Kaucka M, Joven Araus A, Tesarova M, Currie JD, Boström J, Kavkova M, Petersen J, **Yao Z**, Bouchnita A, Hellander A, Zikmund T, Elewa A, Newton PT, Fei JF, Chagin AS, Fried K, Tanaka EM, Kaiser J, Simon A, Adameyko I. Altered developmental programs and oriented cell divisions lead to bulky bones during salamander limb regeneration. ***Nat Commun***. 2022 Nov 14;13(1):6949. doi: 10.1038/s41467-022-34266-w. PMID: 36376278; PMCID: PMC9663504.

Elewa A, Wang H, Talavera-López C, Joven A, Brito G, Kumar A, Hameed LS, Penrad-Mobayed M, **Yao Z**, Zamani N, Abbas Y, Abdullayev I, Sandberg R, Grabherr M, Andersson B, Simon A. Reading and editing the Pleurodeles waltl genome reveals novel features of tetrapod regeneration. ***Nat Commun***. 2017 Dec 22;8(1):2286. doi: 10.1038/s41467-017-01964-9. PMID: 29273779; PMCID: PMC5741667.

CONTENTS

LIST OF ABBREVIATIONS

aHyp	alar hypothalamus
BAMs	Border associated macrophages
bHyp	basal hypothalamus
CB	CALB1 or Calbindin
ch	Choroid plexus
CR	CALB2 or Calretinin
CRISPR	Clustered Regulatory Interspaced Short Palindromic Repeat
DEG	Differentially expressed genes
Di	Diencephalon
EdU	Ethynyl deoxyuridine
ESCs	Embryonic stem cells
FACS	Fluorescence-Activated Cell Sorting
GO	Gene ontology
HMEJ	Homology-mediated end joining
HR	Homologous recombination
iDA	Induced dopamine-releasing
IHC	immunohistochemistry
iPSCs	Induced pluripotent stem cells (iPSCs)
ISH	*in situ* hybridization
MMEJ	Microhomology-mediated end joining
NFI	Nuclear Factor I
NHEJ	Non-homologous end joining
OPCs	Oligodendrocyte precursor cells

PC	Principal component
PCA	Principal component analysis
PD	Parkinson’s disease (PD)
POA	Preoptic area
QC	Quality control
r0	Isthmus
RNAseq	RNA sequencing
RrF	Retrorubral field
scRNAseq	Single-cell RNA sequencing
SN or SNpc	Substantia nigra pars compacta
SNpcd	Substantia nigra pars compacta dorsal tiers
SNpvc	Substantia nigra pars compacta ventral
snRNAseq	Single-nucleus RNA sequencing
TALEN	Transcription Activator-Like Effector Nucleases
Tx	Triton X-100
VMb	Ventral midbrain
VST	Variance stabilizing transformations
VTA	Ventral tegmental area
ZFN	Zinc-Finger Nucleases

1. INTRODUCTION

1.1. Parkinson's disease

Parkinson's disease (PD) is the second most common neurodegenerative disease after Alzheimer's disease. PD results from the degeneration of dopaminergic neurons in the substantia nigra of midbrain, which leads to a decrease in the neurotransmitter dopamine (Chinta and Andersen, 2005). The clinical symptoms of PD include bradykinesia, rigidity, and resting tremor (Kalia and Lang, 2015). There is no cure for PD at present. Current treatments are effective to temporarily relieve the symptoms of the disease, for example, by administration of levodopa (L-DOPA) or related substances and by deep brain stimulation (Reich and Savitt, 2019). The main reason for the lack of cure for PD is that no treatment can lead to the repair or regenerate the damaged midbrain dopaminergic system.

Cell replacement therapy is considered as an alternative to pharmacological treatment and brain stimulation. Human fetal ventral midbrain (VMb) tissues were transplanted into patients' brain in several human clinical trials. These trials provided proof of concept for cell replacement therapy in PD (Lindvall and Bjorklund, 2004, 2011). Importantly, some patients showed recovery for several years (Kefalopoulou et al., 2014). However, this approach has several limitations: 1. The available human fetal brain tissues for transplantation is scarce; 2. It is hard to standardize human fetal sources, leading to variable results; 3. In some cases, undesirable side effects like graft-induced dyskinesias can occur (Ásgrímsdóttir and Arenas, 2020; Barker et al., 2015; Lindvall and Bjorklund, 2004; Parmar et al., 2020).

An alternative cell replacement strategy is to produce dopaminergic progenitors or neurons from Embryonic stem cells (ESCs) or Induced pluripotent stem cells (iPSCs), followed by transplanting those into the brains of PD patients. Compared with using human fetal VMb tissues, the application of ESCs or iPSCs have several advantages: 1. Easier to produce them in large amount; 2. Easier to get higher purity; 3. Easier to standardize the manufacturing process; 4. Cells may be cryopreserved (Nolbrant et al., 2017; Parmar et al., 2020; Wakeman et al., 2017). At the same time, the following challenges are still not resolved fully: 1. How to accurately generate the right cell types? 2. Into which part of the brain should the cells be grafted for optimal outcomes? 3. How to support the viability of the grafted cells after the transplantation? 4. Can the transplanted neurons innervate the appropriate targets? 5. How to avoid immunological rejections from the patients? 6. Ethical considerations, especially related to the use of ESCs (Barbuti et al., 2021; Guo et al., 2021; Parmar et al., 2020). A series of animal experiments were conducted to test the feasibility of this approach and human clinical trials have been started, whose outcomes are yet to be determined (Barbuti et al., 2021; Guo et al., 2021; Kikuchi et al., 2017; Kriks et al., 2011; Parmar et al., 2020; Parmar et al., 2023; Takahashi, 2019; Wang et al., 2018; Xiong et al., 2021).

The third strategy is the direct reprogramming of non-neuronal cell types, for example astrocytes, into dopaminergic neurons *in vivo* (Arenas, 2020; Arenas et al., 2015). The difficulties here include how to make the precise targeting and reprogramming at the correct areas *in vivo*, and if the reprogramed neurons can survive, integrate, and function as normal dopaminergic neurons in the niche. In a previous study with a mouse model of PD, astrocytes in striatum were converted into "induced dopamine-releasing (iDA) neurons" leading to partial correction of motor deficits (Rivetti di Val Cervo et al., 2017). However, these iDA neurons

were not able to form distant neuronal connections, and motor behavior could not be comprehensively restored (Arenas, 2020; Rivetti di Val Cervo et al., 2017). More recently, two studies targeted PTBP1 gene to achieve direct reprogramming of dopaminergic neurons *in vivo* (Qian et al., 2020; Zhou et al., 2020). Both studies claimed efficient reprogramming of astrocytes into dopaminergic neurons, as well as the restoration of motor behavior. In one of the studies PTBP1 was depleted in astrocytes in the striatum while in the in the substantia nigra in the other study. However, the efficacy achieved by depleting PTBP1 has become controversial and needs further confirmations (Chen et al., 2022; Guo et al., 2022a; Guo et al., 2022b; Hao et al., 2023; Hoang et al., 2023; Hoang et al., 2022; Hoang et al., 2021; Hoang et al., 2020; Maimon et al., 2021; Wang et al., 2021; Wang and Zhang, 2022, 2023; Xie et al., 2022; Yang et al., 2023a; Yang et al., 2023b).

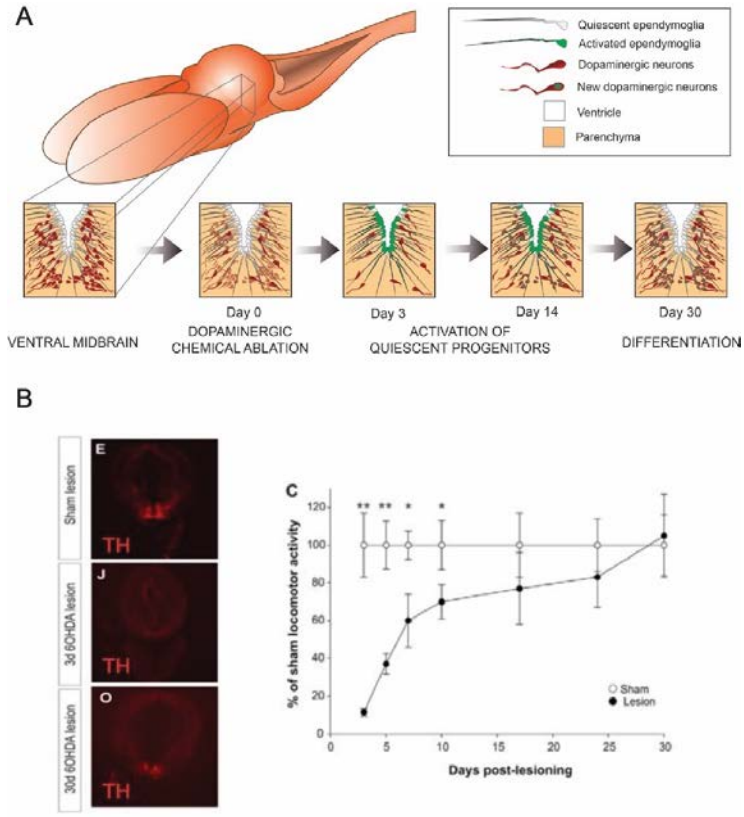

Fig. 1 | Midbrain dopaminergic regeneration in newts. (A) Schematic diagram showing the regeneration after dopaminergic damages. Figure modified from (Joven et al., 2019), reprinted with permission from the publisher: The Company of Biologists. **(B)** Midbrain dopaminergic neuron regeneration and recovery of locomotor performance in newts. Tyrosine hydroxylase (TH) in red. The figure was from (Parish et al., 2007), reprinted with permission from the publisher: The Company of Biologists.

The fourth strategy would be the awakening of the endogenous quiescent stem cells or dopaminergic progenitors in the adult brains *in situ*. This approach is what the thesis focuses on. The Simon lab has previously shown that such a regeneration process is involved in the

restoration of the dopaminergic system in newts, which are semiaquatic salamanders (Parish et al., 2007) **(Fig. 1)**. Furthermore, it was established that dopaminergic progenitors displaying stem cell features remain present in the adult mammalian midbrain. Similar like newts, these cells in the mouse are responsive to dopamine signaling, and it was possible to extend the normal embryonic dopaminergic neurogenic period by administration of dopamine receptor antagonist (Hedlund et al., 2016). These results indicate the feasibility of promoting dopaminergic neurogenesis in the adult mammalian midbrain as well and that it is possible to impose regenerative traits to mammalian cells based on experiments performed in newts. Two main difficulties are: (1) the exact identification of the relevant progenitors in newts and mammals, and (2) establishing methods for their activation in the mammalian brain so that they would produce new dopaminergic neurons. An additional challenge is to restore the innervation from the midbrain to the forebrain. Importantly, previous experiments showed the feasibility of creating new nigro-striatal connections of dopaminergic neurons in the adult brain, though this was achieved by transplanted cells (Torper et al., 2015).

This thesis focuses on the newt midbrain to create entry points for rigorous cross-species comparisons in the future. It examines the evolutionary conservation of the dopaminergic system in the newt midbrain, and examines processes involved in the cell cycle regulation of stem/progenitor cells both during ontogeny as well as a response to injury. The work leverages on and refines recently developed genomic tools for newts.

Table. 1 | Taxonomy of animal species commonly used for research

Kingdom	Phylum	Class	Order	Family	Genus-Species
Animalia	Chordata	Mammalia	Primates	Hominidae	*Homo sapiens* (Human)
			Rodentia	Muridae	*Mus musculus* (Mouse)
					Rattus rattus (Rat)
			Lagomorpha	Leporidae	*Oryctolagus cuniculus* (Rabbit)
		Aves	Galliformes	Phasianidae	*Gallus gallus* (Chicken)
		Reptilia	Crocodilia	Alligatoridae	*Alligator sinensis* (Alligator)
			Squamata	Agamidae	*Pogona vitticeps* (Lizard)
		Amphibia	Anura	Pipidae	*Xenopus laevis* (Frog)
				Pipidae	*Xenopus tropicalis* (Frog)
			Urodela (Salamander)	Salamandridae	***Pleurodeles waltl*** (Newt)
					Notophthalmus viridescens (Newt)
					Cynops pyrrhogaster (Newt)
					Cynops orientalis (Newt)
				Plethodontidae	*Bolitoglossa ramosi*
				Ambystomatidae	*Ambystoma mexicanum* (Axolotl)
		Actinopterygii	Cypriniformes	Cyprinidae	*Danio rerio* (Zebrafish)

1.2. Newts

1.2.1. Newts as regeneration model organisms

Newts are vertebrates with extraordinary regeneration abilities (**Fig. 2A**). Several newt species have been used as regeneration models, and the organs or tissues that have been reported to regenerate in newts including limbs, tail, spinal cord, lens, parts of heart, intestine, upper and lower jaw, male gonads, and brain (Joven et al., 2019) **(Fig. 2A-B)**. While cellular and molecular details of newt limb and heart regeneration have been explored in more details, fewer is known about the mechanisms that control regeneration of midbrain dopaminergic neurons. Taxonomically, newts belong to the Family "Salamandridae", Order "Urodela" (Salamanders), Class "Amphibia" (**Fig. 2B**) **(Table. 1)**. The axolotl is the most frequently used regeneration model among Urodela with significant genomic information and methods, some of the methods are appropriate to be used in newts as well because of the high degree of similarity between newts and axolotl. (Echeverri et al., 2022; Joven et al., 2019). Nevertheless, there are important differences between newts and axolotls in terms of their life cycle, regeneration repertoire, and genomic composition (Joven et al., 2019), justifying the studies of both types of animals and to create genomic tools for newts as well. Some of the important tools will be introduced later in the thesis.

In previous studies, two species of newt models have been used for studying dopaminergic development and regeneration: The American red spotted newt (*Notophthalmus viridescens*) and the Iberian ribbed newt (*Pleurodeles waltl*) (reviewed in (Joven and Simon, 2018), **Fig. 2A**). I mainly used the Iberian newt (*Pleurodeles waltl*) in this thesis because of the emerging availability of genomic and transcriptomic data (Brown et al., 2022; Elewa et al., 2017; Matsunami et al., 2019), as well as genetically modified lines (reviewed in (Joven et al., 2019)).

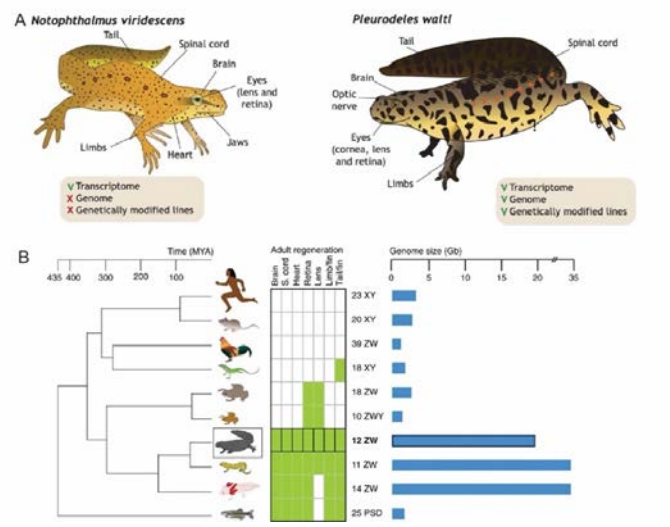

Fig. 2 | Newts and their genome. (A) Most often used newt species in regeneration research. Figure from (Joven et al., 2019), reprinted with permission from the publisher: The Company of Biologists. **(B)** The genome sizes and regeneration ability in different species. Figure from (Elewa et al., 2017), reprinted with the Creative Commons license: https://creativecommons.org/licenses/by/4.0/.

1.2.2. Development of genome and transcriptome resources for newt species

Without genomic data it is not possible to reveal the molecular mechanisms behind newts' excellent regeneration abilities. However, genomes and transcriptomes of newts have only recently been sequenced due to technical limitations (Brown et al., 2022; Elewa et al., 2017; Matsunami et al., 2019). Different from the human genome with around 3 Gb in size, genomes in salamander species are much larger: around 20 Gb in the newt *Pleurodeles waltl*, around 35 Gb in newt *Notophthalmus viridescens*, around 39 Gb in the newt *Cynops pyrrhogaster*, around 40 Gb in the newt *Cynops orientalis*, around 25 Gb in the newt *Bolitoglossa5ntegri*, and around 35 Gb in the axolotl *Ambystoma mexicanum* (Arenas Gomez et al., 2017; Brown et al., 2022; Elewa et al., 2017; Litvinchuk et al., 2007; Wilhelm et al., 2003) **(Fig 2)**. Another unique feature of the salamander genomes is the large number of long repetitive sequences, making the assembly very difficult without long sequencing reads (Brown et al., 2022; Elewa et al., 2017). Among newts, transcriptomes of *Notophthalmus viridescens*, *Cynops pyrrhogaster*, and *Cynops orientalis* were sequenced (Abdullayev et al., 2013; Biscotti et al., 2020; Looso et al., 2013; Nakamura et al., 2014; Wang et al., 2023; Yu et al., 2019). However, no genome of these species was sequenced, mainly because of the heavy cost and the difficulty of sequencing long repetitive areas as mentioned before. These species are not suitable either for making transgenic lines because of their complex life cycle. For example, *Notophthalmus viridescens* has generation of time of at least 2 years, involving aquatic and terrestrial transitions which are cumbersome to mimic in animal facilities (Joven et al., 2019).

Pleurodeles waltl is relatively easy to breed under laboratory conditions and amenable for genomic modifications (Joven et al., 2019). The first genetically modified *Pleurodeles* were being generated a decade ago using Tol2- and SceI-mediated transgenesis (Hayashi et al., 2019; Hayashi and Takeuchi, 2015; Hayashi et al., 2013; Joven et al., 2018), as well as CRISPR/Cas9-directed mutagenesis, including mutants for tyrosinase ($Tyr^{-/-}$), $Pax3^{-/-}$, $Pax6^{-/-}$, $Pax7^{-/-}$ and $Tbx5^{-/-}$ (Elewa et al., 2017; Suzuki et al., 2018). The first genome and transcriptome of *Pleurodeles waltl* was published in 2017 (Elewa et al., 2017). The transcriptome was derived from 10 different tissues/organs at 3 developmental stages and 2 regenerative stages. The genome was sequenced, the size was estimated to 20 Gb but the assembly remained fragmented because of the short sequencing reads from Illumina sequencing (Elewa et al., 2017). Unique features of *Pleurodeles waltl* were revealed, for example the expansion of Harbinger transposable elements and the expansion of miRNAs with embryonic stem cell-specific seed sequences (Elewa et al., 2017). In 2019, an additional transcriptome was published, generated from 12 different tissues/organs, unfertilized egg, or embryos at 8 developmental stages and 2 regenerative stages (Matsunami et al., 2019). Very recently, my laboratory used advanced PacBio long sequencing reads to sequence the genome again. Combined with Hi-C reads for chromosome scaffolding and iso-sequencing of mRNAs from brain, limb, and spleen (Brown et al., 2022), the new genome showed a great improvement: it could be assembled into 1183 pieces, 99.6% of which scaffolded into 12 chromosomes (Brown et al., 2022). Although the annotation of the *Pleurodeles waltl* genome is still not complete, it was possible to use the sequencing data to reveal fundamental aspects of the evolution of the vertebrate forebrain (Woych et al., 2022). I will present the application of these new genome resources in my studies later in this thesis.

1.3. Midbrain dopaminergic system

1.3.1. Mammalian midbrain dopaminergic neurons

Midbrain dopaminergic neurons were defined in the 1960s. In 1964, along with the identification of monoamine-containing neurons in brain, neurons in substantia nigra pars compacta (SNpc) of ventral midbrain were identified as dopaminergic neurons, which projected to dorsal striatum (the caudate and putamen) (Anden et al., 1964; Dahlstroem and Fuxe, 1964, 1965; Fuxe, 1965a, b).

Although dopaminergic neurons constitute a relatively small cell population in the midbrain, they are important in regulating multiple functions in the body (Chinta and Andersen, 2005). Dysregulation of the dopaminergic system is associated with not only PD but also disorders like schizophrenia, restless legs syndrome and attention deficit hyperactivity disorder (Chinta and Andersen, 2005).

In earlier studies, midbrain dopaminergic neurons were classified based on their anatomical locations. In mammals, dopaminergic neurons are distributed in three distinct nuclei in the midbrain: 1) substania nigra pars compacta (SNpc, A9 group). 2) ventral tegmental area (VTA, A10 group). 3) retrorubral field (RrF, A8 group) (Arenas et al., 2015; Dahlstroem and Fuxe, 1964). Distinct midbrain dopaminergic neurons project to different brain areas and exert various functions. A VTA dopaminergic neuron subpopulation projects to nucleus accumbens (ventromedial striatum), olfactory tubercle, septum, amygdala, and hippocampus, and it is known as mesolimbic dopaminergic system (Chinta and Andersen, 2005). Another VTA dopaminergic neuron subpopulation projects to prefrontal, cingulate and perirhinal cortex, and this is called the mesocortical dopaminergic system (Chinta and Andersen, 2005). The VTA dopaminergic neurons control emotional behavior, natural motivation, reward, and cognitive function (Arenas et al., 2015). This cell population is also linked to psychiatric disorders, for example, anxiety and depression (Arenas et al., 2015). SNpc dopaminergic neurons project to dorsolateral striatum (the caudate and putamen) as mentioned before, forming the nigrostriatal dopaminergic system. This cell population plays a significant role in controlling voluntary motor movement (Chinta and Andersen, 2005). In PD, though multiple types of neurons degenerate, these are the cells among midbrain dopaminergic neurons that are mostly affected. VTA dopaminergic neurons are also diminished in PD but not to the same extent as SNpc dopaminergic neurons (Arenas et al., 2015; Chinta and Andersen, 2005) (**Fig. 3**).

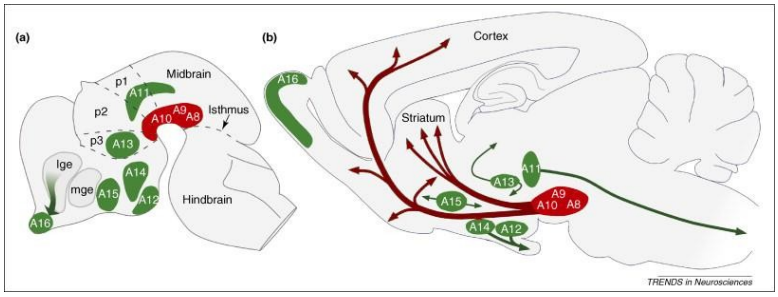

Fig. 3 | Brain regions with dopaminergic neurons in development (A) and adult rodent brain (B). Figure was adapted from "(Bjorklund and Dunnett, 2007)", and reprinted with permission from the publisher: Elsevier.

1.3.2. Cellular composition and dopaminergic regeneration of the newt midbrain

Similar to mammals, the midbrain of newts has both neural and non-neural cellular components. Although anatomically simplified, the functional equivalents can be identified of all major areas of the vertebrate brain (Joven and Simon, 2018). Despite the similarities, important differences have also been identified. The cells lining the ventricular system of the newt brain is one such example with special relevance for this thesis. These cells are generally denoted as ependymoglial cells. These cells are in an "ependymal" position and simultaneously express glial markers, such as the intermediate filament GFAP (Arsanto et al., 1992; Benraiss et al., 1996; Berg et al., 2010). Ependymoglial cells give also rise to neurons both during development and as a response to neuronal loss (Berg et al., 2010).

Work in zebrafish highlighted an interplay between ventricular neuronal progenitors and immune system. In the brain activation of ventricular neuronal progenitors was shown to depend on signals from microglia (Kyritsis et al., 2012). Microglia has also been identified in the newt brain and manipulation of the inflammatory response impinged on the regeneration of dopaminergic neurons (Kirkham et al., 2011). Though previous studies have shown the multiple roles of microglia in regulation development, regeneration and function in different models, few studies have been done in newts (Mehl et al., 2022). An important question that was explored in this thesis was if there is a specific response among microglia/macrophages after dopaminergic injury.

In the newt brain, neurons constitute the largest cell population. It is a heterogenous group of cells with different neurotransmitter identity, such as dopaminergic, cholinergic, serotonergic, GABAergic neurons, glutamatergic neurons (Joven et al., 2018). Although previous work using immunohistochemical analyses and *in situ* hybridizations unraveled targeted neuronal subtypes, our understanding is limited at higher molecular resolution. Detailed molecular profiling is important to define heterogeneity and correlate to functionality, and to determine the extent of evolutionary conservation, including the putative identification of unique newt-specific populations. This knowledge is important to uncover processes that lead to regeneration in newts and to carry out cross-species comparisons.

1.3.3. Attributes of the newt dopaminergic system

In general comparison with mammals, homologous regions with conserved gene expression patterns and connectivity are often present in the newt brain, despite of the scarce migration of neuronal cells during newt brain development (Joven and Simon, 2018).

The first studies of the dopaminergic system in salamanders determined the expression patterns of both dopamine and tyrosine hydroxylase (TH) from a comparative neuroanatomical point of view (Dubé and Parent, 1982; Gonzalez and Smeets, 1991). TH expression has been used as a proxy for dopaminergic neurons as it is catalyzing the rate limiting step in dopamine biosynthesis (UniProt, 2023). These studies showed that in contrast to teleosts, there is a dopaminergic population in the VMb. This should not be taken as an indication that teleosts do not possess functionally equivalent midbrain dopaminergic neurons. Rather, it is believed that they are located more rostrally at posterior tuberculum of prosomere P3 in diencephalon (Rink and Wullimann, 2001; Yamamoto and Vernier, 2011).

The sequential appearance of the dopaminergic subpopulations during development in the brain of *Pleurodeles waltl* was firstly described by detailed immunohistochemical analyses, followed by quantitative tracing approaches that revealed different subpopulations (González et al., 1995; Joven et al., 2018). Several features of the dopaminergic systems are conserved in newts compared to other vertebrates, such as the expression domains of dopaminergic neurons and the functional consequences of their loss: the modulation of complex behaviors, such as instrumental learning, fear processing and decision making (González et al., 1995; González et al., 1996; Gonzalez and Smeets, 1991; Joven et al., 2018; Marín et al., 1997a, b). An important conserved feature is that the newt striatum is innervated by dopaminergic fibers originating from the ventral midbrain (Marín et al., 1997a, b). TH^+ fibers were found to be widespread in the newt brains , but their precise role and targets have not been investigated in great details (González et al., 1995; Gonzalez and Smeets, 1991); and it is likely that the higher complexity of motor repertoire an animal species displays, the more complex are the dopaminergic projections. However, it cannot be excluded that there are newt-specific projection patterns. An example for such a species-specific diversity is the projection from midbrain to prefrontal cortex (PFC) in mammals, which is thought to correspond the projection to nidopallium caudolateral in avians (Güntürkün, 2005; Mogensen and Divac, 1982). An important difference to mammals is that the laterally migrated dopaminergic neurons are absent in the newt midbrain, suggesting the absence of the SNpc in newts (Smeets and Reiner, 1994). More studies are required to confirm this absence, as alternatively the functional heterogeneity of dopaminergic midbrain subpopulations may just not be reflected anatomically in the newt midbrain.

Besides dopaminergic neurons, attention should be given to newt dopamine receptors. In previous studies, an evolution pattern in subtypes of dopamine receptors has been revealed across different species (Callier et al., 2003; Yamamoto and Vernier, 2011). It would be worthwhile to confirm if newts follow this pattern, and if their dopamine receptors can play a role in dopaminergic regeneration (Berg et al., 2011).

1.4. Neurogenesis during regeneration

As described above, ependymoglial cells constitute a source for new dopaminergic neurons (Berg et al., 2010; Berg et al., 2011; Joven et al., 2018; Kirkham et al., 2014). Upon elimination of dopaminergic neurons in the mature non-proliferative midbrain, quiescent ependymoglial cells become reactivated to proliferate and differentiate into new dopaminergic neurons, fueling the recovery of locomotor activity (Berg et al., 2010; Berg et al., 2011; Hameed et al., 2015; Joven et al., 2018; Parish et al., 2007) **(Fig. 1B)**. Dopamine signaling has been shown to be crucial in the activation of ependymoglial cells as it can be suppressed by administration of L-dopa, which also efficiently inhibits regeneration. Furthermore quiescent ependymoglia re-enter the cell cycle after treatment with dopamine receptor antagonist, even if without the loss of dopaminergic neurons (Berg et al., 2011). The three main unsolved questions related to ependymoglial cells that I aimed to explore are: 1. How do ependymoglial cells become quiescent during normal development. 2. How do quiescent ependymoglial cells resume proliferation after neuronal damage? 3. To what extent are the ependymoglial cells in the quiescent newt midbrain a homogenous or a heterogenous population? Throughout this thesis I will refer to ependymoglial cells as stem/progenitor cells as it is unclear how to make the distinction between their long-term self-renewal and neurogenic proliferation.

1.5. Quiescence of midbrain neural stem/progenitor cells in newts and mammals

In mammals, it was long thought that neurons are not born in the adult brain. However, adult stem cell proliferation was detected in hippocampus and striatum in the human brain, as well as hippocampus and olfactory bulb in the mouse brain (Bergmann et al., 2012; Boldrini et al., 2018; Eriksson et al., 1998; Ernst et al., 2014; Moreno-Jimenez et al., 2019; Spalding et al., 2013; Tobin et al., 2019). A study however claimed that human hippocampal neurogenesis is restricted to the first years of life (Sorrells et al., 2018). Homeostatic or lesion-induced neurogenesis in the mammalian midbrain has not been conclusively detected.

In both newts and mammals, midbrain dopaminergic neurons are derived from neural stem cells during development. Ependymoglial cells are retained throughout the entire life of the animal, acquiring a quiescent state as the brain grows during development (Joven and Simon, 2018; Joven et al., 2018). In adult *Pleurodeles waltl* brain, some regions are largely quiescent areas, such as the midbrain, while other regions, such as the telencephalon remain more proliferative (Joven and Simon, 2018; Joven et al., 2018; Kirkham et al., 2014). Although the extent of proliferative regions slightly varies also among newt species, in general there is a decrease in proliferation rate and an increase in the cell cycle length during development, associated to the appearance of a more mature phenotype in the ependymoglia, denoted type-1 ependymoglia (Joven and Simon, 2018; Joven et al., 2018; Kirkham et al., 2014). The accumulation of this slow-dividing type-1 ependymoglia coincides with the brain regions becoming quiescent. Importantly, quiescent ependymoglial cells can resume proliferation and differentiate into dopaminergic neurons after midbrain dopaminergic lesion (Berg et al., 2010; Berg et al., 2011; Joven et al., 2018; Parish et al., 2007). This is a key difference between newts and mammals, and understanding the underlying mechanisms is a main object of this thesis.

1.6. Heterogeneity of neural stem/progenitor cells

An important question in neurogenesis is whether there are subtype specific stem/progenitor cells whose lineage identities are predetermined by the transcription factors they express. Several midbrain dopaminergic determinants were identified in mammals, such as Lmx1a, Lmx1b, Otx2, Engrailed1, Engrailed2, Msx1, Msx2, Neurogenin2 and Mash1 (Ang, 2006). scRNAseq and snRNAseq experiments provided molecular cues for further classification and defined species-specific differences (La Manno et al., 2016). In a study of mammalian midbrain, five groups of neural stem cells, five groups of early progenitor cells and four groups of neuroblasts were defined; and in murine midbrain, three groups of neural stem cells, one group of early progenitor cells, and eight groups neuroblasts were defined (La Manno et al., 2016). Multiple midbrain cell types were matched well between human and mouse, though unique traits also exist in each species (La Manno et al., 2016).

Very little is known about the heterogeneity of newt ependymoglial cells, especially in the midbrain. As mentioned before, previous studies identified 2 types of ependymoglial cells in newts' brain: type-1 ependymoglia are $GFAP^{+}GS^{+}$ cells which show stem cell features as they are resistant to AraC treatment, and type-2 ependymoglia correspond to $GFAP^{+}GS^{-}$ cells with transit-amplifying characteristics and sensitive to AraC treatment (Joven and Simon, 2018; Joven et al., 2018; Kirkham et al., 2014). Type-2 cells are actively cycling, they are predominately located in proliferative areas, show short cell cycle length, and are $Notch1^{-}$. Type-1 cells are largely quiescent, they are predominately located in quiescent areas, show long cell cycle length, and are $Notch1^{+}$. It was found that the $GFAP^{+}GS^{-}$ ependymoglial cells

gradually become $GFAP^{+}GS^{+}$ as the brain matures. Furthermore, in response to neuronal injury, type-1 cells are notch signaling dependent while type-2 cells are not (Joven and Simon, 2018; Joven et al., 2018; Kirkham et al., 2014). Similar to mammals, some transcription factors such as Pax6 and Nkx gene family members are expressed in restricted dorsoventral domains in the VMb of *Pleurodeles* (Joven et al., 2013b), but to what extent ependymoglial cells in the newt midbrain express dopaminergic determinants that were identified in mammals was not known.

1.7. Genome editing techniques in salamanders

A significant hurdle for salamander research has long been the lack of genetic loss of function assays. "RNA interference" has not been established in salamanders, and it has been speculated that this may be due to naturally high activities of RNases in these species (Echeverri et al., 2022). Although morpholino-mediated knock down has been used in salamanders (Madhavan et al., 2006; Schnapp and Tanaka, 2005; Tsonis et al., 2011), this method has never become sufficiently effective. Establishing CRISPR (Clustered Regulatory Interspaced Short Palindromic Repeat) /Cas9 mediated genomic modifications in salamanders (Elewa et al., 2017; Fei et al., 2017; Fei et al., 2014) has also revolutionized the field of salamander regeneration research. Below, I will briefly review methods tested on salamanders.

1.7.1. I-SceI meganuclease system

I-SceI meganuclease is an intron-encoded homing endonuclease originally isolated from the yeast *Saccharomyces cerevisiae* (Jacquier and Dujon, 1985). By co-injection of I-SceI meganuclease enzyme with plasmids containing DNA flanked by I-SceI meganuclease sites into the eggs, DNA integration can be made to generate transgenic animals. Usually, a precondition of using the tool is identifying the regulatory sequences of the genes of interest, for example, the promoter region. The system has been reported to work in *Pleurodeles waltl*, *Cynops pyrrhogaster*, and axolotls (Casco-Robles et al., 2011; Currie et al., 2016; Gerber et al., 2018; Hayashi et al., 2013; Khattak et al., 2009; Khattak et al., 2013; Kragl et al., 2009; Monaghan and Maden, 2012; Sobkow et al., 2006).

1.7.2. Tol2 transposase system

Tol2 is an autonomous transposase belonging to the hAT family of transposons. It was first isolated from the genome of teleost fish medaka *Oryzias latipes* (Koga et al., 1996). Because the initially identified Tol2 *cis* sequence was long, optimization experiments were conducted, and subsequently a "minimal" Tol2 element was isolated (Balciunas et al., 2006; Urasaki et al., 2006). The method is based on the co-injection of DNA flanked by Tol2 elements with the mRNAs of Tol2 transposase (synthesized *in vitro*) into the eggs, leading to the integration of the desired sequences into the genome. Tol2 transposase system has been shown to be able to carry a DNA insert at least up to 70 kb with no reduction in transpositional activity (Balciunas et al., 2006; Suster et al., 2009). Knowing the regulatory sequences of the interesting genes, for example, the promoter sequences, is still a prerequisite in using this tool. Successful examples were shown in both newt *Pleurodeles waltl* and axolotl (Eroglu et al., 2022; Joven et al., 2018; Khattak et al., 2014; Khattak et al., 2013; Sandoval-Guzman et al., 2014; Woodcock et al., 2017).

1.7.3. PiggyBac transposase system

PiggyBac transposase system was initially identified from cabbage looper moth Trichoplusia ni (Fraser et al., 1996). Similar like the Tol2 transposase system, it is conducted by co-injecting DNA flanked by PiggyBac transposase elements with the transposase mRNAs into the eggs. PiggyBac transposase system has been reported with the capacity of carrying more than 100 kb in insert size (Li et al., 2011; Rostovskaya et al., 2012). Again, knowledge of the regulatory sequences in the interesting genes is needed before applying the tool. Unpublished data from our laboratory indicates its feasibility in newt *Pleurodeles waltl*.

1.7.4. ZFN system

Developed in late 1990s and optimized in 2000s, ZFN (Zinc-Finger Nucleases) is the first system which achieved specific targeting in genomes (Gaj et al., 2013). ZFN includes fusions of the nonspecific DNA cleavage domain from the FokI restriction endonuclease and zinc-finger proteins. When it comes to genomic modification, ZFN can be guided to a specific genomic site based on the specificity of the designed zinc-finger domain, before inducing double-strand breaks and stimulating DNA damage response pathways at the targeted sequences by the ZFN dimer (Gaj et al., 2013). ZFN was screened and tested in axolotls, and precise modification at axolotl Oct4 genomic locus was made using the obtained ZFN pair (Echeverri et al., 2022). However, ZFN might have unspecific toxicity which could cause early embryonic lethality in axolotl (Echeverri et al., 2022), and has not been used frequently in salamanders.

1.7.5. TALEN system

TALEN (Transcription Activator-Like Effector Nucleases) was developed around 2010 (Wei et al., 2013). It is based on the fusions of the FokI cleavage domain with the DNA-binding domains derived from TALE proteins. The TALE proteins contain multiple 33–35-amino-acid repeat domains each recognizing a single base pair (Gaj et al., 2013). Similar to ZFN, TALEN also induces double-strand breaks and stimulates DNA damage response pathways at the targeted sequences (Gaj et al., 2013). TALEN was also adapted in salamander models and proved to be more successful than the ZFN system. In a first pilot trial targeting endogenous tyrosinase gene or eGFP in transgenic axolotls, gene-specific loss-of-expression was observed (Echeverri et al., 2022). In addition, TALEN was found to more efficient and less toxic than ZFN in axolotl models, and the modified genomic alleles in F0 generations could readily be transmitted to F1 progeny (Echeverri et al., 2022). Several TALEN constructs were successfully employed in both newts and axolotls (Hayashi et al., 2014; Kuo et al., 2015; Woodcock et al., 2017).

1.7.6. CRISPR/Cas9 system

The CRISPR/cas9 method originates from the adaptive immune system of prokaryotes. It became a milestone among genome editing tool during the first half of the 2010s (Cong et al., 2013; Deltcheva et al., 2011; Jinek et al., 2012; Lander, 2016; Mali et al., 2013). The method has, similarly to other organisms, proved to be functional and efficient in salamander models by the co-expression of gRNAs against specific sites in the genome together with Cas9 protein

or mRNA (Cai et al., 2019; Elewa et al., 2017; Fei et al., 2016; Fei et al., 2018; Fei et al., 2017; Fei et al., 2014; Flowers et al., 2014; Furukawa et al., 2023; Gerber et al., 2018; Joven et al., 2018; Oliveira et al., 2022; Sousounis et al., 2020; Suzuki et al., 2018; Takeuchi et al., 2022; Yu et al., 2022). Due to its efficacy it has become the dominating tool for genome modifications, both to mutate genes in loss of function studies as well for generating knock-ins, for example, for cell tracking studies (Echeverri et al., 2022; Fei et al., 2018). There are mainly four ways to conduct CRISPR/Cas9-mediated knock-ins: homologous recombination (HR), microhomology-mediated end joining (MMEJ), non-homologous end joining (NHEJ), and homology-mediated end joining (HMEJ) (Yao et al., 2017). NHEJ has been reported work successfully in axolotls (Fei et al., 2017; Oliveira et al., 2022; Sousounis et al., 2020). However, its efficiency was not high. Also, it introduced random directions in integration and various types of indels at the junctions, making an easy frameshift of the knock-in gene. Our laboratory tested HR in *Pleurodeles waltl* (unpublished studies). Although successful, its efficiency was low. Recent advance in techniques of gBlocks and HDR Donor Blocks may pave a new way for using HMEJ. By combination of the linear high-fidelity gBlocks or HDR Donor Blocks, instead of plasmids, with the small molecules acting as homology-directed repair (HDR) enhancer, the efficiency of knock-in could be increased (IDT, 2023).

1.8. Gene expression profiling using scRNAseq/snRNAseq and spatial transcritpmics in salamanders

Another facet of the molecular tools that was important to adapt for salamanders are scRNAseq/snRNAseq. Multiple platforms for scRNAseq/snRNAseq have been developed, for example, Drop-seq and Smart-seq (Hwang et al., 2018; Jovic et al., 2022). Drop-seq techniques like 10xGenomics can efficiently recover up to 10000 singlets per run in droplets, the number of genes detected per singlet is not high. Smart-seq is a sensitive method that can detect high number of genes per singlet. However, the techniques require singlets to be isolated into separated wells for reactions, and the whole procedures are more time-consuming. The scRNAseq/snRNAseq techniques have been applied to salamanders to reveal cellular heterogeneity during regeneration of limb, heart, and brain (Eroglu et al., 2022; Gerber et al., 2018; Leigh et al., 2018; Lust et al., 2022; Subramanian et al., 2023; Woych et al., 2022). In this thesis, I have used 10xGenomics platform, given the high number of cells/nuclei I need to define the cell population in ventral midbrain**.**

While RNAseq data from dissociated tissues are useful and instrumental to cluster cells that could define cell (sub)types as well as differentiation trajectories, they do not reveal the spatial location of cells in tissues and organs. To overcome this limitation, spatial transcriptome techniques have been developed (Marx, 2021; Ståhl et al., 2016). Often, there is trade-off between spatial resolution and sequencing depth. The field is rapidly progressing, and a recently developed Stereoseq method, allowing for genome-wide expression analyses at spatial resolution equivalent to a cell, unraveled overlapping neurogenic processes during development and regeneration in the axolotl brain (Wei et al., 2022).

2. RESEARCH AIMS

The studies in this thesis aimed to solve the following aims:

AIM I. **Testing and implementing new genomic tools.**

AIM II. Defining the cell populations in the newt ventral midbrain.

AIM III. Revealing the cellular and molecular transitions in the newt ventral midbrain during development.

AIM IV. Characterizing cellular and molecular responses after dopaminergic damages in the newt ventral midbrain.

3. MATERIALS AND METHODS

3.1. Animals

Pleurodeles waltl were raised in the animal facility of Karolinska Institute under standard conditions (Joven et al., 2015). The newts were maintained at 12 hours light/12 hours darkness, 18-24 °C and staged according to (Gallien, 1957; Joven et al., 2015; Shi and Boucaut, 1995). All the experiments were performed in compilation with Swedish and European ethical permits N211/15, Dnr 9091-2018, and Dnr 3581-2022.

3.2. Generation of genetically modified animals by egg injection

Tol2-mediated or CRISPR-mediated transgenesis by egg injection was conducted based on previous protocols (Fei et al., 2018; Khattak et al., 2014). In Tol2-mediated plasmid integration: a solution of Tol2 mRNAs (50 ng/ul) and the plasmid with Tol2 elements (10 ng/ul) was made, and each newt egg (fertilization was checked) was injected with 5-10 nl of the solution. In CRISPR-mediated transgenesis: (1). For CRISPR-mediated mutation, a 5-10 nl solution of gRNAs and Cas9 protein in 1x Cas9 buffer (CRISPR/Cas9 system), or a 5-10 nl solution of crRNAs and Cas12a protein (CRISPR/Cas12a system) was injected into newt eggs (fertilization was checked) based on the protocols (Fei et al., 2018). (2). For CRISPR-mediated knock-in, a 5-10 nl solution of gRNAs, Cas9 protein, and linear gBlocks doner in 1x Cas9 buffer (CRISPR/Cas9 system), or a 5-10 nl solution of crRNAs, Cas12a protein and linear gBlocks doner (CRISPR/Cas12a system) was injected into newt eggs (which's fertilization were checked) based on the protocols (Fei et al., 2018). Next, the eggs were maintained for hatch and development. Later, genotyping was conducted to examine the transgenic modifications.

3.3. *In vitro* generation of Tol2 transposase mRNAs

Synthesis of Tol2 transposase mRNAs was conducted based on previous description (Khattak et al., 2014). In brief, the plasmid containing "T7 promoter: Transposase" element was linearized by a restriction enzyme, then Tol2 transposase mRNAs was synthesized *in vitro* by HiScribe® T7 ARCA mRNA Kit (with tailing) (New England Biolabs, E2026S). Later, the synthesized mRNAs were purified by LiCl precipitation and dissolved in dNase-/rNase-free water. The Tol2 transposase mRNAs were stored at -80 °C before use.

3.4. Design of gRNAs (Cas9) or crRNAs (Cas12a) for CRISPR system

The genome assembly and RNA seq data in (Brown et al., 2022) was used to target the sequences of the interesting genome areas. Next, the PAM sites of CRISPR/Cas9 system were identified, and the gRNAs were designed using the online tool from Integrated DNA Technologies (IDT) (IDT, 2023). Finally, the potential off-target sites of the gRNAs were examined across the newt genome. See all primers and gRNA sequences used in **Supplementary Table. 1**.

3.5. Genotyping

I performed genotyping by extracting DNA from the putative transgenic newts, designing primers to amplify the donor plasmid sequences by PCR (see all primers and gRNA sequences used in **Supplementary Table. 1**). The PCR product was cut from the gels, purified, and sent for Sanger sequencing.

3.6. Tamoxifen administration

According to published methods for axolotl (Fei et al., 2017; Khattak et al., 2014), a 25.84mM tamoxifen stock solution was prepared for intraperitoneal injections by dissolving 100 mg of 4-hydroxytamoxifen in 10 ml of DMSO. For water-based induction (20 mM), 77.4 mg of 4-hydroxytamoxifen was dissolved in 10 ml of DMSO. The solutions were aliquoted to avoid freeze-thaw cycles and kept at −80 °C for up to 6 months. Each aliquot was used once and protected from light.

Animals were anesthetized and weighted to determine the amount of 4-OH tamoxifen injection volume necessary, calculating 5 µl of per gram of body weight as a starting point. The adult animals were injected at a final dose of 50µg/g (Tamoxifen/animal weight). For larval animals, animals were weighted in groups and two groups were defined: 1.5-2cm larvae were injected with 0.3µl stock (1x1mm glass capillary mark) to achieve an approximate dose of 0.06g/animal; 3cm larvae were injected with 1.4µl stock (4x1mm glass capillary mark) to achieve an approximate dose of 0.28g/animal.

The analysis of the tissue was performed at least 7 days after the tamoxifen administration, as it has been reported that in axolotls the earliest recombination event is visible 5–7 d after 4-OH tamoxifen treatment (Fei et al., 2017; Khattak et al., 2014).

3.7. Edu administration

Edu (5-Ethynyl-2′-deoxyuridine) is a thymidine analog used to assay DNA synthesis and track proliferation cells in multiple biological systems including the newts (Joven et al., 2018). Edu (900584, MERCK) was dissolved in saline (0.9% NaCl) to make a stock at 2 mg/ml. Later the EdU stock was injected intraperitoneally into the newts at a dose of 50 µg/g (Edu/body weight) at the decided time points.

3.8. Dopaminergic chemical ablation in newt brain

The dopaminergic chemical ablation protocol was adapted from our previous studies, which used drug 6OHDA (6-hydroxydopamine) to specifically ablate the midbrain dopaminergic neurons (Berg et al., 2010; Berg et al., 2011; Hameed et al., 2015; Joven et al., 2018; Parish et al., 2007). In short, ascorbic acid (A92902, MERCK) was dissolved in 0.9% NaCl to make the stock solution (0.2mg/ml), followed by dissolving 6OHDA (H4381, MERCK) into this ascorbic acid stock solution to make a 20 µg/µl 6OHDA solution. Later at the decided time points, this 6OHDA solution was delivered to ventral midbrain by intraventricular injection in newt *Pleurodeles waltl*. The dose used was 4-8µg/g (6OHDA/newt body weight). Sham injured

newts generated by intraventricular injection using the same dose but with the ascorbic acid solution. Control newts suffered no intraventricular injection. The effects of the ablation were examined by the loss of TH^+ neurons in the ventral midbrain, or the absence of TH^+ fibers in the striatum by immunohistochemistry.

3.9. PLX3397 -mediated microglia/macrophage depletion

PLX3397 (Pexidartinib) has been used to deplete microglia/macrophage populations by inhibiting CSF1R (Colony Stimulating Factor 1 Receptor) in animal models (Elmore et al., 2014). The PLX3397 solution was made by mixing 50 mg PLX3397 powder, 1 ml DMSO, 4 ml PEG300, 500 µl Tween-80, and 4.5 ml saline into a 10 ml stock solution (5 µg/µl of PLX3397), and the vehicle solution was made by mixing 1 ml DMSO, 4 ml PEG300, 500 µl Tween-80, and 4.5 ml saline into a 10 ml solution. Later, PLX3397 solution or vehicle solution were delivered to newts by intraperitoneal injection at the decided time points. The dose used was 50 µg/g (PLX3397/newt body weight). The effects of microglia/macrophage ablation were measured by immunohistochemistry.

3.10. Tissue processing

The *Pleurodeles waltl* newts were deeply anesthetized by immersion in a solution of MS222 (MERCK) at a range of concentrations (0.02% for small larvae, 0.05% for large larvae, and 0.1% for adults). Then the heads of newts were cut and transferred into 4% PFA for overnight fixation at 4 °C. After fixation, the brains were dissected out and immersed in a solution of 30% sucrose in PBS (14190144, Thermo Fisher Scientific) until they sank at 4 to 37 °C. For immunohistochemistry, the brains were pre-embedded at 37°C for 6-12 hours in 3.5% gelatin with 30% sucrose in PBS, then embedded in 7.5% gelatin with 30% sucrose in PBS for 6-12 hours, and quickly frozen with dry ice. The frozen blocks were immediately cut or stored at -80 °C. Sections of 20 µm were cut on a cryostat (Leica, CM3050S) at -30 °C in the transverse planes, collected on SuperFrost slides (Menzel Gläser Superfrost Plus) in three to five series depending on the sample sizes. Slides were immediately processed or stored at −80 °C until use. For *in situ* hybridization (ISH), the procedure was the same, except for the brains were embedded in Tissue-Tek® O.C.T. Compound (SAKURA) instead of gelatin and the sectioning temperature was -20 °C.

3.11. Immunohistochemistry

Immunohistochemistry procedures were adapted from the protocols in our previous study (Joven et al., 2018). First, slides of sections were permeabilized either in PBST (PBS+0.25% Triton X-100 (Tx, MERCK)) at 37 °C for 30 mins followed by either another 30 min of PBST at 37 °C, or 15-20 mins of 1X antigen retrieval buffer (DAKO S1699) depend on the primary antibodies used later (for details, see **Supplementary Table. 2**). After washing 3 times in PBST for 5-10 mins (last wash washed with PBS), the edges of slides were sealed with a hydrophobic barrier pen (ImmEdge), and blocked using blocking buffer (0.2% BSA, 0.2% fish skin gelatin [MERCK] and 0.2% Tx in PBS) at room temperature for 1 hour. The slides were then incubated with primary antibodies overnight at proper concentrations (see **Supplementary Table. 2**) at room temperature. The slides were washed with PBST for 3 times for 5-10 mins and incubated with the proper secondary antibodies (from: Donkey anti-Mouse IgG (H+L) Highly Cross-Adsorbed Secondary Antibody, Alexa Fluor™ 488 (A-21202, Thermo Fisher Scientific),

Donkey anti-Mouse IgG (H+L) Highly Cross-Adsorbed Secondary Antibody, Alexa Fluor™ 555 (A-31570, Thermo Fisher Scientific), Donkey anti-Mouse IgG (H+L) Highly Cross-Adsorbed Secondary Antibody, Alexa Fluor™ 647 (A-31571 ,Thermo Fisher Scientific), Donkey anti-Rabbit IgG (H+L) Highly Cross-Adsorbed Secondary Antibody, Alexa Fluor™ 488 (A-21206, Thermo Fisher Scientific), Donkey anti-Rabbit IgG (H+L) Highly Cross-Adsorbed Secondary Antibody, Alexa Fluor™ 555 (A-31572, Thermo Fisher Scientific), Donkey anti-Rabbit IgG (H+L) Highly Cross-Adsorbed Secondary Antibody, Alexa Fluor™ 647 (A-31573, Thermo Fisher Scientific), Donkey anti-Goat IgG (H+L) Cross-Adsorbed Secondary Antibody, Alexa Fluor™ 488 (A-11055, Thermo Fisher Scientific), Donkey anti-Sheep IgG (H+L) Cross-Adsorbed Secondary Antibody, Alexa Fluor™ 488 (A-11015, Thermo Fisher Scientific), Donkey anti-Rat IgG (H+L) Highly Cross-Adsorbed Secondary Antibody, Alexa Fluor™ 488 (A-21208, Thermo Fisher Scientific), Donkey anti-Chicken IgY (H+L) Highly Cross Adsorbed Secondary Antibody, Alexa Fluor™ 488 (A78948, Thermo Fisher Scientific)) for 2 hours at room temperature, followed by 30 min incubation of DAPI for 0.5-3 hours, and 3 times washing of PBST. If Edu staining was needed, it was performed at this point by incubating sections with 100 mM Tris pH 8.5, 1 mM CuSO4, 50-100 μM fluorescent azide, and 100 mM ascorbic acid as previously described (Salic and Mitchison, 2008). Finally, slides were mounted under coverslips with non-fluorescent mounting medium (DAKO).

3.12. RNA probe synthesis and *in situ* hybridization

Total RNA Purification Kits (NORGEN, 37500) and SuperScript™ IV Reverse Transcriptase (Thermo Fisher Scientific, 18090010) were used to generate the total cDNA from fresh dissected newt brains. Using the identified the newt orthologues, the RNA probe sequences were manually designed (**Supplementary Table. 4**), the DNA templates (with T7 and T3 promoter at the two ends) of the probes were amplified from the total cDNA of brain using Phusion™ High-Fidelity DNA Polymerase (2 U/μL) (Thermo Fisher Scientific, F-530XL). Next, the RNA probes (antisense or sense) were synthesized with DIG RNA Labeling Mix (11277073910, Merck), T7 RNA Polymerase (New England Biolabs, M0251S), and T3 RNA Polymerase (New England Biolabs, M0378S).

In situ hybridization was conducted in a similar way as described before (Subramanian et al., 2023). In the first day, the slides were dried at 53 °C for 2 h and immersed in cold 100% methanol at -20 °C for 10 min. After Proteinase K (Thermo Fisher Scientific, EO0491) treatment at 5 μg/ml for 7-10 min, the sections were acetylated in triethanolamine/acetic anhydride solution for 5 min. Next, the slides were pre-hybridized with 50% formamide/H_2O/5M NaCl at 53-55 °C for 2 h, and hybridized with probes (0.75 ng/μL, the probes were heated at 80 °C for 5 min and chilled on ice for 5 min before used) at 53 °C for 20-22 h. In the second day, the slides were firstly washed at 53 °C in 4x SSC/0.3% CHAPS 5 min, 2x SSC/0.3% CHAPS/50% formamide 20 min, 2x SSC/0.3% CHAPS – 15 min, 0.2x SSC/0.3% CHAPS – 10 min, then washed at room temperature in (1:1) 0.2% SSC/PBST 10 min, before the final wash of PBST 5min. Then the slides were blocked with blocking buffer (10% goat serum, containing 1% BSA in PBST) for 1 h, before incubated in alkaline phosphatase conjugated anti-digoxigenin antibody (Roche) (1:1000) for 2 h. Next after washing the antibody with PBST, the sections were washed 3x for 5 min each in freshly prepared alkaline phosphatase buffer (100mM Tris-HCl pH 9.5, 50 mM MgCl2, 100mM NaCl, 0.1% Tween-20). Later the slides were incubated in BM Purple (Roche) before the color development was

terminated by incubating the sections in 0.5M EDTA. Finally, the slides were mounted with VectaMount AQ Mounting Medium (Vector Laboratories).

3.13. Molecular cloning of plasmids for transfection in cell culture and newt brain electroporation

Then the open reading frame (ORF) of newt NFIA was amplified from the total brain cDNA purified before with Phusion™ High-Fidelity DNA Polymerase (2 U/μL) (Thermo Fisher Scientific, F-530XL). The plasmid pT2K-p53DN-T2A-copGFP (a gift from Martine Roussel, Addgene plasmid # 109229 ; http://n2t.net/addgene:109229 ; RRID:Addgene_109229) was digested by BbvCI (New England Biolabs, R0601S) and EcoRI-HF (New England Biolabs, R3101S), before the amplified ORF of nFiA was infused by Gibson Assembly® Cloning Kit (New England Biolabs, E5510S) to generate the CMV: NFI-T2A-copGFP plasmid (Kawauchi et al., 2017).

3.14. HEK293t cell transfection and immunocytochemistry

HEK293t cells were cultured and transfected with either CMV: NFI-T2A-copGFP plasmids or CAG: GFP-loxp-cherry plasmids (as control) using Lipofectamine™ 2000 Transfection Reagent (Thermo Fisher Scientific, 11668019). Next the cells were fixed in 4% PFA, washed in PBST (0.25% Tx), blocked by 0.2% BSA, 0.2% fish skin gelatin (MERCK) and 0.2% Tx in PBS (blocking buffer), and incubated with primary antibodies at room temperature for 6-12 hours. Then the cells were washed in PBST (0.25% Tx) and incubated with secondary antibodies and DAPI, before finally washed in PBST (0.25% Tx) and mounted with non-fluorescent mounting medium (DAKO). Images of the sections were taken by Zeiss LSM880 confocal microscope.

3.15. Plasmid electroporation to ependymoglia of newt midbrain

Plasmid electroporation was performed based on previous protocols (Joven et al., 2018; Kirkham and Joven, 2015). In brief, late larval newts were injected intraventricularly with either “CMV: NFI-T2A-copGFP” plasmids or “CAG: GFP-loxp-cherry” plasmids (as control). Larvae were placed in agarose chambers as previously described (Joven et al., 2018). Then, electroporation was performed with the (+) towards the ventral side of the larvae to achieve labelling of the ventral or lateral walls of the ventricle. A NEPA21 electroporator (Nepagene) attached to tweezers with round platinum plate electrodes 4 mm in diameter was used. Using “unidirectional setting (+)”, the brains were exposed to a first single pulse of 135 mV/cm (voltage), 5 cm (pulse length), 95 ms (pulse interval), and 0% (decay), followed by 5 pulses of 99 mV/cm (voltage), 50 cm (pulse length), 999 ms (pulse interval), and 10% (decay).

3.16. Imaging and image processing

For slides of IHC, Zeiss (Axio Imager Z2) and confocal (LSM 700, LSM 880) microscopes were used to examine slides. The microscope was equipped with fluorescence illumination (HXP120V, HXP120C) and ZEN software (Zeiss) was used to take images. Brightness and contrast adjustments of images were processed in Fiji: ImageJ software. Morphological and quantitative analyses from confocal images were performed in Fiji: ImageJ. Cell counter was used to quantify positive cells and determine proportions of cell subpopulations. For

morphological quantitative analysis of the microglia, the shape of each microglia/macrophage cell in the interesting areas of the images was manually outlined. Then the circularity of each microglia/macrophage cell was measured by Fiji: ImageJ. Data were collected, processed and graphs were generated using Microsoft Excel as well as GraphPad Prism. For slides of *in situ* hybridization, a Leica DM5500 B Microscope was used for imaging the sections. Brightness and contrast adjustments of images were processed in Fiji: ImageJ software.

3.17. Phylogram

The protein sequences of the orthologues from different species were extracted from UniProt database or the new genome resource of Pleurodeles waltl (Brown et al., 2022; UniProt, 2023). Next the protein sequences were analyzed in Clustal Omega by selecting "PROTEIN" (Omega, 2023). The phylogram was generated by choosing "Phylogenetic Tree". Finally, the phylogram was processed in Adobe Illustrator software.

3.18. BulkRNAseq and data processing

Newt ventral midbrains were freshly dissected out, and their RNA was purified using Total RNA Purification Kits (NORGEN, 37500). Then, the extracted RNA was sent to Novogene Co to generate "eukaryotic strand-specific transcriptome library".

To process the raw data, Cutadapt package was used to trim the adapter sequences from paired-end reads (Martin, 2011):

```
cutadapt -a ADAPTER_FWD -A ADAPTER_REV -o out.1.fastq -p out.2.fastq reads.1.fastq reads.2.fastq
```

Next, STAR 2.7.9a package was used to make the index of newt genome, and then the RNAseq transcripts were mapped to the index (Brown et al., 2022; Dobin et al., 2013):

```
STAR \
--runMode genomeGenerate \
--runThreadN 16 \
--genomeDir ./indexed_genome \
--genomeFastaFiles $genome_file \
--sjdbGTFfile $full_annotation.gtf\
--sjdbOverhang 124 \
--limitGenomeGenerateRAM 55000000000

STAR --runMode alignReads --quantMode GeneCounts --runThreadN 16 --
genomeDir ./indexed_genome --outSAMtype BAM SortedByCoordinate --
readFilesCommand zcat --readFilesIn rnaseq1_1.fq.gz rnaseq1_2.fq.gz --sjdbGTFfile
full_annotation.gtf --sjdbGTFfeatureExon exon --outFileNamePrefix rnaseq1_tr
```

Then Subread package was used to count reads to genomic features (Liao et al., 2013, 2014):

```
featureCounts -a full_annotation.gtf -o count_out -p -s 2 -T 10 -F GTF -t CDS
*.bam >counts_out.log
```

The differential expression was analyzed with DESeq2 package in R (Love et al., 2014). The sample-to-sample distances were calculated and visualized by PCA plot, or heatmap using pheatmap package. The top differentially expressed genes were visualized using volcano plot.

The genes that showed a statistically significant difference in gene expression (padj<0.05) were selected for functional gene ontology (GO) enrichment analysis. The human gene orthologues of the annotated genes were found using Uniprot conversion from transcript to gene name. The lists of genes were used to perform functional gene ontology (GO) enrichment analysis using the web server g:Profiler (Raudvere et al., 2019).

3.19. Tissue dissociation and fluorescence-activated cell sorting (FACS) for scRNAseq and snRNAseq

Tissues from newt ventral midbrain were dissociated either into single-cell suspension or single-nucleus suspension before FACS. For single-cell suspension, newt ventral midbrains were freshly dissected out and dissociated in one of the three enzymes: (1) 20 units/ml papain (Worthington, LK003176) in 70% EBSS (E6267-500ml, Sigma-Aldrich) with 0.5 mM EDTA (15575020, Thermo Fisher Scientific), 1 mM L-cysteine (C121800, Sigma-Aldrich), and 240 units/ml DNase (58C18143, Worthington) at 27 °C for 30 min. (2) 2 mg/ml collagenase/dispase enzyme (11097113001, Roche) in 70% PBS at 27 °C for 30 min. (3) 10 mg/ml *Bacillus licheniformis* (BL) enzyme (P5380-25MG, MERCK) in 70% PBS at 4 °C (in cold room) for 30-60 mins. Later the liquid was filtered with a 100 µm strainer and resuspended in 70% PBS with 2% BSA. This cell suspension was sent for FACS to enrich live singlets by cell viability and morphology into a collection tube.

For single-nucleus suspension, first a lysis buffer (0.32M sucrose, 5 mM CaCl2, 3 mM MgAc, 0.1 mM Na_2EDTA, and 10mM Tris-HCl) was made, then a lysis solution was freshly prepared by mixing 5 ml lysis buffer, 50 µl complete inhibitor (MERCK, 11873580001, one 1 tablet in 500 µl Ultrapure nuclease free H_2O), 50 µl DTT (0.1M), 50 µl 10% Triton X-100, and 25 µl rNase inhibitor (TAKARA, 2313A) Next the newt ventral midbrains were freshly dissected out and dissociated in a douncer with 2.5 ml of the lysis solution. The tissues were dounced firstly with loose, then tight pistons. After the dissociation, the solution was centrifuged at 500 g, 4 °C, 5 min. Then the nuclei were resuspended in 1 ml 70% DPBS with 2% BSA and 10 µl rNase inhibitor. Later, the nuclei suspension was filtered by a 70 µm nylon cell strainer into a FACS tube (pre-coated by 2% BSA). Finally, 7AAD stock (50 µg/ml in 70% PBS) was added to the suspension at 1:50 to stain the nuclei, and proceeded to FACS. Based on the fluorescence property of 7AAD (excited by 488 laser light and detected in the far-red range of the spectrum (650 nm long-pass filter)), the singlets of nuclei were sorted into a collection tube.

3.20. scRNAseq/snRNAseq of newt ventral midbrains

3.20.1. Single-cell/-nucleus capture, library construction, and sequencing

Following the procedures of Chromium Next GEM Single Cell 3' Reagent Kits v3.1 (Dual Index), the single-cell/-nucleus suspension obtained from previous dissociations were loaded into 10x Chromium Chip G and ran on the chromium controller. Then cDNA amplification and library construction were conducted for each sample. The quality of the cDNAs and libraries was examined using agilent 2100 bioanalyzer system. Finally, the library of each sample was sequenced on Illumina NovaSeq 6000-S2 v1.5.

3.20.2. Mapping

A genome index for scRNAseq / snRNAseq analysis was generated using kallisto and bustool programs (Bray et al., 2016; Melsted et al., 2021). Then the reads of the samples were mapped to the index, and a count matrix was created for each library (Bray et al., 2016; Melsted et al., 2021).

3.20.3. QC and filtering

Knee plots were generated for each library after creating the count matrix of each library. Libraries were processed independently to filter out the droplets with low UMI counts, using the manually supplied cutoff based on inflection. R package Seurat was used to generate individual Seurat object from each filtered matrix (Hao et al., 2021). One more filtration was conducted on the Seurat objects to only keep the droplets with nFeature_RNA > 200, nFeature_RNA < 6500 and for the snRNAseq analysis in Chapter 3 an additional filter of nCount<15000 was applied. Next, R package DoubletFinder was used to detect and exclude doublet cells (McGinnis et al., 2019). The filtered Seurat objects were saved for the analyses in the later steps.

3.20.4. Data integration and clustering

The Seurat objects generated in the previous steps were integrated and clustered with R package Seurat (Hao et al., 2021). The Seurat objects were combined and split into a list with each dataset as an element. Then after identifying anchors using the FindIntegrationAnchors function, the anchors were passed to the IntegrateData function, which returned as an integrated Seurat object. The integrated data was scaled, and dimensionality reduction was conducted by PCA, TSNE, and UMAP. Louvain, K-means, and hierarchical clustering were tested on the integrated data. Louvain integration was chosen for further analysis.

3.20.5. Differential expression across conditions in specific cell types

In general, the function FindAllMarkers from R package Seurat was used to identify the top differentially expressed genes in each cluster (Hao et al., 2021). Then, the Louvain resolution (CCA_snn_res) that better explained cell types was selected on the basis of top expressed marker genes which orthologues were described in the literature. Seurat package in R was further used to visualize gene expression in UMAPs and violin plots. For a comprehensive analysis on event composition's origin among samples and clusters, the total counts per cluster and condition were extracted, normalized and plotted using excel and graphpad Prism.

3.21. Bias mitigation

To avoid sampling bias not related to experimental conditions, sexes were evenly distributed among experimental groups and all groups were assigned similar sized animals.

To confirm the absence of bias in data acquisition, quantification, and processing, samples were assessed by two researchers independently from each other.

3.22. Statistical analyses

The number of values for each graph is always shown as individual dots. The variability is shown as mean ±SEM. Statistical significance was determined using Student's t-test for two group comparisons. One-way ANOVA with Bonferroni's post-hoc test was used to analyze the differences of one independent variable between more than two groups. ANOVA with Bonferroni's post-hoc test was used to analyze the differences of two independent variables between multiple groups.

4. RESULTS AND DISCUSSION

4.1. Applying and refining the genomic toolkits for *Pleurodeles waltl*

The recent progress in generating genomic resources and developing transgenic techniques has led to novel tools for newt research (Brown et al., 2022; Elewa et al., 2017; Hayashi and Takeuchi, 2015; Hayashi et al., 2013; Matsunami et al., 2019; Suzuki et al., 2018). In this chapter, I present the advances I made in using these new resources for increasing our understanding of newt regeneration.

4.1.1. Identifying gene orthologues for study of the ventral midbrain

I first identified the newt protein and mRNA orthologues by blasting human/mouse orthologue proteins against newt transcriptome databases using the annotations and assemblies published in (Brown et al., 2022; Elewa et al., 2017; Matsunami et al., 2019). By blasting the mRNA against the genome, I identified gene elements, including 5' upstream regions, exons, introns, 3' downstream regions, and chromosomal locations of selected genes. The last version of the genome assembly that I use in most of this thesis contains 56,783 conserved protein coding isoforms, which are named "gene1", "gene2", and so on. For the purpose of gene nomenclature and downstream analysis in this thesis, genes were given a Uniprot ID based on the highest homology found in the database (Brown et al., 2022). Hereafter, the format "gene12345" means there was no hit on Uniprot and "gene12345-Uniprot ID" when isoforms were assigned to a given Uniprot ID.

My main focus was to find genes related to the ventral midbrain development and dopaminergic neurogenesis reported in other species (La Manno et al., 2016; Saunders et al., 2018). An emphasis was on key dopaminergic determinants, such as tyrosine 3-hydroxylase, which catalyzes the rate-limiting step in the biosynthesis of catecholamines, dopamine, noradrenaline, and adrenaline (Hook et al., 2018; Salmani et al., 2023; Tiklova et al., 2019; UniProt, 2023). I found two tyrosine hydroxylase (*Th/Ty3h*) genes (*gene28570-TH* and *gene36549-TH*) in the *Pleurodeles waltl* genome, located on two different chromosomes (chromosome 3 and 4). Different to mammals, where a secondary loss of *Th2* gene is assumed, other vertebrates also contain 2 genes enconding for *Th* (Yamamoto et al., 2010). This result indicates that *Pleurodeles walt* contains two copies like teleost fish and the presumed ancestor of jawed vertebrates. I also identified the dopamine receptors D1a, D1b (dopamine D5 receptor), and D1c (which belong to D1-like family) as well as D2, D3, and D4 (which belong to D2-like family) in *Pleurodeles waltl*. Most of the gene orthologues related to dopaminergic subpopulations had only one copy in *Pleurodeles waltl,* such as *Nurr1, Otx2, Lmx1a, Lmx1b, Aldh1a1, Calb1* (Calbindin), *Calb2* (Calretinin), *En1* and *En2* (Ang, 2006; Arenas et al., 2015). Interestingly, *Pitx3* which is known to be important for the survival of a subset of dopaminergic neurons (Hwang et al., 2003; Maxwell et al., 2005; Nunes et al., 2003; van den Munckhof et al., 2003), was not found in the newt genome. More research is necessary to confirm whether this lack of *Pitx3* is real and not due to annotation problems. A limitation of this study is that the annotation is not final and future versions will likely improve the resolution of these findings.

In relation to other key cell types in the ventral midbrain, I found both evolutionary conservation and divergence. An important mechanism for acquiring new genes and creating genetic novelty in organisms is gene duplication (Magadum et al., 2013). I found, for example, a duplication of the oligodendrocyte marker *Mbp* on chromosome 2 (*gene19846-Mbp* and *gene19872-Mbp*) (**Fig. 4**). For the microglia/macrophage marker *Mpeg1*, three gene variants were detected on chromosome 4 (*gene31079-Mpeg1, gene31082-Mpeg1* and *gene31083-Mpeg1*) (**Fig. 5**). Two variants of the ependymoglial marker gluthamine synthesase gene (*Gs/Glna/Glul*) were identified in *Pleurodeles waltl* on two different chromosomes (*gene32391-Glna* in chromosome 4 and *gene49443-Glna* in chromosome 6). Molecular phylogeny analysis of protein orthologues by Clustal Omega suggested that both *GLNA* proteins of *Pleurodeles waltl* have a counterpart in the frog, while the teleost and mammalian proteins are divergent (Omega, 2023) (**Fig. 6**). These results illustrate examples for conserved and divergent proteins, as well as suggesting a loss of the GLNA isoforms in the mammalian and bird lineages. Alternatively, one *Glna* gene was present in the common ancestor of vertebrates, undergoing duplication events in teleosts, amphibians and reptiles.

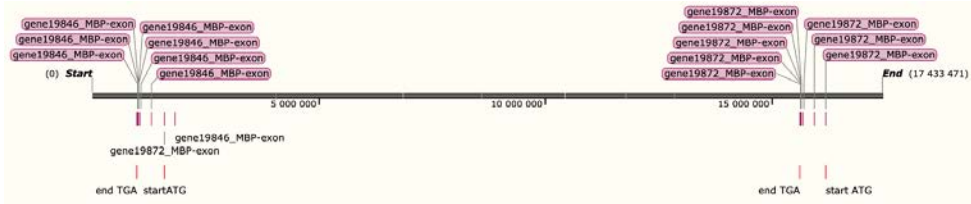

Fig. 4 | Duplication of the oligodendrocyte marker MBP was found on newt chromosome 2. The purple vertical lines represent exons (9 exons in *gene19846-Mbp* and 8 exons in *gene19872-Mbp*). The red vertical lines mark the start and end of the gene.

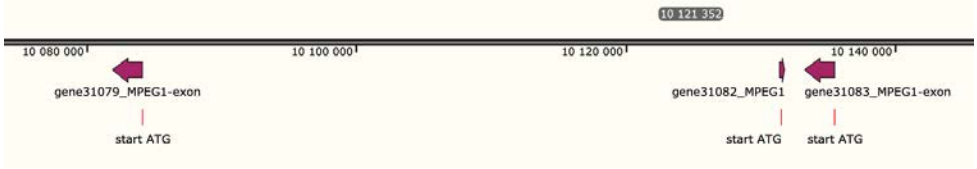

Fig. 5 | Three versions of the macrophage marker MPEG1 (*gene31079-Mpeg1, gene31082-Mpeg1*, and *gene31083-Mpeg1*) were found on newt chromosome 4 genes (represented by purple arrows). The purple arrows represent genes. The red vertical lines mark the start of each gene.

4.1.2. Generation of genetically modified newts

Transgenic *Pleurodeles* expressing fluorescent proteins in specific cell types have been generated by manipulating their genome using various techniques in one-cell-stage embryos (Elewa et al., 2017; Eroglu et al., 2022; Hayashi et al., 2013; Joven et al., 2018). Gene regulatory elements in newts are largely unexplored. One approach to generate genetically modified newts is by integrating a donor plasmid into their genome. The donor plasmid expresses a protein of interest under the genomic regulatory element to target a specific cell type. This approach has been successful in several cases in newts and other species (Kawakami, 2007; Tsissios et al., 2023). Another alternative I chose was to use CRISPR/Cas9 technology to target specific loci

in the genome. CRISPR/Cas9 is used to generate loss of function mutants, but it can also be used to integrate donor sequences in a locus of interest for cell tracing (Fei et al., 2017). I made several constructs to target ependymoglial cells and their progeny in the dopaminergic lineage. I chose to start with these early during the thesis work because creating these genetically modified animals is time consuming. Not only do newts have a long generation time, but there could have arisen technical problems as well. However, I was hopeful that if any of these lines succeeded, it could move the projects of this thesis forward and provide important tools for subsequent studies beyond this thesis. Given the unpredictability of successful generation of genetically modified animals, I tested several constructs. These would allow for conditional and non-conditional expression of fluorescent cell trackers as well as mutation of genes known to be important in dopaminergic neurogenesis in mammals. Below I present the genetically modified newts I was involved in generating to target ependymoglial cells and their putative progeny.

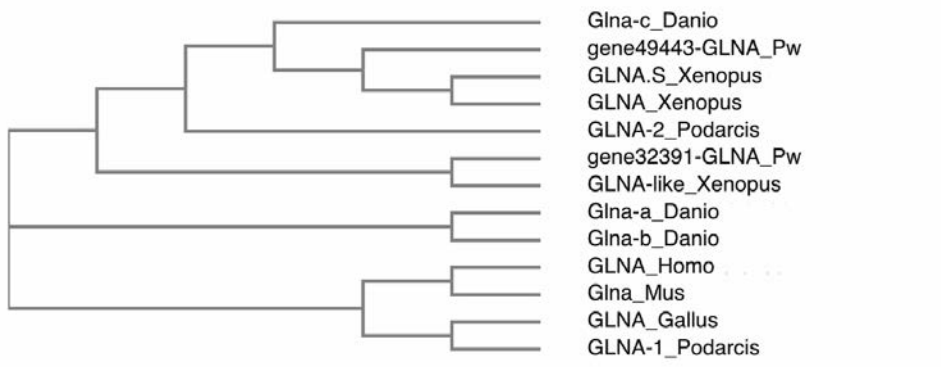

Fig. 6 | Phylogram tree of the GLUL (GLNA) genes from *Danio rerio* (zebrafish), *Pleurodeles waltl* (Pw), *Xenopus laevis* (frog), *Podarcis muralis* (Wall lizard), *Gallus gallus* (Chicken), *Mus musculus* (Mice), and *Homo sapiens* (Human). Three isoforms were detected in zebrafish and *Xenopus laevis*. Two isorforms were detected in *Podarcis muralis.* Only one GLNA protein was detected in *Homo sapiens, Mus musculus* (Mice) and *Gallus gallus.* Both isoforms from *Pleurodeles waltl* show some distances to the mammalian genes. Two isoforms of *Xenopus laevis* and one of *Danio rerio* are close to one isoform (gene49443) of *Pleurodeles waltl*, while another isoform of *Xenopus laevis* is close to the other isoform of *Pleurodeles waltl* (gene32391).

4.1.2.1 Tol2-mediated transgenesis

In order to integrate a donor plasmid into a salamander genome, the Tol2 transposase is one of the most widely used procedures (Berg et al., 2010; Eroglu et al., 2022; Tilley et al., 2022). The procedure involves injecting a mixture of Tol2 mRNA and a donor plasmid that contains the sequences of a regulatory element, followed by gene(s) of interest, and both of them flanked by Tol2 elements.

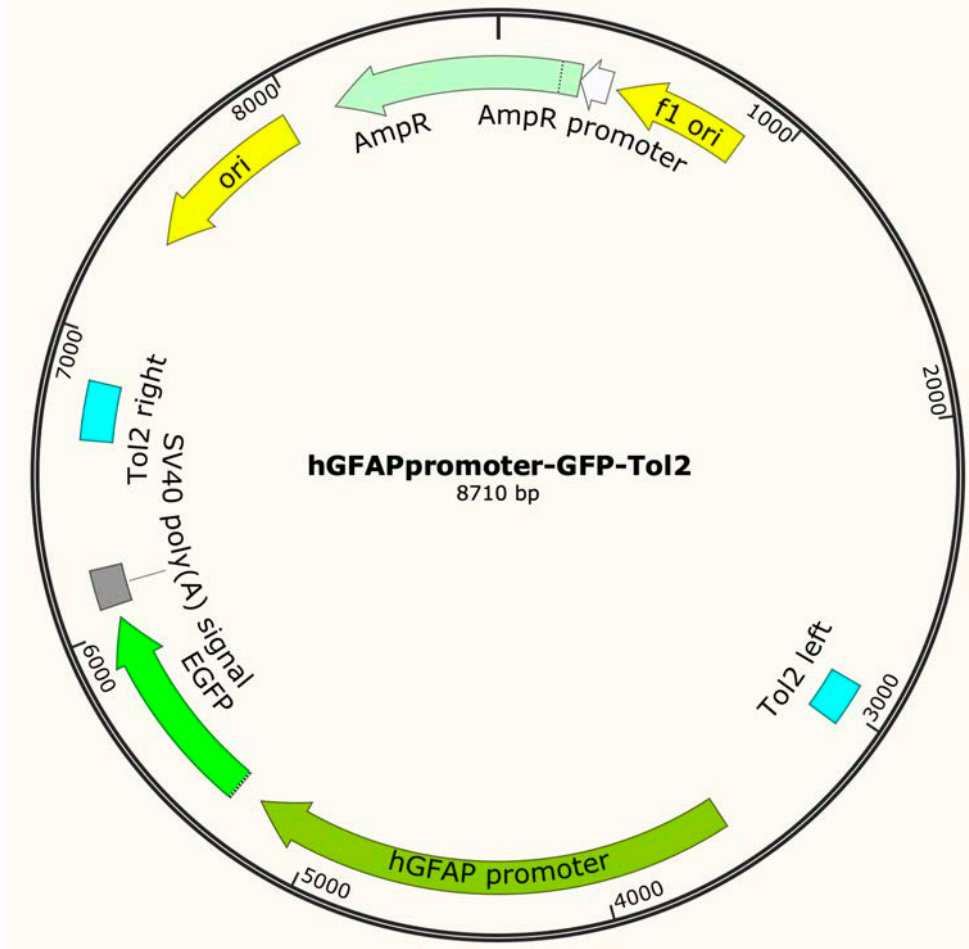

Fig. 7 | Map of the plasmid Tol2-human GFAP: GFP-Tol2 (hGFAP:GFP). An EGFP is under control of the human GFAP promoter, while both of them were flanked by the Tol2 elements.

4.1.2.1.1 Generation and validation of transgenic newts

I have designed and produced multiple plasmids by molecular cloning and amplification (**Fig. 7, Sup. Fig. S1**). These plasmids were used to inject single cell fertilized embryos to try to generate F_0 founders of new transgenic lines (see **Table. 2**). Of note, *Pleurodeles waltl* needs one year to reach adulthood, which means that I needed to wait at least that time to confirm germline transmission by breeding. I then confirmed the transgenesis in the first generation by genotyping and/or phenotyping (see example of tgTol2(Hsa.*GFAP:GFP*)^{Simon} in **Fig. 8**). Before the transgenic line tgTol2(Hsa.*GFAP:GFP*)^{Simon} was generated, our lab relied on electroporation techniques to visualize and trace the progeny of GFAP$^+$ cells (Berg et al., 2010). With a transgenic line the efficiency of electroporation would no longer pose a problem, and it would also allow for long term tracing of GFAP+ expressing cells. Similar to its application in axolotls,

the limitation of this method is that it relies on conserved promoters/enhancers and the expression of reporter proteins need to be validated for each case (Tilley et al., 2022).

Table. 2 | The plasmids generated for Tol2-mediated transgenesis in different cell types

Plasmid	Promoter source	Expected phenotype	Phenotyped	Genotyped
tgTol2(Hsa.*GFAP:GFP*)^{Simon}	(Berg et al., 2010)	GFP in ependymoglia	Epifluorescence and immunostaining	Yes
tgTol2(Dre.Dat:*GFP*)^{Simon}	(Xi et al., 2011)	GFP expression in dopaminergic neurons	Epifluorescence	No
tgTol2(Hsa.*GFAP:NLStdTomatoNLS*)^{Simon}	(Berg et al., 2010)	tdTomato in nuclei of ependymoglia	Epifluorescence	No
tgTol2(Mmu.*Th:NLStdTomatoNLS*)^{Simon}	(Chan et al., 2017)	tdTomato in nuclei of dopaminergic neurons	Epifluorescence	No
tgTol2(Rno.*TH:GFP*)^{Simon}	(Oh et al., 2009)	GFP in dopaminergic neurons	No	No

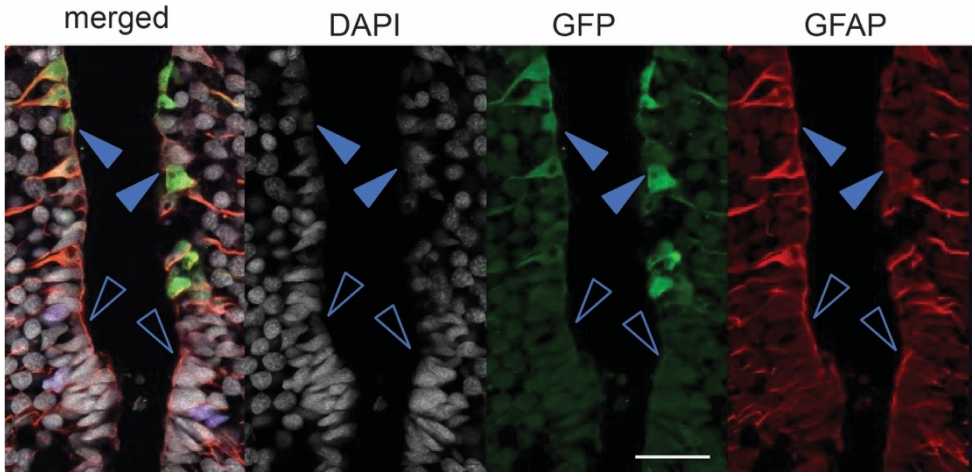

Fig. 8 | Analysis of tgTol2(Hsa.GFAP:GFP)^{Simon} by IHC. The GFP under the control of the human GFAP promoter co-localized with GFAP expression in ependymoglia (filled arrowheads). Some ventricular cells containing GFAP protein did not express GFP (empty arrowheads). Scale bar: 100 µm.

4.1.2.1.2 Tol2-mediated transgenesis and test of the Ert2-Cre-Ert2 system

ER^{T2}-Cre-ER^{T2} is a useful system that allows temporal control of Cre recombinase expression upon tamoxifen administration. In combination with the loxP system, this can be used to trace the progeny of specific cells when recombination results in the expression of a fluorescent tracer (Fei et al., 2017). I designed and cloned a plasmid containing the *ER^{T2}-Cre-ER^{T2}* cassette in order to be able to label the ependymoglia and their progeny in the context of regeneration: I started with the *Col1A2:TFPnls-T2a-ER^{T2}-Cre-ER^{T2}* plasmid (**Fig. 9A;** kindly donated by E.M. Tanaka) (Gerber et al., 2018), in which I replaced the *Col1A2* promoter and the TFP by H2b-EBFP (a sequence to express blue-fluorescent protein in the nucleus and also kindly donated by E.M. Tanaka; **Fig. 9B).** The generated sequence was confirmed by Sanger sequencing (**Fig. 9C**). Next, I added a human GFAP promoter to generate tgTol2(Hsa.*GFAP:h2b-EBFP-T2a-ER^{T2}-Cre-ER^{T2}*)^{Simon} (**Fig. 9D**).

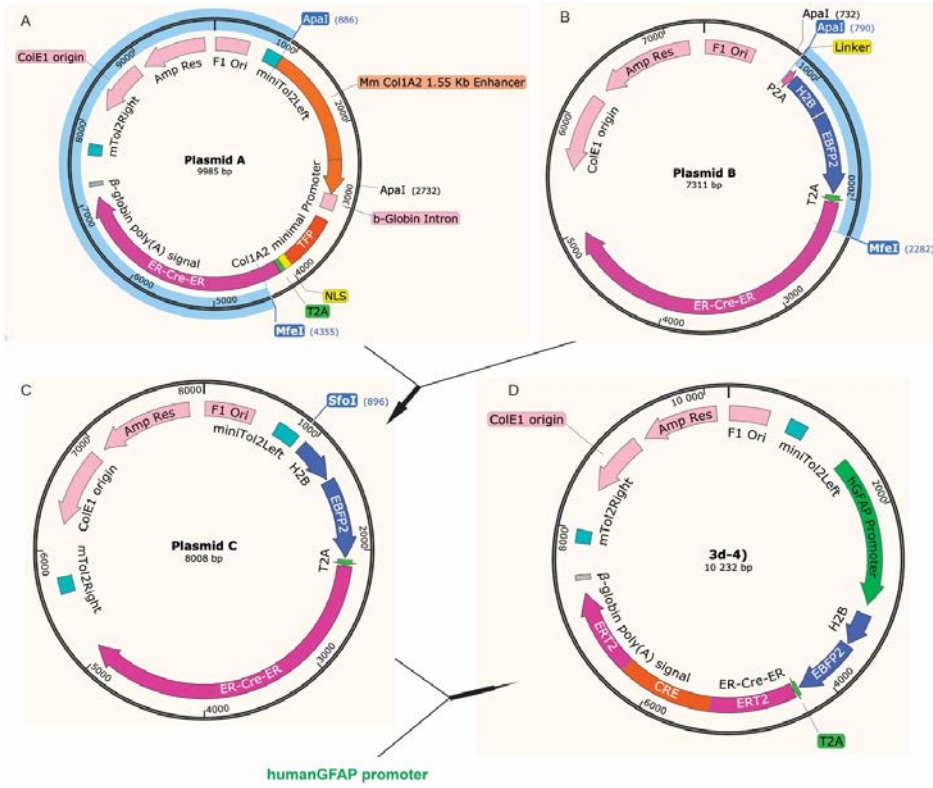

Fig. 9 | Generation of the plasmid for inserting the Ert2CreErt2 system into ependymoglia for Tol2-mediated transgenesis. After integrating the Ert2creErt2 and EBFP from Plasmids **(A)** and **(B)** to generate Plasmid **(C)**, a human GFAP promoter was inserted into Plasmid (C) to generate the plasmid **(D)**, which contained tgTol2(Hsa.GFAP:h2b-EBFP-T2a-ERT2-Cre-ERT2)^{Simon}.

Single-cell fertilized cells were then injected with the Tol2 enzyme plus the plasmid D shown in Fig. 9D. The F_0 animals were screened by epifluorescence (**Fig. 10A**) and genotyped by PCR (**Fig. 10B**). The positive animals were named according to the standardized nomenclature for

transgenic salamanders (Nowoshilow et al., 2022; Yun et al., 2022) as: tgTol2(Has.*Gfap:h2b-EBFP-T2a-ER^{T2}-Cre-ER^{T2}*)^{Simon} ; hereafter I use standard abbreviation with the Simon-lab label for *Pleurodeles waltl* (Pw): (Pw$^{GFAP:\ EBFP\text{-}CreERT2}$). F_0 positive larvae were raised to adulthood and directly bred with other transgenic lines expressing the LoxP system available in our facility (**Fig. 10C**). These were:

- *Pw^{NucCyt}* [tgTol2(*CAG:loxN-lox2272-loxP-H2B:EBFP2-loxN-H2B:mEYFP-lox2272-H2B:mCherry-loxP-H2B:mCeru;CAG:loxN-lox2272-loxP-H2B:EBFP2-loxN-tdTomato-lox2272-H2B:mCeru/mTq2-loxP-mEYFP*)^{Simon}] (Joven et al., 2018)

- *Pw$^{GFP\text{-}loxP\text{-}Cherry}$* [tgSceI(*CAG:loxP-GFP-loxP-Cherry*)^{Simon}] (Joven et al., 2018)

- *Pw$^{Cherry\text{-}loxP\text{-}H2B:YFP}$* [tgTol2(*CAG:loxP-Cherry-loxP-H2B:YFP*)^{Simon}] (Eroglu et al., 2022)

We selected animals that expressed either EBFP or CRE in the tail as well as the fluorescent protein of interest. These were the readouts for germline transmission in the first generation that resulted in expression of the transgenes after the crossing. In the absence of tamoxifen, Cre-LoxP recombination did not occur, as confirmed in the three types of crossings (**Fig. 10D**). Unfortunately, no color change was observed after the tamoxifen treatment, despite several trials of administration (either in water or intraperitoneal injections), in either larvae or adults (**Fig. 10E**). This system test yielding negative results could be caused by several reasons: 1. The integration of the tol2 constructs in the genome is random (Kawakami, 2007). This means that the expression of the transgenes could be inhibited if the integration happens inside a silenced genomic area (Hansen, 2020). 2. To our knowledge, tamoxifen-mediated recombination has never been demonstrated in the newt. Future studies can be done to test further concentrations and administration methods in order to optimize the efficiency of tamoxifen.

4.1.2.2. CRISPR/Cas 9-mediated gene editing

CRISPR/Cas9-mediated genomic modifications have been successfully implemented in recent years but not yet extensively applied because of the preliminary nature of the annotation and assembly of the genome. I designed three gRNAs to target the first exon of Lmx1b, a known dopaminergic determinant (Yan et al., 2011), as well as primers for genotyping (**Fig. 11A**). The most efficient gRNA was gRNA12. The F_0 generation was genotyped and animals carrying mutations in the Lmx1b gene (**Fig. 11B**) were allowed to breed with each other. The offspring was screened by genotyping. Heterozygous F_1:*Lmx1b$^{+/-}$* newts were kept for breeding and the two homozygous F_1:*Lmx1b$^{-/-}$* mutants were euthanized after metamorphosis as they were not growing well. Examination of the mutant brains showed a trend of decrease in the number of TH^+ cells (**Fig. 11C-D**). Currently, the heterozygous F_1:*Lmx1b$^{+/-}$* is maintained in the lab. This result shows that I succeeded generating *Lmx1b* mutant newts and suggests that *Lmx1b* is a key gene for the correct development of dopaminergic neurons in the newt ventral midbrain, like in mammals (Deng et al., 2011; Doucet-Beaupre et al., 2016; Laguna et al., 2015; Yan et al., 2011).

I next tested NHEJ-, MMEJ-, and HMEJ- mediated knock-in of on *Lmx1b* gene in order to be able to visualize the lineage derived from Lmx1b expressing cells in the newt ventral midbrain. To this end, I generated donor plasmids containing *EBFP-T2A-ER^{T2}-Cre-ER^{T2}* combined with gRNAs targeting the first or last exon of Lmx1b. (**Fig. 12**). However, after egg

injections, PCR on the *Lmx1b* cutting site only showed mutations at the site of gRNAs targets; no knock-in were detected for any of the three methods (data not shown). This result is in line with the poor efficiency of CRISPR-directed knock in reported in axolotl (Fei et al., 2018; Fei et al., 2017).

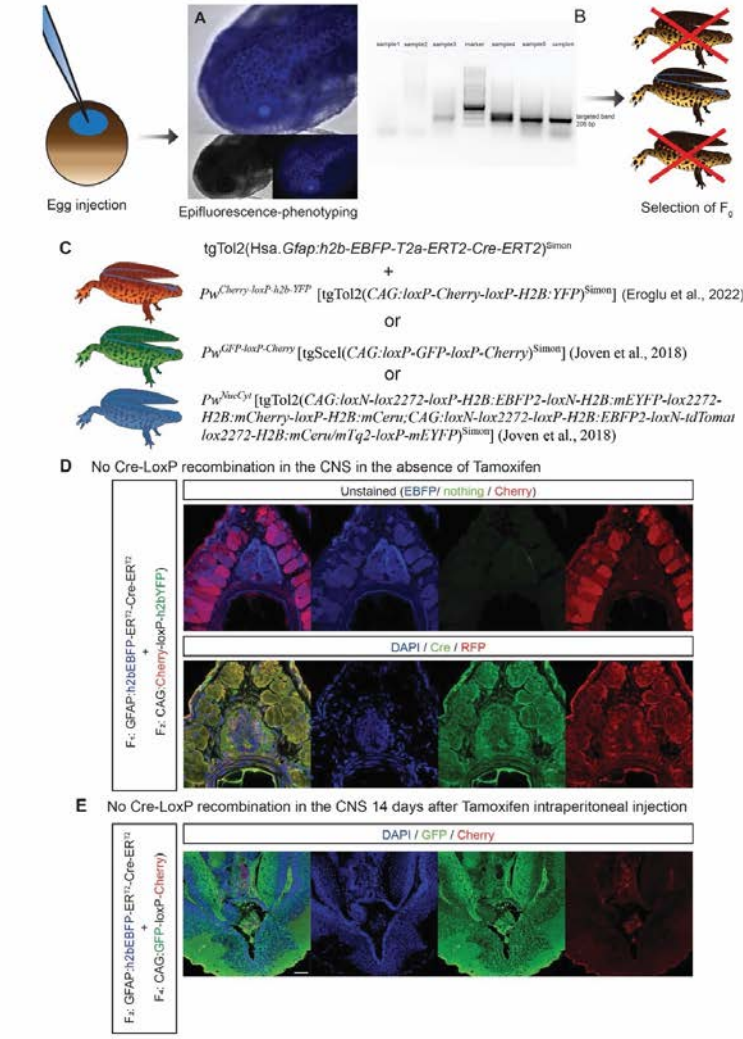

Fig. 10 | Production and testing of the new transgenic line tgTol2(Hsa.*Gfap:h2b-EBFP-T2a-ER^{T2}-Cre-ER^{T2}*)^{Simon}. (A) Screening of the F_0 animals based on phenotype; the larva in the image shows EBFP in the central nervous system (CNS). **(B)** Examples of genotyping by PCR. Both EBFP and Cre were amplified to select the positive F_0s. **(C)** Schematic drawing showing the crossings performed with other lines previously produced in the Simon laboratory in order to test the Cre-LoxP recombination system. **(D)** Example of a tail section used for selection of F_1s obtained by the breeding depicted in (C) using phenotyping by immunohistochemistry. Note that in the absence of tamoxifen, no Cre-LoxP recombination occurs in the animals. **(E)** Example of a brain section where Cre-LoxP recombination was not observed after tamoxifen administration. Despite multiple trials, the *ER^{T2}-Cre-ER^{T2}* system did not work in my hands. Scale bar in (E) is valid for all images: 100µm.

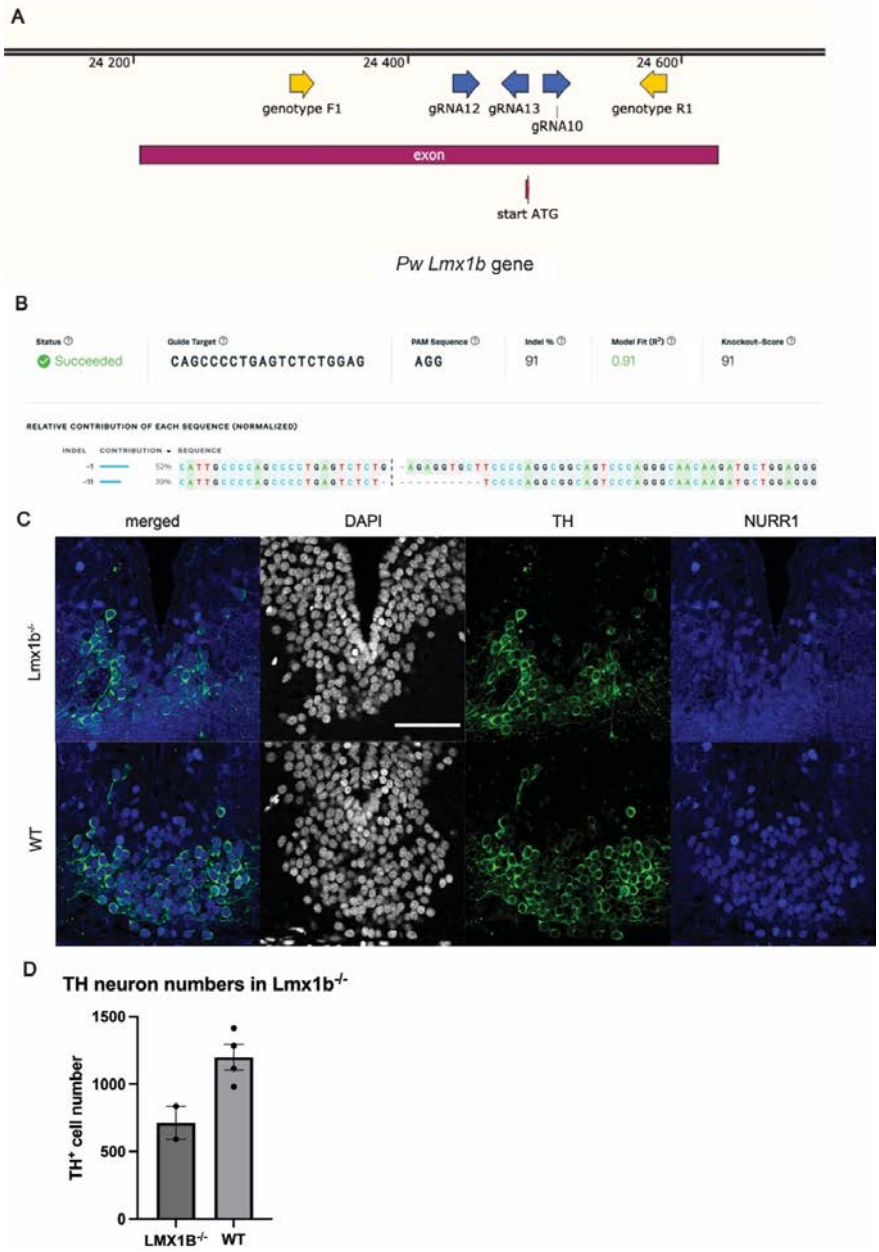

Fig. 11 | Genetic modifications of *Lmx1b* gene in the newt. (A) Genomic location of *Lmx1b* first exon in chromosome 6. Blue arrows represent gRNAs; yellow arrows show primers for genotyping. **(B)** Frameshift mutations detected in a F_1:*Lmx1b*$^{-/-}$ mutant embryo. **(C)** Representative image showing TH staining in ventral midbrains of wildtype (left) and mutant F_1:*Lmx1b*$^{-/-}$ (right). **(D)** The animals shown had similar size and weight, but the F_1:*Lmx1b* mutants showed fewer TH cells. Statistical analysis could not be conducted due to the low number of samples available (only 2 Lmx1b$^{-/-}$ newts), but it shows a trend of decreased TH$^+$ cells in F_1:*Lmx1b*$^{-/-}$. Scale bar: 100 μm.

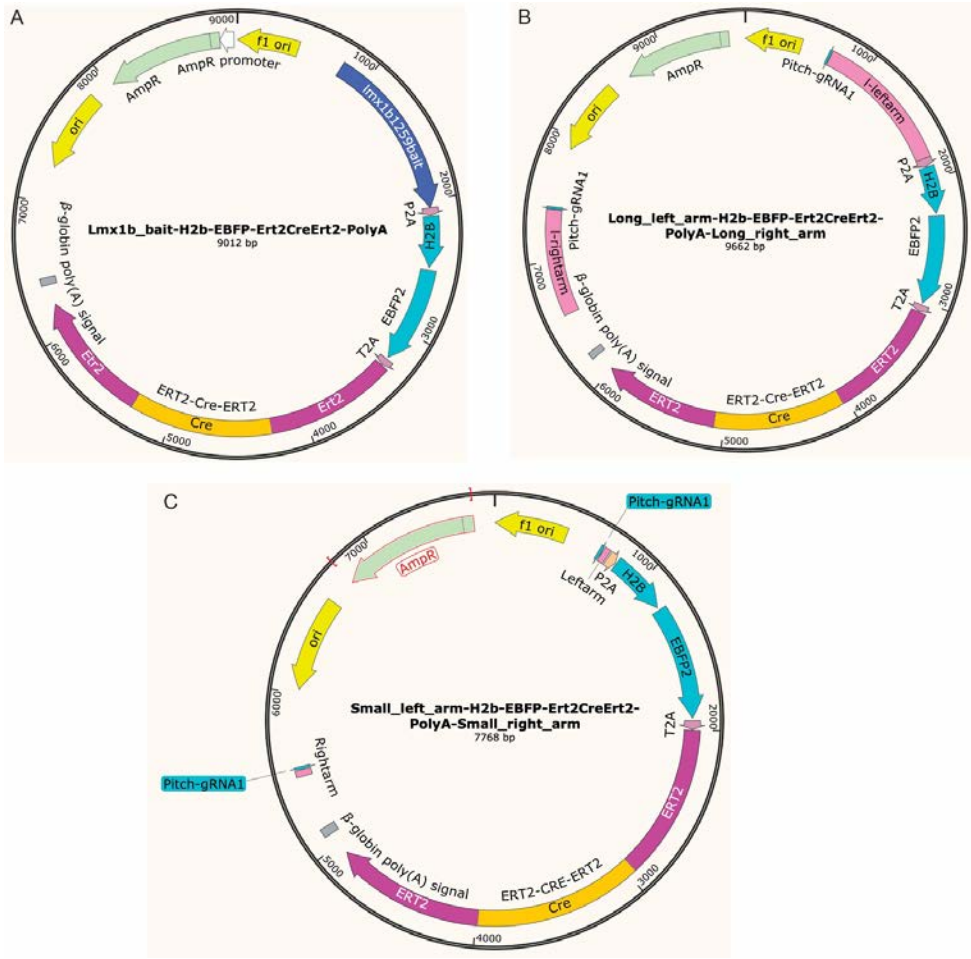

Fig. 12 | Donor plasmids. Used for **(A)** NHEJ-, **(B)** HMEJ-, and **(C)** MMEJ- mediated knockins of "H2b-EBFP-T2A-Ert2CreErt2" at the newt *Lmx1b* gene.

4.1.3. Predicting cross-species antibody reactivities

To be able to visualize different cell types in the ventral midbrain, I screened commercially available antibodies because very few antibodies have been raised specifically against newt proteins. Aiming to improve the process of antibody screening, I used the transcriptomic resources to predict if an antibody might work cross-species based on the degree of sequence homology. I screened commercial antibodies in which the amino acid identity of the antigen was at least 40% (most of them were 60-90%). The cross-reactivity in the newt was accepted if the antibody gave the expected staining pattern as it does in mammals. As an example, the antigen sequence for the commercial antibody "goat anti-human Otx2 antibody (AF1979, R&D/Novus)" was blasted to the predicted newt Otx2 protein sequence, and high antigen identity (90%) was detected (**Fig. 13A**). Subsequently, I performed IHC and, based on the expected staining (in this case I used TH to confirm anatomical location and catecholaminergic

identity), this antibody was categorized to be effective in the newt brain (**Fig. 13B-E**). In this way, I first predicted cross-reactivity and then performed IHC in newt brain tissue for a large number of antibodies. Positive control tests for the antibodies in the species they were raised against for were not performed because the antibodies may require modified staining conditions in the newt (**Table. 3**). I observed that the highest identities did not sufficiently ensure the efficiency of the antibodies tested (using the T-test between percentages of antibodies that showed cross-reactivity versus those that did not, p=0.3773). In several cases, I observed cross-reactivity despite a low degree of homology; this result indicates that the tridimensional protein structure might be more relevant than the actual amino acid sequence conservation to predict cross-species reactivity of antibodies.

Table. 3. Antibodies tested by IHC after predicting identities of their antigens to the newt protein orthologues.

Antibody	Catalog number and Producer	Expected labeling	Identity with the antigen (%)	Cross-reactivity
Human Otx2 Antibody	AF1979, R&D/Novus	neural stem/ progenitor cell, neuron	95	Yes
Anti-Otx1 + Otx2 antibody	Ab21990, Abcam	neural stem/ progenitor cell, neuron	93	Yes
OTX2 Recombinant Rabbit Monoclonal Antibody (14H14L5)	701948, Thermo Fisher Scientific	neural stem/ progenitor cell, neruon	75	No
Anti-SOX2 antibody	ab97959, Abcam	neural stem/ progenitor cell, neruon	Not known; the antigen sequence is proprietary	Yes
AIF-1/Iba1 Antibody	NB100-1028, R&D/Novus	microglia/macrophage	75	Yes
Anti Iba1, Rabbit	019-19741, Wako	microglia/macrophage	75	Yes
Tyrosine Hydroxylase Antibody	NB300-110, R&D/Novus	dopaminergic neuron	87	Yes
Tyrosine Hydroxylase Antibody	NB300-109, R&D/Novus	dopaminergic neuron	74	Yes
Anti-Tyrosine Hydroxylase Antibody, clone LNC1	MAB318, MERCK	dopaminergic neuron	69	Yes
Anti-Tyrosine Hydroxylase Antibody	AB152, MERCK	dopaminergic neuron	74	Yes
GFAP Antibody	NBP1-05198, R&D/Novus	neural stem cell	84	Yes
Anti-GFAP−Cy3™ antibody, Mouse monoclonal	C9205, MERCK	neural stem cell	86	Yes
Anti-Vimentin Antibody	AB5733, MERCK	neural stem cell	78	Yes

Antibody	Catalog number and Producer	Expected labeling	Identity with the antigen (%)	Cross-reactivity
Human/Mouse/Rat Vimentin Alexa Fluor® 647-conjugated Antibody	IC2105R, R&D/Novus	neural stem cell	78	Yes
SOX6 Polyclonal Antibody	PA5-34616, Thermo Fisher Scientific	dopaminergic neuron, neural progenitor	86	No
SOX6 Antibody	NBP1-86149, R&D/Novus	dopaminergic neuron, neural progenitor	78	Yes
Human/Mouse Nurr1/NGFI-B beta /NR4A2 Antibody	AF2156, R&D/Novus		98	Yes
Nurr1/Nur77 Antibody (E-20)	sc-990, Santa Cruz	neural progenitor, neuron	100	No
Nurr1 Polyclonal Antibody	PA5-22830, Thermo Fisher Scientific	neural progenitor, neuron	100	No
GPR37-3	#GPR37-3, MABTechnologies	oligodendrocyte	94	No
Human GPR37 Antibody	MAB44502, R&D/Novus	oligodendrocyte	74	No
Human/Mouse Aldehyde Dehydrogenase 1-A1/ ALDH1A1 Antibody	AF5869-SP, R&D/Novus	dopaminergic neuron	78	No
Anti-ALDH1A1 antibody	ab9883, Abcam	dopaminergic neuron	79	No
Anti-LMX1b antibody	ab129306, Abcam	dopaminergic neuron, neural progenitor	86	No
LMX1B Polyclonal Antibody	PA5-34471, Thermo Fisher Scientific	dopaminergic neuron, neural progenitor	92	No
LMX1A Polyclonal Antibody	PA5-34470, Thermo Fisher Scientific	dopaminergic neuron, neural progenitor	65	No
c-Fos (E-8) Antibody	sc-166940, Santa Cruz	neural stem/progenitor cell, microglia/macrophage	96	Yes
Calbindin D-28k	300, Swant	neurons	83	Yes
Calretinin	7697, Swant	neurons	84	Yes
NFIA Antibody	PCRP-NFIA-2C6, DSHB	neural stem/ progenitor cell, neuron	97	Yes
Monoclonal Anti-NFIX antibody produced in mouse	SAB1401263, MERCK	neural stem/ progenitor cell, neuron	93	Yes
PTBP1 Rabbit pAb	A6107, Abclonal	neural progenitor cell	83	Yes
Human HNF-3 beta /FoxA2 Antibody	AF2400, R&D/Novus	neural stem/ progenitor cell, neuron	64	No
FOXA2 Polyclonal Antibody	PA518169, Thermo Fisher Scientific	neural stem/ progenitor cell, neuron	100	No

Antibody	Catalog number and Producer	Expected labeling	Identity with the antigen (%)	Cross-reactivity
FOXA2 Antibody	PCRP-FOXA2-3A2, DSHB	neural stem/ progenitor cell, neuron	86	No
HNF-3β Antibody (M-20)	sc-6554, Santa Cruz	neural stem/ progenitor cell, neuron	83	Yes
Human/Mouse/Rat MBP Antibody	MAB42282, R&D/Novus	oligodendrocyte	60	No
MBP Antibody (12)	NB600-717, R&D/Novus	oligodendrocyte	86	Yes
MOG Antibody (CL2858)	NBP2-46634, R&D/Novus	oligodendrocyte	45	No
Human/Mouse/Rat Olig2 Antibody	AF2418, R&D/Novus	oligodendrocyte precursor cell, oligodendrocyte	65	No
Human/Rat SOX10 Antibody	MAB2864, R&D/Novus	oligodendrocyte, schwann cell	69	No
Human SOX10 Antibody	AF2864, R&D/Novus	oligodendrocyte, Schwann cell	70	Yes
FoxO1/FKHR Antibody (83N7F8) - BSA Free	NBP2-31376, R&D/Novus	microglia/ macrophage	68	No
Human EGR1 Antibody	MAB2818, R&D/Novus	microglia/ macrophage	95	No
Stat1 (D1K9Y) Rabbit mAb	14994, Cell Signaling Technology	microglia/ macrophage	83	No
Human LYPD1 Antibody	AF6855, R&D/Novus	dopaminergic neuron	84	No
VIP Antibody (576721)	MAB6079, R&D/Novus	dopaminergic neuron	100	No
Mouse/Rat Wnt-5a Antibody	AF645, R&D/Novus	neural stem/ progenitor cell	91	No

A

```
Score:508 bits(1307), Expect:0.0,
Method:Compositional matrix adjust.,
Identities:261/289(90%), Positives:276/289(95%), Gaps:0/289(0%)

Query  1    MMSYLKQPPYAVNGLSLTTSGMDLLHPSVGYPATPRKQRRERTTFTRAQLDVLEALFAKT  60
            MMSYLKQPPY VNGLSLT+SGMDLLHPSVGYPATPRKQRRERTTFTRAQLDVLEALFAKT
Sbjct  1    MMSYLKQPPYTVNGLSLTSSGMDLLHPSVGYPATPRKQRRERTTFTRAQLDVLEALFAKT  60

Query  61   RYPDIFMREEVALKINLPESRVQVWFKNRRAKCRQQQQQQQNGGQNKVRPAKKKTSPARE  120
            RYPDIFMREEVALKINLPESRVQVWFKNRRAKCRQQQQQQQ+GGQ+K RPAKKK SP RE
Sbjct  61   RYPDIFMREEVALKINLPESRVQVWFKNRRAKCRQQQQQQQQSGGQSKTRPAKKKNSPGRE  120

Query  121  VSSESGTSGQFTPPSSTSVPTIASSSAPVSIWSPASISPLSDPLSTSSSCMQRSYPMTYT  180
            VSSESG SGQFTPP +T+VPTI+S+SAPVSIWSPASISPLSDPLSTSSSCMQRSYPMTY+
Sbjct  121  VSSESGASGQFTPPPTTAVPTISSTSAPVSIWSPASISPLSDPLSTSSSCMQRSYPMTYS  180

Query  181  QASGYSQGYAGSTSYFGGMDCGSYLTPMHHQLPGPGATLSPMGTNAVTSHLNQSPASLST  240
            QA  Y+QGY+GS+SYFGGMDCGSYL+PMHHQL G GATLSPMGTN V+SHL+QSPASLST
Sbjct  181  QAPAYTQGYSGSSSYFGGMDCGSYLSPMHHQLTGAGATLSPMGTNGVSSHLSQSPASLST  240

Query  241  QGYGASSLGFNSTTDCLDYKDQTASWKLNFNADCLDYKDQTSSWKFQVL  289
            QGYGASSLGFN+TTDCLDYKDQ  SWKLNFNADCLDYKDQTSSWKFQVL
Sbjct  241  QGYGASSLGFNTTTDCLDYKDQATSWKLNFNADCLDYKDQTSSWKFQVL  289
```

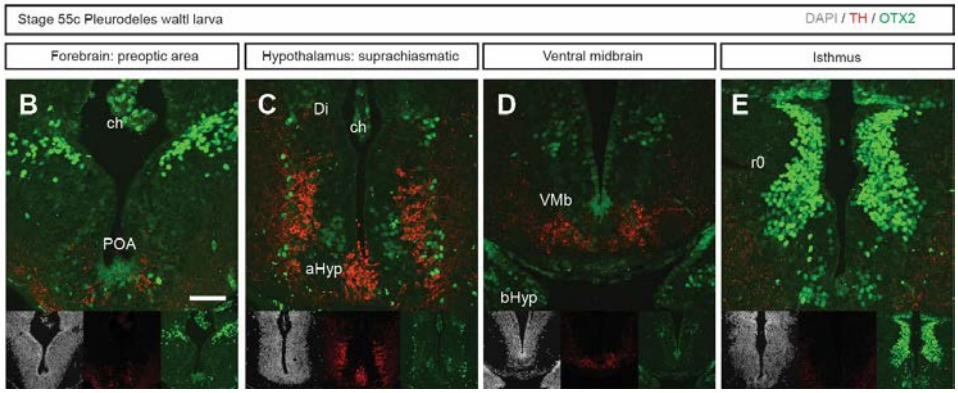

Fig. 13 | Screening and testing of OTX2 antibody for the newts. (**A).** Blast results comparing the sequence of the antigen of goat anti-human Otx2 antibody (AF1979, R&D/Novus) and the newt Otx2 orthologue. **(B-E).** IHC with goat anti-human Otx2 antibody (AF1979, R&D/Novus, shown in green) labeled brain regions including telencephalon (B), choroid plexus ("ch" in B), hypothalamus (C), diencephalon, mIcephalon (D) and isthmus (E), in agreement with previous literature in other vertebrates (Hoch et al., 2015; Larsen et al., 2010; Puelles et al., 2006; Puelles et al., 2004). All fluorescent microscopy images were taken with the same settings to depict the different intensities found in each brain region. TH staining (red) is shown to facilitate the anatomical interpretation. Abbreviations: aHyp: alar hypothalamus; bHyp: basal hypothalamus; ch:choroid plexus; Di: diencephalon; POA: preoptic area; r0: isthmus; VMb: ventral midbrain. Scale bar in (B) is valid for all images: 100μm.

4.1.4. Designing RNA probes for single and multiplexed mRNA detection

An alternative method to immunohistochemical analyses to detect gene expression is *in situ* hybridization (ISH) that detects mRNA in the tissue. ISH methods have been significantly developed the past years by the RNAscope technology that allows for detection of multiple

mRNAs in the same section (Wang et al., 2012). I made use of all available transcriptomes for newts to identify mRNAs of genes with relevance for defining cell types as well as their functions. **Supplementary Table. 3** lists the genes I generated probes for by blasting the target mRNA orthologues of other species against the available transcriptomes data sets (Brown et al., 2022; Elewa et al., 2017; Matsunami et al., 2019). ISH showed variable success. *GFAP* mRNA was detected in the ependymoglial cell layer, as expected (**Fig. 14A-B**). ISH for *Lmx1b* showed strong expression in the ventral midbrain, in the area where the TH^{+} neurons are located (**Fig. 14C-D**). This results probe that the genomic and transcriptomic resources of *Pleurodeles waltl* can be used to design probes that can be used to visualize gene expression patterns in the tissue.

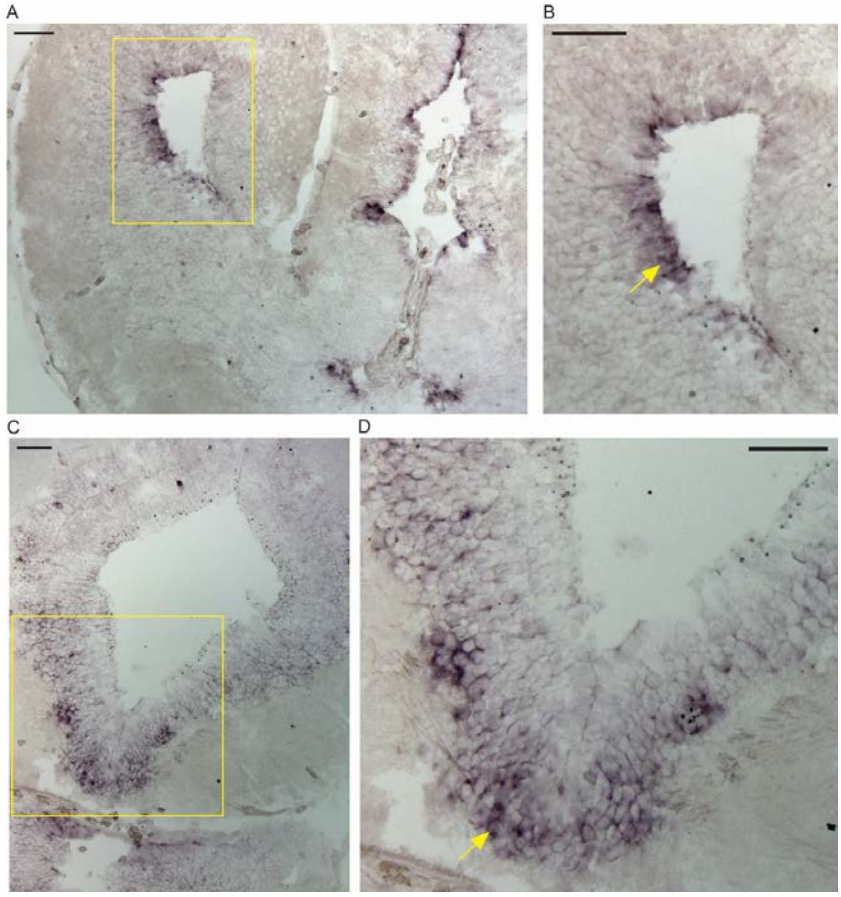

Fig. 14 | *In situ* hybridization by digoxigenin-labelled probes in the newt brain. (**A)-(B)** Representative image of a forebrain section (late active larval stage) showing expression of *Gfap* in the ventricular zone (arrows). **(C)-(D)** Representative image of a midbrain section (late active larval stage) showing expression of *Lmx1b* in the mantle zone of the ventral midbrain (arrows). Scale bar: 100 µm.

4.2. Defining cell populations in the development of *Pleurodeles waltl* ventral midbrain

At the start of this project, previous studies had defined a limited number of cell types in the newt midbrain. To understand the molecular and cellular underpinnings of neurogenesis and regeneration, a detailed map of the cell population is required. This knowledge is a prerequisite to study the complex interplay likely to govern the injury response that leads to functional regeneration. It is also important to determine heterogeneity among known cell types and define them in molecular terms. Likewise, it is important to characterize the events in the newt brain and to carry out cross-species comparisons with non-regenerative species. These comparisons could highlight cellular and molecular components that allow or disallow successful regeneration to occur.

A particular feature of the newt brain is that it retains the radial glial cell-like ependymoglial cells throughout its lifetime. This could mean the newt brain remains in a more immature state compared to mammals, which gradually lose radial glial cells in most parts of the brain during ontogeny. Hence, I had two major aims in this project: first, to determine the cellular composition of the newt brain, and second, to compare the cellular diversity in larval, adult, and aged newts. To do that, I generated and analyzed single-cell and single-nucleus RNA sequencing datasets (scRNAseq and snRNAseq). *In silico*-defined cell clusters based on molecular profiles were validated by IHC, with a special focus on the dopaminergic development.

4.2.1. Adaptation and comparison of dissociation protocols for scRNAseq and snRNAseq in ventral midbrain of the newt

When this project started, neither scRNAseq nor snRNAseq studies had been conducted in the newt CNS. Methods needed to be generated for tissue dissociation, cell and nuclei purification, and for single-cell or single-nucleus library preparation. To overcome this, I first adapted cell dissociation methods for rodent brains, then tested them on newt brain tissues (Tiklova et al., 2019). Ventral midbrains (from either larval stage 54 newts or young adults) were freshly dissected out on ice (**Fig. 15A**), pooled and homogenized by gentle pipetting in dissociation media. I tested tissue dissociation using three different methods: papain dissociation for 30-60 min at 27 °C, collagenase/dispase for 30-60 min at 27 °C, and a protease from *Bacillus licheniformis* for 30-60 min at 4 °C. I first compared papain versus collagenase/dispase and found that the enzymes did not make a difference in cell viability (**Fig. 15B**). The recovered live cells of both methods ranged between 300 to 4000 cells per ventral midbrain. I successfully optimized FACS-sorting for newt cells, which are much bigger than the mammalian ones. Subsequently, protease from *Bacillus licheniformis* was tested and found that this enzyme recovered many more live cells (35094 cells from 3 ventral midbrains at st56) compared to the previous two methods (**Fig. 15C**), hence this protocol was used for further experiments. RNAlibrary preparations and sequencing were conducted by the ESCG facility at SciLifeLab (Stockholm).

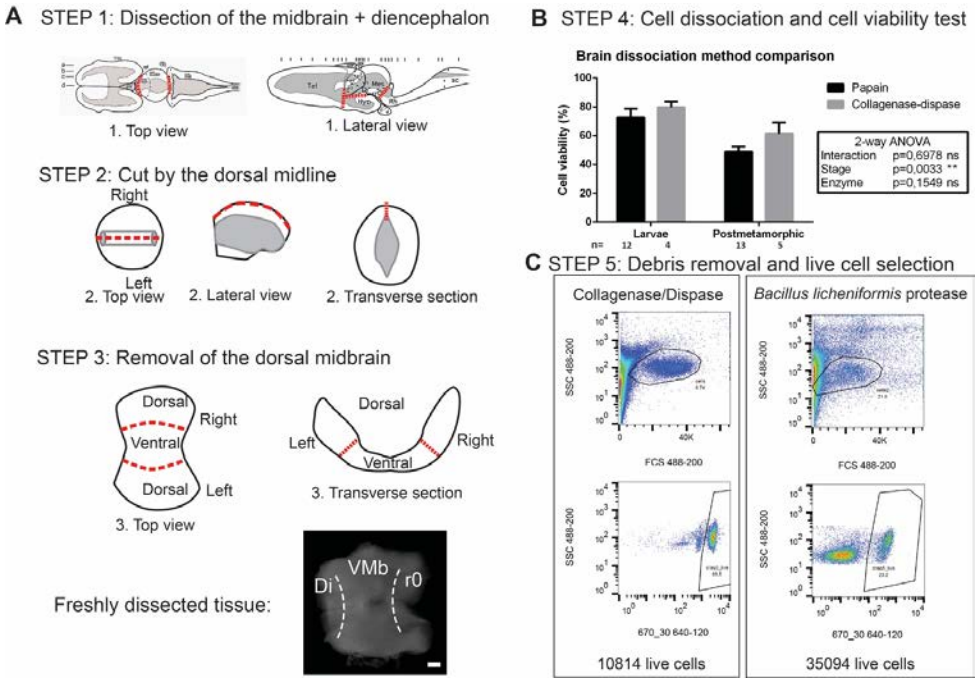

Fig. 15 | Workflow to obtain single cell suspensions for scRNAseq. (A) Step-by-step depictions of the ventral midbrain dissection process. Red dashed lines indicate from where the tissue was excised. On the bottom, a representative image of a freshly dissected ventral midbrain is shown. Di=diencephalon, r0=isthmus, VMb=ventral midbrain. White dashed lines indicate the border between brain segments. Scale bar: 200µm. The brain schematic drawings in the top of (A) are from (Joven et al., 2013a). **(B)** Comparison of two protocols using different enzymes did not show statistically significant differences in cell viability. Cell viability was found to be higher in larvae compared with adults. 2-way ANOVA was used. The numbers of samples analyzed are labelled under the histogram, each sample consisted of 2-5 pooled ventral midbrains. **(C)** The cell suspensions were purified by FACS to select for live cells and discard dead cells and cellular debris. Note that the Bacillus licheniformis protease yielded more live cells that the collagenase/dispase method. Each sample consisted of 3 ventral midbrains of the same batch of newts at st56.

Unfortunately, the number of cells recovered in the sequencing was still very low. In our first attempts, only 3756 single cells passed the quality control (QC) using six larval VMb from one trial plus 11 young adult VMb from a second trial (see **Supplementary Table. 5**). I decided to try an alternative, so I adapted a method of single nuclei dissociation to newt brain tissues which had yielded good results in rodent brains (Salmani et al., 2023). The four main differences with the previous single-cell dissociation method were: the tissue was not fresh but snap-frozen, all procedures were performed in ice, RNase inhibitor was incorporated, and the dissociation in lysis buffer was mechanical not enzymatic. Newt ventral midbrains of larvae (n= 15 VMb from two trials), young adults (n= 7 VMb from two trials), and old adults (n= 3 VMb from one trial) were dissociated and purified by FACS (**Supplementary Table. 5**). The suspended nuclei were selected by FACS using the far-red dye 7AAD. Next, the single-cell libraries were prepared using the Chromium Next GEM Single Cell 3' Reagent Kits v3.1 (Dual Index), which were

sequenced at National Genomics Infrastructure (NGI, Stockholm) to achieve 25000-50000 reads per singlet for each of the samples. The reads of scRNAseq and snRNAseq were mapped to the new newt genome. After QC filtering and doublet removal, 3756 single-cell transcriptomes and 25,429 single-nucleus transcriptomes were obtained, indicating an improvement of the snRNAseq protocol over the scRNAseq one. Nevertheless, when comparing scRNAseq with snRNAseq, I found that scRNAseq detected more transcripts per event for both larvae and adults (**Fig. 16**). Unsupervised clustering of the datasets separately showed more clusters in the nucleus dataset, probably due to the higher number of events (**Sup. Fig. S2**). This indicates that despite of fewer transcripts being detected per event using the snRNAseq protocol, higher numbers of events can be recovered and the genes detected are sufficient to illustrate cell diversity, making it better than using the scRNAseq protocol. In conclusion, I favored the single-nucleus dissociation method, which gave many more events than the single-cell one.

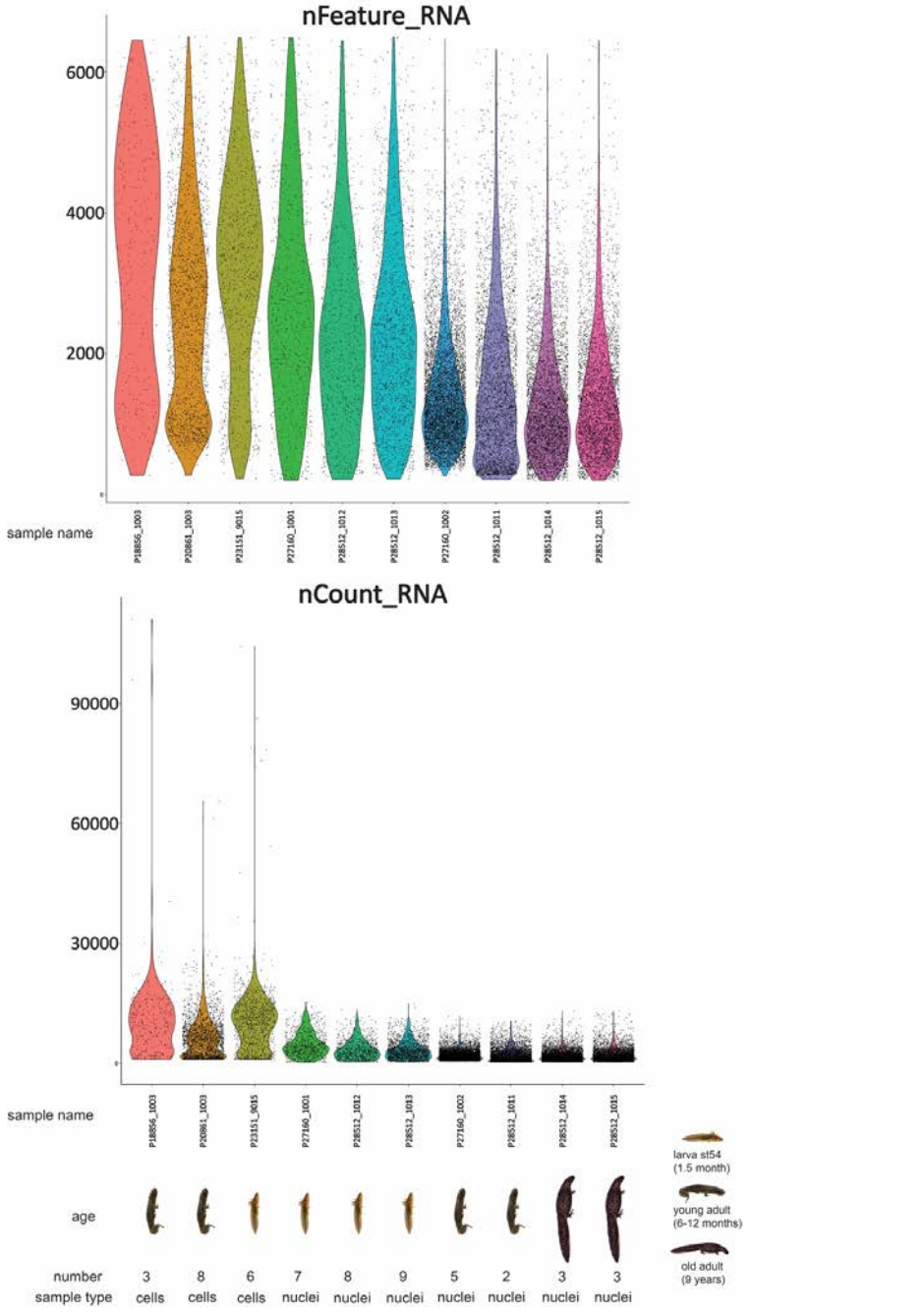

Fig. 16 | Quality control (QC) of each sample. Violin plots showing the number of genes (nFeatures_RNA) or transcripts (nCounts_RNA) per cell or nucleus (black dots). See **Supplementary Table. 5** for details on the samples shown.

4.2.2. Cell type diversity of the newt ventral midbrain in homeostasis

To get an overview of the cell type diversity of the newt ventral midbrain, I merged the scRNAseq and the snRNAseq datasets. Unsupervised Louvain clustering of the combined data classified 29,185 events in 11 to 38 clusters (**Fig. 17A**). The integrated events were distributed in all the clusters within the UMAP space on both sample type (cell/nucleus) (**Fig. 17B, C**) and stage (larva, young adult, and old adult) (**Fig. 17D-F**). Thus, neither the method nor the stage had a strong bias towards specific cell types.

I then computed the differential expression of genes at different levels of resolution and obtained the lists of genes that define each cluster. Based on the expression of the newt orthologues of conserved genes (La Manno et al., 2016; Linnarsson, 2023; Lust et al., 2022; UniProt, 2023; Woych et al., 2022) (**Fig. 18A)**, I selected the clustering resolution CCA_snn_res.1.5 that best explained the cell diversity (including some degree of heterogeneity of major cell types) and assigned cell identities to clusters. Twelve major cell populations were identified, including: neural stem/progenitor cells, microglia/macrophages, oligodendrocytes, oligodendrocyte precursor cells (OPCs), meningeal fibroblasts, erythrocytes, intermediate progenitor cells/immature neurons, and five types of differentiated neurons (including dopaminergic, serotonergic, cholinergic, GABAergic and glutamatergic neuronal subtypes) (**Fig. 18B-C**).

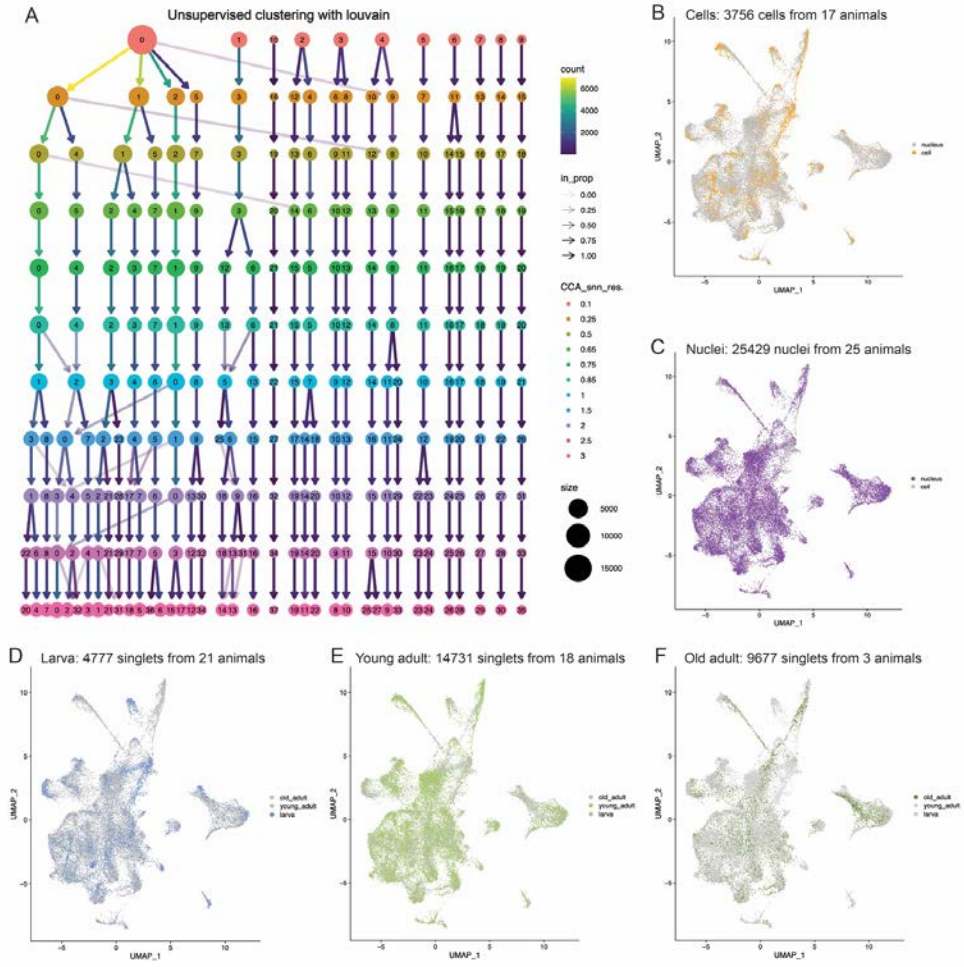

Fig. 17 | Integration of scRNAseq/snRNAseq dataset. (A) Hierarchical tree indicating the levels (CCA_snn_res.) obtained after unsupervised clustering by Louvain of the scRNAseq/snRNAseq combined dataset. UMAP showing the distribution of events, in the combined dataset, coming from scRNAseq **(B)**, snRNAseq **(C)**, larvae **(D)**, young adults **(E)**, and old adults **(F)**.

In brief, I detected all the expected major cell types that have been described in the mouse ventral midbrain (Linnarsson, 2023), which means a high degree of conservation of all major cell types between *Pleurodeles waltl* and other vertebrates including mammals, as previously described (Joven and Simon, 2018). The cell categories and their subtypes are explained in detail in the following subheadings.

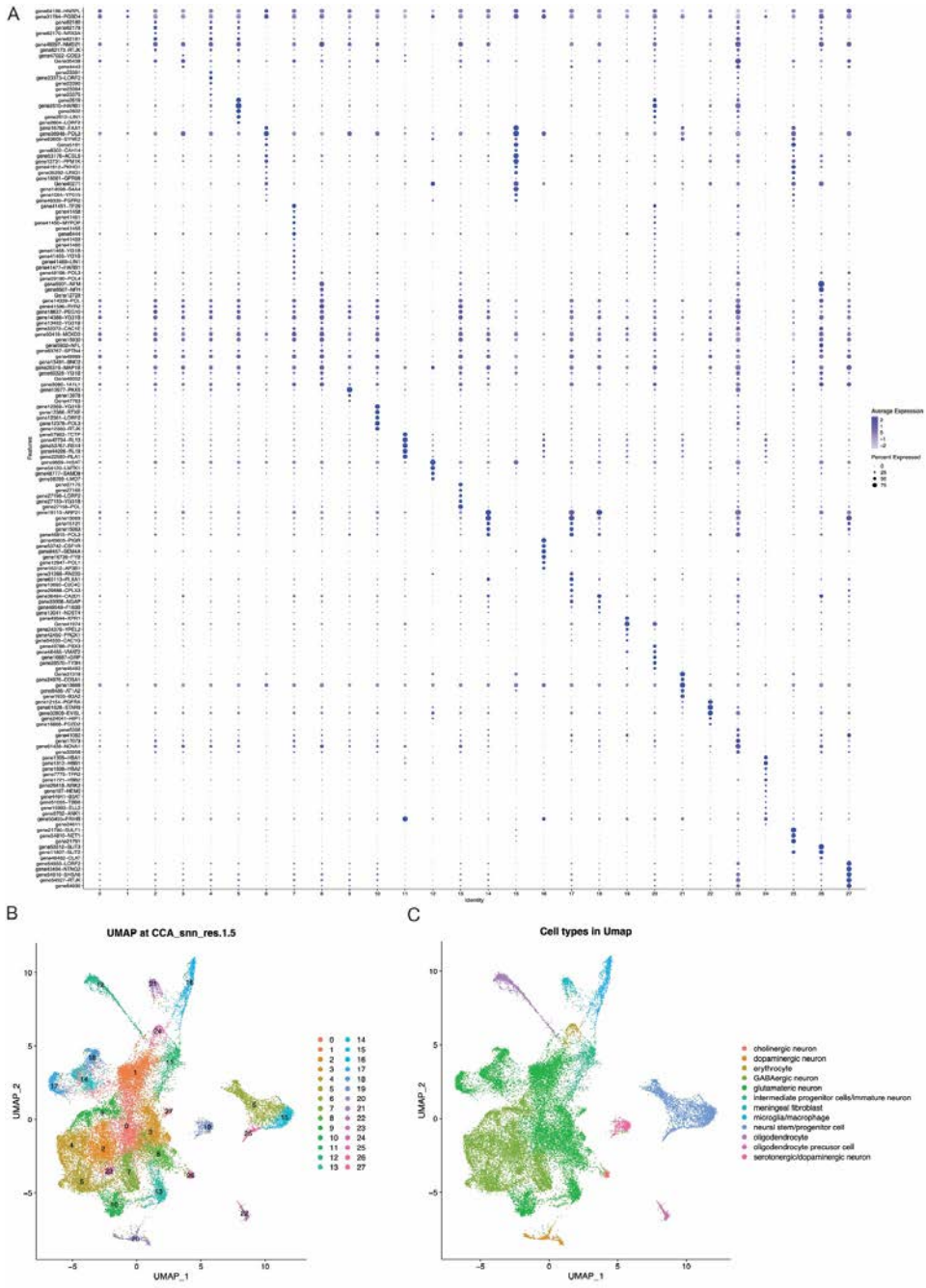

Fig. 18 | Integrated UMAP with cell types identified. (**A)** Dot-plot showing the top expressed genes in each cluster of the scRNAseq+snRNAseq combined dataset. **(B)** UMAP of 29185 singlets at CCA_snn_res.1.5. classified the data set in 28 clusters. **(C)** Cell type manual curation based on key conserved markers grouped the clusters into 12 main categories.

4.2.2.1. Neural stem/progenitor cells (ependymoglia)

Cluster 6 shared top expressed genes with clusters 15 and 25 at the selected CCA_snn_res.1.5. **(Fig. 19A**), so they were scrutinized together. Among the top expressed genes, *gene49443-Glna, gene4266-Sox2,* indicated that these cells could represent ependymoglia, the neural stem/progenitor cell population in the newt (Joven and Simon, 2018; Joven et al., 2018; Kirkham et al., 2014). In line with previous studies (reviewed in (Joven and Simon, 2018)), the proliferation marker *gene47101-Ki67* was higher in cluster 6 and 25 than cluster 15 **(Fig. 19G)**, while *gene49443-Glna* showed a opposite expression pattern **(Fig. 19C)**. This observation suggests that cluster 15 may contain low-proliferative (quiescent) type-1 ependymoglia, while clusters 6 and 25 likely probably harbor highly-proliferative (active) type-2 ependymoglia. Other genes found in these three clusters included genes that have been previously described as markers of neural progenitors in other species (Linnarsson, 2023): *gene31687-Nfia, gene16792-Eaa1* (orthologue of human astrocytic marker SLC1A3/GLAST), and *gene32540-Nfix* (**Fig. 19B-F**). I used the markers *gene49795-Lmx1b, gene11807-Slit2, gene16061-Gpr98* and *gene21790-Sulf1* (Linnarsson, 2023) to tentatively identify cluster 25 as the dopaminergic progenitor ependymoglia. It is known that the dopaminergic neurons that arise from ependymoglial cells after 6-OHDA lesion (Berg et al., 2010). However, whether, dopaminergic neurons come from a restricted subpopulation of progenitors, like in mammals (Andersson et al., 2006; Yan et al., 2011), has not been described. My data show that there are at least three transcriptionally distinguishable subtypes of ependymoglia, one of them resembling the mammalian dopaminergic progenitors. To visualize the spatial location of these three clusters in the tissue, I performed IHC for some of the markers mentioned above. SOX2, GS and NFIA were detected to visualize this population **(Fig. 20**).

4.2.2.2. Oligodendrocyte precursor cells

Oligodendrocyte precursor cells (OPCs) are a cell type indispensable to regenerate mature oligodendrocytes, the myelin producing cells (Chamberlain et al., 2016). They are a cell population difficult to detect by traditional techniques in newts and, to our knowledge, only described for the first time in the *Pleurodeles* forebrain using scRNAseq (Woych et al., 2022). I identified this population in our new dataset (cluster 22) using newt orthologues of the mammalian markers (Miron et al., 2011): *gene12154-Pgfra, gene29841-Cspg4* (mammalian Ng2), the proteoglycan *gene16130-Cspg2, gene60537-Olig1, gene60536-Olig2, gene16868-Pdzd2,* and *gene29924-Otu7a* **(Fig. 21A-G, O)**. I found genes that were expressed in both OPCs and ependymoglial cells, such as *gene44685-Gfap*, *gene21783-Prex2* and *gene36616-Sox5* **(Fig. 21H-J, L-N)**. Interestingly, this gene combination is unique to one cluster in the developing mouse brain. However, it does not correspond to OPCs in mouse, but to dorsal forebrain radial glia (Linnarsson, 2023). In the adolescent mouse, *GFAP*, *Prex2* and *Sox5* are co-expressed in midbrain astrocyte clusters, but not in OPCs or oligodendrocytes (Linnarsson, 2023). This suggests that the newt OPC cell cluster described herein may contain a subset of the mammalian astrocyte counterpart. On another note, some unannotated newt genes were found highly expressed in the population, for example, *gene8919* **(Fig. 21K)**. More research on these transcripts and their genomic location are needed to clarify the relevance and potential novelty of these unannotated genes. I tried to visualize this subpopulation in the tissue using Olig2 IHC, but unfortunately this antibody did not work in newt tissue (see **Table. 3**).

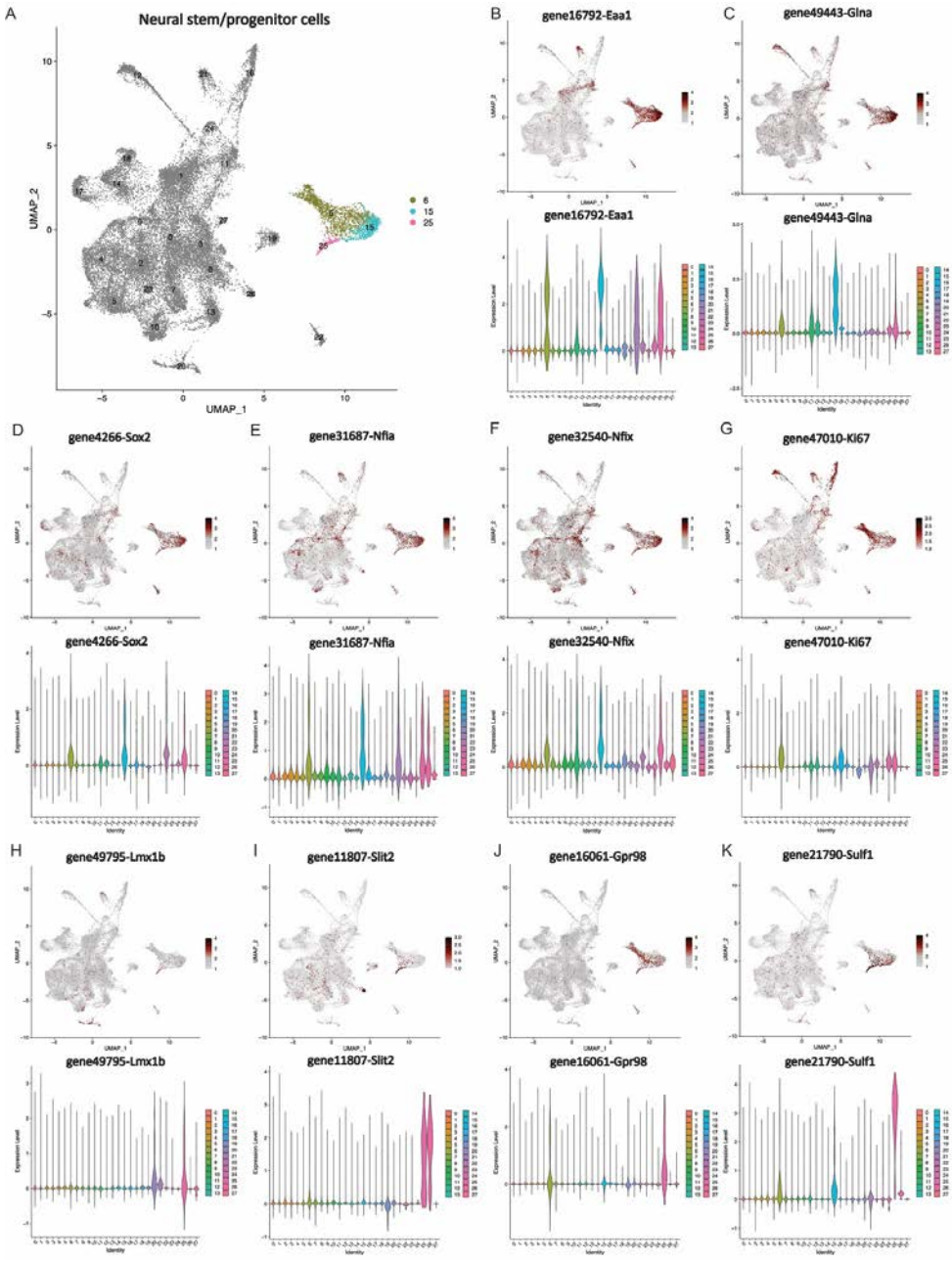

Fig. 19 | The neural stem/progenitor cell (ependymoglia) clusters and selected markers. (A) The ependymoglial cell population was characterized as clusters 6, 15 and 25 in the UMAP at CCA_snn_res.1.5. **(B)-(K)** Top expressed genes in the three clusters of ependymoglia suggest that cluster 25 may represent the dopaminergic progenitor one.

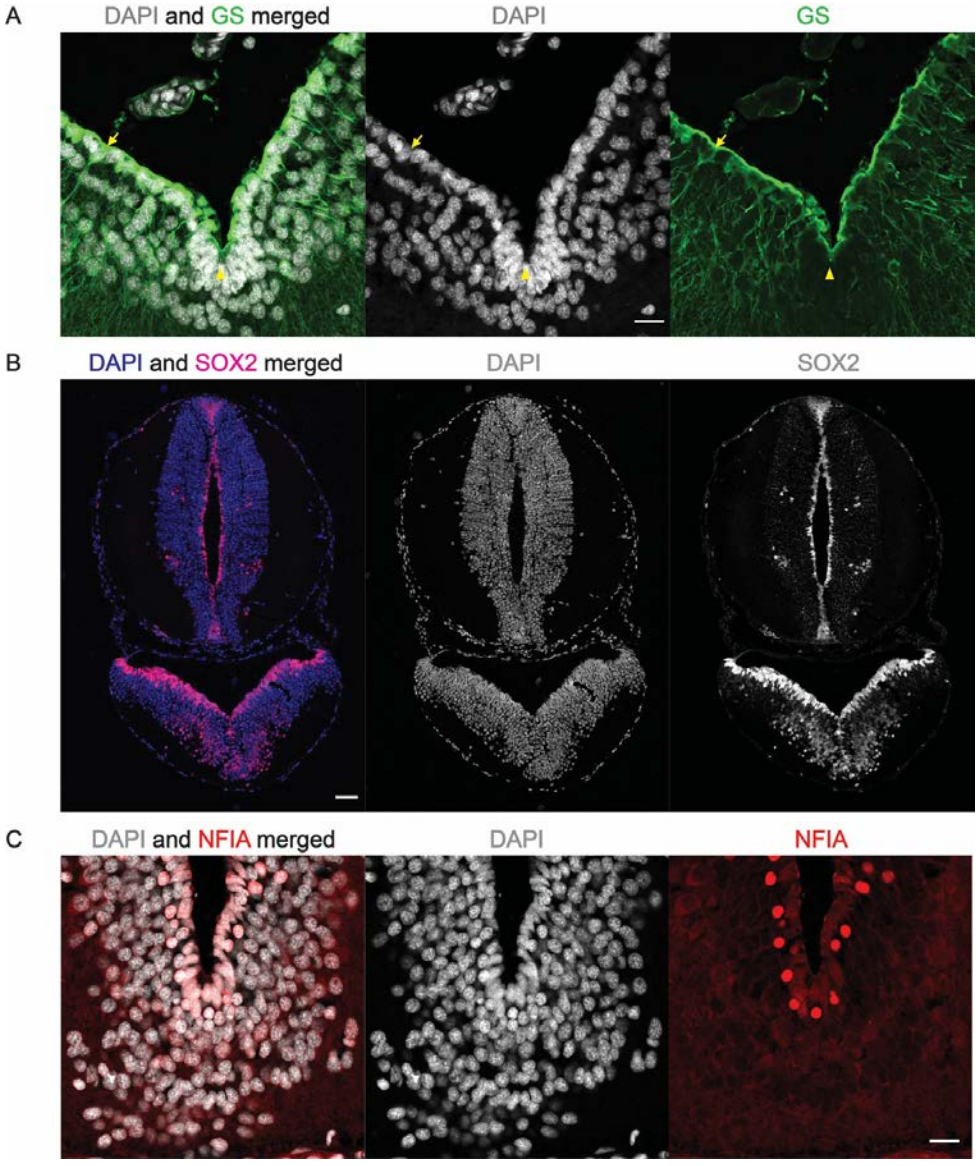

Fig. 20 | IHC in the newt midbrain to detect stem/progenitor cells. (A). GS staining in adult newt. Arrows point to type-1 ependymoglia **(**GS^+), and arrowheads point to type-2 ependymoglia (GS^-). **(B).** SOX2 staining in larva (Conducted by Dr. Laura Lahti). **(C).** NFIA staining in adult newt. Scale bar**:** 100μm.

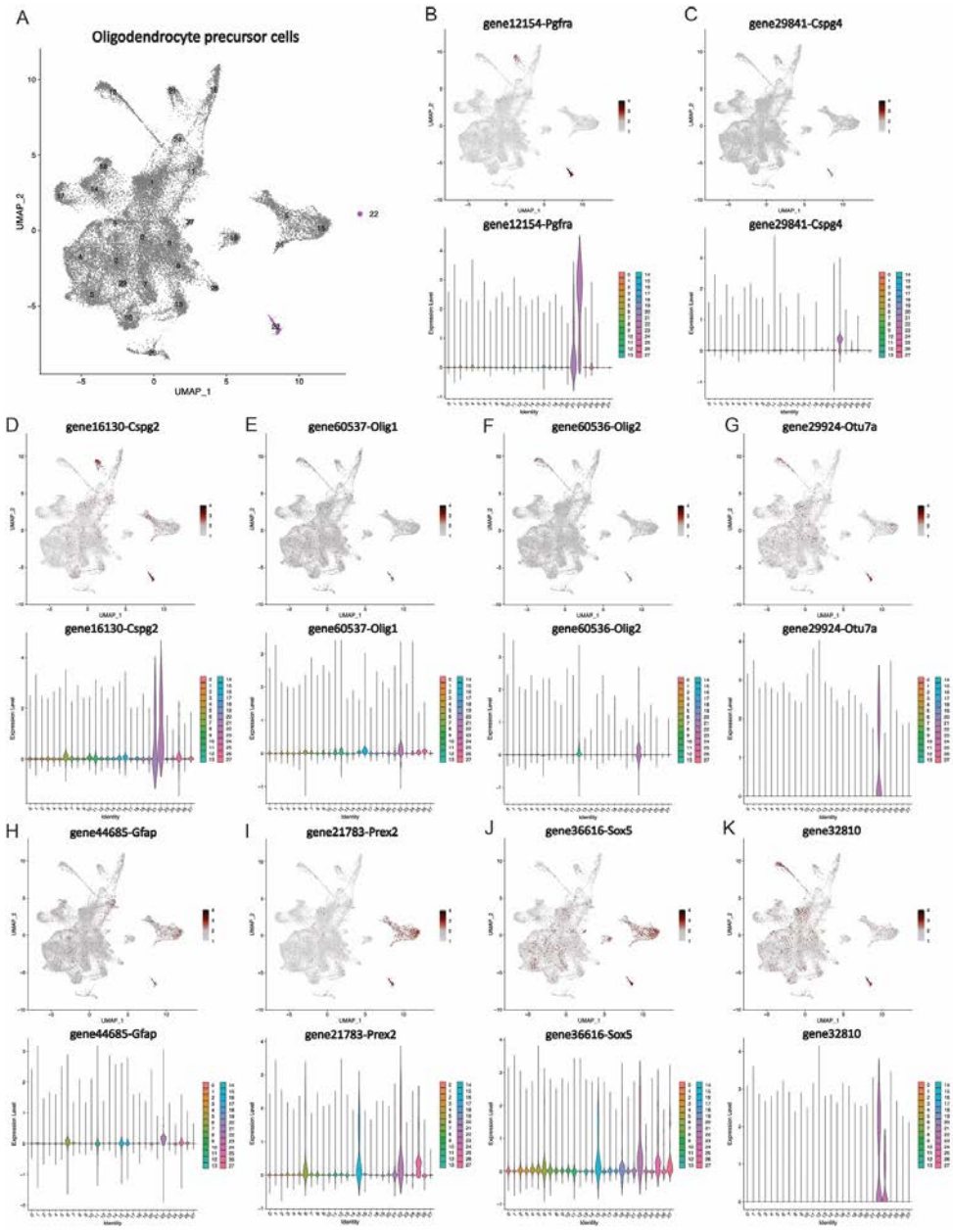

Fig. 21 | The OPC cell cluster and selected markers. (A) OPC population was characterized as cluster 22 in the UMAP at CCA_snn_res.1.5. **(B)-(K)** Top expressed genes in the cluster of OPC. **(L)-(O)** Singlets of cluster 22 were extracted and stained again to show clearer expression of *Gfap, Prex2, Sox5, and Pdfra.*

4.2.2.3. Oligodendrocytes

Mature oligodendrocytes are detrimental to dendritic and axonal regeneration as they express myelin and neurite growth inhibitory proteins that inhibit branch formation, growth and plasticity (Silver et al., 2014). Oligodendrocytes were identified as cluster 12 at CCA_snn_res.1.5 of the combined dataset **(Fig. 22A)**. In mammals, the classical markers include *Mypr, Cd9, Sox10, Cn37* and *Mbp* (Miron et al., 2011; Yadav et al., 2023). I found the *Pleurodeles* counterparts *gene18940-Mypr, gene36735-Cd9, gene33288-Sox10, gene44357-Cn37*. Both *Mbp* genes mentioned in section 4.1 (*gene19872-Mbp* and *gene19846-Mbp,* **Fig. 4**) were strongly expressed in this cluster (**Fig. 22B-G**). Interestingly, an unannotated newt gene (*gene19847)* that neighbors *gene19846-Mbp* was restrictedly expressed in oligodendrocytes (**Fig. 22I**). This finding suggests that this area of the genome could be crucial for the function of oligodendrocytes. Moreover, *gene35256-Gpr37* which encodes for the newt orthologue of the receptor of the neuroprotective and glioprotective factor prosaposin (Meyer et al., 2013), was highly enriched in oligodendrocytes (**Fig. 22H**). This gene has been reported to be enriched in mammalian oligodendrocytes (Yang et al., 2016). To visualize cluster 12, I did IHC for the aforementioned markers MBP and GPR37 (**Fig. 22J**). Newt oligodendrocytes are an understudied cell type, despite their importance as inhibitors of CNS regeneration demonstrated in many other animal models (Silver et al., 2014). The present RNAseq results provide new information on this cell type, opening new avenues for comparative and regenerative studies.

4.2.2.4. Microglia/Macrophages

In the CNS, resident microglia and blood monocytes initiate and maintain an injury-induced, long-lasting inflammatory response. Depending on the context, this can be beneficial or detrimental for regeneration (Silver et al., 2014). Although they share a myeloid lineage, microglia are the CNS-resident macrophages that enter the brain parenchyma early in development, while the so-called border associated macrophages (BAMs) reside in the meninges, the choroid plexus, and the perivascular spaces (Utz et al., 2020). Microglia/macrophages were identified as an individual cluster with newt orthologues of mammalian classical markers including *gene45605-Pigr, gene16736-Fyb, gene53742-CSF1R, gene47418-C1qc, gene53490-* and *gene43680-Aif1* (IBA1) **(Fig. 23A-F)**. As mentioned before, three *Mpeg1* genes were detected in the newt genome (**Fig. 5**). However, only *gene31079-MPEG1* was detected in my RNAseq dataset, suggesting that the other two copies found could represent pseudogenes **(Fig. 23G).** Despite the low number of transcripts of *Mpeg1* gene in the dataset, immunohistochemistry for GFP and IBA1 in transgenic mpeg1:GFP newts demonstrated that both proteins are co-expressed in the majority of the microglia and BAMs (**Fig. 23H**). In chapter 3, I have used these markers to shed light on this cell subpopulation in a regenerative context.

Fig. 22 (next page) | The cluster and markers of oligodendrocytes. (A) The oligodendrocyte population was characterized as cluster 12 in the UMAP at CCA_snn_res.1.5. **(B)-(I)** Top expressed genes in the cluster of OPC. **(J)** Immunohistochemistry of MBP and GPR37 in the newt ventral midbrain. Both markers were found primarily in the myelin in the fiber zone. Arrows point to the co-localization of MBP and GPR37. Scale bar: 50 µm.

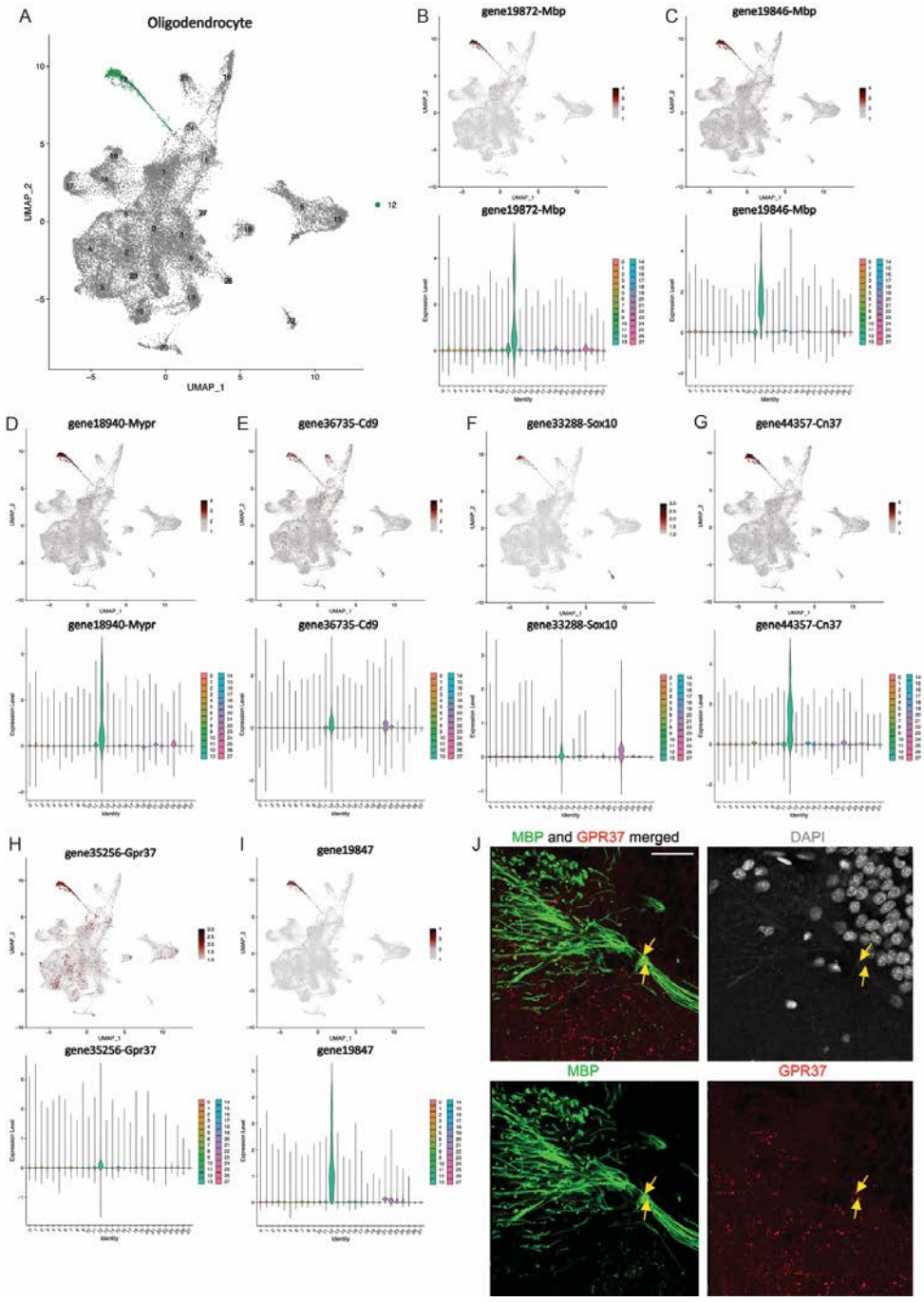
A
Oligodendrocyte
UMAP_2
UMAP_1
12
B
gene19872-Mbp
C
gene19846-Mbp
D
gene18940-Mypr
E
gene36735-Cd9
F
gene33288-Sox10
G
gene44357-Cn37
H
gene35256-Gpr37
I
gene19847
J
MBP and GPR37 merged
DAPI
MBP
GPR37

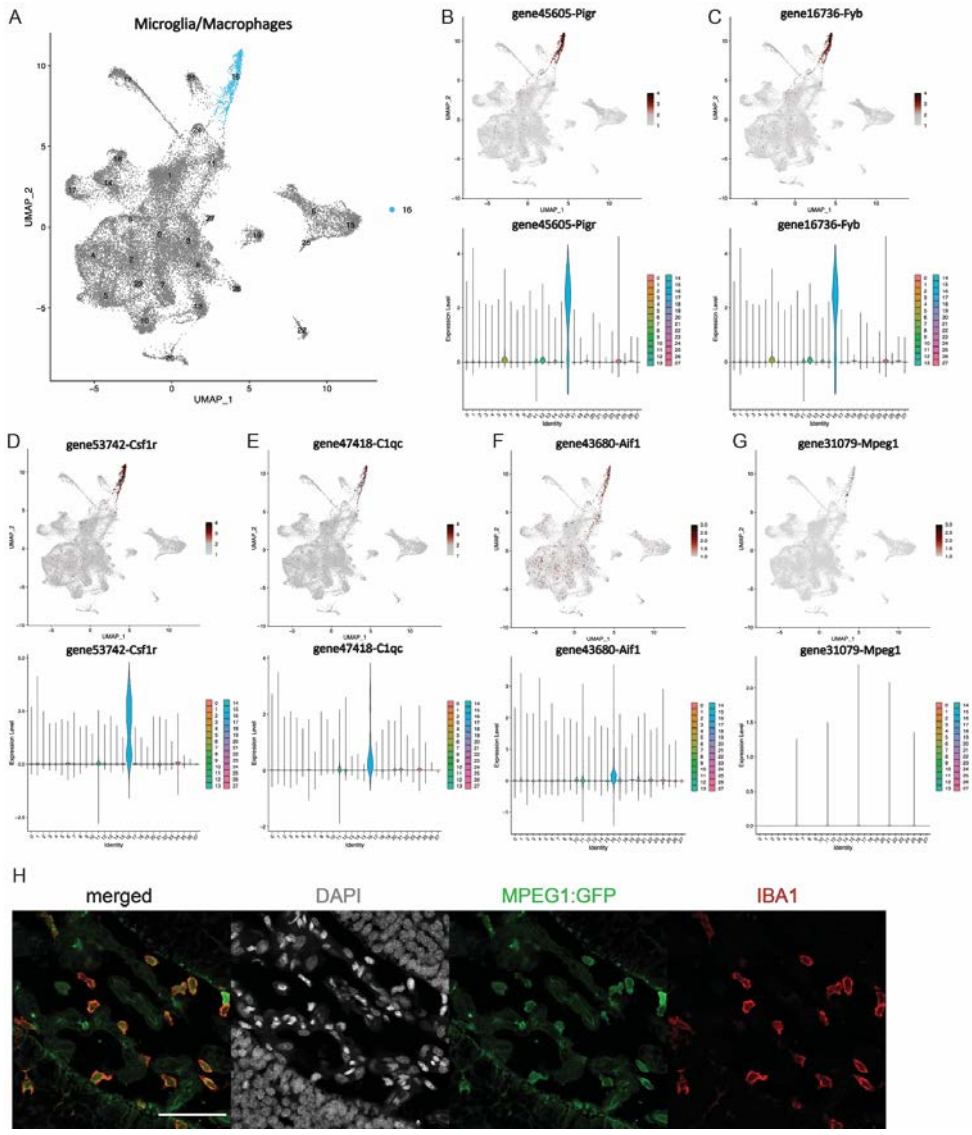

Fig. 23 | The cluster and markers of microglia/macrophages. (A) The microglia/macrophage population was characterized as cluster 16 in the UMAP at CCA_snn_res.1.5. **(B)-(G)** Top expressed genes in the cluster of microglia/macrophages. **(J)** Immunohistochemistry of GFP and IBA1 in the brain of MPEG1: GFP transgenic newt. Scale bar**:** 100µm.

4.2.2.5. Meningeal fibroblasts

The leptomeninges (arachnoid and pia layers) have vascular, immune, and mainly fibroblast cell types. There is increasing evidence of the role of meningeal fibroblasts in physiological responses to CNS pathology (Dorrier et al., 2022). Perivascular fibroblast classical markers include *collagen-1, laminin α1* and platelet-derived growth factor receptor-α (*PDGFRα*)

(Hannocks et al., 2018; Kelly et al., 2016; Vanlandewijck et al., 2018). I confirmed the presence of these classical markers in cluster 21 and found additional genes among the top expressed transcripts of this cell population, including *gene28851-Tmem2, gene24976-Co3a1, gene61918-Nid2, gene10168-At8b3, gene6106-Aebp1, gene36084-S38a4* and *gene32391-GLNA* **(Fig. 24A-H).** The orthologue genes of mouse label the cell population of meningeal fibroblasts in a mouse database (Linnarsson, 2023). Of special interest is the case of *GLNA*. According to the UniProt database (UniProt, 2023), mammals have only one *Glul* (*Glna*) gene copy that encodes for glutamine synthetase. This gene is expressed not only in meningeal fibroblasts, but also in all glial cell types, vascular-related cell types, and in a few neuronal subpopulations (Linnarsson, 2023). As mentioned before, I found two *Glna* genes in *Pleurodeles* (**Fig. 6**). Interestingly, the two genes show divergent expression patterns in our dataset. *Gene49443-GLNA* marks neural stem/progenitor cells (ependymoglia), microglia/BAMs and oligodendrocytes **(Fig. 6)**, while *gene32391-GLNA* marks the meningeal fibroblast cluster **(Fig. 24H)**. Not only GLNA, but also *gene63609-Syne2* and *gene8486-AT1A2* showed co-expression in fibroblasts and glial cells **(Fig. 24I-J)**. These results indicate that newts have meningeal fibroblasts similar like the ones described in mammals. The finding of the two newt *Glna* genes with differential cell type-specific expression patterns requires more investigation, as these two genes may have diverged in function, thereby providing an evolutionary advantage.

4.2.2.6. Erythrocytes

Like in most non-mammalian vertebrates, newt erythrocytes (red blood cells) are nucleated (Claver and Quaglia, 2009), which allows them to be detected using snRNAseq. The small cluster 24 was identified as erythrocytes **(Fig. 25A)** using the UniProt database (UniProt, 2023). Among the top-expressed transcripts I found genes encoding for the alpha or beta globin chains of hemoglobin (*gene1698-Hba2, gene1309-Hba1*). Other genes defining this cluster included *gene197-Hem0, gene29418-Nrk2, gene7775-Tfr2,* and *gene44641-B3at* **(Fig. 25B-E)**. Unlike humans, which have only one *HBB* gene, the newt expressed *gene1312-Hbb1*, and *gene1721-Hbb2,* indicating there has been a duplication in the beta globin chain gene (**Fig. 25F-G**). Interestingly, some cells in the neighboring intermediate progenitor cells/immature neuron cluster also expressed genes encoding the alpha or beta globin chains of hemoglobin (*gene1309-Hba1, gene1698-Hba2, gene1312-Hbb1*, or *gene1721-Hbb2*) while *Hba2* and both *Hbb* newt transcripts were also found in differentiated neurons (**Fig. 25B-G**). Few transcripts of *Hbb1* and *Hbb2* were detected in the dopaminergic neurons (cluster 20, will be discussed later) of the newts (see the violin plot in **Fig. 25F-G**). *Hba-a2* and *Hbb* transcripts have been reported to occur in rat and human neurons, including A9 dopaminergic neurons in the substantia nigra (Richter et al., 2009). Expression of hemoglobin in these neurons may be associated with cellular susceptibility in Parkinson disease (Codrich et al., 2017). The finding that hemoglobin in dopaminergic neurons could be a conserved feature in vertebrates further emphasizes the relevance of using newts as animal model for Parkinson disease research.

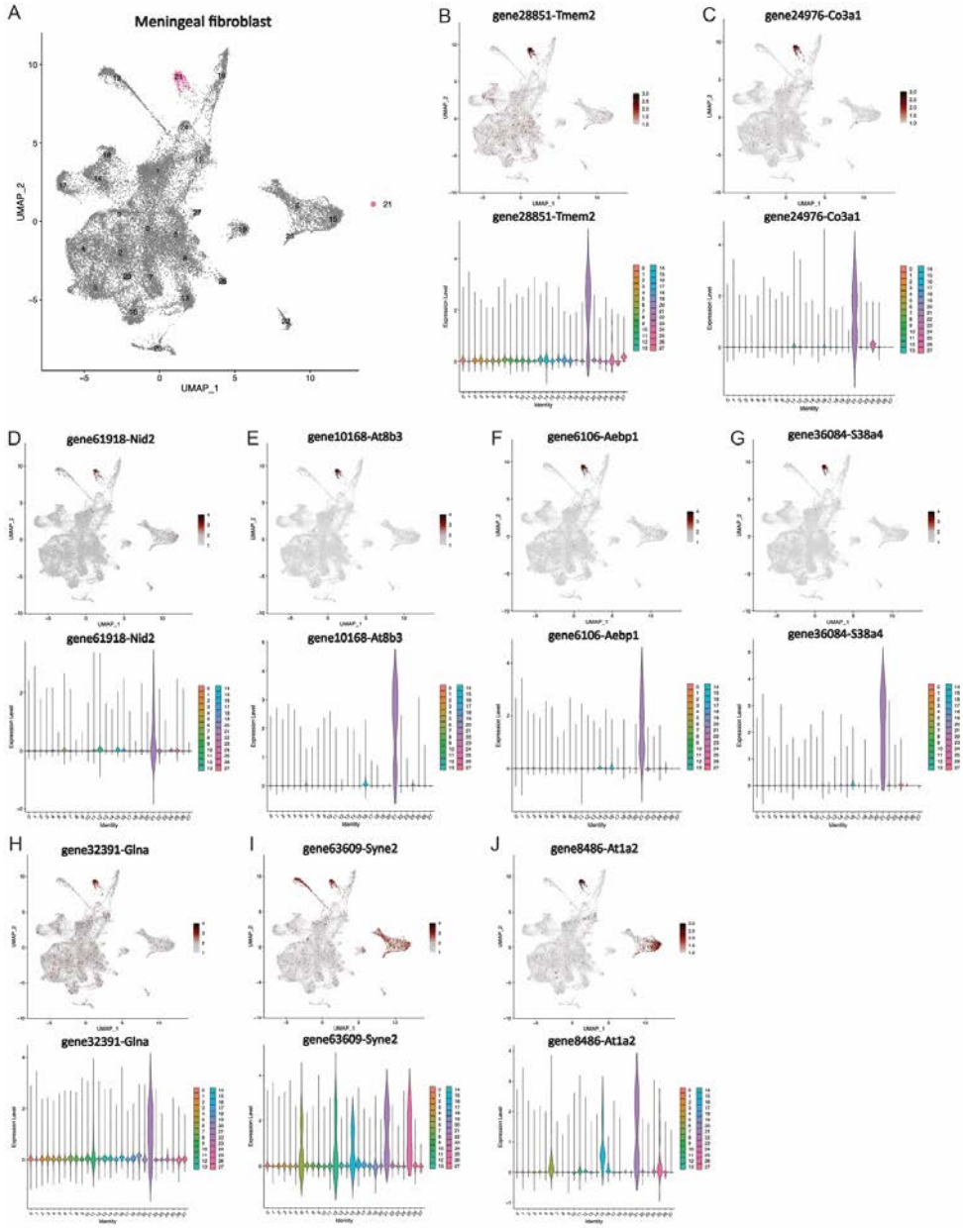

Fig. 24 | The cluster and markers of meningeal fibroblasts. (A) Meningeal fibroblast cell population was characterized as cluster 21 in the UMAP at CCA_snn_res.1.5. **(B)-(J)** Top expressed genes in the cluster.

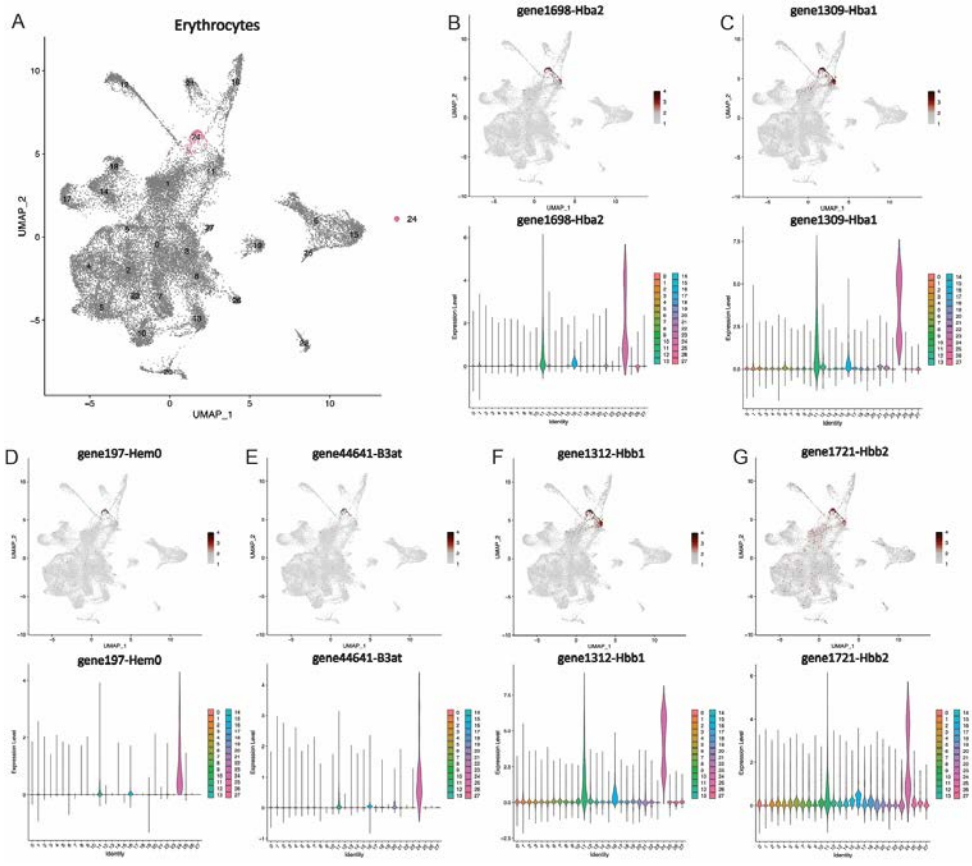

Fig. 25 | The cluster and markers of erythrocytes. (A) The erythrocyte population was characterized as cluster 24 in the UMAP at CCA_snn_res.1.5. **(B)-(G)** Top expressed genes in the cluster.

4.2.2.7. Neurons

Most of events in our combined dataset were identified as neurons by their expression of the newt orthologues of the pan-neuronal marker genes *gene32565-ELAV3*, *gene31466-ELAV4*, and *gene7866-DLG4* (**Fig. 26A-C**). At CCA_sn_res.1.5, IHC showed ELAV3/4^{+} (HUC/D^{+}) neurons were mostly restricted to the SVZ and MZ of ventral midbrains, and all the TH^{+} cells were ELAV3/4^{+} (**Fig. 26D**). Eighteen clusters were included in the category of "neuron", including clusters 0, 2-5, 7-11, 13, 17-20, 23, 26 and 27 (see **Fig. 18C** to visualize the extent of neurons grouped together). A closer look into each of these clusters allowed me to define neuronal subtypes (see below).

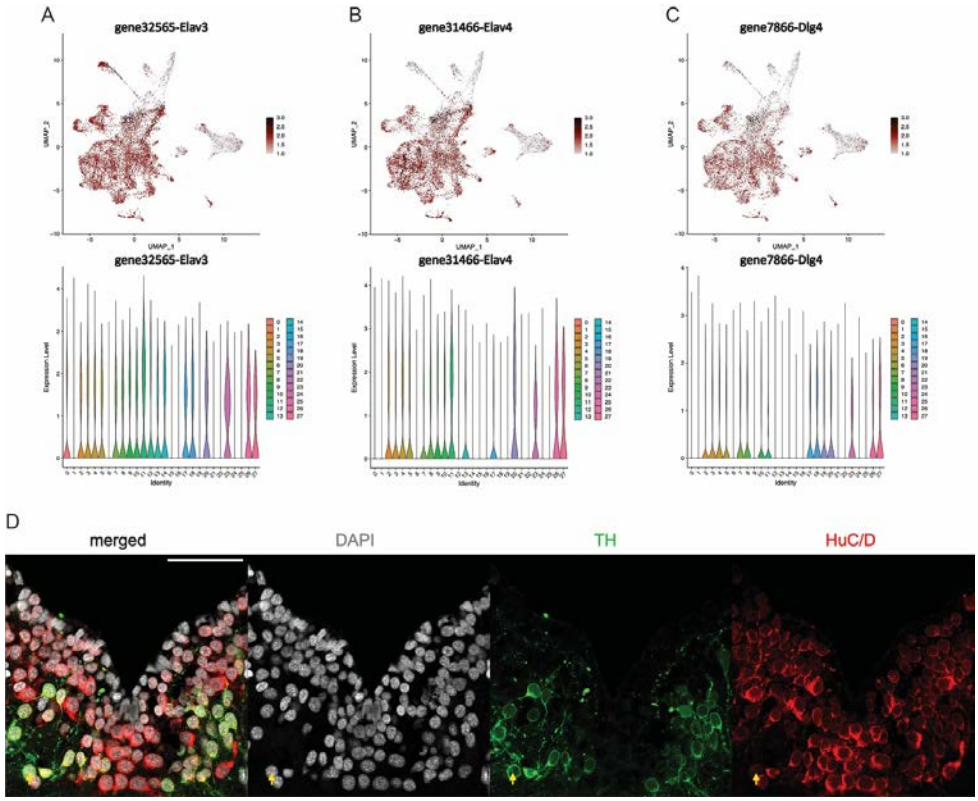

Fig. 26 | The clusters and markers of differentiated neurons. (A)-(C) Expressions of pan-neuron genes. **(D)** Immunohistochemistry of HuC/D with TH. Arrows point to the co-localization of TH neuron with HuC/D staining. Scale bar**:** 100μm.

Cluster 11 was characterized by showing both ependymoglial (see **Fig. 19B-G**) and neuronal **(Fig. 26A-C)** markers. Because of this peculiarity, together with the expression of *Tbb* and *Dcx* genes in the cluster **(Fig. 27A-D),** I defined this cluster as intermediate progenitor cells/immature neurons. Interestingly, the majority of the nuclei/cells in this cluster came from the larval samples, and very few nuclei coming from old newts populate this cluster (**Fig. 17D-F**).

Differentiated neurons were categorized based on the expression of well-known neurotransmitters and neurotransmitter-related molecules. Using this method, I could detect monoaminergic neurons (**Fig. 28A-D**) (including dopaminergic ones cluster 20, **Fig. 28E-H**, and serotonergic ones cluster 19, **Fig. 29I-L**), cholinergic neurons (cluster 19, **Fig. 29A-D**), glutamatergic neurons (clusters 0, 1, 3, 10, 13, 14, 17, 18 and 27, **Fig. 29E-H**) and GABAergic neurons (clusters 2, 4, 5, 7, 9 and 23, **Fig. 29I-L**).

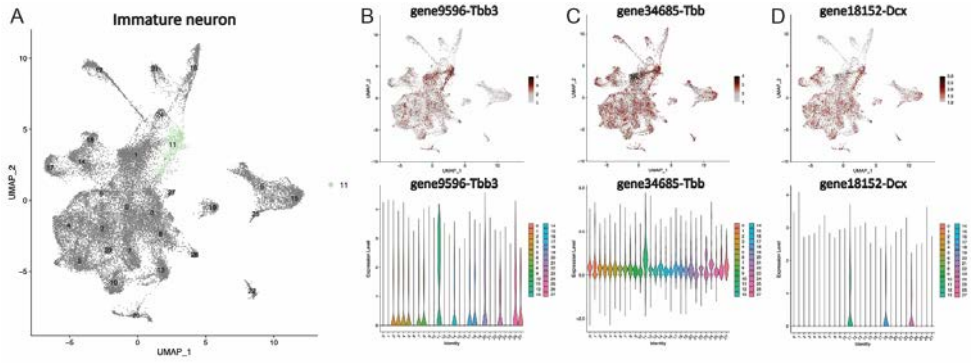

Fig. 27 | The intermediate progenitor cells/immature neuron cluster and selected markers. (A) Intermediate progenitor cell/immature neuron population was characterized as cluster 11 in the UMAP at CCA_snn_res.1.5. **(B)-(G)** Top expressed genes in the cluster.

Monoaminergic neurons were allocated in clusters 19 and 20 (**Fig. 28A)**, defined by the expression of the synaptic vesicular amine transporter *gene46485-Vmat2* (**Fig. 28B)** and the aromatic-L-amino-acid decarboxylase *gene19440-Ddc* (**Fig. 28C**). In addition, two unannotated newt genes, *gene46483* (**Fig. 28D**) and *gene46484* (data not shown), were detected in both clusters. These two genes were the neighbors of *gene46485-Vmat2*, indicating that this genome area was crucial for both dopaminergic neurons and serotonergic neurons. I found two different transcripts that are encoded by the newt genes: *gene28570-Ty3h* and *gene36149-Ty3h*. This finding agrees with the duplication of *TH* genes already reported in other in amphibians (Yamamoto and Vernier, 2011). Interestingly, the expression of these two genes was cluster-specific, implying the diversification of the regulatory elements and potentially also of protein functions. High expression of *gene28570-Ty3h* (denoted as orthologue of TH1 in zebrafish) (Yamamoto et al., 2010) was detected in cluster 20, which was identified as dopaminergic neurons by the co-expressions of *gene49795-Lmx1b*, *gene32788-Lmx1a*, and *gene16887-GRP* **(Fig. 19H, 28E-H)**. As mentioned before, *gene49795-Lmx1b* is also expressed in the neural progenitor cluster 25, indicating that the dopaminergic cells of cluster 20 could develop from this neural progenitor cell population **(Fig. 19H)**. Interestingly, the mammalian SN dopaminergic marker *gene28059-Sox6* (Poulin et al., 2020) was detected in cluster 20 (**Fig. 28L**) though in very few singlets. This indicates that some dopaminergic neurons located in the newt VMb may functionally act like the SN dopaminergic neurons in mammals. It should be noted also that *gene28059-Sox6* was highly expressed in OPCs (cluster 22), and this is conserved with previous findings in mammals (Baroti et al., 2016; Stolt et al., 2006; Wittstatt et al., 2019). Unlike calbindin, which was not found to be expressed in the dopaminergic cluster, other dopaminergic markers of SNpc (eg: Aldh1a1 and Girk2) or VTA (eg: Otx2) were detected in cluster 20, but the number of singlets were also very few (data not shown). This can be explained by the low number of total dopaminergic neurons recovered in the dataset. The second TH gene, *gene36149-Ty3h* (denoted as orthologue of TH2 in zebrafish) (Yamamoto et al., 2010), was detected in some cells of cluster 19 (**Fig. 28I-J**). This cluster also contained serotonergic neuron markers, as determined by the expression of tryptophan 5-hydroxylase 1. This enzyme catalyses the rate-limiting step in the synthesis of serotonin and is encoded by the newt gene *gene27993-Tph1* **(Fig. 28K)**. Though one previous study in zebrafish suggested the $TH2^+$ neurons were dopamine-synthesizing neurons (Yamamoto et al., 2010), a later study found TH2 was actually responsible for the function of serotonin, making TH2 a marker gene of serotonergic neurons

(Ren et al., 2013). For this reason, cluster 19 was identified as serotonergic neurons. I have used anti-TH antibodies to visualize these cells (see **Table. 3**); however, it is unclear whether those antibodies recognized one or both proteins that I found in the sequencing data. The existence of dopaminergic and serotonergic neurons in the newt brain was reported more than 40 years ago (Dubé and Parent, 1982). Subsequent studies have demonstrated their homology with the mammalian counterparts (reviewed in (Joven and Simon, 2018)), but until now there are no studies describing two separate TH genes which are expressed by two distinct subpopulations. My next step will be to generate probes and detect where those two catecholaminergic cell types are located in the tissues.

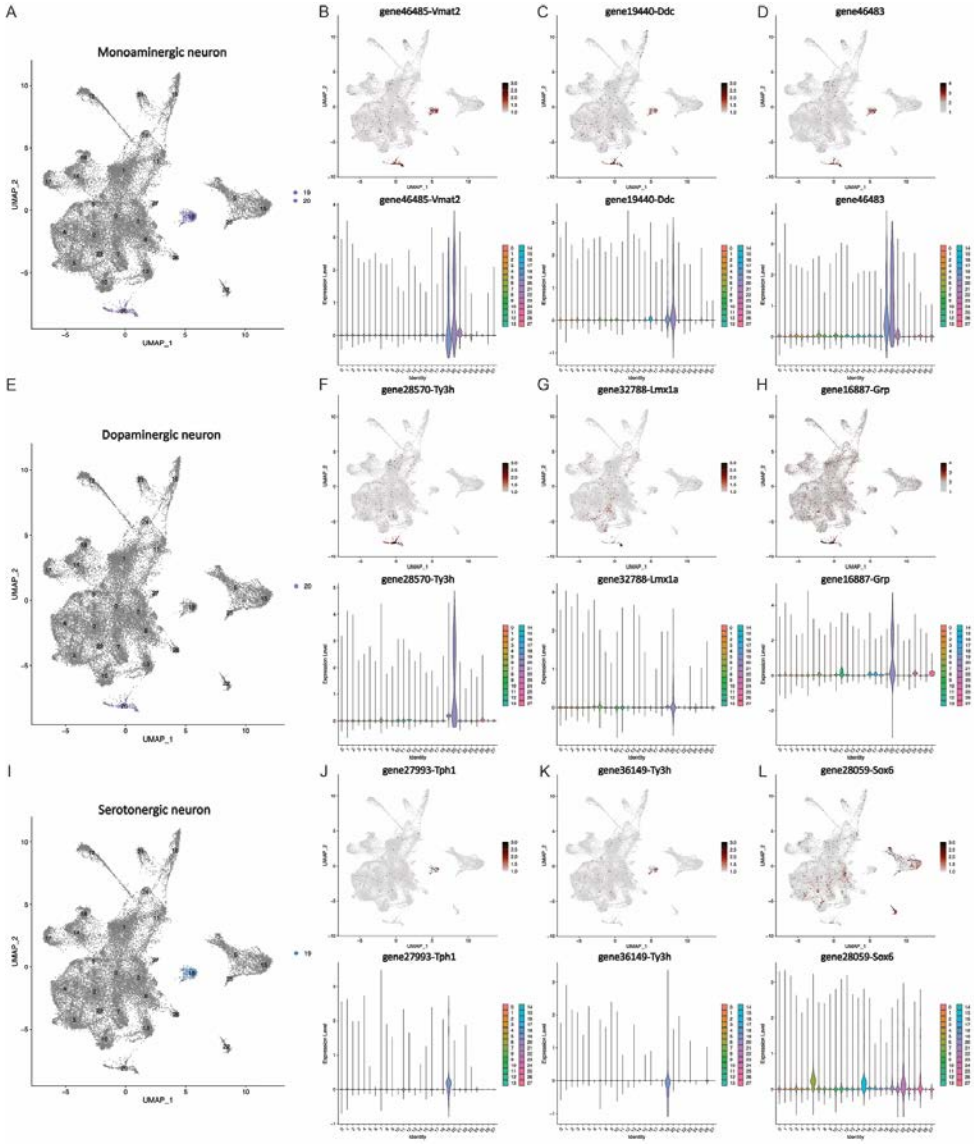

Fig. 28 (previous page) | Differentiated neuron clusters and selected markers (1 of 2). (A)-(D) Monoaminergic neurons (clusters 19 and 20) express *Vmat2* (**B**), *Ddc* (**C**), and *gene46483* **(D)**. **(E)-(H)** Dopaminergic neuron cluster 19 **(E)** was defined by the expression of one of the two newt genes found encoding for tyrosine hydroxylase, *gene28570-Ty3h* (**F**), *Lmx1a* (**G**), and *Grp* **(H)**. **(I)-(K)** Serotonergic neuron cluster 20 **(I)** was defined based on the expression of *Tph1* (**J**). Additionally, a second newt gene encoding for tyrosine hydroxylase, *gene36149-Ty3h*, was differentially expressed in this cluster (**K**). Furthermore, *Sox6* was detected in both clusters with a higher expression in cluster 20 **(L)**.

The cholinergic neurons were identified as the cluster 26 (**Fig. 29A**), expressing the newt orthologue that encodes for choline O-acetyltransferase, *gene48482-Clat* (**Fig. 29B**). Other genes detected in the cluster included *gene16650-Isl1*, *gene11807-Slit2*, and *gene53512-Slit3*

(**Fig. 19I, 29C, D**), which are known to play roles in cholinergic neuron development (Linnarsson, 2023). Interestingly, *gene11807-SLIT2* was also detected in the neural progenitor cluster 25 expressing *gene49795-Lmx1b* (**Fig. 19H, I**). This observation led me to hypothesize that both monoaminergic neurons and cholinergic neurons could develop from the same neural progenitor population, which can be addressed with future experimental validations. The anatomical description of cholinergic system in the *Pleurodeles* brain is available in the literature (Marín et al., 1997c). Based on the dissected areas selected for sequencing, the cholinergic cells defined in this study may correspond to the few cell bodies described in the posterior tubercle, oculomotor and trochlear nuclei, and the isthmic tegmentum (Marín et al., 1997c).

The remaining neuronal populations found in this study have not been previously described in newts. As a first approach, I classified them based on their putative excitatory or inhibitory nature.

Inhibitory neurons (GABAergic neurons) were distributed in six clusters at CCA_snn_res.1.5 (**Fig. 29E**). I classified them as inhibitory neurons based on the expression of newt orthologues that putatively encode for the glutamate decarboxylases 1 and 2, *gene25603-DCE1* and *gene2770-DCE2* (**Fig. 29F-G**), together with the *gene51578-VIAAT* (**Fig. 29H**) which encodes for the newt's vesicular inhibitory amino acid transporter (orthologue of SLC32A1). The data outlined here contain an unprecedented resource regarding the neuronal heterogeneity of the newt ventral midbrain.

Excitatory neurons (Glutamatergic neurons) were a large population consisting of nine different clusters at CCA_snn_res.1.5 (**Fig. 29I**). The newt orthologues encoding for the vesicular glutamate transporters *gene55427-VGLU1* and *gene30102-VGLU2* were used to define these clusters as glutamatergic **(Fig. 29J-K)**. The gene *gene35336-VGLU3* was also present but very few reads were detected (**Fig. 29L**).

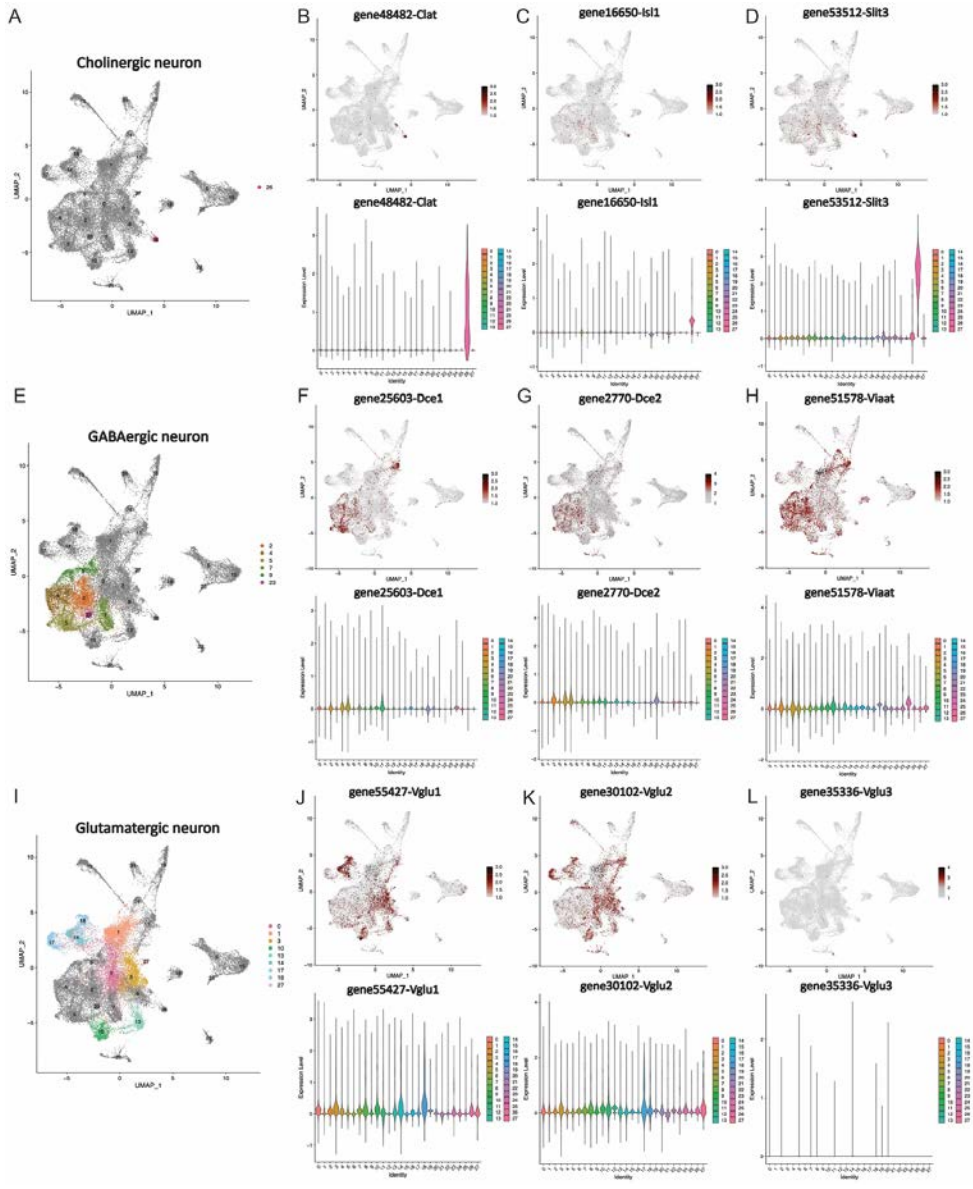

Fig. 29 | Differentiated neuron clusters and selected markers (2 of 2). (A)-(D) Cholinergic neurons (cluster 26) in the newt midbrain express *Clat* (**B**), *Isl1* (**D**), and *Slit3* (**D**). (**E)-(H)** GABAergic neurons were composed of 6 different clusters (2, 4, 5, 7, 9 and 23). Glutamate decarboxylase-encoding genes *Dce1* (**F**), and *Dce2* (**G**) together with *VIAAT* (**H**) were used to characterize this cluster. (**I)-(L)** Glutamatergic neuron diversity in the newt midbrain was highlighted by 9 clusters at CCA_sn_res_1.5 (). These cell clusters were characterized as glutamatergic based on the expression of *gene55427-Vglu1* (**J**), *gene30102-Vglu2* (**K**) and *gene35336-Vglu3* (**L**).

4.2.3. Cellular composition of newt ventral midbrain changes during life span.

In this chapter, I present the cellular and molecular changes I found in the transitions from larval to mature to aged newt ventral midbrain using single-nucleus RNAseq analysis in combination with IHC.

4.2.3.1. The main cell types of the ventral midbrain are established at late active larval stage.

An important question to explore in brain development is when the different cell populations appear. Some neuronal subpopulations such as dopaminergic and cholinergic neurons in the VMb are present from early larval stages, although the number of neurons and complexity of their innervation pattern increases during a developmental time window (Joven et al., 2018). It is unknown whether this could be a rule that applies to all neuronal subpopulations and other cell types in the CNS. To tackle this question with transcriptomics, I excluded the scRNAseq data to prevent a method-biased analysis of the results and integrated the data obtained from single nuclei (**Fig. 30A**). By analyzing the snRNAseq integrated dataset of late active larvae, 1year old young adults, and 9 years old adults, all the cell types described in chapter 4.2.2 could be identified at CCA_snn_res.2 (**Fig. 30A-B)**. Importantly, the nuclei contributing to each of the clusters originated from samples from the 3 life stages **(Fig. 30C-E)**. This indicates that the cellular heterogeneity found in the mature newt ventral midbrain is already established at late active larval stage. This resembles the situation in the *Pleurodeles* forebrain, where all adult neuronal subtypes are already getting established during development (Woych et al., 2022).

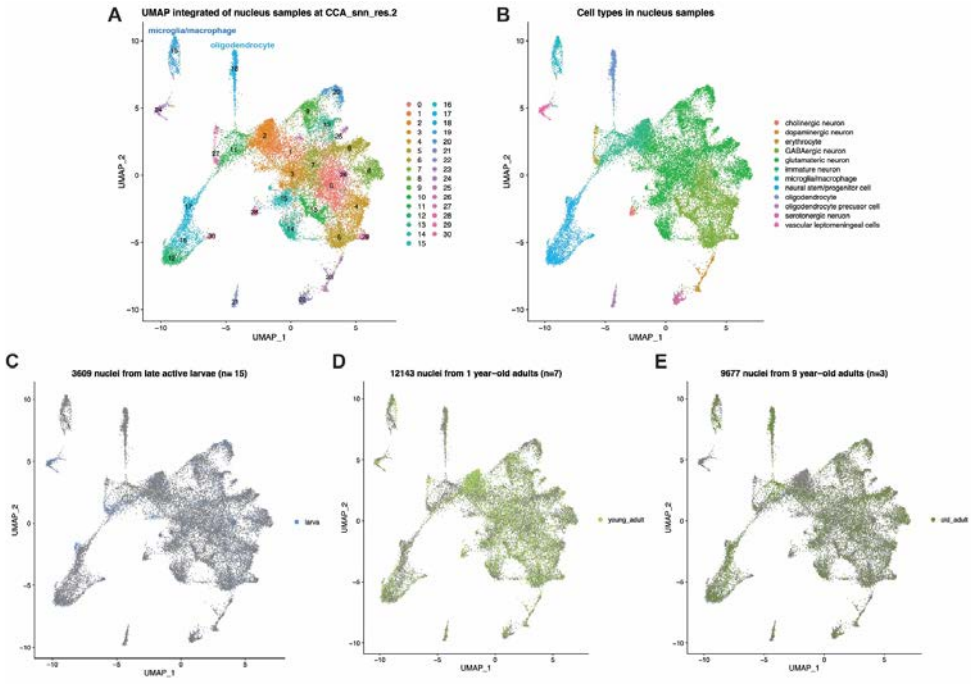

Fig. 30 (previous page) | Late larvae have established the main cell populations in their ventral midbrains. **(A)** UMAP of the snRNAseq integrated dataset of late active larvae, young adults, and old adults at CCA_snn_res.2. Both microglia/macrophages and oligodendrocytes were identified as single clusters at this resolution. **(B)** Cell categories in the snRNAseq integrated dataset of the 3 stages. **(C-E)** Individual plotting of late active larvae, young adults (1 year old), and old adults (9 years old) on the UMAP.

4.2.3.2. The cellular composition changes with maturation and aging.

Previous studies have described the cellular composition of the mammalian ventral midbrain at different life stages (Braun et al., 2022; La Manno et al., 2016; Siletti et al., 2022). However, it is not known if the cellular composition changes in newt brain with maturation and ageing. To visualize potential dynamic changes in the composition of ventral midbrain cell types during the life span of the newts, I plotted the percentages of nuclei's origin (by stages) in all the clusters (**Fig. 31A**). I found that among all clusters, the clusters 18 and 19 contained very few nuclei of larval origin, while clusters 24 and 26 were scarce in events of aged origin (**Fig. 31A**). I then normalized the percentage of nuclei's origin by life stage total nuclei numbers. Relative proportion of clusters 18 and 19 representing microglia/macrophages and oligodendrocytes by each life stage suggest that these populations are already present in larvae, but their numbers expand with age (**Fig. 31B-C**). The relative amount of cells belonging to clusters 24 and 26 along the life span of newts suggests that there is a decline of meningeal fibroblasts and circuit-forming neurons in the aged newt ventral midbrains (**Fig. 31D-E**). The oligodendrocyte expansion was confirmed by immunohistochemical analyses of MBP and GPR37 expression **(Fig. 31F)**. These results indicate that both immune cells and myelinating oligodendrocytes in newt ventral midbrain are minor components of the larval brains, which greatly increase in numbers during brain maturation and aging. Similar patterns of microglia and oligodendrocytes increase are found in mammalian development and aging (Barry-Carroll et al., 2023; Nishiyama et al., 2021). Previous studies have shown that interactions among microglia, oligodendrocyte and neurons are crucial in brain development (Kalafatakis and Karagogeos, 2021; Mehl et al., 2022; Peferoen et al., 2014). It would be valuable to explore if similar cell interactions occur in newts. In contrast, meningeal fibroblasts and circuit-forming neurons displayed a decline in percentages with maturation and aging. Interestingly, previous studies showed that specific leptomeningeal cells have neurogenic potential (Bifari et al., 2017; Nakagomi and Matsuyama, 2017). It would be interesting to explore whether the newt leptomeningeal cells have neurogenic potential, and its relation to newt regeneration ability. Cluster 26 marker genes are related to roles in sculpting neural circuits in brain development (Luhmann et al., 2016; Penn and Shatz, 1999). The decline in this neuronal subtype in aged brains suggests that newts experience a decrease in neural plasticity with age, like other vertebrates.

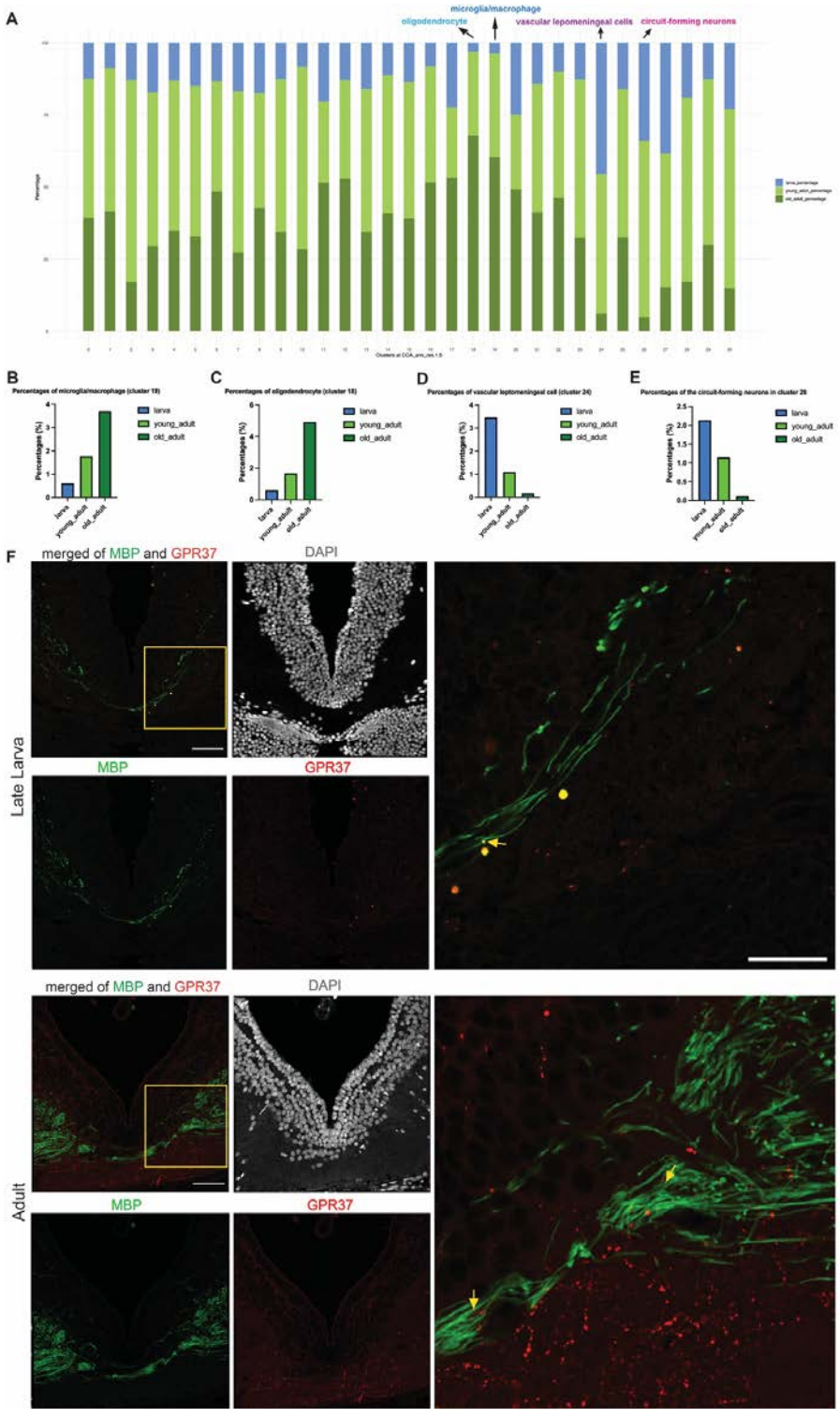
A
microglia/macrophage
oligodendrocyte
vascular lepomeningeal cells
circuit-forming neurons
B
Percentages of microglia/macrophage (cluster 19)
C
Percentages of oligodendrocyte (cluster 18)
D
Percentages of vascular leptomeningeal cell (cluster 24)
E
Percentages of the circuit-forming neurons in cluster 28
Percentages (%)
larva
young_adult
old_adult
F
merged of MBP and GPR37
DAPI
MBP
GPR37
Late Larva
Adult

Fig. 31 (previous page) | Cellular composition changes with maturation and aging. (A) Percentages of the nucleus from late active larvae, young adults, and old adults in each cluster at CCA_snn_res.2. **(B)-(E)** The percentages of the nuclei in clusters (at CCA_snn_res.2) of microglia/macrophages (B), oligodendrocytes (C), meningeal fibroblasts (D), and circuit-forming neurons (cluster 26) across the 3 stages. **(F)** The expansion of oligodendrocytes from late larva to adult was detected by IHC of MBP and GPR37. The yellow squared areas were enlarged in the right panels. Arrows point to the co-expression of GPR37 and MBP. Scale bar**:** 100μm in the left images and 50μm in the right enlarged images.

4.2.3.3. Potential dopaminergic subpopulations

While mammalian dopaminergic neurons are found in both VTA and SN in mammals, newts do not have laterally migrated TH^+ cells in the midbrain (Smeets and Reiner, 1994). This could indicate either that dopaminergic neurons corresponding to mammalian SN neurons are not present in the newt midbrain or that they are located also in the VTA. While only functional analyses along with analyses of projections could fully resolve this question, a good starting point is the analysis of marker genes that are differently expressed in the VTA and SN in mammals. I first tried to analyze the scRNAaseq and snRNAseq data but the yield for dopaminergic neurons was too low. Therefore, I used immunohistochemical analyses instead.

I first analyzed the expression of calbindin (CALB1 or CB), which marks VTA dopaminergic population in the mammalian midbrain dopaminergic neurons (La Manno et al., 2016). As previously reported (Joven et al., 2013c), CALB1 was not detected in newt midbrain dopaminergic neurons (marked by TH and NURR1), but it was expressed in more dorsally located cells, whose exact identity is yet to be determined **(Fig. 32A)**.

Fig. 32 (next page) | CB and CR expression in ventral midbrain of the newt. (A) IHC of CB with TH and NURR1 in adult midbrain. No co-expression was detected. Scale bar: 100 μm. **(B)** IHC of CR and TH in midbrains of newts from st45 to st56. Arrows point to CR^+TH^+ cells. Scale bar: 100 μm. **(C)** Quantifications of the percentages of CR^+ cells in midbrain dopaminergic neurons (marked by TH) from st37 to st56. Each dot represents the percentage of CR^+ cells in TH^+ neurons of one newt in the whole ventral midbrain. 7 newts were counted at st45 while 3 newts were counted in each of the other stages. 31-286 TH^+ cells were counted per newt, the lower values corresponding to early developmental stages. Ordinary one-way ANOVA with Bonferroni's multiple comparisons test. **p<0.01, ***p<0.001, ****p<0.0001. Means ± s.e.m. are shown. **(D)** Quantifications of the percentages of CR^+TH^+ cells along the rostrocaudal axis at st55c. 3 newts were counted. 254-308 TH^+ cells were counted per newt. Ordinary one-way ANOVA with Bonferroni's multiple comparisons test. *p<0.05. Means ± s.e.m. are shown. **(E)** Quantifications of the percentages of CR^+TH^+ cells along the rostrocaudal axis at st56. 3 newts were counted. 235-286 TH^+ cells were counted per newt. Ordinary one-way ANOVA with Bonferroni's multiple comparisons test. **p<0.01. Means ± s.e.m. are shown.

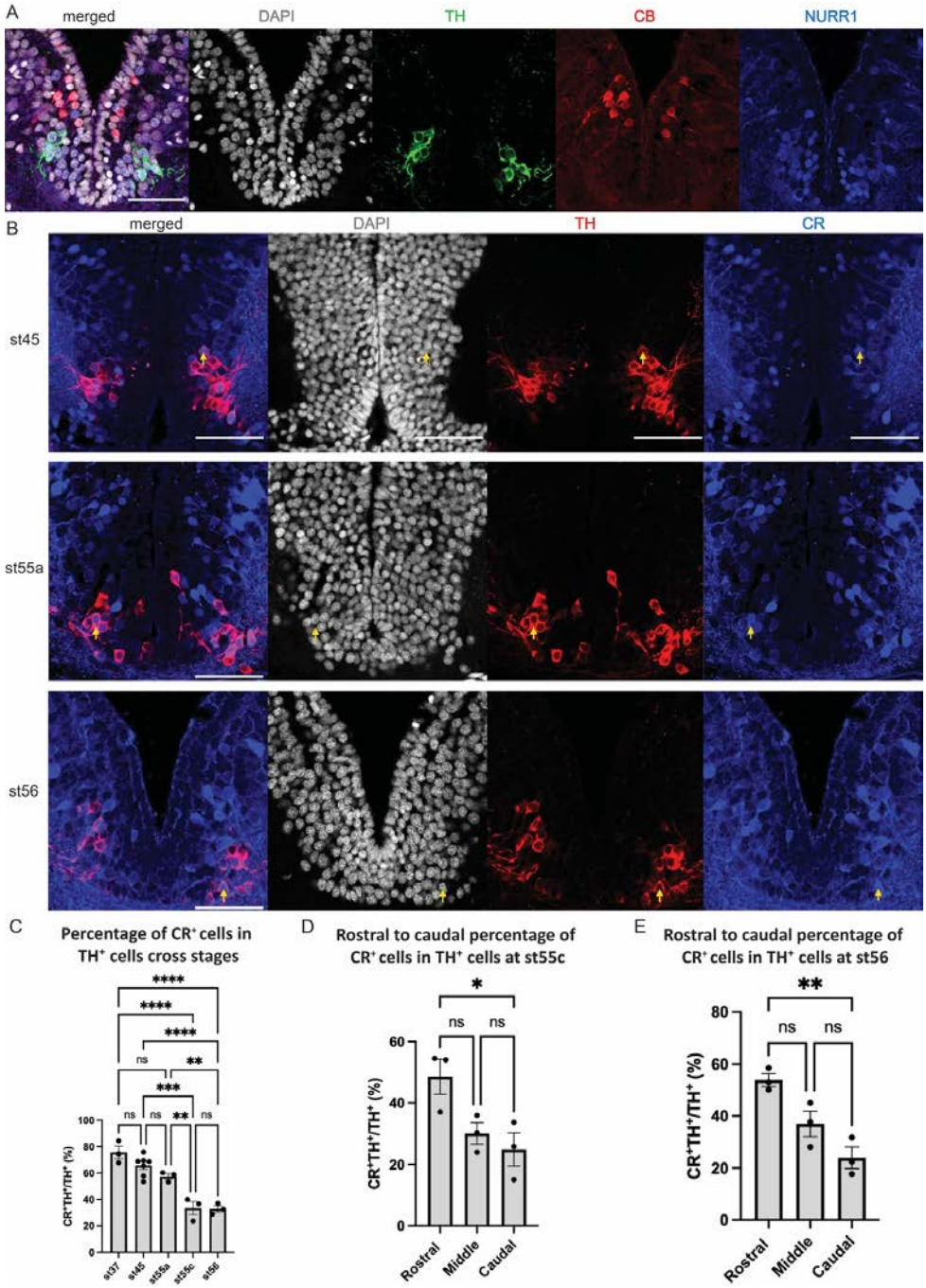
A
merged
DAPI
TH
CB
NURR1
B
merged
DAPI
TH
CR
st45
st55a
st56
C
Percentage of CR+ cells in TH+ cells cross stages
CR+TH+/TH+ (%)
st37
st45
st55a
st55c
st56
D
Rostral to caudal percentage of CR+ cells in TH+ cells at st55c
CR+TH+/TH+ (%)
Rostral
Middle
Caudal
E
Rostral to caudal percentage of CR+ cells in TH+ cells at st56
CR+TH+/TH+ (%)
Rostral
Middle
Caudal

In contrast, the expression of calretinin (CALB2 or CR), another calcium-binding protein with neuroanatomical distribution has been reported in *Pleurodeles* (Joven et al., 2013c), was detected in some of the newt midbrain dopaminergic neurons **(Fig. 32B)**. I found that the percentages of CR^+ cells among TH-expressing neurons in the VMb gradually decreased during ontogeny **(Fig. 32C)**. Interestingly, these cells were more abundant in rostral VMb **(Fig. 32D, E).** Determining the significance of this observation would need further experimentation. Next, I analyzed the expression patterns of OTX2 and SOX6 as they are key transcription factors for the specification of the mammalian VTA and SN (Panman et al., 2014). I found that SOX6 and OTX2 labeled mostly mutually excluding subpopulations within TH^+ VMb cells **(Fig. 33A)**. This resembles the situation reported previously in mouse development from stage 13.5 to 18.5 (Panman et al., 2014). Quantifications indicated that the proportions of some of these subpopulations change during development **(Fig. 33B)**: while the percentages of $OTX2^+/SOX6^-$ and $OTX2^+/SOX6^+$ cells remained constant, the $OTX2^-/SOX6^-$ subpopulation increased and the $OTX2^-/SOX6^+$ decreased with age **(Fig. 33B, 33C)**. This is consistent with the reports in mice, where Sox6 expression decreases during development (Panman et al., 2014). Given the rostrocaudal differences I found in the distribution of CR^+/TH^+ cells **(Fig. 32D-E)**, I analyzed the distribution of $SOX6^+/TH^+$cells and found that they are less abundant in the caudal part of the VMb, suggesting that the putative SN in the newt occupy mostly the rostral and middle aspects of the VMb **(Fig. 33D)**." In mammals, OTX2 has a higher expression in VTA than in SN (Poulin et al., 2020). I did not find differences in the proportion of $OTX2^+/ TH^+$ between developmental and adult stages **(Fig. 34A)**. The distribution of $OTX2^+/TH^+$ expressing neurons showed a low-to-high gradient in a rostral-to-caudal direction **(Fig. 34B-D)**. This may suggest that the heterogeneity among the dopaminergic neurons that is manifested in lateral migration in mammals could be traced to a rostral-caudal distribution in newts. Altogether, these data indicate that although partially intermingled, the putative SN in the newt may occupy more rostral portions of the VMb, while the VTA cells may be preferentially located in more caudal areas.

Due to the low number of dopaminergic neurons in my dataset, it was hard to explore their transcriptional heterogeneity at a high resolution. Generation of transgenic newt lines, like Th: GFP or Dat1: GFP (which the Simon lab is in the process to produce) should allow to increase the resolution by enriching for sufficient number of dopaminergic neurons using FACS prior to scRNAseq/snRNAseq, as performed in previous studies in mammals (Salmani et al., 2023; Tiklova et al., 2019). Another potential option to increase the resolution is to apply scRNAseq/snRNAseq techniques that can catch more features per singlets, for example Smart-seq3 (Hagemann-Jensen et al., 2020; Hagemann-Jensen et al., 2022).

Fig. 33 (next page) | SOX6 and OTX2 highlight dopaminergic subpopulations in the newt ventral midbrain. **(A)** Representative image of immunohistochemistry of SOX6, OTX2 and TH in a postmetamorphic newt (st56). Scale bar: 100 µm. The solid arrow points a $TH^+SOX6^+OTX2^-$ cell, the hollow arrow points a $TH^+SOX6^-OTX2^-$ cell, the solid arrowhead points a $TH^+SOX6^-OTX2^+$ cell, the solid arrowhead points a $TH^+SOX6^+OTX2^+$ cell. **(B)** Analysis of the percentages of $OTX2^+/SOX6^-$, $OTX2^+/SOX6^+$, $OTX2^-/SOX6^-$ and $OTX2^-/SOX6^+$ in dopaminergic neurons (marked by TH) at two different stages. Two-way ANOVA (****p<0.0001, not shown in the graph) with Bonferroni's multiple comparisons test showed statistically significant differences only in the $OTX2^+/SOX6^-$ subpopulation (****p<0.0001, not shown in the graph) and the $OTX2^-/SOX6^+$ subpopulation (***p=0.0002, not shown in the graph). Means ± s.e.m. are shown. **(C)** The percentages of $SOX6^+$ cells at st53 and st56. Each dot represents the percentage of cells of one newt in the whole rostrocaudal extent of the ventral midbrain. N=3-6 newts were used in each stage. Student's T test. ****p<0.0001. Means ± s.e.m. are shown. **(D)** Quantifications of $SOX6^+$ cells in dopaminergic neurons in rostral, medial and caudal levels in newts at st56. 6 newts were used for counting. Each dot represents the cell percentage of one newt in the areas. Ordinary one-way ANOVA with Bonferroni's multiple comparisons test. *p<0.05, **p<0.01. Means ± s.e.m. are shown. For (B), (C), and (D), 144-283 TH^+ cells were counted per newt.

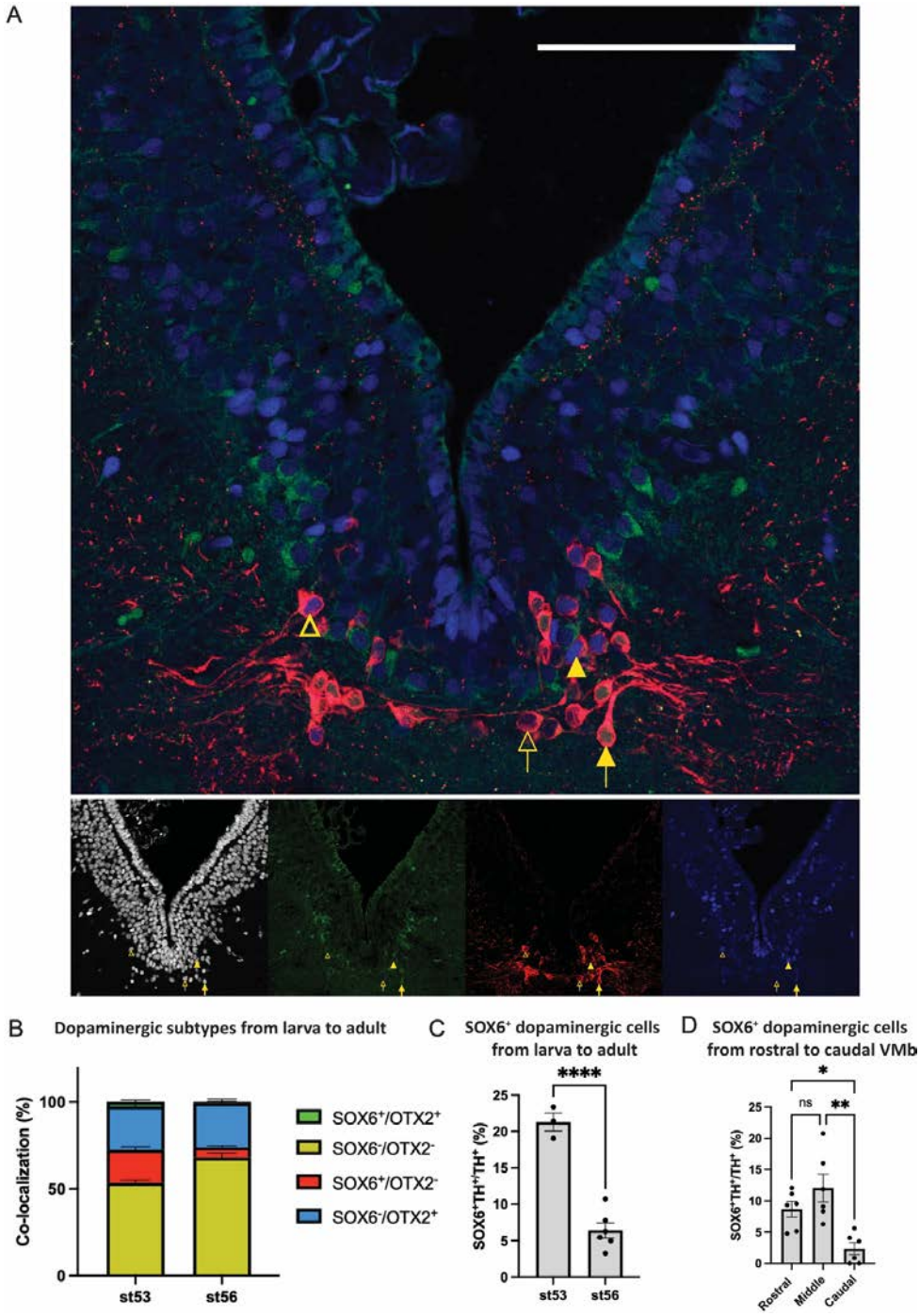
A
B
Dopaminergic subtypes from larva to adult
Co-localization (%)
100
50
0
st53
st56
SOX6+/OTX2+
SOX6-/OTX2-
SOX6+/OTX2-
SOX6-/OTX2+
C
SOX6+ dopaminergic cells from larva to adult
****
SOX6+TH+/TH+ (%)
25
20
15
10
5
0
st53
st56
D
SOX6+ dopaminergic cells from rostral to caudal VMb
*
ns
**
SOX6+TH+/TH+ (%)
25
20
15
10
5
0
Rostral
Middle
Caudal

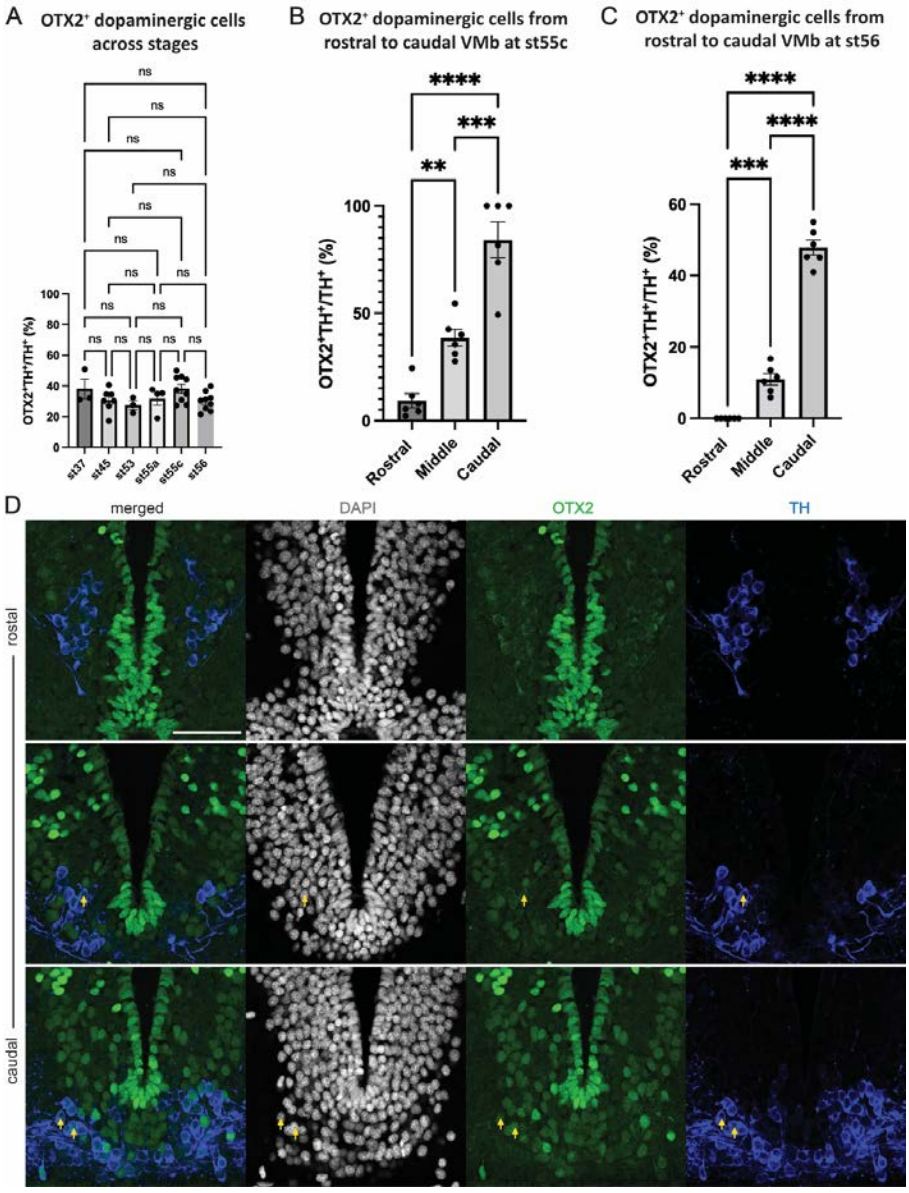

Fig. 34| OTX2⁺ dopaminergic subpopulation in the newt ventral midbrain. (A) The percentages of OTX2⁺ cells in dopaminergic neurons (marked by TH) from st37 to st56. Each dot represents the percentage of cells of one newt in the whole rostrocaudal extent of the ventral midbrain. N=3-9 newts were used in each stage. **(B)** Quantifications of OTX2⁺ cells in dopaminergic neurons in rostral, medial and caudal levels in newts at st55c. 6 newts were used for counting. **(C)** Quantifications of OTX2⁺ cells in dopaminergic neurons in rostral, medial and caudal levels in newts at st56. 6 newts were used in counting. In (B) and (C), each dot represents the cell percentage of one newt in the different areas. For (A), (B), and (C), 31-158 TH⁺ cells were counted per newt, the lower values corresponding to early developmental stages. Ordinary one-way ANOVA with Bonferroni's multiple comparisons test. *p<0.05, **p<0.01, ***p<0.001, ****p<0.0001. Means ± s.e.m. are shown. **(D)** Immunohistochemistry of OTX2⁺ cells in dopaminergic neurons from rostral (section 0) to caudal (section 4) at st55c. Scale bar: 100 µm.

4.2.4. Molecular transitions between various cell types

Besides the changes in the proportions of various cell types, molecular transitions occur within different cell types during midbrain maturation and aging (Braun et al., 2022; Joven et al., 2018; Kirkham et al., 2014; La Manno et al., 2016; Siletti et al., 2022). However, the molecular changes in key cell types of the newt VMb are largely unknown. To gain new understanding of the molecular transitions during newt's life span, I analyzed the snRNAseq dataset containing nuclei from larvae, 1 year old adults, and 9-year-old adults (**Fig. 16**). I selected the suitable Louvain resolution for each cell type, as different cell types were best visualized at different Louvain resolutions on the UMAP. To tackle this, the top differentially expressed genes were identified for the clusters of "ependymoglia" (clusters 3 of the snRNAseq dataset at CCA_snn_res.0.25), "intermediate progenitor cells/immature neurons" (clusters 1 of the snRNAseq dataset at CCA_snn_res.0.65) and "dopaminergic neurons" (clusters 23 of the snRNAseq dataset at CCA_snn_res.2) (**Fig. 35**). Then the differentially expressed transcripts across life stages in the defined cluster of the cell type were analyzed. Given the focus of this thesis in the dopaminergic neurogenesis, I tried to uncover the transcriptional changes underlying quiescence acquirement by ependymoglia, formation of new neurons and dopaminergic maturation.

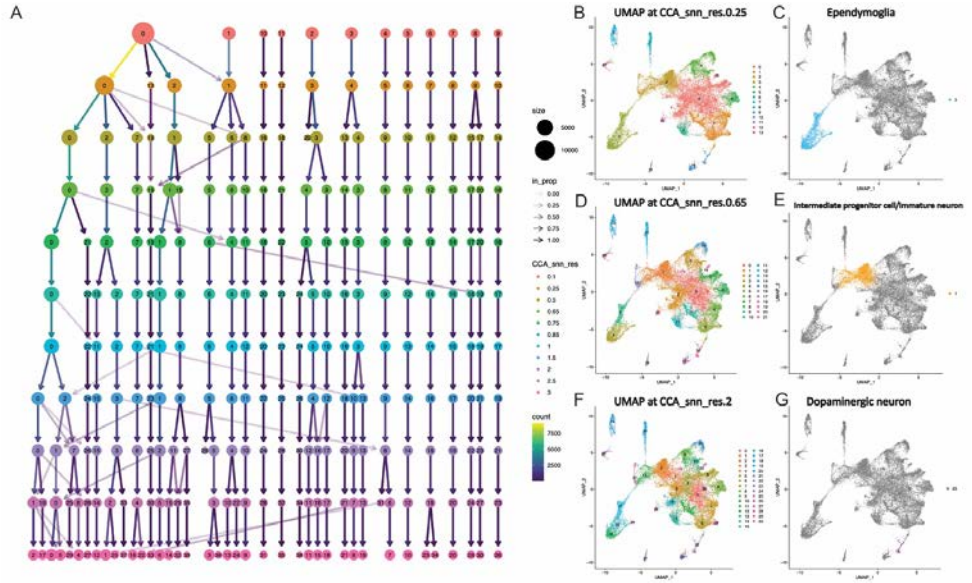

Fig. 35| Selection of each cell type for analysis at the suitable Louvain resolution. (A) Hierarchy tree of Louvain clustering. **(B)-(C)** Selecting ependymoglia in cluster 3 at CCA_snn_res.0.25. **(D)-(E)** Selecting intermediate progenitor cells/immature neurons in cluster 1 at CCA_snn_res.0.65. **(F)-(G)** Selecting dopaminergic neurons in cluster 23 at CCA_snn_res.2.

As mentioned before, quiescence acquirement of ependymoglia is a key process in brain maturation (Joven and Simon, 2018; Joven et al., 2018; Kirkham et al., 2014), making ependymoglia as an indispensable target population for analysis. I first confirmed the expected higher expression of proliferation markers such as *gene47010-KI67*, and lower expression of quiescent, Type-1 ependymoglial marker *gene49443-GLNA* in larval stage compared to adult stages **(Fig. 36A)**. This is consistent with the previous studies (Joven et al., 2018; Kirkham et

al., 2014), strengthening the validity of this method to uncover molecular changes at the population level**.** I then performed unbiased analysis to discover the most DEG in ependymoglia along the newt life span. In support of the major presence of highly proliferative, type-2 ependymoglia in the larval brain, two ribosomal protein genes showed higher enrichment in larva compared with adult stages **(Fig. 36A)**. This agrees with the previous finding about the upregulation of ribosomal proteins in activated neural stem cells (Baser et al., 2017; Llorens-Bobadilla et al., 2015). Neuronal membrane glycoprotein *gene59244-GPM6B* was found at a higher expression in larval stage **(Fig. 36A)** when the ependymoglia is more active. A previous study showed the expression of its orthologue in reactive astrocytes after traumatic brain injury (Choi et al., 2013). It would be interesting to explore if there is an upregulation of this gene upon brain injury also in newts. Interesting, increased expression of *gene63609-SYNE2* was detected along brain maturation and aging **(Fig. 36A)**. Given SYNE2 has been described to be involved in centrosome attachment in neural progenitors, it would be valuable for future research to explore if (and how) SYNE2 regulates ependymoglial quiescence (Wallis et al., 2021). Furthermore, I identified a upregulation of *gene19770-JARD2* along brain maturation and aging (**Fig. 36A**), which orthologue is known as a regulator of histone methyltransferase complexes and can act as an accessory subunit for the core PRC2 complex (Chen et al., 2020; Chen et al., 2018; Pasini et al., 2010). This agrees with previous studies showing its regulatory roles in stem cell quiescence, activation, and differentiation (Berg et al., 2010; Celik et al., 2018; Ishibashi et al., 2021; Mejetta et al., 2011).

The intermediate progenitors/immature neurons clusters share some marker genes with neural stem cells and astrocytes in mammals (Beckervordersandforth et al., 2010; Codega et al., 2014; Pilz et al., 2018; Urban et al., 2019). This led me to hypothesize that these cells may suffer similar dynamical regulation in the process of quiescence acquirement, as well as being another potential pool to replenish neurons in the adult brain upon injury. In my analysis, I found the differential expression of *gene19770-JARD2* and several ribosomal protein genes (**Fig. 36B**), which are similar to what I found in ependymoglia (**Fig. 36A**). This indicates that newt intermediate progenitors/immature neurons share some similar transcriptional changes with ependymoglia. Interestingly, *gene43450-AIF1L*, which's mammalian orthologue was known to promote actin bundling, showed upregulation after brain maturation. This result is in coherence with a recent study which showed the increase of *aif1l* during maturation of *Xenopus* midbrain (Ta et al., 2022) **(Fig. 36B)**. More studies are needed to clarify the significance of this gene regulation.

The heterogeneity of midbrain dopaminergic neurons across different life stages has been a topic of intense research in mammals during the last decade (Hook et al., 2018; La Manno et al., 2016; Poulin et al., 2018; Poulin et al., 2020; Poulin et al., 2014; Salmani et al., 2023; Saunders et al., 2018; Tiklova et al., 2019). An important question for the understanding of Parkinsonian models and the human disease is the vulnerability of dopaminergic neurons as well as the effect of aging (Branch et al., 2014; Chan et al., 2010; Kamath et al., 2022; Pereira Luppi et al., 2021; Salmani et al., 2023). Given the regenerative neurogenic potential of newts upon dopaminergic damage (Berg et al., 2010; Berg et al., 2011; Joven et al., 2018; Parish et al., 2007), a question that remains to be answered is whether newts show transcriptional changes in the VMb dopaminergic cells with maturation and aging. In this analysis, I found a higher expression of *gene2556-PTPR2* in larval compared to adult stages **(Fig. 36C)**. In one previous study, reduced levels of dopamine, serotonin, and norepinephrine were found in mouse with deletion of the gene orthologue and IA-2 protein (Nishimura et al., 2009). Another study showed decreased expression of the gene orthologue in human patients of Parkinson's disease (Grunblatt

et al., 2004). Thus, the lower expression of the *gene2556-PTPR2* in the population of adult newts may imply an increased tendency of degeneration in the dopaminergic neurons upon aging. On the other hand, *gene53784-GPX3,* whose orthologue protects from oxidative damages (Esworthy et al., 1991), showed a downregulation in old adult newt cells **(Fig. 36C)**. This suggested a decreased ability of reducing hydrogen peroxide, lipid peroxides and organic hydroperoxide in dopaminergic neurons of the aged newts, which could make them more vulnerable. This may support the model with a conserved vertebrate program in age-related degeneration of dopaminergic cells. *gene2984-SIA8F* displayed a higher expression in old adult newts **(Fig. 36C)**. Downregulation of the human orthologue of *gene2984-SIA8F* in dopaminergic neurons from postmortem brains of patients with Parkinson's disease has been reported (Huang et al., 2023). Also, an anti-inflammatory and neuroprotective effect was shown by overexpression of *gene2984-SIA8F* in dopaminergic neurons of MPTP-treated mice (Huang et al., 2023). The results indicate that a protection against dopaminergic degeneration in old adult newts by *gene2984-SIA8F.* Furthermore, I explored the signaling pathways predicted by the upregulated genes of larval dopaminergic neurons compared to adult stages using the web server g:Profiler (Raudvere et al., 2019). While multiple signaling pathways for neural development were predicted, pathways involved in the response to oxygen-containing compounds were also found **(Fig. 36D)**. This may suggest a stronger resistance to oxidative stress in larval dopaminergic neurons.

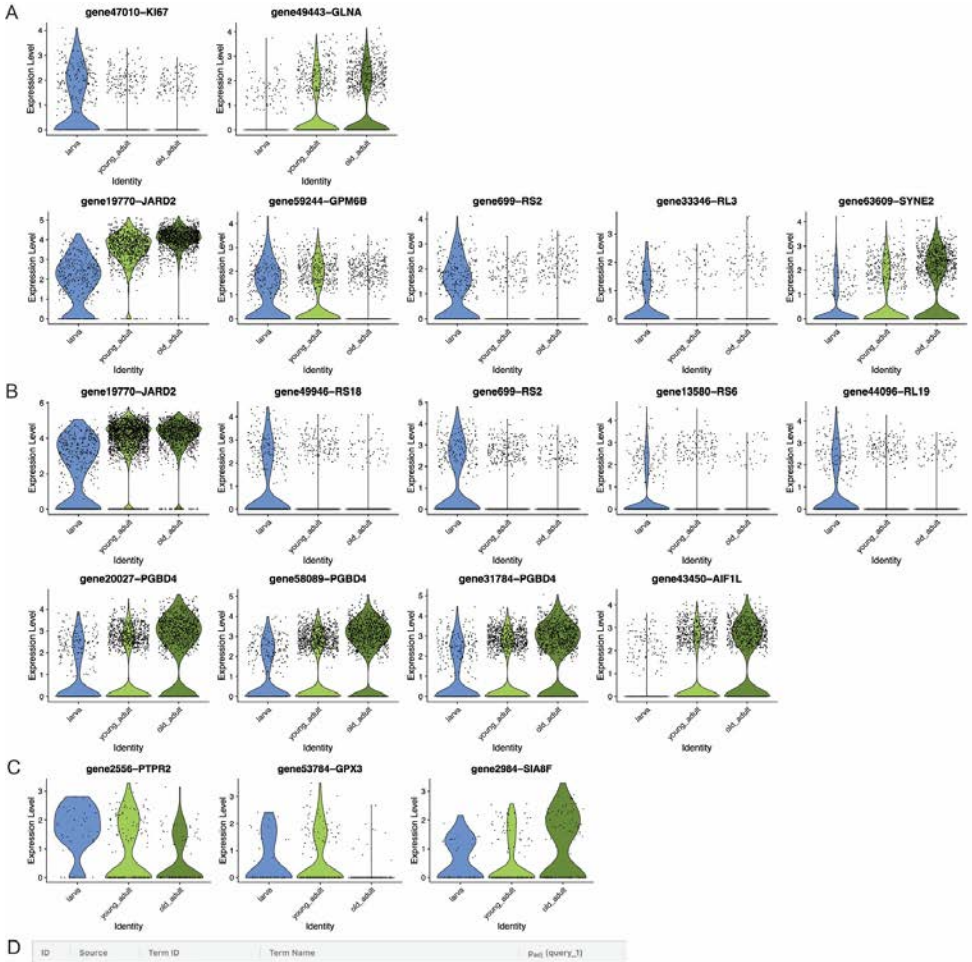

D

ID	Source	Term ID	Term Name	P_{adj} (query_1)
1	GO:MF	GO:0005515	protein binding	3.056×10^{-3}
2	GO:MF	GO:0003729	mRNA binding	4.043×10^{-3}
3	GO:BP	GO:0048812	neuron projection morphogenesis	8.338×10^{-6}
4	GO:BP	GO:0032879	regulation of localization	9.250×10^{-6}
5	GO:BP	GO:0048858	cell projection morphogenesis	1.470×10^{-5}
6	GO:BP	GO:0032990	cell part morphogenesis	2.470×10^{-5}
7	GO:BP	GO:0007399	nervous system development	3.663×10^{-5}
8	GO:BP	GO:0120039	plasma membrane bounded cell projection morphogenesis	1.287×10^{-5}
9	GO:BP	GO:0060341	regulation of cellular localization	4.687×10^{-5}
10	GO:BP	GO:0048667	cell morphogenesis involved in neuron differentiation	2.547×10^{-4}
11	GO:BP	GO:0030030	cell projection organization	3.084×10^{-4}
12	GO:BP	GO:0031175	neuron projection development	8.778×10^{-4}
13	GO:BP	GO:1901700	response to oxygen-containing compound	3.673×10^{-3}
14	GO:BP	GO:1901701	cellular response to oxygen-containing compound	4.521×10^{-4}
15	GO:BP	GO:0048856	anatomical structure development	4.718×10^{-3}
16	GO:CC	GO:0030424	axon	1.576×10^{-10}
17	GO:CC	GO:0043005	neuron projection	1.338×10^{-8}
18	GO:CC	GO:0045202	synapse	1.443×10^{-9}
19	GO:CC	GO:0030054	cell junction	3.493×10^{-9}
20	REAC	REAC:R-HSA-9675108	Nervous system development	6.972×10^{-4}
21	REAC	REAC:R-HSA-422475	Axon guidance	1.678×10^{-3}
22	REAC	REAC:R-HSA-6794362	Protein-protein interactions at synapses	3.691×10^{-3}
23	REAC	REAC:R-HSA-112316	Neuronal System	3.083×10^{-6}

Fig. 36 (previous page) | Differentially expressed genes and analysis in ependymoglia cluster **(A)**, intermediate progenitor cells/immature neuron cluster **(B)**, and dopaminergic neuron cluster across the three stages **(C)**. Wilcox test was used for the statistical analysis, and genes with |log2FC|>0.2 and P value<0.01 were screened. A selection of these genes are displayed in figure (A)-(C). The predicted signaling pathways from upregulated genes in larval dopaminergic neuron population are displayed in **(D)**.

4.2.5. NFI transcription factors in newt ventral midbrain development

Nuclear Factor I (NFI) transcription factors were identified as key factors that promote the quiescence of stem cells during brain development (Clark et al., 2019; Martynoga et al., 2013). To see if there are similar mechanisms in the newt, I explored the expression of *Nfi* genes in the ependymoglia cluster from the previous snRNAseq dataset. I speculated that NFI genes would be upregulated, given the regulative roles of NFI in neural quiescence (Hoang et al., 2020). Except for gene39658-NFIA, the NFI genes did not show upregulation in mean expressions, though trends of more high-expressing cells of the genes could be observed along development. A reasonable explanation for this may be that although more NFI^+ cells appear along development, more NFI^- neural progenitors were also generated, making the mean expression level more or less constant. I next used IHC to analyze these potential changes in ventral midbrain tissue sections during the development of the midbrain dopaminergic neuron population (**Fig. 38**). I used the TH staining in this case as an anatomical reference, to ensure that I was analyzing the same brain area across stages. I found that NFI IHC showed no expression at early active larval stage 37, when proliferation is very active in the developing larvae (Joven et al., 2018). Starting at late active larval stage 45, when ependymoglia begins to undergo quiescence in the *Pleurodeles* larval brainstem (Joven et al., 2018), I detected NFIA expression in the VZ; this remained high at later stages including after metamorphosis **(Fig. 38)**. Note that the strongest $NFIA^+$ cells in adult ventral midbrain were not the ependymoglia along the VZ, but the specific cells in the SVZ **(Fig. 38)**. These results showed similar a role of NFI found in stem cells before (Clark et al., 2019), indicating this function of promoting quiescence is conserved in brain of *Pleurodeles.*

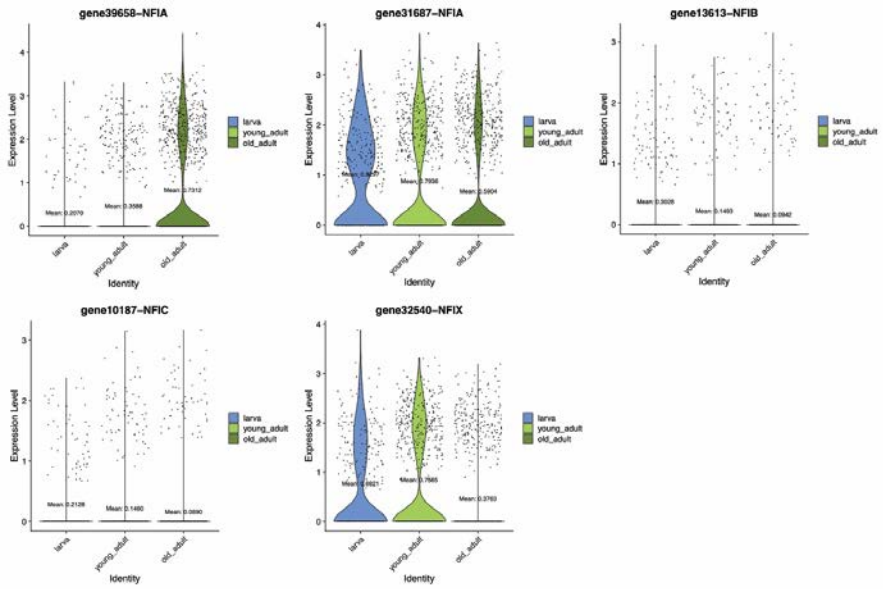

Fig. 37 | Violin plots showing changes of gene expression of NFI transcription factors in ependymoglia across the newt life span. Only the gene39658-NFIA among the NFI factors showed increased expression during ontogeny (Wilcox test of |log2FC|>0.2 and P value<0.01). The other NFI genes only show a trend as newts mature.

Because I found that upregulation of NFI factors (**Fig. 38**) occurred at the same developmental stages than the acquisition of the quiescent state by ependymoglial cells (Joven et al., 2018), next I explored whether the ependymoglial quiescence can be accelerated by manipulating NFI . I generated a plasmid expressing NFiA with GFP (CMV: NFIA -t2A-GFP) and validated the NFIA expression in cell culture **(Fig. 39A)**. Next, I electroporated the "CMV: NFI -t2A-GFP" plasmid or control plasmid "CAG: GFP-loxP-Cherry" into the ependymoglia of developing newt midbrain at a developmental stage when these cells are still highly proliferative (Joven et al., 2018). I found a marked reduction of MCM2+ /GFP+ cells after NFIA overexpression compared to the brains electroporated with the control plasmid, indicating an accelerated cell cycle exit by ependymoglial cells, as a result of NFIA overexpression **(Fig 39B-D)**. Again, the result agrees with the previous manipulation study in cultured neural stem cells (Martynoga et al., 2013).

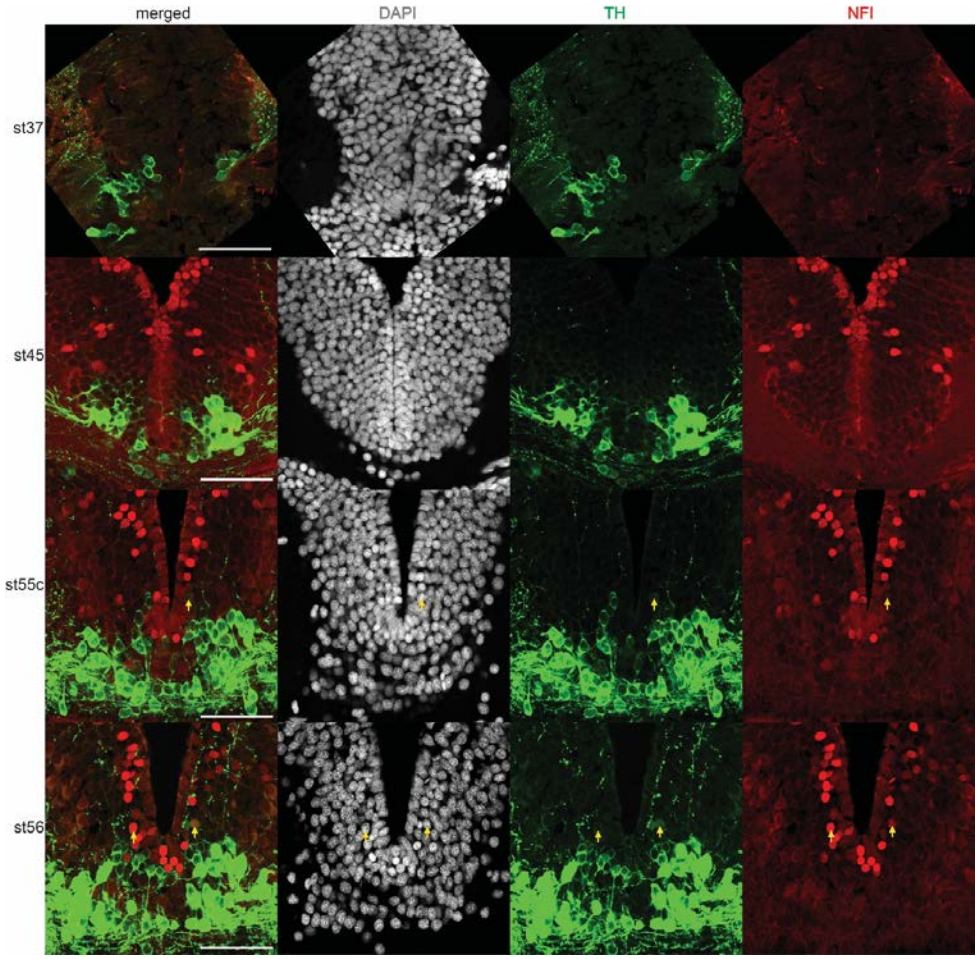

Fig. 38 | Co-staining and counting of NFI with TH in ventral midbrain of the adult newt. The expression of NFI in midbrain with dopaminergic neurons (marked by TH) in the newts from st37 to st56. Arrows point $NFI^{+}TH^{+}$ cells. Scale bar: 100 µm.

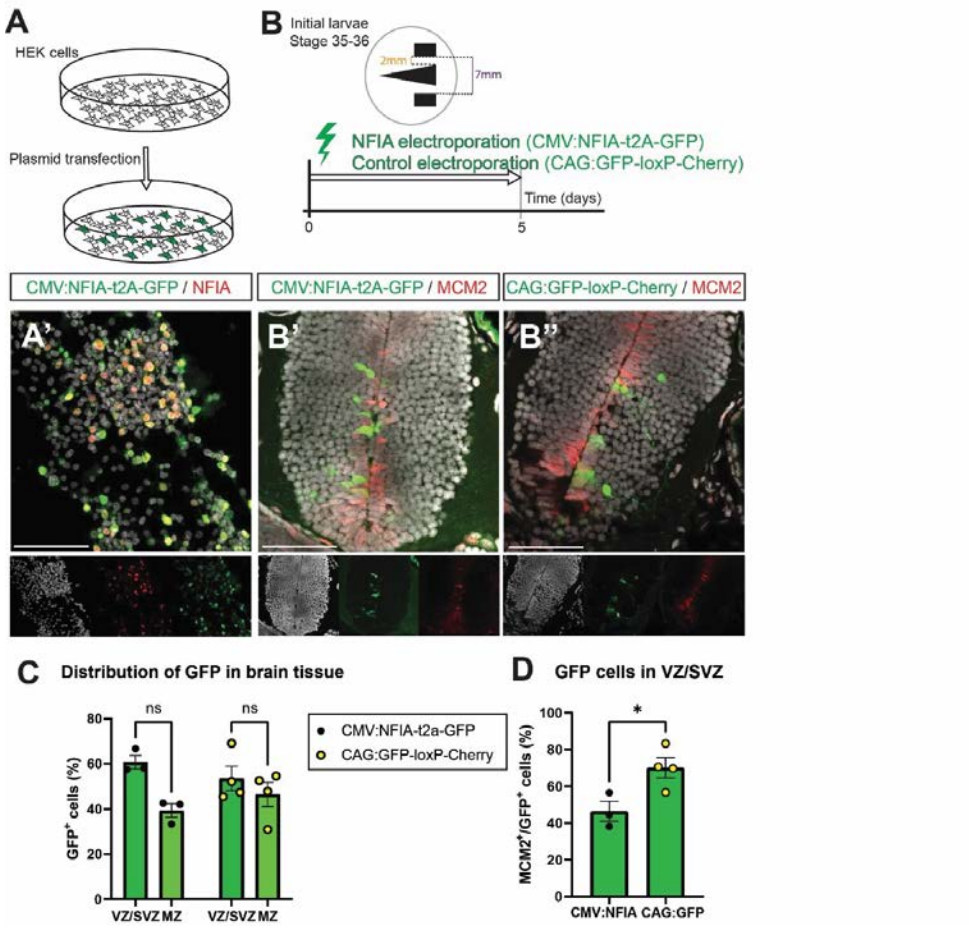

Fig. 39 | (A) Experimental design of in vitro plasmid test. HEK cells were electroporated with the plasmid CMV: NFIA -t2A-GFP. A'.Immunostaining for GFP and NFIA demonstrates that the plasmid generated can induce the production of both GFP and NFIA in HEK cells. Scale bar: 100 µm. **(B)** Experimental design for larva electroporation. Stage 35-36 larvae were electroporated with either the plasmid CMV: NFIA -t2A-GFP or a control plasmid expressing GFP. Tissue was collected 5 days later for analysis. B'., B''. Representative images of sections analyzed. Scale bar: 100 µm. (C) Quantification of the percentage of GFP+ cell distribution showed no statistically significant differences between groups. Two-way ANOVA with Bonferroni's multiple comparisons test. *$p<0.05$. Means ± s.e.m. are shown. (D) The GFP+ cells containing ectopic expression of NFIA proliferated less than the control electroporation ones. T-test. Means ± s.e.m. are shown.

4.3. Dopaminergic injury response in the newt midbrain

Our laboratory has elucidated cellular and molecular mechanisms of dopaminergic regenerative neurogenesis in a 6-OHDA-induced Parkinsonian model in newts (Berg et al., 2010; Berg et al., 2011; Hameed et al., 2015; Joven et al., 2018; Parish et al., 2007)). In this section, I describe my findings using the latest technologies. These findings increase our understanding of the early response to dopaminergic ablation, the innate immune system, and the re-activation of stem cells. In the following experiments I always compared three conditions: 6-OHDA intraventricular injection (6-OHDA), sham intraventricular injection (sham) and uninjured controls (control).

4.3.1. The role of NFI in dopaminergic injury response

In the previous section, I showed how NFI expression first appears in the developing ventral midbrains when the ependymoglia is acquiring quiescence, and how overexpression of these transcription factors decreases proliferation. These observations led me to hypothesize that *Nfi* factors may also play a role during the injury response, as it has been shown in zebrafish (Hoang et al., 2020). First NFIA expression patterns was determined after dopaminergic injury (**Fig. 40A**). As predicted, NFIA labeling was weak in the 6-OHDA treated animals at 14 days post injury (d.p.i.) (**Fig. 40B**). Quantifications of TH^+ cells were used to confirm successful dopaminergic ablations (**Fig. 40C, F**). The percentage of NFI^+ cells in the innermost layer which was closest to the ventricle (SVZ) confirmed a downregulation of NFI in both 6-OHDA and sham groups at 7 d.p.i. (**Fig. 40D**), which correlated with a non-significant trend of increased proliferation, as measured by the percentage of $MCM2^+$ ependymoglia (**Fig. 40E**). This downregulation of NFI in sham implies that the instant injury response could also inhibit the expression of NFI in neural progenitor cells. However, at 14 d.p.i., the downregulation of NFI was only seen in the 6-OHDA group **(Fig. 40G)**, together with a significant increase in ependymoglial cell proliferation **(Fig. 40H)**. These results indicate a difference between *Pleurodeles* and mammals in regulating injury response: *Pleurodeles* induces ventricular glial cell proliferation by a long-lasting downregulation of NFI, while mammals do not (Hoang et al., 2020).

Given the relationship between NFI expression levels and proliferative activity of ependymoglia showed in both development and dopaminergic injury response, I wanted to explore if the proliferation of ependymoglia after dopaminergic injury could be suppressed by manipulating NFI expression as shown in a previous study (Martynoga et al., 2013). To fulfil the goal, I conducted dopaminergic ablation on late active larvae. Eleven days after ablating the dopaminergic neurons, intraventricular injection was performed followed by electroporation of either the plasmid "CMV: NFiA-t2A-tGFP" or a control plasmid "CAG: GFP-loxp-Cherry", i.e., the two plasmids mentioned before (**Fig. 41A, B)**. The success of the dopaminergic ablation was determined: TH^+ cells were significantly reduced in both 6-OHDA groups, with no differences in the amount of TH^+ cells irrespective of which plasmid was electroporated. (**Fig. 41C).** The proliferation activity of the GFP^+ cells at 13 d.p.i. upon dopaminergic damage decreased when NFiA was overexpressed (**Fig. 41D)**. In combination with my results in **Fig. 40**, this result indicates that NFI factors could directly or indirectly regulate ependymoglial proliferation after dopaminergic lesion in newts. To really define if NFIA is important for generation of TH neurons from the ependymoglia upon 6-OHDA, genetic lineage tracing experiments linked to overexpression of NFIA is the next set of experiments to be performed.

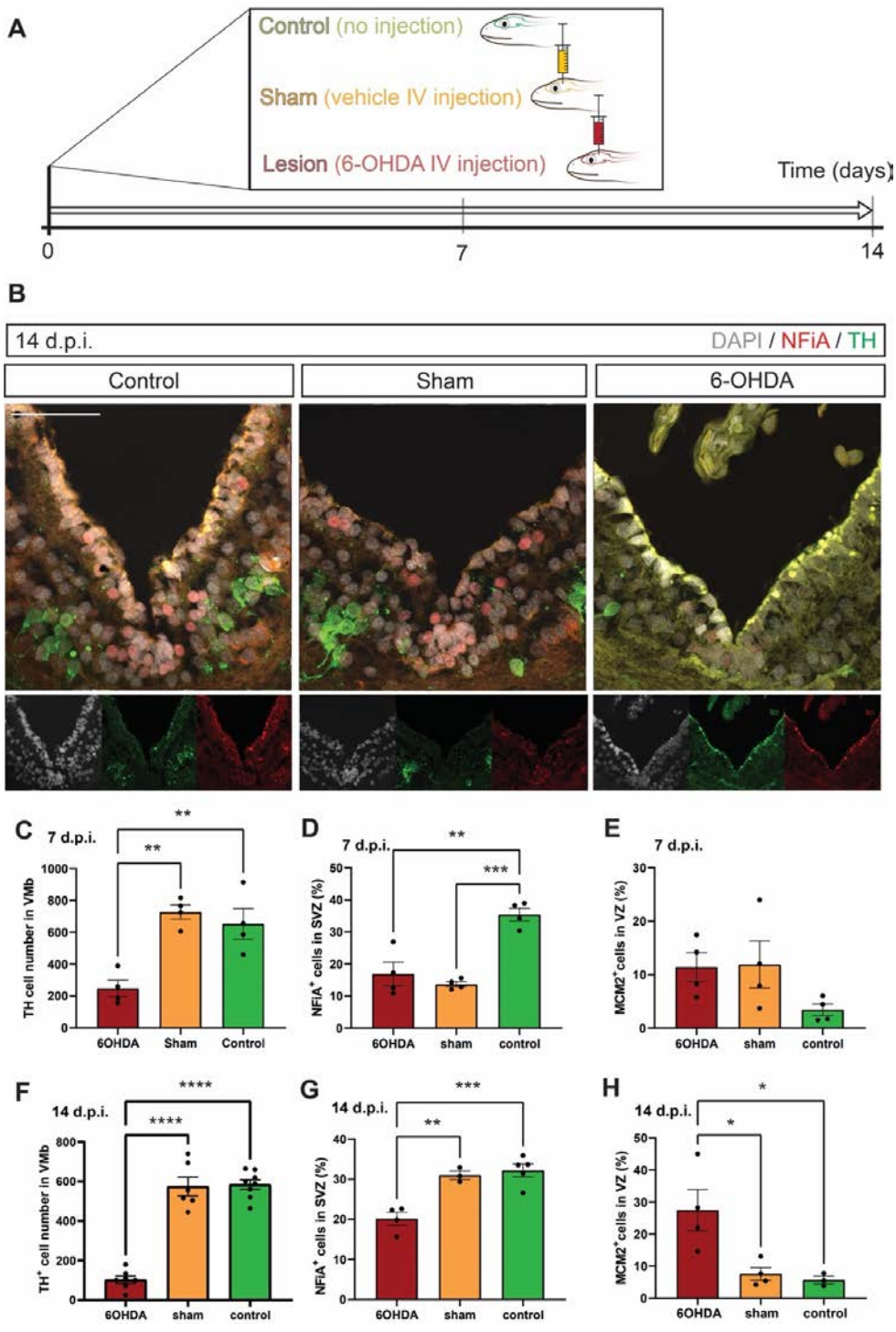
A
Control (no injection)
Sham (vehicle IV injection)
Lesion (6-OHDA IV injection)
Time (days)
0
7
14
B
14 d.p.i.
DAPI / NFiA / TH
Control
Sham
6-OHDA
C
7 d.p.i.
TH cell number in VMb
6OHDA
Sham
Control
D
7 d.p.i.
NFiA+ cells in SVZ (%)
6OHDA
sham
control
E
7 d.p.i.
MCM2+cells in VZ (%)
6OHDA
sham
control
F
14 d.p.i.
TH+ cell number in VMb
6OHDA
sham
control
G
14 d.p.i.
NFiA+ cells in SVZ (%)
6OHDA
sham
control
H
14 d.p.i.
MCM2+cells in VZ (%)
6OHDA
sham
control

Fig. 40 (previous page) | Expression of NfiA in newt ventral midbrain after 6-OHDA-mediated dopaminergic lesion. (A) Schematic drawing showing the experimental design. Adult newts were used (n=4-7 animals/timepoint and condition). **(B)** Representative images of ventral midbrain sections showing the expression of NFIA and TH at 14 d.p.i.. Scale bar: 100 µm. **(C)-(E)** Quantifications at 7 d.p.i.. **(F)-(H)** Quantifications at 14 d.p.i.. **(C)** and **(F)** show total number of TH^+ cells. **(D) and (G)** show percentage of $NFIA^+$ cells in the SVZ (quantification was conducted in the innermost layer which was closest to the ventricle). **(E)** and **(H)** show percentage of $MCM2^+$ cells in the VZ. Ordinary one-way ANOVA with Bonferroni's multiple comparisons test. *p<0.05, **p<0.01, ***p<0.001, ****p<0.0001. Means ± s.e.m. are shown.

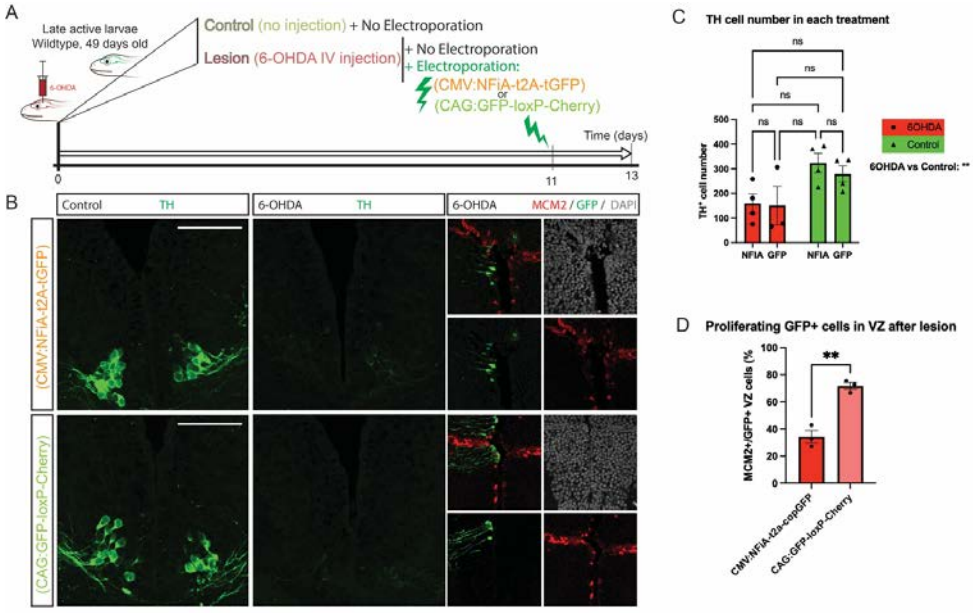

Fig. 41 | Manipulation of NfiA in ependymoglia of midbrain after dopaminergic lesion. (A) Schematic drawing showing the experimental design. Larval newts were used (n=4 animals/timepoint and condition). **(B)** Representative images of ventrally-electroporated brain sections showing the expression of TH, GFP and MCM2 at 13 d.p.i. after 6-OHDA. The electroporated plasmid is indicated in the left. Scale bar: 100 µm. **(C)** Quantifications at 13 d.p.i. showing the total number of TH^+ cells. Two-way ANOVA with Bonferroni's multiple comparisons test. **p<0.01. Mean ± s.e.m. is shown. **(D)** Percentage of $MCM2^+$ cells in the GFP^+ ependymoglia at 13 d.p.i. shows a significant decrease in proliferation upon overexpression of NfiA. T-test. **p=0.0021. Mean ± s.e.m. is shown.

4.3.2. Bulk RNAseq of newt ventral midbrains reveals gene regulatory networks

Dopaminergic injury response is a complex process which cannot be achieved solely with NFI (Berg et al., 2011; Hameed et al., 2015; Joven et al., 2018). To uncover the genes involved in the 6-OHDA-mediated re-activation of ependymoglial proliferation, I performed bulk RNAseq, a powerful next generation sequencing method for monitoring changes in gene expression under different conditions. I sequenced samples from freshly dissected ventral midbrains (n=2 samples per condition, each sample was pooled with 2 ventral midbrains) at 14 d.p.i., when the proliferation of ependymoglia is at its peak in 6-OHDA condition but not significantly increased in the sham group compared to control **(Fig. 40 H)**.

After processing the raw data, I first assessed sample-to-sample variability. The data was normalized by variance stabilizing transformations (VST) and plotted the samples in a distance plot and a PCA **(Fig. 42)**. The injured and the control samples clustered separately by PC2, but not by PC1. 31% of the variance between the experimental groups could be explained by PC2 **(Fig. 42B)**. Although it would have been beneficial to include additional samples, the present results (displayed and discussed later) were enough to reveal several of the molecular pathways implicated in the injury responses. I compared the conditions between them and found multiple up- and downregulated genes. I then analyzed the genes that fulfilled the criteria of a statistically significant difference in gene expression (padj<0.05) as well as a |log2FC|>1. I next added the annotations and found the human gene orthologues where possible. I used the latter lists of genes to perform functional gene ontology (GO) enrichment analysis using the web server g:Profiler (Raudvere et al., 2019). This analysis was used to uncover key biological processes and transcription factors involved in the newt midbrain response to 6OHDA injury.

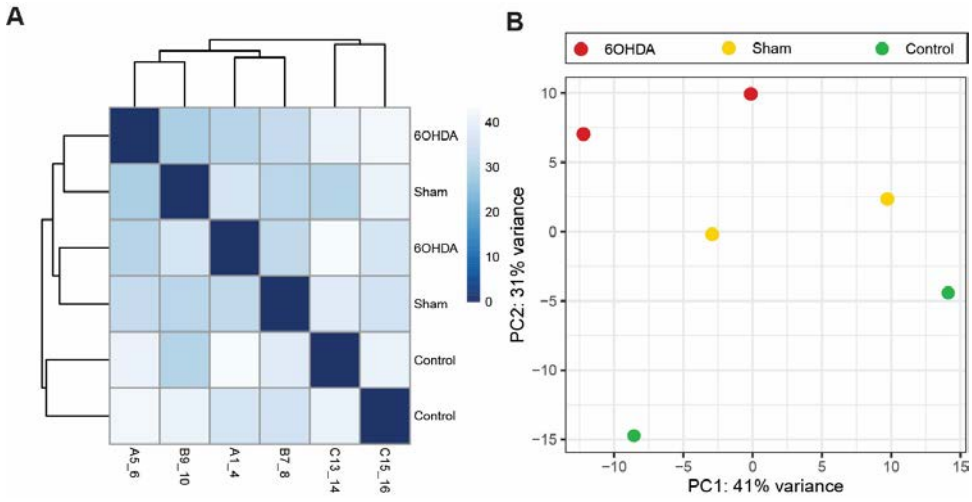

Fig. 42 | Assessment of sample-to-sample variability. (A) Distance plot of the samples analyzed. **(B)** PCA showing the variability among the samples analyzed by bulk RNAseq.

Given injury responses happened in both 6-OHDA and sham conditions, the first step was to characterize the responses that were not unique from dopaminergic damage. To fulfil the goal, I first compared sham versus control samples. I found 16 downregulated and 81 upregulated newt genes (**Fig. 43**). Of the 16 downregulated genes, 13 had a human orthologue. The 13 orthologues showed few hits in the GO analysis: miRNA:hsa-miR-335-5p and skin disease related signaling pathways (**Fig. 44**). 52 out of the 81 upregulated newt genes could be analyzed using human orthologues for GO, showing strong upregulation of immune system-related processes (**Fig. 44**). The results agree with the expectation of immune responses which are usually turned on after injury (Kirkham et al., 2011).

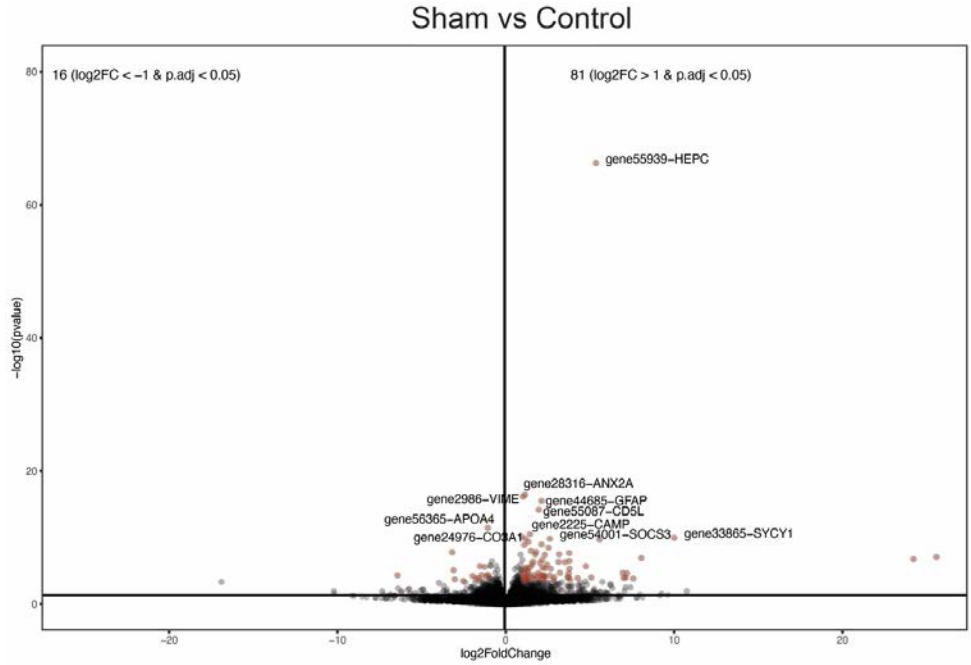

Fig. 43 | Volcano plot showing the differentially expressed genes (dots) in sham versus control experimental conditions. Genes with both a p.adj<0.05 and $|\log_2 FC|>1$ are shown in red (16 downregulated genes and 81 upregulated genes). For clarity, only the top 10 hits are annotated in the figure.

Since ependymoglial reactivation only happened after dopaminergic injury, it can be assumed that certain elements specific in 6-OHDA samples are responsible for the reactivation. Before pinpointing the elements, the total responses from 6-OHDA samples need to be analyzed. I compared 6-OHDA samples to control samples, found 27 downregulated and 364 upregulated genes (**Fig. 45**). Of these, 17 and 266, respectively could be assigned a human orthologue. As expected, dopaminergic neuron-related biological processes were significantly downregulated (**Fig. 46A**). The most significantly upregulated genes were still related to immune response processes, and vesicle-related signaling pathways showed higher expression in 6-OHDA. (**Fig. 46B**). Noticing many immune response processes and vesicle-related signaling pathways were also detected in "sham vs control" (**Fig. 44B**), it can be speculated that these signaling pathways are not specific for inducing ependymoglial reactivation.

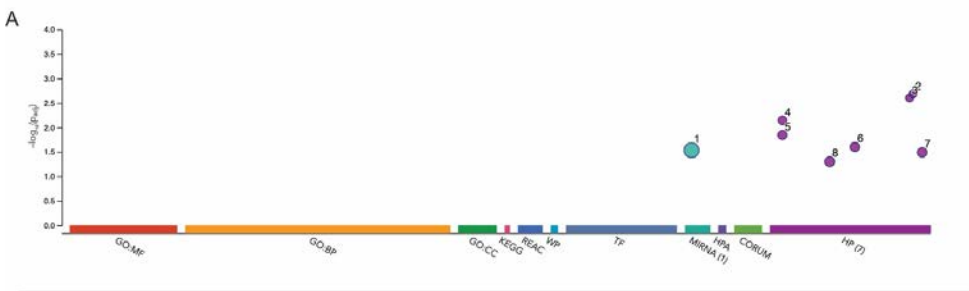

ID	Source	Term ID	Term Name	p_{adj} (query_1)
1	MIRNA	MIRNA:hsa-miR-335-5p	hsa-miR-335-5p	2.926×10^{-2}
2	HP	HP:0045059	Hyperkeratotic papule	2.069×10^{-2}
3	HP	HP:0040154	Acne inversa	2.483×10^{-3}
4	HP	HP:0001806	Onycholysis	7.147×10^{-3}
5	HP	HP:0001805	Onychogryposis	1.422×10^{-2}
6	HP	HP:0012514	Lower limb pain	2.505×10^{-2}
7	HP	HP:0200035	Skin plaque	3.239×10^{-2}
8	HP	HP:0009763	Limb pain	4.988×10^{-2}

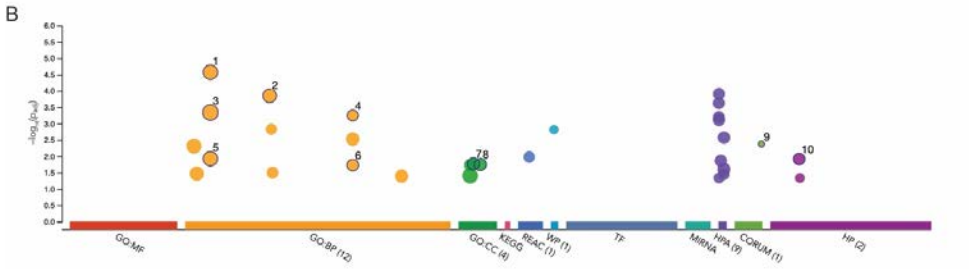

ID	Source	Term ID	Term Name	p_{adj} (query_1)
1	GO:BP	GO:0006955	immune response	2.652×10^{-5}
2	GO:BP	GO:0034097	response to cytokine	1.399×10^{-4}
3	GO:BP	GO:0006950	response to stress	4.551×10^{-4}
4	GO:BP	GO:0071346	cellular response to type II interferon	5.607×10^{-4}
5	GO:BP	GO:0006952	defense response	1.186×10^{-2}
6	GO:BP	GO:0071356	cellular response to tumor necrosis factor	1.868×10^{-2}
7	GO:CC	GO:0034774	secretory granule lumen	1.692×10^{-2}
8	GO:CC	GO:0060205	cytoplasmic vesicle lumen	1.781×10^{-2}
9	CORUM	CORUM:7385	DTX3L-PARP9-STAT1 complex	4.192×10^{-3}
10	HP	HP:0004332	Abnormal lymphocyte morphology	1.213×10^{-2}

Fig. 44 | g:GOSt multiquery Manhattan plot of downregulated (A) and upregulated (B) genes in sham compared to control experimental conditions. X-axis shows the functional terms grouped and colour-coded by data source. The most significant biological processes are shown as pinned circles with a numeric ID and are described in more detail in the table below the image.

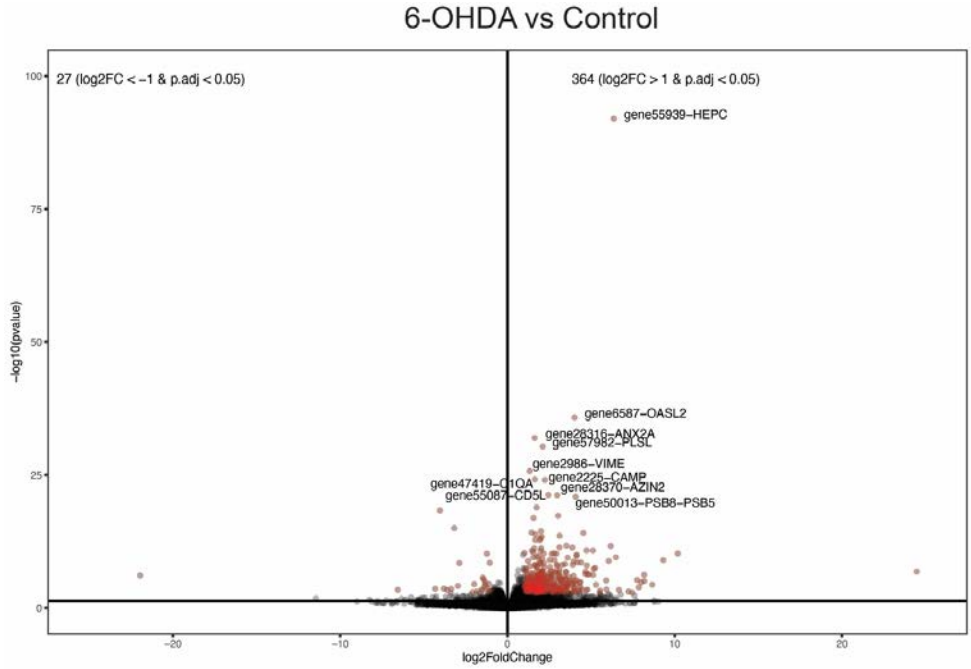

Fig. 45 | Volcano plot showing the differentially expressed genes (dots) in 6-OHDA versus control experimental conditions. Genes with both a p.adj<0.05 and $|\log_2 FC|>1$ are shown in red (27 downregulated genes and 364 upregulated genes). For clarity, only the top 10 hits are annotated in the figure.

To uncover the genes involved in the specific response to ependymoglial reactivation after dopaminergic loss, I compared 6-OHDA samples to sham samples. In the 6-OHDA, I found 22 downregulated and 45 upregulated genes with padj<0.05 and |log2FC|>1 cutoff (**Fig. 47**). The top downregulated genes included *gene40104-ST3A1, gene6704-SC6A4, gene28570-TY3H* and *gene62032-GCH1*, which again confirmed the successful ablation of dopaminergic neurons. Interestingly, multiple processes related to Parkinson disease were found to be related to these genes, including cognition, learning and memory, social behavior, dopamine biosynthesis, monoamine transport and postural tremor (**Fig. 48**). This is an expected result further supporting the successful dopaminergic lesion. Two of the upregulated genes identified here were *gene57982-PLSL* and *gene49975-2B1A*, which are related to the immune system. Of the downregulated genes, 17 were assigned to a human orthologue. The Reactome results pointed to a downregulation of genes involved in NGF-stimulated transcription, nuclear events (kinase and transcription factor activation) and NTRK1 signaling (**Fig. 48A**). I found 34 upregulated genes that could be assigned to human orthologues. The GO analysis showed upregulated processes including cell adhesion molecule binding, podosome, CAPG-PRMT5 complex, extracellular organization and immune response (**Fig. 48B**). Considering that the functions of immunity in salamander regeneration are not well understood (Bolanos-Castro et al., 2021), I had a closer look into the immune upregulated processes. Among the immune signaling pathways, I found upregulation of MHC protein complex binding, type-II interferon signaling, IL-4, IL-13, IL-6 and IL-18 signaling pathways.

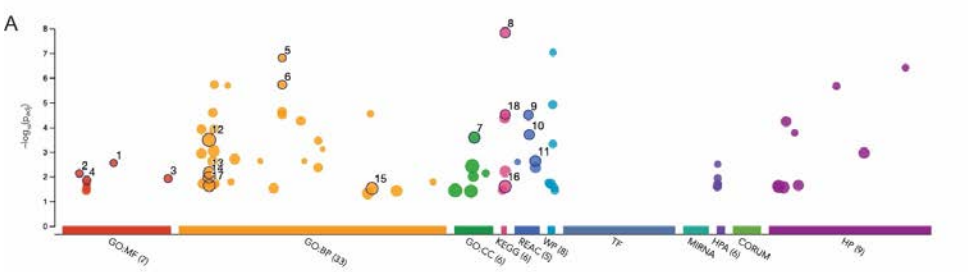

ID	Source	Term ID	Term Name	p_{adj} (query_1)
1	GO:MF	GO:0035240	dopamine binding	2.795×10^{-3}
2	GO:MF	GO:0008504	monoamine transmembrane transporter activity	7.309×10^{-3}
3	GO:MF	GO:1901338	catecholamine binding	1.208×10^{-2}
4	GO:MF	GO:0015378	sodium:chloride symporter activity	1.393×10^{-2}
5	GO:BP	GO:0042416	dopamine biosynthetic process	1.550×10^{-7}
6	GO:BP	GO:0042423	catecholamine biosynthetic process	1.867×10^{-6}
7	GO:CC	GO:0044306	neuron projection terminus	2.576×10^{-4}
8	KEGG	KEGG:05031	Amphetamine addiction	1.455×10^{-8}
9	REAC	REAC:R-HSA-9031628	NGF-stimulated transcription	3.181×10^{-5}
10	REAC	REAC:R-HSA-198725	Nuclear Events (kinase and transcription factor activation)	1.988×10^{-4}
11	REAC	REAC:R-HSA-187037	Signaling by NTRK1 (TRKA)	2.287×10^{-3}
12	GO:BP	GO:0007610	behavior	3.226×10^{-4}
13	GO:BP	GO:0007612	learning	6.787×10^{-3}
14	GO:BP	GO:0007568	aging	1.073×10^{-2}
15	GO:BP	GO:0099003	vesicle-mediated transport in synapse	3.006×10^{-2}
16	KEGG	KEGG:05012	Parkinson disease	2.487×10^{-2}
17	GO:BP	GO:0007626	locomotory behavior	2.295×10^{-2}
18	KEGG	KEGG:05030	Cocaine addiction	3.069×10^{-5}

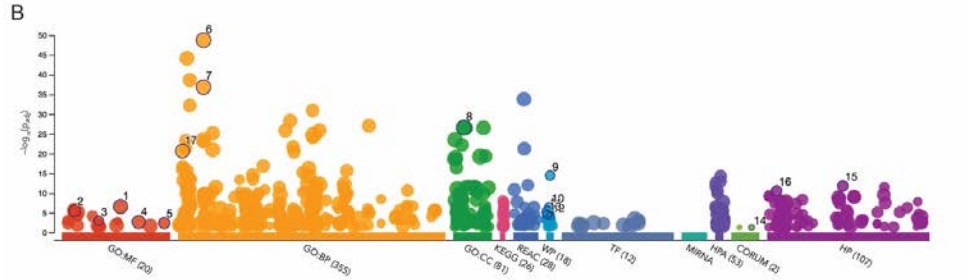

ID	Source	Term ID	Term Name	p_{adj} (query_1)
1	GO:MF	GO:0044877	protein-containing complex binding	2.521×10^{-7}
2	GO:MF	GO:0005178	integrin binding	3.231×10^{-6}
3	GO:MF	GO:0023023	MHC protein complex binding	9.708×10^{-4}
4	GO:MF	GO:0050839	cell adhesion molecule binding	2.105×10^{-3}
5	GO:MF	GO:0140375	immune receptor activity	3.852×10^{-3}
6	GO:BP	GO:0006955	immune response	1.698×10^{-49}
7	GO:BP	GO:0006952	defense response	1.270×10^{-37}
8	GO:CC	GO:0031410	cytoplasmic vesicle	2.789×10^{-27}
9	WP	WP:WP3937	Microglia pathogen phagocytosis pathway	3.342×10^{-15}
10	WP	WP:WP619	Type II interferon signaling	3.700×10^{-7}
11	WP	WP:WP5090	Complement system in neuronal development and plasticity	4.747×10^{-6}
12	WP	WP:WP4146	Macrophage markers	6.825×10^{-5}
13	WP	WP:WP545	Complement activation	3.006×10^{-5}
14	CORUM	CORUM:6418	C1q complex	4.973×10^{-2}
15	HP	HP:0011450	Unusual CNS infection	1.575×10^{-12}
16	HP	HP:0001287	Meningitis	2.494×10^{-11}
17	GO:BP	GO:0001775	cell activation	2.059×10^{-21}

Fig. 46 | g:GOSt multiquery Manhattan plot of downregulated (A) and upregulated (B) genes in 6-OHDA compared to control experimental conditions. X-axis shows the functional terms grouped and colour-coded by data source. The most significant biological processes are shown as pinned circles with a numeric ID and are described in more detail in the table below the image.

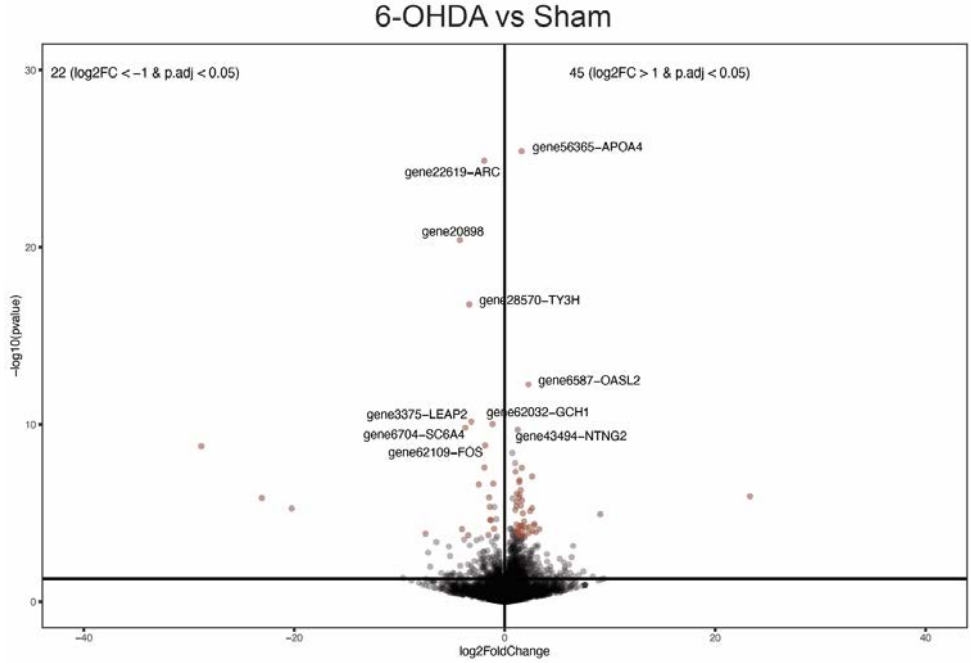

Fig. 47 | Volcano plot showing the differentially expressed genes (dots) in 6-OHDA versus sham experimental conditions. Genes with both a p.adj<0.05 and $|\log_2 FC|>1$ are shown in red (22 downregulated genes and 45 upregulated genes). For clarity, only the top 10 hits are annotated in the figure.

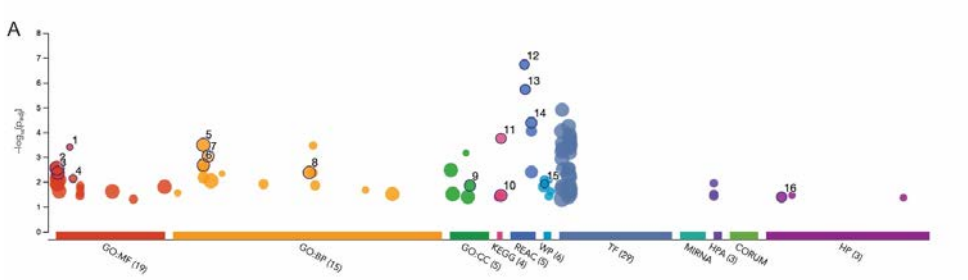

ID	Source	Term ID	Term Name	p_{adj} (query_1)
1	GO:MF	GO:0005335	serotonin:sodium:chloride symporter activity	4.000×10^{-4}
2	GO:MF	GO:0000978	RNA polymerase II cis-regulatory region sequence-specific DNA binding	2.747×10^{-3}
3	GO:MF	GO:0001228	DNA-binding transcription activator activity, RNA polymerase II-specific	4.332×10^{-3}
4	GO:MF	GO:0008504	monoamine transmembrane transporter activity	7.309×10^{-3}
5	GO:BP	GO:0007610	behavior	3.226×10^{-6}
6	GO:BP	GO:0007611	learning or memory	2.080×10^{-3}
7	GO:BP	GO:0009636	response to toxic substance	9.057×10^{-4}
8	GO:BP	GO:0050890	cognition	4.156×10^{-3}
9	GO:CC	GO:0044306	neuron projection terminus	1.401×10^{-2}
10	KEGG	KEGG:05012	Parkinson disease	3.485×10^{-2}
11	KEGG	KEGG:05031	Amphetamine addiction	1.761×10^{-4}
12	REAC	REAC:R-HSA-9031628	NGF-stimulated transcription	1.862×10^{-7}
13	REAC	REAC:R-HSA-198725	Nuclear Events (kinase and transcription factor activation)	1.898×10^{-6}
14	REAC	REAC:R-HSA-187037	Signaling by NTRK1 (TRKA)	4.146×10^{-5}
15	WP	WP:WP3944	Serotonin and anxiety-related events	1.205×10^{-2}
16	HP	HP:0002174	Postural tremor	4.096×10^{-2}

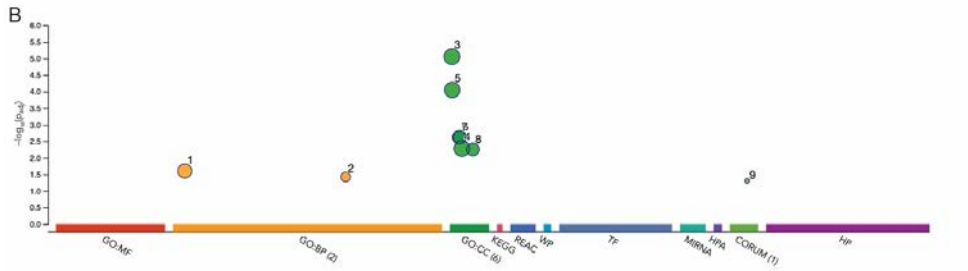

ID	Source	Term ID	Term Name	p_{adj} (query_1)
1	GO:BP	GO:0002684	positive regulation of immune system process	2.486×10^{-2}
2	GO:BP	GO:0071711	basement membrane organization	3.768×10^{-2}
3	GO:CC	GO:0005576	extracellular region	8.719×10^{-6}
4	GO:CC	GO:0031982	vesicle	5.214×10^{-3}
5	GO:CC	GO:0005615	extracellular space	8.854×10^{-5}
6	GO:CC	GO:0031012	extracellular matrix	2.365×10^{-3}
7	GO:CC	GO:0030312	external encapsulating structure	2.392×10^{-3}
8	GO:CC	GO:0062023	collagen-containing extracellular matrix	5.569×10^{-3}
9	CORUM	CORUM:5691	TALL1 homo-oligomer complex	4.968×10^{-2}

Fig. 48 | g:GOSt multiquery Manhattan plot of downregulated (A) and upregulated (B) genes in 6-OHDA and sham conditions. The X-axis shows the functional terms grouped and colour-coded by data source. The most significant biological processes are shown as pinned circles with a numeric ID and are described in more detail in the table below the image.

4.3.3. Newt brain injury response: cellular players and molecular mechanisms indicated by snRNAseq

The bulkRNAseq analysis indicates that specific immune responses could be crucial for ependymoglial reactivation. To reveal a higher resolution of the genes involved in newt brain response to injury, both 6-OHDA and sham injuries were performed followed by snRNAseq. I

analyzed these new data together with the subset of uninjured (naïve) brains of young adults presented in chapter 2, as the nuclei were obtained in the same way and the libraries had similar quality control values (see nFeature and nCount in **Sup. Fig. S3A**). Interestingly, following hierarchical clustering, this dataset contained more clusters at the same resolution values than the previous developmental dataset (compare UMAPs in **Fig. 18B** with **Sup. Fig. S3B**, or ClusTrees in **Fig. 17A** with **Sup. Fig. S3C**), suggesting that additional cell types or states appear in the newt ventral midbrain upon brain injury. Keeping this in consideration, I decided to first analyze the data using a low value of CCA_snn_res, as this clustering was sufficient for me to distinguish the main cell subpopulations of interest based on key markers (**Fig. 49A-B**, **Sup. Fig. S4-S5**). In this dataset, approximately 10000 ±2250 nuclei represent each of the experimental conditions (the exact number of nuclei per condition are provided in **Fig. 49C-E**). The proportion of cell origin for each of the clusters is shown in **Fig. 49F**. All clusters are composed of cells from the three experimental conditions, although in cluster 9, characterized as erythrocytes, the contribution of cells coming from the naïve brains is minor. Remarkably, the 6-OHDA samples contributed with low numbers in the monoaminergic neurons (cluster 8), and with high proportions to several other clusters, including microglia/BAMs (cluster 4), meningeal fibroblasts (cluster 5), OPCs (cluster 7), and neuronal subtypes clusters 12 and 13) **(Fig. 49F)**. While the increase of microglia/BAMs agrees with our bulk RNAseq results (see **4.3.1.**) and previous reports (Kirkham et al., 2011), the increase of meningeal fibroblasts could represent fibrotic scarring or formation of reticular networks similar to the ones reported after neuroinflammation (Dorrier et al., 2022). On the other hand, the increase of OPCs and oligodendrocytes could indicate a stronger protection from myelination on neurons against toxins or immune stresses (Simons and Nave, 2015).

I then decided to explore the differentially expressed genes, with a major focus on trying to understand how the 6OHDA experimental group differed from the other two conditions. I first looked into the expression of the up- and downregulated genes that were found in the previous chapter by bulkRNAseq analysis. Splitting the data by either cluster or experimental condition, I plotted all the hits in violin plots, which highlighted both the number of cells that express a given gene as well as the expression level at which they do so. For most of the cases the snRNAseq correlated well with the pattern predicted by bulkRNAseq analysis (**Sup. Fig. S6-S9**). First, by plotting the RNA assay data into the defined clusters, I could visualize which cell types accounted for the gene expression changes observed in the bulk RNA seq (**Sup. Fig. S6, S8**). I then confirmed these observations by plotting the expression data by experimental condition (**Sup. Fig. S7, S9**). As a proof of concept for this type of analysis, I plotted dopaminergic-related genes and observed a clear downregulation of *Th* genes and *Dat* expression in the 6-OHDA group compared to sham and controls (**Sup. Fig. S10A-C**). On the contrary, *Lmx1b* gene was found to be upregulated after dopaminergic ablation (**Sup. Fig. S10D**).

To illustrate cell-type specific differential gene regulation, I selected three genes from the sham versus 6-OHDA comparison shown in **Fig. 47** that had unveiled information on three clusters of interest in the snRNAseq dataset at CCA_snn_res.0.1 (**Fig. 50 A-F**). Agreeing with the expectation, the newt orthologue of *Ty3h* (TH1) was found to be strongly expressed in cluster 24, the dopaminergic population. For 6-OHDA, fewer cells and transcripts were detected, in line with the bulkRNAseq results (**Fig. 50A-C, Sup. Fig. S10**). *Oasl2*, which is an antiviral enzyme that plays a critical role in cellular innate antiviral response (Eskildsen et al., 2003; Kakuta et al., 2002), was found predominantly in microglia/macrophage cluster and overexpressed specifically in the 6-OHDA lesioned cells (**Fig. 50D-H**). These results indicate that cell type-specific gene expression changes are consistently underlying the response to injury leading to

newt brain regeneration. To reveal more of these unknown cell type-specific changes, I did subsets of the clusters of interest and performed unbiased DEG analysis in the snRNAseq data (**Fig. 50G, Sup. Fig. S11-S12**). This method uncovered a large number of genes with expression changes in different cell types. This provides a framework for generating new hypotheses that will eventually lead to the understanding of cellular and molecular mechanisms by which newts regenerate dopaminergic cells upon injury.

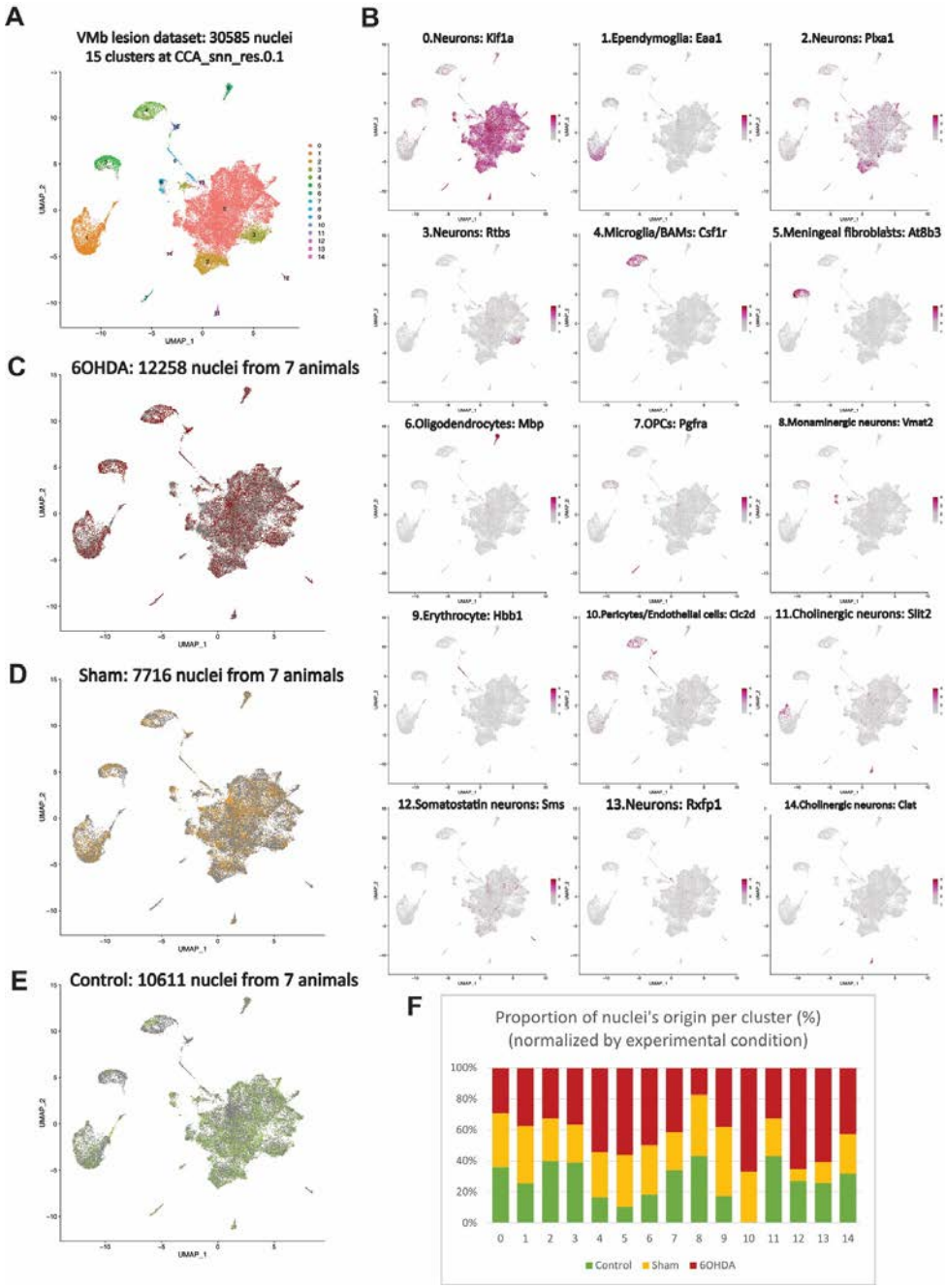

Fig. 49 | Single-nucleus RNAseq analysis of 6OHDA, sham, and control ventral midbrain of young adult newts at 14 d.p.l.. (A) UMAP of 30585 nuclei at CCA_snn_res.0.1. **(B)** Key marker gene of each cluster in the UMAP at CCA_snn_res.0.1. **(C)-(E)** Nucleus of each treatment conditions (6OHDA, sham, and control) on the UMAP. **(F)** Proportions of nucleus of each treatment condition in each cluster at CCA_snn_res.0.1.

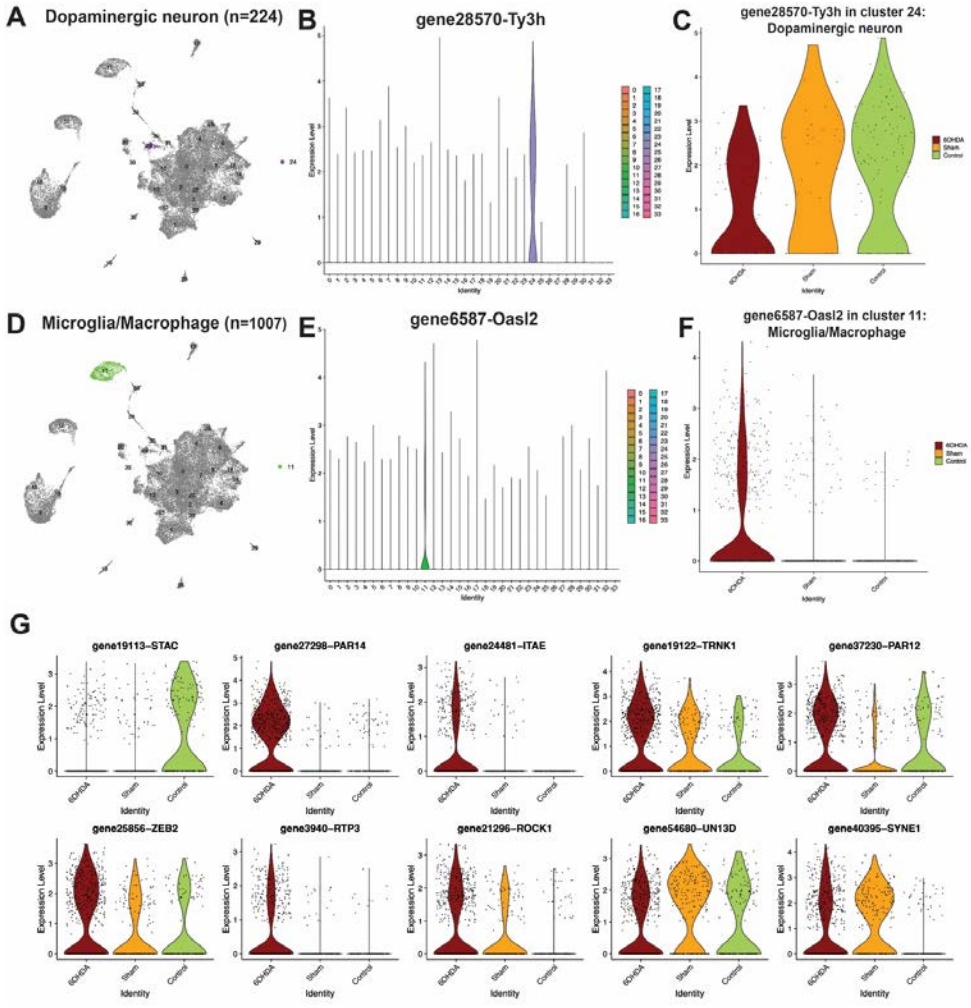

Fig. 50 | BulkRNAseq-based and unbiased DEG analysis in single-nucleus RNAseq dataset. (A)–(F) Analysis of the DEG screened from bulkRNAseq in single-nucleus RNAseq dataset at CCA_snn_res.1. **(G)** Unbiased DEG analysis of microglia/BAMs in single-nucleus RNAseq dataset. All the genes in this figure fulfil Wilcox test of |log2FC|>0.2 and P value<0.01.

4.3.4. Microglia and macrophages are required for the reactivation of ependymoglial cell proliferation

CNS-resident macrophages are composed of parenchymal microglia and border-associated macrophages (BAMs), both contributing to CNS development, homeostasis and diverse pathological states (Mundt et al., 2022). Despite the importance of the innate immune cells in the CNS, the mechanisms by which these cells may act upon neuron-producing glia are unknown. Here, I present the experiments on how BAMs and microglia activate a regenerative response after 6-OHDA injection.

4.3.4.1. Microglia and BAMs' infiltration precedes entry to cell cycle by ependymoglial cells in the VMb

As mentioned before, most of the top differentially expressed genes that was found in the bulk RNAseq data are related to immune processes. Supported by the *in silico* results, I tested the hypothesis that microglia/macrophages may play a key role in the ependymoglial proliferation. I first characterized the midbrains of the transgenic line tgTol2(Dre.mpeg1:eGFP)$^{MHY/SIMON}$ (referred as mpeg1:GFP henceforth) (Tsissios et al., 2023) that had been generated to trace microglia/macrophages. Analysis of co-expression of GFP with IBA1 (Kirkham et al., 2011) **(Fig. 51A-B)** showed that 93.20% of the GFP-expressing cells were positive for IBA1 (n=955 cells). This indicated that the mpeg1:GFP *Pleurodeles* transgenic line is suitable for visualizing innate immune macrophages and resident microglia in the newt brain **(Fig. 51C)**.

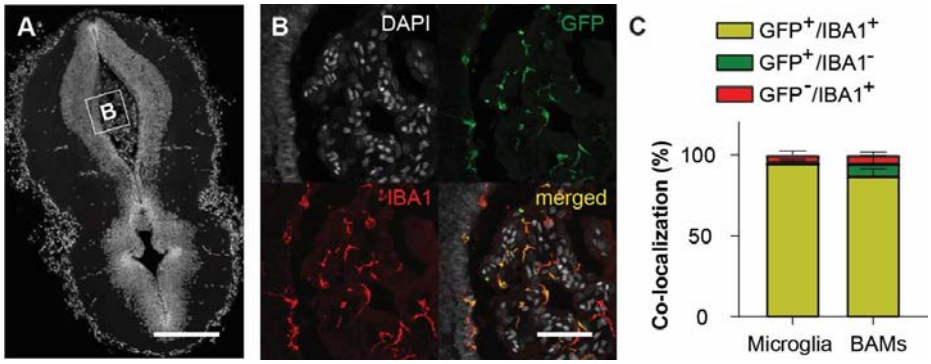

Fig. 51 | Assessment of the expression of IBA1 in mpeg1:GFP positive cells from transgenic newts. (A) Overview of a midbrain section with quantifications were performed. The inset shows the region depicted in (B), containing parenchyma as well as choroid plexus. Scale bar: 500μm. **(B)** Representative image showing IHC against GFP to detect mpeg1+ cells and the use of IBA1 to detect microglia and BAMs. Scale bar: 200μm. **(C)** Quantifications indicated that 95.07% of microglia and 86.99% of BAMs were double labelled by GFP and IBA1. Quantifications were performed on 11 newts (n=435 microglia cells and n=520 BAMs). Mean±SEM.

I next examined the ventral midbrain after 6-OHDA administration. Both naïve brains (uninjured) and sham injured (which entails a mechanical injury by the intraventricular injection procedure, in these cases a similar volume of vehicle was injected) were used as controls **(Fig. 52A)**. From 7 d.p.i., GFP$^+$ cells increased significantly in the 6-OHDA injected brains compared to controls, and the GFP$^+$ cell numbers remained elevated for 30 days **(Fig. 52B-C)**. At 14 d.p.i., I found that the number of GFP$^+$ cells did not significantly differ between sham and control ventral midbrains. However, there were multiple GFP$^+$ cells in the dorsal midbrain, around the area where the brain had been mechanically injured **(Fig. 52C)** . One week later, these cells seemed to have spread throughout the entire midbrain. This was indicated by the increased number in the ventral midbrain at 21 d.p.i. in the sham group, when it reached similar numbers to those observed in the 6-OHDA-injected samples **(Fig. 52C)** . At 28 d.p.i., both 6-OHDA and sham groups displayed fewer GFP$^+$ cells, indicating that the inflammatory response was resolving **(Fig. 52C)** . Next, quantification of MCM2$^+$ in the VZ was used as a proxy to understand the dynamics of ependymoglial proliferation. Importantly, I only detected a statistically significant increase of MCM2$^+$ ependymoglial cells after 6-OHDA injection, the

increase was significant and peaked at 14 d.p.i **(Fig. 52D)**. These results suggest that microglia/macrophages could have a role in ependymoglial reactivation. This indicates a specific early response to 6-OHDA by microglia, since the increased number of microglia at 21 d.p.i. does not lead to an increase in MCM2^{+} ependymoglial cells after sham injury.

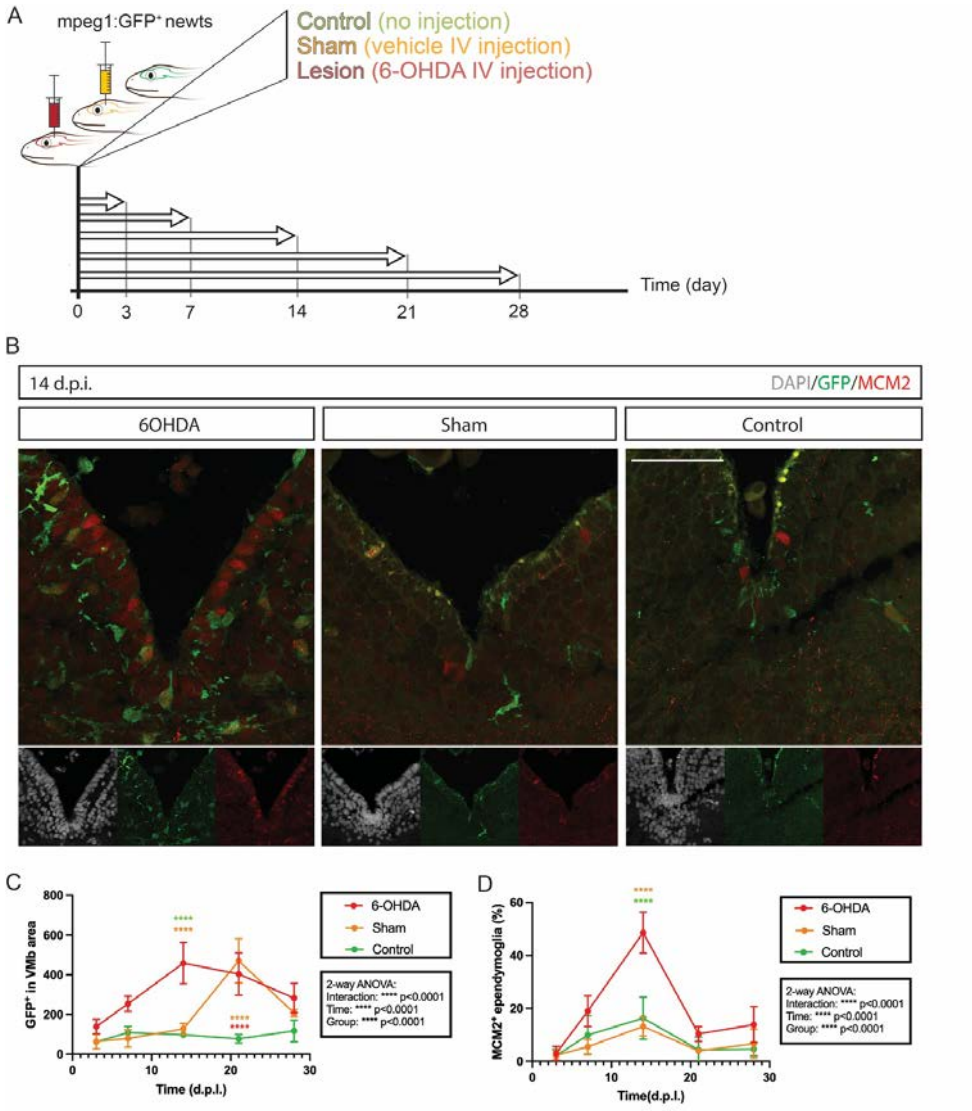

Fig. 52 | Infiltration of microglia/BAMs and reactivation of ependymoglia after dopaminergic injury. (A) Experimental design. **(B)** Representative images of VMb showing GFP+ cells and cells in proliferation (MCM2^{+}) at 14 d.p.i.. Scale bar: 100 µm. **(C)** Quantifications showing GFP+ cell dynamic presence in the VMb after injury. **(D)** The percentage of proliferating VZ cells (MCM2^{+}) indicates the dynamics of ependymoglial proliferation in the VMb. Mean±SEM. In (C) and (D), 2-way ANOVA with Bonferroni's multiple comparisons test was conducted. The statistical details are specified in the figure (n=3-6 newts per condition).

4.3.4.2. Phenotypic changes in microglia/BAMs after lesion

RNA sequencing analyses indicated regulation of immune genes involved in cell motility and shape, but it was unclear if these changes in gene expression could induce noticeable changes in the cell phenotypes of microglia and BAMs in *Pleurodeles*. To test this, I performed a morphological quantitative analysis comparing the circularity of GFP^+ cells across the three conditions. Similar analyses have linked cellular morphology with the diversity of microglial subtypes or states (Paasila et al., 2019). No differences in GFP^+ cell circularity at 7 d.p.i were observed. In addition to the increase in GFP^+ cell number mentioned before **(Fig. 53A)**, changes in the morphology of microglia were detected in 6OHDA and sham at 14, 21, and 28 d.p.i., as well as in BAMs at 21 d.p.i **(Fig. 53B-C)**. Interestingly, the morphology in the microglia at 14 d.p.i. and the BAMs at 21 d.p.i was more dendritic for the 6OHDA group than in the shams **(Fig. 53B-C)**. These results support the hypothesis that the changes in gene expression have a direct effect in the phenotype of VMb-located microglia and BAMs.

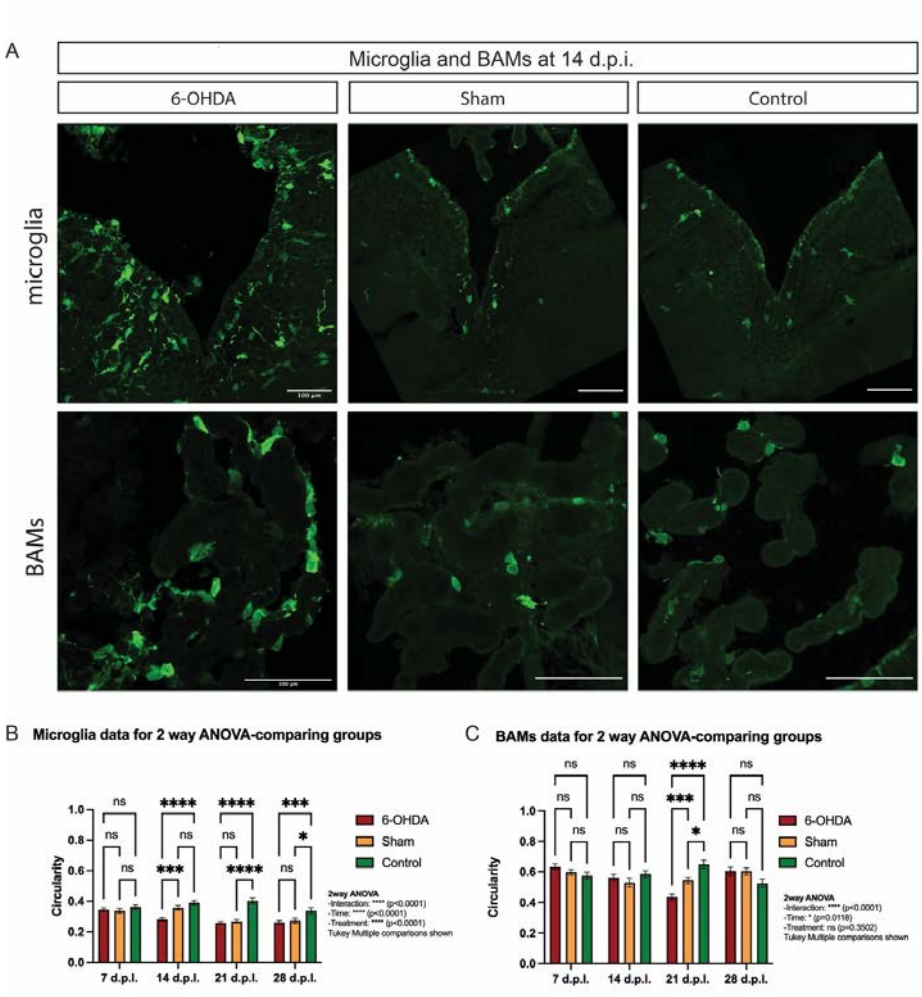

Fig. 53 (previous page) | Circularity of microglia and BAMs. (A) Representative images showing microglia (top row) and BAMs (bottom row) observed at 14 d.p.i.. Scale bar: 100 µm. **(B)** Quantitative analysis on the circularity of GFP^+ cells found in the brain parenchyma indicates a phenotypic transition of microglia towards a more amoeboid morphology in the ventral midbrain. This is noticeable from 14 d.p.i. onwards in the 6-OHDA group and from 21 d.p.i in the sham group. Mean±SEM. Two-way ANOVA with Bonferroni's multiple comparisons test. The statistical details are specified in the figure (n=3 newts per condition). **(C)** Quantitative analysis on the circularity of GFP+ cells found in the choroid plexus and outside of the meninges indicates a transient phenotypic change of BAMs towards a more amoeboid morphology in the ventral midbrain proximity from 14 d.p.i. onwards in the 6-OHDA group and from 21 d.p.i in the sham group. Mean±SEM. Two-way ANOVA with Bonferroni's multiple comparisons test. The statistical details are specified in the figure (n=3 newts per condition).

4.3.4.3. Pharmacological depletion of microglia/BAMs inhibited ependymoglia reactivation in the ventral midbrain after 6-OHDA injection

My results in previous sections as well as the studies from other groups have indicated the indispensable role of microglia/BAMs in ependymoglial reactivation (Mehl et al., 2022). To test the functional significance of the presence of microglia/BAMs, the CSF1R inhibitor PLX3397 was administered, which is a widely used drug to ablate microglia and macrophages (Elmore et al., 2014). I then explored the consequences of immune cell ablation in the context of brain injury **(Fig. 54A)**. Using mpeg1:GFP newts, I next confirmed experimentally that the drug depleted GFP^+ cells in the brain without affecting the ependymoglial population (data not shown). As predicted, the PLX3397 administration did not affect the TH^+ population in any of the experimental conditions **(Fig. 54B)**. Importantly, the CSF1R gene is expressed specifically in the cluster characterized as microglia/BAMs, which suggested that the drug could target these cells also in the newt brain **(Fig. 54C)**. I observed a strong reduction in the number of GFP^+ cells **(Fig. 54D-E)**, leading to a marked reduction in the number of $MCM2^+$ ependymoglial proliferation cells to the levels seen in sham-injected and naïve brains **(Fig. 54D, F)**. This result indicates that the infiltration of activated microglia/macrophages is indispensable for the reactivation of ependymoglial proliferation after dopaminergic injury in the newt ventral midbrain. Studies in recent years have revealed that microglia/macrophages are significant players in mediating repairs or regenerations in both newts and mammals (Bellver-Landete et al., 2019; Kyritsis et al., 2012; Li et al., 2020; Tsissios et al., 2023). One previous study revealed a role of microglia/macrophages in regulating ependymoglia proliferation after dopaminergic lesion in zebrafish (Caldwell et al., 2019). However, this study did not examine the effect after a specific ablation of the microglia/macrophages, also it did not explore the roles of subtypes of microglia/macrophages. My data of microglia/macrophage ablation and RNAseq can fill in this gap. Furthermore, it will be valuable to conduct cross-species comparison on their populations and examine if they make a difference in regulating the regeneration ability.

Fig. 54 (next page) | Microglia/BAMs ablation after dopaminergic damage. (A) Experimental design: at 7 d.p.i. after 6-OHDA injection/sham, the CSF1R inhibitor PLX3397 was administered intraperitoneally every 48h to mpeg1:GFP transgenic *Pleurodeles waltl*, except for the last dose which was given 24 hours after the previous one. Tissue analysis was performed at 14 d.p.i. **(B)** The PLX3397 treatment did not affect the numbers of TH^+ cells in the VMb in any of the experimental groups. **(C)** UMAP showing the expression of CSF1R in the snRNAseq injury dataset (top). Violin plot demonstrating that the CSF1R expression is specific of the microglia/BAMs cluster (bottom). **(D)** Representative images showing the effect of dopaminergic chemical ablation followed by microglia/BAMs depletion on the presence of GFP+ cells and the proliferation of ependymoglia. Scale bar: 100 µm. **(E)** PLX3397 treatment strikingly reduced the GFP+ cells in the VMb after 6-OHDA. **(F)** PLX3397 treatment prevented the 6-OHDA injury-induced proliferative response of ependymoglia, not affecting the baseline in the other two experimental groups. For (B), (E), and (F), Mean±SEM. Two-way ANOVA with Bonferroni's multiple comparisons test. The statistical details are specified in the figure (**$p<0.05$, ***$p<0.001$, ****$p<0.0001$; n=3 to 6 newts per condition).

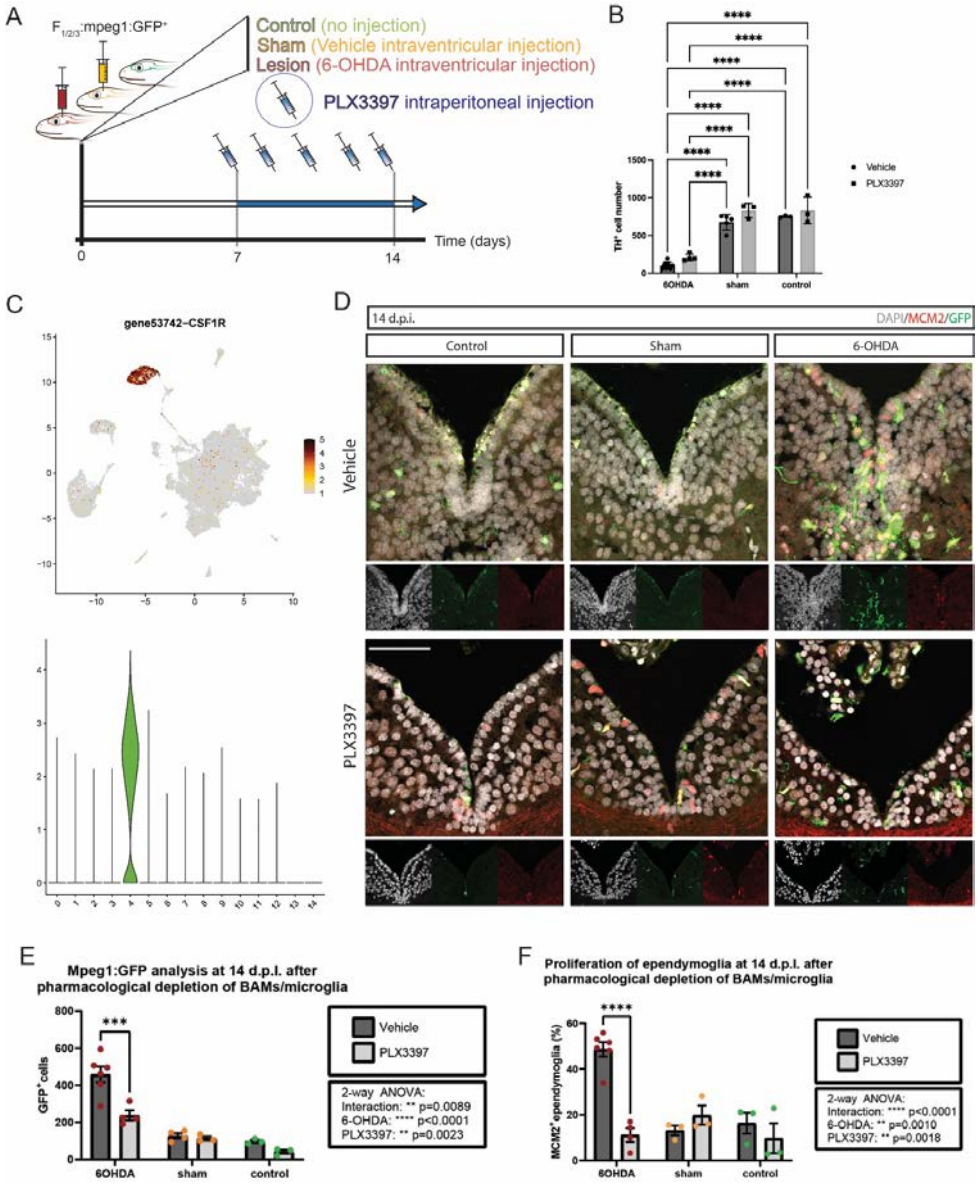
A
F1/2/3:mpeg1:GFP+
Control (no injection)
Sham (Vehicle intraventricular injection)
Lesion (6-OHDA intraventricular injection)
PLX3397 intraperitoneal injection
Time (days)
0
7
14
B
TH+ cell number
6OHDA
sham
control
Vehicle
PLX3397
C
gene53742-CSF1R
D
14 d.p.i.
DAPI/MCM2/GFP
Control
Sham
6-OHDA
Vehicle
PLX3397
E
Mpeg1:GFP analysis at 14 d.p.i. after pharmacological depletion of BAMs/microglia
GFP+cells
Vehicle
PLX3397
2-way ANOVA:
Interaction: ** p=0.0089
6-OHDA: **** p<0.0001
PLX3397: ** p=0.0023
F
Proliferation of ependymoglia at 14 d.p.i. after pharmacological depletion of BAMs/microglia
MCM2+ependymoglia (%)
2-way ANOVA:
Interaction: **** p<0.0001
6-OHDA: ** p=0.0010
PLX3397: ** p=0.0018

5. PERSPECTIVE

5.1. *Pleurodeles waltl* in the genomic era: progress and limitations

The genomic toolkit for newt research has dramatically improved during the past decade. The advance comes mainly from two areas: genome and transcriptome sequences as well as methods for genetic modifications such as transgenesis and mutations using CRISPR technologies. While random insertion of exogenous DNA into the genome has been feasible for a long time, the recent chromosome scale assembly of the of *Pleurodeles waltl* genome provides unprecedented opportunities to functionally probe key genes during development and regeneration by targeting various loci. The available sequences also allow for identification of both evolutionarily conserved as well species-specific genomic elements. An important example for the latter is the expansion of certain transposable elements and miRNAs (Brown et al., 2022; Elewa et al., 2017). However, a current limitation is the still preliminary nature of gene annotations resulting in a substantial number of unannotated sequences (Brown et al., 2022). It remains to be seen whether these sequences represent bona fide species-specific innovations or that they will be classified as non-coding regions as the community will refine the annotation. Relating the unannotated sequences to RNA sequences in transcriptomes could be a way forward to identify those that are never expressed in any of the analyzed tissues. There are also several examples of gene duplications in the *Pleurodeles waltl* genome. At present it is not totally known either if in the cases of duplicated genes, both copies are used in different contexts or if one of the copies represents a pseudogene. Although there are several examples of such duplications, the *Pleurodeles waltl* genome does not seem to have undergone major genome wide duplication of the kind that is observed in teleosts (Jaillon et al., 2004). This poses also a challenge to predict which loci should be targeted using CRISPR/Cas9 mediated genome modifications. Nevertheless, the existing tools offer already today a variety of versatile approaches to functionally probe various signaling pathways and to track cells as well as their progeny during regeneration.

5.2. Cross-species comparative analyses of cell types

scRNAseq /and snRNAseq analyses are powerful to discern cell types from each other in a mixed population. It is of course important to make a distinction between the notion of cell cluster generated by an algorithm and a cell type. The analyses presented in this thesis were performed in a way that the clustering was biased towards cell types defined in other species. This is a common way of handling RNA sequencing data, and it helps to identify homologous cell types in a cross-species comparative setting. As such several cell types were identified as conserved in *Pleurodeles waltl* compared to mammals, such as neurons, microglia. macrophages, oligodendrocytes, oligodendrocyte precursor cells, meningeal fibroblasts, and erythrocytes. Also, among neurons it was possible to define clusters with gene expression profile characteristic for various subtypes. When it comes to dopaminergic neurons in the midbrain, it has been previously shown that a laterally migrated population is missing in newts (Smeets and Reiner, 1994) indicating that newts do not have a group of dopaminergic neurons that correspond anatomically to those found in the substantia nigra in mammals. However, I observed dopaminergic subpopulations within the newt VMb defined by the co-expression of calretinin and/or Otx2. The scRNAseq/snRNAseq data in this thesis identified some dopaminergic neurons in the midbrain that do express SOX6 (**Fig. 27L**), which marks dopaminergic neurons in the mammalian substantia nigra. These results corroborate the notion

that the dopaminergic population in the newt midbrain is functionally heterogeneous and some cells in the newt VTA are functionally equivalent to cells found in the mammalian substantia nigra. The dopaminergic innervation of the striatum and the behavioral changes observed upon 6-OHDA ablation (Joven et al., 2018) also support the existence of a functional equivalent of the mammalian substantia nigra. Further studies to refine the connectivity and spatial expression patterns should be performed to confirm the existence and localization of the putative substantia nigra in *Pleurodeles waltl*.

The thesis also dealt with neural stem/progenitor cells in the newt. The results in this thesis represent a useful resource to disentangle seemingly homogenous cells from each other that today are collectively denoted as ependymoglia in the newt. Characterizing this cell population in terms of heterogeneity and function both during homeostasis as well as during regeneration is important to understand key differences compared to their mammalian counterparts. Two questions are important to explore in this context: 1. What is the relationship between the ependymoglia of newts and the astrocytes of adult mammals? 2. Could the existence of unique cell type "ependymoglia" be an important reason behind the regenerative ability of the newt brain? Several studies indicated that in mammalian brain ventricular radial glia act as NSCs in development, while astrocytes are NSCs in specialized niches in the adult brain (Chojnacki et al., 2009; Zhao and Moore, 2018). The parenchyma of the adult newt brain is largely devoid of GFAP-expressing nuclei, which was interpreted as an indication of the lack of astrocytes. However, an alternative hypothesis is that a subpopulation of ependymoglia could directly correspond to mammalian astrocytes, the main difference is that these cells retain their contact with the ventricles. Ependymoglial cells express typical mammalian astrocytic markers (present results) and their dendritic arborizations are in contact with both neurons, blood vesseles and meninges (Joven et al., 2018), just like the mammalian astrocytes. In line with this hypothesis, astrocytes in the mammalian brain express $GLNA^+$ (GS^+) similarly to some of the ependymoglia in the newt brain. For addressing the second question it is imperative to comprehensively compare the injury responses between newt ependymoglia and mammalian radial glia/astrocytes. The existence of radial glia-like cells in the mouse midbrain that are retained postnatally (Hedlund et al., 2016) provides an ideal platform for systematic cross-species comparison. A promising starting point for such studies is the regulation of the transcription factors belonging to the NFI family, which show similar regulation during ontogeny in newts and mammals, and which appear to have a regulatory function in newts (see results).

It is also likely that signaling from other cellular components of the brain will have an impact on the fate NSCs. The thesis highlighted a role for microglia/macrophages in the activation of ependymoglia. The results suggesting that microglia stimulate ependymoglial cells are in line with observations made in another non-mammalian regenerative species, the zebrafish, both during brain and spinal cord regeneration (Cavone et al., 2021; Kanagaraj et al., 2022). It will be important to elucidate whether the same paracrine factors are involved in the zebrafish as in the newt. Similarly, it will be important to understand why microglia activation does not lead to an inflammatory response with a detrimental effect in these anamniote species. It is possible that the immune system in zebrafish and newts produces the right cocktail of pro- and anti-inflammatory cytokines to promote regeneration and not a scar as in mammals. Interestingly, manipulating the innate immune response during newt lens regeneration can lead to scar formation instead of regeneration (Tsitssios et al., 2023). It is also possible that the lack of parenchymal astrocytes in the newt (and zebrafish for that matter) is a reason for the lack of the cytokine-mediated self-amplifying loop between astroglia and microglia activation, which

is observed in mammals, and which leads to sustained inflammation (Crotti and Glass, 2015). Hence the interplay between microglia and macroglia, including also oligodendrocytes should be a target of future experiments in the newt brain (Peferoen et al., 2014; Song et al., 2022).

5.3. Activation of neural stem/progenitor cells by cellular and molecular manipulations

An important aim of my study is to pinpoint possible means to activate resident neural stem/progenitor cells. Given the considerable cellular and molecular conservations between newts and mammals as this thesis and other studies (e.g. (Woych et al., 2022)) revealed, it is not unconceivable that manipulation of selected targets identified in *Pleurodeles waltl* could promote regeneration in mammals. The feasibility of such an approach is indicated by the extension of normal developmental dopaminergic neurogenesis by dopamine antagonist administration in mice (Hedlund et al., 2016). This method was based on findings in newts that showed an important role for dopamine in the regulation of ependymoglia quiescence.

One such possible target could be *JARD2* which is a regulator of histone methyltransferase complexes, (Chen et al., 2020; Chen et al., 2018; Pasini et al., 2010) and whose regulation is highlighted in this thesis. In previous studies, *JARD2* has been assigned regulative roles in stem cell quiescence, activation, and differentiation (Celik et al., 2018; Ishibashi et al., 2021; Mejetta et al., 2011). Interestingly, *JARD2* was identified as a differential regulated in the *Notophthalmus viridescens* brain after 6-OHDA mediated lesion (Berg et al., 2010). In addition to ependymoglia, *JARD2* showed a differential regulation in intermediate progenitor cells/immature neurons as well, further suggesting the broad impact of this factor in neurogenesis.

In addition to evolutionarily conserved genes, it is possible that newt specific factors also play a role in the regulation of cellular quiescence. For example, the unannotated sequence, gene10576, was found as a differentially expressed gene in bulkRNAseq data, and it was also enriched in microglia/BAMs in scRNAseq/snRNAseq data. In this context it is relevant to refer to *Prod1* which determines the positional identity of cells during newt limb regeneration and is only found in the genomes of salamanders (Garza-Garcia et al., 2010; Geng et al., 2015). Thus, it will also be interesting to elucidate if and how species-specific innovations may re-orchestrate evolutionary conserved regulatory loops in a way that is permissive for regeneration.

5.4. Concluding remarks

This thesis represents the successful application of genomic tools to the study of brain regeneration in *Pleurodeles waltl*. I have managed to implement new methodologies and produce resources upon which our understanding of newt CNS regeneration is being built. The new transcriptomic data presented in this thesis is a valuable resource for understanding not only cellular heterogeneity, ageing and regeneration in the newt brain, but also a hypothesis generator and the ground for future comparative studies.

6. ACKNOWLEDGEMENTS

I would like to thank you, my main supervisor, **Andras**. You were the person who took me to the world of salamander and regeneration. While sharing endless love, wisdom, and enthusiasm with me, you taught me the meaning of persistence when facing difficulties in scientific research. I enjoyed your humorously and intelligent words in our discussions, as well as when we played chess. I am super sure that your smile and kind words have touched not only me but also many other people you met.

Alberto, my co-supervisor, maybe you do not remember, our first meeting was because I needed your help to dissect a brain when I was working on one of my master's projects. That time I could not imagine the high sense of responsibility and the impressive surgery hands you showed me much later after you became my co-supervisor. Also, I will never forget "the Dance of Happy Dragons" which you wrote and surprised me!

Ahmed, my co-supervisor, you were the person who led me to the world of bioinformatics. It was with your help that I found coding was not always that difficult by knowing the tricks. By the way, the pizza in your home was very delicious!

Per, my co-supervisor, you were the person that took me to the world of dopaminergic system, making me intoxicated with the complexity and the delicacy of brains. I still remember the beautiful view watching from the top of the CMM building!

Matti, the first time I met you was in a master course in the old CMB building. Since then, I have been impressed by your strictness and kindness. I was moved when you reminded me to follow the rules of the course while kindly emailing me "fly safe" when I was rushing for an airplane.

Linda, thank you for your endless help during my whole Ph.D time for my courses!

Thank you, **Eva** and **Thomas (Becker)**, the external reviewers, for your suggestions and very helpful comments to improve this thesis!

Thank you, **Terese**, for professional language editing.

Thanks to the people who helped with my projects. **Enric**, thanks for your broad knowledge and assistance in single-cell/single-nucleus RNAseq techniques. **Sarantis**, thanks for your amazing FACS techniques! **Vincent**, **Anna**, and **Asa** thank you for not only aiding me but also teaching me bioinformatic analysis! **Thomas (Perlmann)**, thanks for the nice talks with you during the meetings in my doctoral study! They inspired me a lot! **Behzard**, thanks for your help with the nucleus dissociation method, it greatly propelled the work! **Laura**, I thought you were a magician of immunohistochemistry every time I saw your staining of the newt brain! **Helena**, thank you for helping me find and order many different reagents during my whole doctoral time! **Ernest**, thanks for your help when I found something weird and interesting in newt dopaminergic neurons! **Shanzheng**, your knowledge and the antibodies you offered assisted me a lot in my study of the dopaminergic system! **Sten**, thanks for your help with the human brain database! **Emelie**, thanks for your help with the cell dissociation method! **Ji-feng**,

thanks for your aid in transgenic techniques! **Emma**, thanks for your help in the histology facility!

Thanks to my current group colleagues. **Matthew**, thanks for your help in almost all aspects of my doctoral study! **Anoop**, I envy your brain, which is just like a computer connected to a comprehensive science database! Also, thanks for your nice help to everyone in the group! **Elaiya**, you did look like a "young king" every time I saw your excellent work! **Elif**, you showed me a very good example of persisting to success. **Chris**, I admire your optimism when facing hardship, also all the best with your following research! **Chad**, thanks for your good care of the animals as well as your kindness, which I can always feel though you may not speak a lot! **Elin**, besides thanking your good care of the animals, I want to say I am touched by your smile and enthusiasm! **Ketan**, thanks for your knowledge in bioinformatics and stem cells, I also hope we can get more knowledge in Malatang! **Ingrid**, I enjoyed the stories you shared about Brazil and Japan! **Zuzana**, lots of times when I saw your work of recording the animals, I thought you could not only become a scientist but maybe also a good director haha! **Monica**, thanks for sharing the knowledge of sea animals with me, which I was curious about but had no idea about before! **Jesus**, hope everything good with your doctoral study!

Thanks to my formal group colleagues for your help and kindness during my early time of doctoral study, including **Heng**, **Shahul**, **Goncalo**, **Tiago**, **Laure**, **Eric**, **Iv**, **Alex (small)**, **Alex (big)**, **Sunny**, **Li (Ma)**, **Arturo**, and **Tobias**. Also, **Argos**, thanks for your happy company in our group BBQ.

To the persons I met in Sweden (before and now): **Yitian**, **Liuting**, **Peipei**, **Li (Shi)**, **ShuangJia**, **Xiaoyang**, and **Tianyang**, I can never forget the colorful life we had in my master time, with the endless card plays, meals, trips, etc. **Jingyan**, **Can**, **TaoTao**, **Lipeng,** and **Yanhua**, I always remember the happy times we had together in the many hotpots and parties. **Xueqi** and **Congru**, thanks for the wonderful time enjoying the water, animals, and stars in Tenerife. Yes, Saturn had a ring that could be seen! **Yuanyuan**, I admire your skills in Guzheng, cooking, and photography. **Tianyu**, yes you were very cool when I saw you play and taught me the fighting sport. **Xiaoqun**, thanks for taking me to the world of Parkinson's research, which I kept studying in my doctoral time. **Jeff**, I always remember and admire your accurate 3-points on the basketball field. **Shuijie**, I felt your kindness and diligence from the first time I met you in Ludwig, hope everything is good with you in your research in China. **Weiwei (Cai)**, thanks for the nice castle trip to Estonia. **Chikai**, thanks for your kind help every time I looked for reagents in my early time of doctoral study. **Lifeng,** I enjoyed our time of basketball play. **Yujiao**, thanks for your help with my questions about the cancer research. **Antony** and **Loay**, thanks for the many nice talks we had in the lab! **Qirong**, I really admire your knowledge of programming and sequencing, hope everything good with your doctoral studies. **Weiwei (Bian)**, thanks for the wonderful time of badminton play. **Danqing**, thanks for the amazing trip under the northern lights!

Thanks to my supervisors in my bachelors, including **Yuping**, **Jian**, **Zan**, and **Zhou**. Thanks to **Yan** who taught me the first course in developmental biology and stem cells.

Finally, thanks to my **parents** and **grandparents**, who have never stopped teaching me the meanings of love, wisdom, persistence, and responsibility. Only after standing on your shoulders that I can see such a beautiful sky.

7. REFERENCES

Abdullayev, I., Kirkham, M., Bjorklund, A.K., Simon, A., and Sandberg, R. (2013). A reference transcriptome and inferred proteome for the salamander Notophthalmus viridescens. Exp Cell Res *319*, 1187-1197.

Anden, N.E., Carlsson, A., Dahlstroem, A., Fuxe, K., Hillarp, N.A., and Larsson, K. (1964). DEMONSTRATION AND MAPPING OUT OF NIGRO-NEOSTRIATAL DOPAMINE NEURONS. Life Sci (1962) *3*, 523-530.

Andersson, E., Tryggvason, U., Deng, Q., Friling, S., Alekseenko, Z., Robert, B., Perlmann, T., and Ericson, J. (2006). Identification of intrinsic determinants of midbrain dopamine neurons. Cell *124*, 393-405.

Ang, S.L. (2006). Transcriptional control of midbrain dopaminergic neuron development. Development *133*, 3499-3506.

Arenas, E. (2020). Method to combat Parkinson's disease by astrocyte-to-neuron conversion. Nature *582*, 489-490.

Arenas, E., Denham, M., and Villaescusa, J.C. (2015). How to make a midbrain dopaminergic neuron. Development *142*, 1918-1936.

Arenas Gomez, C.M., Gomez Molina, A., Zapata, J.D., and Delgado, J.P. (2017). Limb regeneration in a direct-developing terrestrial salamander, Bolitoglossa ramosi (Caudata: Plethodontidae): Limb regeneration in plethodontid salamanders. Regeneration (Oxf) *4*, 227-235.

Arsanto, J.P., Komorowski, T.E., Dupin, F., Caubit, X., Diano, M., Géraudie, J., Carlson, B.M., and Thouveny, Y. (1992). Formation of the peripheral nervous system during tail regeneration in urodele amphibians: ultrastructural and immunohistochemical studies of the origin of the cells. J Exp Zool *264*, 273-292.

Ásgrímsdóttir, E.S., and Arenas, E. (2020). Midbrain Dopaminergic Neuron Development at the Single Cell Level: In vivo and in Stem Cells. Frontiers in Cell and Developmental Biology *8*.

Balciunas, D., Wangensteen, K.J., Wilber, A., Bell, J., Geurts, A., Sivasubbu, S., Wang, X., Hackett, P.B., Largaespada, D.A., McIvor, R.S.*, et al.* (2006). Harnessing a high cargo-capacity transposon for genetic applications in vertebrates. PLoS Genet *2*, e169.

Barbuti, P.A., Barker, R.A., Brundin, P., Przedborski, S., Papa, S.M., Kalia, L.V., Mochizuki, H., and Committee, M.D.S.S.I. (2021). Recent Advances in the Development of Stem-Cell-Derived Dopaminergic Neuronal Transplant Therapies for Parkinson's Disease. Mov Disord *36*, 1772-1780.

Barker, R.A., Drouin-Ouellet, J., and Parmar, M. (2015). Cell-based therapies for Parkinson disease-past insights and future potential. Nat Rev Neurol *11*, 492-503.

Baroti, T., Zimmermann, Y., Schillinger, A., Liu, L., Lommes, P., Wegner, M., and Stolt, C.C. (2016). Transcription factors Sox5 and Sox6 exert direct and indirect influences on oligodendroglial migration in spinal cord and forebrain. Glia *64*, 122-138.

Barry-Carroll, L., Greulich, P., Marshall, A.R., Riecken, K., Fehse, B., Askew, K.E., Li, K., Garaschuk, O., Menassa, D.A., and Gomez-Nicola, D. (2023). Microglia colonize the developing brain by clonal expansion of highly proliferative progenitors, following allometric scaling. Cell Rep *42*, 112425.

Baser, A., Skabkin, M., and Martin-Villalba, A. (2017). Neural Stem Cell Activation and the Role of Protein Synthesis. Brain Plast *3*, 27-41.

Beckervordersandforth, R., Tripathi, P., Ninkovic, J., Bayam, E., Lepier, A., Stempfhuber, B., Kirchhoff, F., Hirrlinger, J., Haslinger, A., Lie, D.C*., et al.* (2010). In vivo fate mapping and expression analysis reveals molecular hallmarks of prospectively isolated adult neural stem cells. Cell Stem Cell *7*, 744-758.
Bellver-Landete, V., Bretheau, F., Mailhot, B., Vallières, N., Lessard, M., Janelle, M.-E., Vernoux, N., Tremblay, M.-È., Fuehrmann, T., Shoichet, M.S*., et al.* (2019). Microglia are an essential component of the neuroprotective scar that forms after spinal cord injury. Nature Communications *10*, 518.
Benraiss, A., Caubit, X., Arsanto, J.P., Coulon, J., Nicolas, S., Le Parco, Y., and Thouveny, Y. (1996). Clonal cell cultures from adult spinal cord of the amphibian urodele Pleurodeles waltl to study the identity and potentialities of cells during tail regeneration. Dev Dyn *205*, 135-149.
Berg, D.A., Kirkham, M., Beljajeva, A., Knapp, D., Habermann, B., Ryge, J., Tanaka, E.M., and Simon, A. (2010). Efficient regeneration by activation of neurogenesis in homeostatically quiescent regions of the adult vertebrate brain. Development *137*, 4127-4134.
Berg, D.A., Kirkham, M., Wang, H., Frisen, J., and Simon, A. (2011). Dopamine controls neurogenesis in the adult salamander midbrain in homeostasis and during regeneration of dopamine neurons. Cell Stem Cell *8*, 426-433.
Bergmann, O., Liebl, J., Bernard, S., Alkass, K., Yeung, M.S., Steier, P., Kutschera, W., Johnson, L., Landen, M., Druid, H*., et al.* (2012). The age of olfactory bulb neurons in humans. Neuron *74*, 634-639.
Bifari, F., Decimo, I., Pino, A., Llorens-Bobadilla, E., Zhao, S., Lange, C., Panuccio, G., Boeckx, B., Thienpont, B., Vinckier, S*., et al.* (2017). Neurogenic Radial Glia-like Cells in Meninges Migrate and Differentiate into Functionally Integrated Neurons in the Neonatal Cortex. Cell Stem Cell *20*, 360-373.e367.
Biscotti, M.A., Carducci, F., Barucca, M., Gerdol, M., Pallavicini, A., Schartl, M., Canapa, A., and Adolfi, M.C. (2020). The transcriptome of the newt Cynops orientalis provides new insights into evolution and function of sexual gene networks in sarcopterygians. Sci Rep *10*, 5445.
Bjorklund, A., and Dunnett, S.B. (2007). Dopamine neuron systems in the brain: an update. Trends Neurosci *30*, 194-202.
Bolanos-Castro, L.A., Walters, H.E., Garcia Vazquez, R.O., and Yun, M.H. (2021). Immunity in salamander regeneration: Where are we standing and where are we headed? Dev Dyn *250*, 753-767.
Boldrini, M., Fulmore, C.A., Tartt, A.N., Simeon, L.R., Pavlova, I., Poposka, V., Rosoklija, G.B., Stankov, A., Arango, V., Dwork, A.J*., et al.* (2018). Human Hippocampal Neurogenesis Persists throughout Aging. Cell Stem Cell *22*, 589-599 e585.
Branch, S.Y., Sharma, R., and Beckstead, M.J. (2014). Aging decreases L-type calcium channel currents and pacemaker firing fidelity in substantia nigra dopamine neurons. J Neurosci *34*, 9310-9318.
Braun, E., Danan-Gotthold, M., Borm, L.E., Vinsland, E., Lee, K.W., Lönnerberg, P., Hu, L., Li, X., He, X., Andrusivová, Ž*., et al.* (2022). Comprehensive cell atlas of the first-trimester developing human brain. bioRxiv, 2022.2010.2024.513487.
Bray, N.L., Pimentel, H., Melsted, P., and Pachter, L. (2016). Near-optimal probabilistic RNA-seq quantification. Nat Biotechnol *34*, 525-527.
Brown, T., Elewa, A., Iarovenko, S., Subramanian, E., Araus, A.J., Petzold, A., Susuki, M., Suzuki, K.-i.T., Hayashi, T., Toyoda, A*., et al.* (2022). Sequencing and chromosome-scale assembly of the giant Pleurodeles waltl genome. bioRxiv, 2022.2010.2019.512763.

Cai, H., Peng, Z., Ren, R., and Wang, H. (2019). Efficient Gene Disruption via Base Editing Induced Stop in Newt Pleurodeles waltl. Genes (Basel) *10*.
Caldwell, L.J., Davies, N.O., Cavone, L., Mysiak, K.S., Semenova, S.A., Panula, P., Armstrong, J.D., Becker, C.G., and Becker, T. (2019). Regeneration of Dopaminergic Neurons in Adult Zebrafish Depends on Immune System Activation and Differs for Distinct Populations. J Neurosci *39*, 4694-4713.
Callier, S., Snapyan, M., Le Crom, S., Prou, D., Vincent, J.D., and Vernier, P. (2003). Evolution and cell biology of dopamine receptors in vertebrates. Biol Cell *95*, 489-502.
Casco-Robles, M.M., Yamada, S., Miura, T., Nakamura, K., Haynes, T., Maki, N., Del Rio-Tsonis, K., Tsonis, P.A., and Chiba, C. (2011). Expressing exogenous genes in newts by transgenesis. Nat Protoc *6*, 600-608.
Cavone, L., McCann, T., Drake, L.K., Aguzzi, E.A., Oprisoreanu, A.M., Pedersen, E., Sandi, S., Selvarajah, J., Tsarouchas, T.M., Wehner, D*., et al.* (2021). A unique macrophage subpopulation signals directly to progenitor cells to promote regenerative neurogenesis in the zebrafish spinal cord. Dev Cell *56*, 1617-1630 e1616.
Celik, H., Koh, W.K., Kramer, A.C., Ostrander, E.L., Mallaney, C., Fisher, D.A.C., Xiang, J., Wilson, W.C., Martens, A., Kothari, A*., et al.* (2018). JARID2 Functions as a Tumor Suppressor in Myeloid Neoplasms by Repressing Self-Renewal in Hematopoietic Progenitor Cells. Cancer Cell *34*, 741-756 e748.
Chamberlain, K.A., Nanescu, S.E., Psachoulia, K., and Huang, J.K. (2016). Oligodendrocyte regeneration: Its significance in myelin replacement and neuroprotection in multiple sclerosis. Neuropharmacology *110*, 633-643.
Chan, C.S., Gertler, T.S., and Surmeier, D.J. (2010). A molecular basis for the increased vulnerability of substantia nigra dopamine neurons in aging and Parkinson's disease. Mov Disord *25 Suppl 1*, S63-70.
Chan, K.Y., Jang, M.J., Yoo, B.B., Greenbaum, A., Ravi, N., Wu, W.L., Sanchez-Guardado, L., Lois, C., Mazmanian, S.K., Deverman, B.E*., et al.* (2017). Engineered AAVs for efficient noninvasive gene delivery to the central and peripheral nervous systems. Nat Neurosci *20*, 1172-1179.
Chen, S., Jiao, L., Liu, X., Yang, X., and Liu, X. (2020). A Dimeric Structural Scaffold for PRC2-PCL Targeting to CpG Island Chromatin. Mol Cell *77*, 1265-1278 e1267.
Chen, S., Jiao, L., Shubbar, M., Yang, X., and Liu, X. (2018). Unique Structural Platforms of Suz12 Dictate Distinct Classes of PRC2 for Chromatin Binding. Mol Cell *69*, 840-852 e845.
Chen, W., Zheng, Q., Huang, Q., Ma, S., and Li, M. (2022). Repressing PTBP1 fails to convert reactive astrocytes to dopaminergic neurons in a 6-hydroxydopamine mouse model of Parkinson's disease. Elife *11*.
Chinta, S.J., and Andersen, J.K. (2005). Dopaminergic neurons. Int J Biochem Cell Biol *37*, 942-946.
Choi, K.M., Kim, J.Y., and Kim, Y. (2013). Distribution of the Immunoreactivity for Glycoprotein M6B in the Neurogenic Niche and Reactive Glia in the Injury Penumbra Following Traumatic Brain Injury in Mice. Exp Neurobiol *22*, 277-282.
Chojnacki, A.K., Mak, G.K., and Weiss, S. (2009). Identity crisis for adult periventricular neural stem cells: subventricular zone astrocytes, ependymal cells or both? Nat Rev Neurosci *10*, 153-163.
Clark, B.S., Stein-O'Brien, G.L., Shiau, F., Cannon, G.H., Davis-Marcisak, E., Sherman, T., Santiago, C.P., Hoang, T.V., Rajaii, F., James-Esposito, R.E*., et al.* (2019). Single-Cell RNA-Seq

Analysis of Retinal Development Identifies NFI Factors as Regulating Mitotic Exit and Late-Born Cell Specification. Neuron *102*, 1111-1126 e1115.
Claver, J.A., and Quaglia, A.I.E. (2009). Comparative Morphology, Development, and Function of Blood Cells in Nonmammalian Vertebrates. Journal of Exotic Pet Medicine *18*, 87-97.
Codega, P., Silva-Vargas, V., Paul, A., Maldonado-Soto, A.R., Deleo, A.M., Pastrana, E., and Doetsch, F. (2014). Prospective identification and purification of quiescent adult neural stem cells from their in vivo niche. Neuron *82*, 545-559.
Codrich, M., Bertuzzi, M., Russo, R., Francescatto, M., Espinoza, S., Zentilin, L., Giacca, M., Cesselli, D., Beltrami, A.P., Ascenzi, P*., et al.* (2017). Neuronal hemoglobin affects dopaminergic cells' response to stress. Cell Death Dis *8*, e2538.
Cong, L., Ran, F.A., Cox, D., Lin, S., Barretto, R., Habib, N., Hsu, P.D., Wu, X., Jiang, W., Marraffini, L.A*., et al.* (2013). Multiplex genome engineering using CRISPR/Cas systems. Science *339*, 819-823.
Crotti, A., and Glass, C.K. (2015). The choreography of neuroinflammation in Huntington's disease. Trends Immunol *36*, 364-373.
Currie, J.D., Kawaguchi, A., Traspas, R.M., Schuez, M., Chara, O., and Tanaka, E.M. (2016). Live Imaging of Axolotl Digit Regeneration Reveals Spatiotemporal Choreography of Diverse Connective Tissue Progenitor Pools. Dev Cell *39*, 411-423.
Dahlstroem, A., and Fuxe, K. (1964). EVIDENCE FOR THE EXISTENCE OF MONOAMINE-CONTAINING NEURONS IN THE CENTRAL NERVOUS SYSTEM. I. DEMONSTRATION OF MONOAMINES IN THE CELL BODIES OF BRAIN STEM NEURONS. Acta Physiol Scand Suppl, Suppl 232:231-255.
Dahlstroem, A., and Fuxe, K. (1965). EVIDENCE FOR THE EXISTENCE OF MONOAMINE NEURONS IN THE CENTRAL NERVOUS SYSTEM. II. EXPERIMENTALLY INDUCED CHANGES IN THE INTRANEURONAL AMINE LEVELS OF BULBOSPINAL NEURON SYSTEMS. Acta Physiol Scand Suppl, Suppl 247:241-236.
Deltcheva, E., Chylinski, K., Sharma, C.M., Gonzales, K., Chao, Y., Pirzada, Z.A., Eckert, M.R., Vogel, J., and Charpentier, E. (2011). CRISPR RNA maturation by trans-encoded small RNA and host factor RNase III. Nature *471*, 602-607.
Deng, Q., Andersson, E., Hedlund, E., Alekseenko, Z., Coppola, E., Panman, L., Millonig, J.H., Brunet, J.F., Ericson, J., and Perlmann, T. (2011). Specific and integrated roles of Lmx1a, Lmx1b and Phox2a in ventral midbrain development. Development *138*, 3399-3408.
Dobin, A., Davis, C.A., Schlesinger, F., Drenkow, J., Zaleski, C., Jha, S., Batut, P., Chaisson, M., and Gingeras, T.R. (2013). STAR: ultrafast universal RNA-seq aligner. Bioinformatics *29*, 15-21.
Dorrier, C.E., Jones, H.E., Pintaric, L., Siegenthaler, J.A., and Daneman, R. (2022). Emerging roles for CNS fibroblasts in health, injury and disease. Nat Rev Neurosci *23*, 23-34.
Doucet-Beaupre, H., Gilbert, C., Profes, M.S., Chabrat, A., Pacelli, C., Giguere, N., Rioux, V., Charest, J., Deng, Q., Laguna, A*., et al.* (2016). Lmx1a and Lmx1b regulate mitochondrial functions and survival of adult midbrain dopaminergic neurons. Proc Natl Acad Sci U S A *113*, E4387-4396.
Dubé, L., and Parent, A. (1982). The organization of monoamine-containing neurons in the brain of the salamander, Necturus maculosus. J Comp Neurol *211*, 21-30.
Echeverri, K., Fei, J., and Tanaka, E.M. (2022). The Axolotl's journey to the modern molecular era. Curr Top Dev Biol *147*, 631-658.

Elewa, A., Wang, H., Talavera-Lopez, C., Joven, A., Brito, G., Kumar, A., Hameed, L.S., Penrad-Mobayed, M., Yao, Z., Zamani, N.*, et al.* (2017). Reading and editing the Pleurodeles waltl genome reveals novel features of tetrapod regeneration. Nat Commun *8*, 2286.
Elmore, M.R., Najafi, A.R., Koike, M.A., Dagher, N.N., Spangenberg, E.E., Rice, R.A., Kitazawa, M., Matusow, B., Nguyen, H., West, B.L.*, et al.* (2014). Colony-stimulating factor 1 receptor signaling is necessary for microglia viability, unmasking a microglia progenitor cell in the adult brain. Neuron *82*, 380-397.
Eriksson, P.S., Perfilieva, E., Björk-Eriksson, T., Alborn, A.M., Nordborg, C., Peterson, D.A., and Gage, F.H. (1998). Neurogenesis in the adult human hippocampus. Nat Med *4*, 1313-1317.
Ernst, A., Alkass, K., Bernard, S., Salehpour, M., Perl, S., Tisdale, J., Possnert, G., Druid, H., and Frisen, J. (2014). Neurogenesis in the striatum of the adult human brain. Cell *156*, 1072-1083.
Eroglu, E., Yen, C.Y.T., Tsoi, Y.L., Witman, N., Elewa, A., Joven Araus, A., Wang, H., Szattler, T., Umeano, C.H., Sohlmer, J.*, et al.* (2022). Epicardium-derived cells organize through tight junctions to replenish cardiac muscle in salamanders. Nat Cell Biol *24*, 645-658.
Eskildsen, S., Justesen, J., Schierup, M.H., and Hartmann, R. (2003). Characterization of the 2'-5'-oligoadenylate synthetase ubiquitin-like family. Nucleic Acids Res *31*, 3166-3173.
Esworthy, R.S., Chu, F.F., Paxton, R.J., Akman, S., and Doroshow, J.H. (1991). Characterization and partial amino acid sequence of human plasma glutathione peroxidase. Arch Biochem Biophys *286*, 330-336.
Fei, J.F., Knapp, D., Schuez, M., Murawala, P., Zou, Y., Pal Singh, S., Drechsel, D., and Tanaka, E.M. (2016). Tissue- and time-directed electroporation of CAS9 protein-gRNA complexes in vivo yields efficient multigene knockout for studying gene function in regeneration. NPJ Regen Med *1*, 16002.
Fei, J.F., Lou, W.P., Knapp, D., Murawala, P., Gerber, T., Taniguchi, Y., Nowoshilow, S., Khattak, S., and Tanaka, E.M. (2018). Application and optimization of CRISPR-Cas9-mediated genome engineering in axolotl (Ambystoma mexicanum). Nat Protoc *13*, 2908-2943.
Fei, J.F., Schuez, M., Knapp, D., Taniguchi, Y., Drechsel, D.N., and Tanaka, E.M. (2017). Efficient gene knockin in axolotl and its use to test the role of satellite cells in limb regeneration. Proc Natl Acad Sci U S A *114*, 12501-12506.
Fei, J.F., Schuez, M., Tazaki, A., Taniguchi, Y., Roensch, K., and Tanaka, E.M. (2014). CRISPR-mediated genomic deletion of Sox2 in the axolotl shows a requirement in spinal cord neural stem cell amplification during tail regeneration. Stem Cell Reports *3*, 444-459.
Flowers, G.P., Timberlake, A.T., McLean, K.C., Monaghan, J.R., and Crews, C.M. (2014). Highly efficient targeted mutagenesis in axolotl using Cas9 RNA-guided nuclease. Development *141*, 2165-2171.
Fraser, M.J., Ciszczon, T., Elick, T., and Bauser, C. (1996). Precise excision of TTAA-specific lepidopteran transposons piggyBac (IFP2) and tagalong (TFP3) from the baculovirus genome in cell lines from two species of Lepidoptera. Insect Mol Biol *5*, 141-151.
Furukawa, H., Mito, S., Nishio, J., Sato, N., Ando, Y., Tominaga, A., Toyama, F., Nakauchi, Y., Takayama-Watanabe, E., and Watanabe, A. (2023). Identification and characterization of sperm motility-initiating substance-2 gene in internally fertilizing Cynops species. Dev Growth Differ *65*, 144-152.
Fuxe, K. (1965a). EVIDENCE FOR THE EXISTENCE OF MONOAMINE NEURONS IN THE CENTRAL NERVOUS SYSTEM. 3. THE MONOAMINE NERVE TERMINAL. Z Zellforsch Mikrosk Anat *65*, 573-596.

Fuxe, K. (1965b). EVIDENCE FOR THE EXISTENCE OF MONOAMINE NEURONS IN THE CENTRAL NERVOUS SYSTEM. IV. DISTRIBUTION OF MONOAMINE NERVE TERMINALS IN THE CENTRAL NERVOUS SYSTEM. Acta Physiol Scand Suppl, Suppl 247:237+.
Gaj, T., Gersbach, C.A., and Barbas, C.F., 3rd (2013). ZFN, TALEN, and CRISPR/Cas-based methods for genome engineering. Trends Biotechnol *31*, 397-405.
Gallien, L. (1957). Table chronologique du developpement chez Pleurodeles waltlii(Michah).
Garza-Garcia, A.A., Driscoll, P.C., and Brockes, J.P. (2010). Evidence for the local evolution of mechanisms underlying limb regeneration in salamanders. Integr Comp Biol *50*, 528-535.
Geng, J., Gates, P.B., Kumar, A., Guenther, S., Garza-Garcia, A., Kuenne, C., Zhang, P., Looso, M., and Brockes, J.P. (2015). Identification of the orphan gene Prod 1 in basal and other salamander families. Evodevo *6*, 9.
Gerber, T., Murawala, P., Knapp, D., Masselink, W., Schuez, M., Hermann, S., Gac-Santel, M., Nowoshilow, S., Kageyama, J., Khattak, S*., et al.* (2018). Single-cell analysis uncovers convergence of cell identities during axolotl limb regeneration. Science *362*.
González, A., Marín, O., and Smeets, W.J. (1995). Development of catecholamine systems in the central nervous system of the newt Pleurodeles waltlii as revealed by tyrosine hydroxylase immunohistochemistry. J Comp Neurol *360*, 33-48.
González, A., Muñoz, A., Muñoz, M., Marín, O., Arévalo, R., Porteros, A., and Alonso, J.R. (1996). Nitric oxide synthase in the brain of a urodele amphibian (Pleurodeles waltl) and its relation to catecholaminergic neuronal structures. Brain Res *727*, 49-64.
Gonzalez, A., and Smeets, W.J. (1991). Comparative analysis of dopamine and tyrosine hydroxylase immunoreactivities in the brain of two amphibians, the anuran Rana ridibunda and the urodele Pleurodeles waltlii. J Comp Neurol *303*, 457-477.
Grunblatt, E., Mandel, S., Jacob-Hirsch, J., Zeligson, S., Amariglo, N., Rechavi, G., Li, J., Ravid, R., Roggendorf, W., Riederer, P*., et al.* (2004). Gene expression profiling of parkinsonian substantia nigra pars compacta; alterations in ubiquitin-proteasome, heat shock protein, iron and oxidative stress regulated proteins, cell adhesion/cellular matrix and vesicle trafficking genes. J Neural Transm (Vienna) *111*, 1543-1573.
Güntürkün, O. (2005). Avian and mammalian "prefrontal cortices": limited degrees of freedom in the evolution of the neural mechanisms of goal-state maintenance. Brain Res Bull *66*, 311-316.
Guo, T., Pan, X., Jiang, G., Zhang, D., Qi, J., Shao, L., Wang, Z., Xu, H., and Zhao, Y. (2022a). Downregulating PTBP1 fails to convert astrocytes into hippocampal neurons and to alleviate symptoms in Alzheimer's mouse models. J Neurosci *42*, 7309-7317.
Guo, T., Pan, X., Jiang, G., Zhang, D., Qi, J., Shao, L., Wang, Z., Xu, H., and Zhao, Y. (2022b). Downregulating PTBP1 fails to convert astrocytes into hippocampal neurons and to alleviate symptoms in Alzheimer’s mouse models. bioRxiv, 2022.2004.2027.489696.
Guo, X., Tang, L., and Tang, X. (2021). Current Developments in Cell Replacement Therapy for Parkinson's Disease. Neuroscience *463*, 370-382.
Hagemann-Jensen, M., Ziegenhain, C., Chen, P., Ramskold, D., Hendriks, G.J., Larsson, A.J.M., Faridani, O.R., and Sandberg, R. (2020). Single-cell RNA counting at allele and isoform resolution using Smart-seq3. Nat Biotechnol *38*, 708-714.
Hagemann-Jensen, M., Ziegenhain, C., and Sandberg, R. (2022). Scalable single-cell RNA sequencing from full transcripts with Smart-seq3xpress. Nat Biotechnol *40*, 1452-1457.

Hameed, L.S., Berg, D.A., Belnoue, L., Jensen, L.D., Cao, Y., and Simon, A. (2015). Environmental changes in oxygen tension reveal ROS-dependent neurogenesis and regeneration in the adult newt brain. Elife *4*.
Hannocks, M.J., Pizzo, M.E., Huppert, J., Deshpande, T., Abbott, N.J., Thorne, R.G., and Sorokin, L. (2018). Molecular characterization of perivascular drainage pathways in the murine brain. J Cereb Blood Flow Metab *38*, 669-686.
Hansen, J.C. (2020). Silencing the genome with linker histones. Proc Natl Acad Sci U S A *117*, 15388-15390.
Hao, Y., Hao, S., Andersen-Nissen, E., Mauck, W.M., 3rd, Zheng, S., Butler, A., Lee, M.J., Wilk, A.J., Darby, C., Zager, M.*, et al.* (2021). Integrated analysis of multimodal single-cell data. Cell *184*, 3573-3587 e3529.
Hao, Y., Hu, J., Xue, Y., Dowdy, S.F., Mobley, W.C., Qian, H., and Fu, X.D. (2023). Reply to: Ptbp1 deletion does not induce astrocyte-to-neuron conversion. Nature *618*, E8-e13.
Hayashi, T., Nakajima, M., Kyakuno, M., Doi, K., Manabe, I., Azuma, S., and Takeuchi, T. (2019). Advanced microinjection protocol for gene manipulation using the model newt Pleurodeles waltl. Int J Dev Biol *63*, 281-286.
Hayashi, T., Sakamoto, K., Sakuma, T., Yokotani, N., Inoue, T., Kawaguchi, E., Agata, K., Yamamoto, T., and Takeuchi, T. (2014). Transcription activator-like effector nucleases efficiently disrupt the target gene in Iberian ribbed newts (Pleurodeles waltl), an experimental model animal for regeneration. Dev Growth Differ *56*, 115-121.
Hayashi, T., and Takeuchi, T. (2015). Gene manipulation for regenerative studies using the Iberian ribbed newt, Pleurodeles waltl. Methods Mol Biol *1290*, 297-305.
Hayashi, T., Yokotani, N., Tane, S., Matsumoto, A., Myouga, A., Okamoto, M., and Takeuchi, T. (2013). Molecular genetic system for regenerative studies using newts. Dev Growth Differ *55*, 229-236.
Hedlund, E., Belnoue, L., Theofilopoulos, S., Salto, C., Bye, C., Parish, C., Deng, Q., Kadkhodaei, B., Ericson, J., Arenas, E.*, et al.* (2016). Dopamine Receptor Antagonists Enhance Proliferation and Neurogenesis of Midbrain Lmx1a-expressing Progenitors. Sci Rep *6*, 26448.
Hoang, T., Kim, D.W., Appel, H., Ozawa, M., Zheng, S., Kim, J., and Blackshaw, S. (2023). Ptbp1 deletion does not induce astrocyte-to-neuron conversion. Nature *618*, E1-e7.
Hoang, T., Kim, D.W., Appel, H., Pannullo, N.A., Leavey, P., Ozawa, M., Zheng, S., Yu, M., Peachey, N.S., and Blackshaw, S. (2022). Genetic loss of function of Ptbp1 does not induce glia-to-neuron conversion in retina. Cell Rep *39*, 110849.
Hoang, T., Kim, D.W., Appel, H., Pannullo, N.A., Leavey, P., Ozawa, M., Zheng, S., Yu, M., Peachey, N.S., Kim, J.*, et al.* (2021). Ptbp1 deletion does not induce glia-to-neuron conversion in adult mouse retina and brain. bioRxiv, 2021.2010.2004.462784.
Hoang, T., Wang, J., Boyd, P., Wang, F., Santiago, C., Jiang, L., Yoo, S., Lahne, M., Todd, L.J., Jia, M.*, et al.* (2020). Gene regulatory networks controlling vertebrate retinal regeneration. Science *370*.
Hoch, R.V., Lindtner, S., Price, J.D., and Rubenstein, J.L. (2015). OTX2 Transcription Factor Controls Regional Patterning within the Medial Ganglionic Eminence and Regional Identity of the Septum. Cell Rep *12*, 482-494.
Hook, P.W., McClymont, S.A., Cannon, G.H., Law, W.D., Morton, A.J., Goff, L.A., and McCallion, A.S. (2018). Single-Cell RNA-Seq of Mouse Dopaminergic Neurons Informs Candidate Gene Selection for Sporadic Parkinson Disease. Am J Hum Genet *102*, 427-446.

Huang, Q., Chen, C., Chen, W., Cai, C., Xing, H., Li, J., Li, M., and Ma, S. (2023). Cell type- and region-specific translatomes in an MPTP mouse model of Parkinson's disease. Neurobiol Dis *180*, 106105.
Hwang, B., Lee, J.H., and Bang, D. (2018). Single-cell RNA sequencing technologies and bioinformatics pipelines. Exp Mol Med *50*, 1-14.
Hwang, D.Y., Ardayfio, P., Kang, U.J., Semina, E.V., and Kim, K.S. (2003). Selective loss of dopaminergic neurons in the substantia nigra of Pitx3-deficient aphakia mice. Brain Res Mol Brain Res *114*, 123-131.
IDT (2023). Genome editing with CRISPR-Cas9.
Ishibashi, J., Taslim, T., Hussein, A., Brewer, D., Liu, S., Harper, S., Nguyen, B., Dang, J., Chen, A., Castillo, D.D*., et al.* (2021). Stem cell quiescence requires PRC2/PRC1-mediated mitochondrial checkpoint. bioRxiv, 2021.2004.2021.440825.
Jacquier, A., and Dujon, B. (1985). An intron-encoded protein is active in a gene conversion process that spreads an intron into a mitochondrial gene. Cell *41*, 383-394.
Jaillon, O., Aury, J.M., Brunet, F., Petit, J.L., Stange-Thomann, N., Mauceli, E., Bouneau, L., Fischer, C., Ozouf-Costaz, C., Bernot, A*., et al.* (2004). Genome duplication in the teleost fish Tetraodon nigroviridis reveals the early vertebrate proto-karyotype. Nature *431*, 946-957.
Jinek, M., Chylinski, K., Fonfara, I., Hauer, M., Doudna, J.A., and Charpentier, E. (2012). A programmable dual-RNA-guided DNA endonuclease in adaptive bacterial immunity. Science *337*, 816-821.
Joven, A., Elewa, A., and Simon, A. (2019). Model systems for regeneration: salamanders. Development *146*.
Joven, A., Kirkham, M., and Simon, A. (2015). Husbandry of Spanish ribbed newts (Pleurodeles waltl). Methods Mol Biol *1290*, 47-70.
Joven, A., Morona, R., Gonzalez, A., and Moreno, N. (2013a). Expression patterns of Pax6 and Pax7 in the adult brain of a urodele amphibian, Pleurodeles waltl. J Comp Neurol *521*, 2088-2124.
Joven, A., Morona, R., González, A., and Moreno, N. (2013b). Spatiotemporal patterns of Pax3, Pax6, and Pax7 expression in the developing brain of a urodele amphibian, Pleurodeles waltl. J Comp Neurol *521*, 3913-3953.
Joven, A., Morona, R., Moreno, N., and González, A. (2013c). Regional distribution of calretinin and calbindin-D28k expression in the brain of the urodele amphibian Pleurodeles waltl during embryonic and larval development. Brain Struct Funct *218*, 969-1003.
Joven, A., and Simon, A. (2018). Homeostatic and regenerative neurogenesis in salamanders. Prog Neurobiol *170*, 81-98.
Joven, A., Wang, H., Pinheiro, T., Hameed, L.S., Belnoue, L., and Simon, A. (2018). Cellular basis of brain maturation and acquisition of complex behaviors in salamanders. Development *145*.
Jovic, D., Liang, X., Zeng, H., Lin, L., Xu, F., and Luo, Y. (2022). Single-cell RNA sequencing technologies and applications: A brief overview. Clin Transl Med *12*, e694.
Kakuta, S., Shibata, S., and Iwakura, Y. (2002). Genomic structure of the mouse 2',5'-oligoadenylate synthetase gene family. J Interferon Cytokine Res *22*, 981-993.
Kalafatakis, I., and Karagogeos, D. (2021). Oligodendrocytes and Microglia: Key Players in Myelin Development, Damage and Repair. Biomolecules *11*.
Kalia, L.V., and Lang, A.E. (2015). Parkinson's disease. Lancet *386*, 896-912.
Kamath, T., Abdulraouf, A., Burris, S.J., Langlieb, J., Gazestani, V., Nadaf, N.M., Balderrama, K., Vanderburg, C., and Macosko, E.Z. (2022). Single-cell genomic profiling of human dopamine

neurons identifies a population that selectively degenerates in Parkinson's disease. Nat Neurosci *25*, 588-595.
Kanagaraj, P., Chen, J.Y., Skaggs, K., Qadeer, Y., Connors, M., Cutler, N., Richmond, J., Kommidi, V., Poles, A., Affrunti, D.*, et al.* (2022). Microglia Stimulate Zebrafish Brain Repair Via a Tumor Necrosis Factor-α-Initiated Inflammatory Cascade. bioRxiv, 2020.2010.2008.330662.
Kaucka, M., Joven Araus, A., Tesarova, M., Currie, J.D., Bostrom, J., Kavkova, M., Petersen, J., Yao, Z., Bouchnita, A., Hellander, A.*, et al.* (2022). Altered developmental programs and oriented cell divisions lead to bulky bones during salamander limb regeneration. Nat Commun *13*, 6949.
Kawakami, K. (2007). Tol2: a versatile gene transfer vector in vertebrates. Genome Biol *8 Suppl 1*, S7.
Kawauchi, D., Ogg, R.J., Liu, L., Shih, D.J.H., Finkelstein, D., Murphy, B.L., Rehg, J.E., Korshunov, A., Calabrese, C., Zindy, F.*, et al.* (2017). Novel MYC-driven medulloblastoma models from multiple embryonic cerebellar cells. Oncogene *36*, 5231-5242.
Kefalopoulou, Z., Politis, M., Piccini, P., Mencacci, N., Bhatia, K., Jahanshahi, M., Widner, H., Rehncrona, S., Brundin, P., Bjorklund, A.*, et al.* (2014). Long-term clinical outcome of fetal cell transplantation for Parkinson disease: two case reports. JAMA Neurol *71*, 83-87.
Kelly, K.K., MacPherson, A.M., Grewal, H., Strnad, F., Jones, J.W., Yu, J., Pierzchalski, K., Kane, M.A., Herson, P.S., and Siegenthaler, J.A. (2016). Col1a1+ perivascular cells in the brain are a source of retinoic acid following stroke. BMC Neurosci *17*, 49.
Khattak, S., Murawala, P., Andreas, H., Kappert, V., Schuez, M., Sandoval-Guzman, T., Crawford, K., and Tanaka, E.M. (2014). Optimized axolotl (Ambystoma mexicanum) husbandry, breeding, metamorphosis, transgenesis and tamoxifen-mediated recombination. Nat Protoc *9*, 529-540.
Khattak, S., Richter, T., and Tanaka, E.M. (2009). Generation of transgenic axolotls (Ambystoma mexicanum). Cold Spring Harb Protoc *2009*, pdb prot5264.
Khattak, S., Schuez, M., Richter, T., Knapp, D., Haigo, S.L., Sandoval-Guzman, T., Hradlikova, K., Duemmler, A., Kerney, R., and Tanaka, E.M. (2013). Germline transgenic methods for tracking cells and testing gene function during regeneration in the axolotl. Stem Cell Reports *1*, 90-103.
Kikuchi, T., Morizane, A., Doi, D., Magotani, H., Onoe, H., Hayashi, T., Mizuma, H., Takara, S., Takahashi, R., Inoue, H.*, et al.* (2017). Human iPS cell-derived dopaminergic neurons function in a primate Parkinson's disease model. Nature *548*, 592-596.
Kirkham, M., Berg, D.A., and Simon, A. (2011). Microglia activation during neuroregeneration in the adult vertebrate brain. Neurosci Lett *497*, 11-16.
Kirkham, M., Hameed, L.S., Berg, D.A., Wang, H., and Simon, A. (2014). Progenitor cell dynamics in the Newt Telencephalon during homeostasis and neuronal regeneration. Stem Cell Reports *2*, 507-519.
Kirkham, M., and Joven, A. (2015). Studying newt brain regeneration following subtype specific neuronal ablation. Methods Mol Biol *1290*, 91-99.
Koga, A., Suzuki, M., Inagaki, H., Bessho, Y., and Hori, H. (1996). Transposable element in fish. Nature *383*, 30.
Kragl, M., Knapp, D., Nacu, E., Khattak, S., Maden, M., Epperlein, H.H., and Tanaka, E.M. (2009). Cells keep a memory of their tissue origin during axolotl limb regeneration. Nature *460*, 60-65.

Kriks, S., Shim, J.W., Piao, J., Ganat, Y.M., Wakeman, D.R., Xie, Z., Carrillo-Reid, L., Auyeung, G., Antonacci, C., Buch, A.*, et al.* (2011). Dopamine neurons derived from human ES cells efficiently engraft in animal models of Parkinson's disease. Nature *480*, 547-551.
Kuo, T.H., Kowalko, J.E., DiTommaso, T., Nyambi, M., Montoro, D.T., Essner, J.J., and Whited, J.L. (2015). TALEN-mediated gene editing of the thrombospondin-1 locus in axolotl. Regeneration (Oxf) *2*, 37-43.
Kyritsis, N., Kizil, C., Zocher, S., Kroehne, V., Kaslin, J., Freudenreich, D., Iltzsche, A., and Brand, M. (2012). Acute inflammation initiates the regenerative response in the adult zebrafish brain. Science *338*, 1353-1356.
La Manno, G., Gyllborg, D., Codeluppi, S., Nishimura, K., Salto, C., Zeisel, A., Borm, L.E., Stott, S.R.W., Toledo, E.M., Villaescusa, J.C.*, et al.* (2016). Molecular Diversity of Midbrain Development in Mouse, Human, and Stem Cells. Cell *167*, 566-580 e519.
Laguna, A., Schintu, N., Nobre, A., Alvarsson, A., Volakakis, N., Jacobsen, J.K., Gomez-Galan, M., Sopova, E., Joodmardi, E., Yoshitake, T.*, et al.* (2015). Dopaminergic control of autophagic-lysosomal function implicates Lmx1b in Parkinson's disease. Nat Neurosci *18*, 826-835.
Lander, E.S. (2016). The Heroes of CRISPR. Cell *164*, 18-28.
Larsen, K.B., Lutterodt, M.C., Mollgard, K., and Moller, M. (2010). Expression of the homeobox genes OTX2 and OTX1 in the early developing human brain. J Histochem Cytochem *58*, 669-678.
Leigh, N.D., Dunlap, G.S., Johnson, K., Mariano, R., Oshiro, R., Wong, A.Y., Bryant, D.M., Miller, B.M., Ratner, A., Chen, A.*, et al.* (2018). Transcriptomic landscape of the blastema niche in regenerating adult axolotl limbs at single-cell resolution. Nat Commun *9*, 5153.
Li, M.A., Turner, D.J., Ning, Z., Yusa, K., Liang, Q., Eckert, S., Rad, L., Fitzgerald, T.W., Craig, N.L., and Bradley, A. (2011). Mobilization of giant piggyBac transposons in the mouse genome. Nucleic Acids Res *39*, e148.
Li, Y., He, X., Kawaguchi, R., Zhang, Y., Wang, Q., Monavarfeshani, A., Yang, Z., Chen, B., Shi, Z., Meng, H.*, et al.* (2020). Microglia-organized scar-free spinal cord repair in neonatal mice. Nature *587*, 613-618.
Liao, Y., Smyth, G.K., and Shi, W. (2013). The Subread aligner: fast, accurate and scalable read mapping by seed-and-vote. Nucleic Acids Res *41*, e108.
Liao, Y., Smyth, G.K., and Shi, W. (2014). featureCounts: an efficient general purpose program for assigning sequence reads to genomic features. Bioinformatics *30*, 923-930.
Lindvall, O., and Bjorklund, A. (2004). Cell therapy in Parkinson's disease. NeuroRx *1*, 382-393.
Lindvall, O., and Bjorklund, A. (2011). Cell therapeutics in Parkinson's disease. Neurotherapeutics *8*, 539-548.
Linnarsson, S. (2023). Mouse Brain Atlas.
Litvinchuk, S.N., Rosanov, J.M., and Borkin, L.J. (2007). Correlations of geographic distribution and temperature of embryonic development with the nuclear DNA content in the Salamandridae (Urodela, Amphibia). Genome *50*, 333-342.
Llorens-Bobadilla, E., Zhao, S., Baser, A., Saiz-Castro, G., Zwadlo, K., and Martin-Villalba, A. (2015). Single-Cell Transcriptomics Reveals a Population of Dormant Neural Stem Cells that Become Activated upon Brain Injury. Cell Stem Cell *17*, 329-340.
Looso, M., Preussner, J., Sousounis, K., Bruckskotten, M., Michel, C.S., Lignelli, E., Reinhardt, R., Höffner, S., Krüger, M., Tsonis, P.A.*, et al.* (2013). A de novo assembly of the newt transcriptome combined with proteomic validation identifies new protein families expressed during tissue regeneration. Genome Biol *14*, R16.

Love, M.I., Huber, W., and Anders, S. (2014). Moderated estimation of fold change and dispersion for RNA-seq data with DESeq2. Genome Biol *15*, 550.
Luhmann, H.J., Sinning, A., Yang, J.W., Reyes-Puerta, V., Stuttgen, M.C., Kirischuk, S., and Kilb, W. (2016). Spontaneous Neuronal Activity in Developing Neocortical Networks: From Single Cells to Large-Scale Interactions. Front Neural Circuits *10*, 40.
Lust, K., Maynard, A., Gomes, T., Fleck, J.S., Camp, J.G., Tanaka, E.M., and Treutlein, B. (2022). Single-cell analyses of axolotl telencephalon organization, neurogenesis, and regeneration. Science *377*, eabp9262.
Madhavan, M., Haynes, T.L., Frisch, N.C., Call, M.K., Minich, C.M., Tsonis, P.A., and Del Rio-Tsonis, K. (2006). The role of Pax-6 in lens regeneration. Proc Natl Acad Sci U S A *103*, 14848-14853.
Magadum, S., Banerjee, U., Murugan, P., Gangapur, D., and Ravikesavan, R. (2013). Gene duplication as a major force in evolution. J Genet *92*, 155-161.
Maimon, R., Chillon-Marinas, C., Snethlage, C.E., Singhal, S.M., McAlonis-Downes, M., Ling, K., Rigo, F., Bennett, C.F., Da Cruz, S., Hnasko, T.S*., et al.* (2021). Therapeutically viable generation of neurons with antisense oligonucleotide suppression of PTB. Nat Neurosci *24*, 1089-1099.
Mali, P., Yang, L., Esvelt, K.M., Aach, J., Guell, M., DiCarlo, J.E., Norville, J.E., and Church, G.M. (2013). RNA-guided human genome engineering via Cas9. Science *339*, 823-826.
Marín, O., González, A., and Smeets, W.J. (1997a). Basal ganglia organization in amphibians: afferent connections to the striatum and the nucleus accumbens. J Comp Neurol *378*, 16-49.
Marín, O., González, A., and Smeets, W.J. (1997b). Basal ganglia organization in amphibians: efferent connections of the striatum and the nucleus accumbens. J Comp Neurol *380*, 23-50.
Marín, O., Smeets, W.J., and González, A. (1997c). Distribution of choline acetyltransferase immunoreactivity in the brain of anuran (Rana perezi, Xenopus laevis) and urodele (Pleurodeles waltl) amphibians. J Comp Neurol *382*, 499-534.
Martin, M. (2011). Cutadapt removes adapter sequences from high-throughput sequencing reads. 2011 *17*, 3.
Martynoga, B., Mateo, J.L., Zhou, B., Andersen, J., Achimastou, A., Urban, N., van den Berg, D., Georgopoulou, D., Hadjur, S., Wittbrodt, J*., et al.* (2013). Epigenomic enhancer annotation reveals a key role for NFIX in neural stem cell quiescence. Genes Dev *27*, 1769-1786.
Marx, V. (2021). Method of the Year: spatially resolved transcriptomics. Nat Methods *18*, 9-14.
Matsunami, M., Suzuki, M., Haramoto, Y., Fukui, A., Inoue, T., Yamaguchi, K., Uchiyama, I., Mori, K., Tashiro, K., Ito, Y*., et al.* (2019). A comprehensive reference transcriptome resource for the Iberian ribbed newt Pleurodeles waltl, an emerging model for developmental and regeneration biology. DNA Res *26*, 217-229.
Maxwell, S.L., Ho, H.Y., Kuehner, E., Zhao, S., and Li, M. (2005). Pitx3 regulates tyrosine hydroxylase expression in the substantia nigra and identifies a subgroup of mesencephalic dopaminergic progenitor neurons during mouse development. Dev Biol *282*, 467-479.
McGinnis, C.S., Murrow, L.M., and Gartner, Z.J. (2019). DoubletFinder: Doublet Detection in Single-Cell RNA Sequencing Data Using Artificial Nearest Neighbors. Cell Syst *8*, 329-337 e324.
Mehl, L.C., Manjally, A.V., Bouadi, O., Gibson, E.M., and Tay, T.L. (2022). Microglia in brain development and regeneration. Development *149*.
Mejetta, S., Morey, L., Pascual, G., Kuebler, B., Mysliwiec, M.R., Lee, Y., Shiekhattar, R., Di Croce, L., and Benitah, S.A. (2011). Jarid2 regulates mouse epidermal stem cell activation and differentiation. EMBO J *30*, 3635-3646.

Melsted, P., Booeshaghi, A.S., Liu, L., Gao, F., Lu, L., Min, K.H.J., da Veiga Beltrame, E., Hjorleifsson, K.E., Gehring, J., and Pachter, L. (2021). Modular, efficient and constant-memory single-cell RNA-seq preprocessing. Nat Biotechnol *39*, 813-818.
Meyer, R.C., Giddens, M.M., Schaefer, S.A., and Hall, R.A. (2013). GPR37 and GPR37L1 are receptors for the neuroprotective and glioprotective factors prosaptide and prosaposin. Proc Natl Acad Sci U S A *110*, 9529-9534.
Miron, V.E., Kuhlmann, T., and Antel, J.P. (2011). Cells of the oligodendroglial lineage, myelination, and remyelination. Biochim Biophys Acta *1812*, 184-193.
Mogensen, J., and Divac, I. (1982). The prefrontal 'cortex' in the pigeon. Behavioral evidence. Brain Behav Evol *21*, 60-66.
Monaghan, J.R., and Maden, M. (2012). Visualization of retinoic acid signaling in transgenic axolotls during limb development and regeneration. Dev Biol *368*, 63-75.
Moreno-Jimenez, E.P., Flor-Garcia, M., Terreros-Roncal, J., Rabano, A., Cafini, F., Pallas-Bazarra, N., Avila, J., and Llorens-Martin, M. (2019). Adult hippocampal neurogenesis is abundant in neurologically healthy subjects and drops sharply in patients with Alzheimer's disease. Nat Med *25*, 554-560.
Mundt, S., Greter, M., and Becher, B. (2022). The CNS mononuclear phagocyte system in health and disease. Neuron *110*, 3497-3512.
Nakagomi, T., and Matsuyama, T. (2017). Leptomeninges: a novel stem cell niche with neurogenic potential. Stem Cell Investig *4*, 22.
Nakamura, K., Islam, M.R., Takayanagi, M., Yasumuro, H., Inami, W., Kunahong, A., Casco-Robles, R.M., Toyama, F., and Chiba, C. (2014). A transcriptome for the study of early processes of retinal regeneration in the adult newt, Cynops pyrrhogaster. PLoS One *9*, e109831.
Nishimura, T., Kubosaki, A., Ito, Y., and Notkins, A.L. (2009). Disturbances in the secretion of neurotransmitters in IA-2/IA-2beta null mice: changes in behavior, learning and lifespan. Neuroscience *159*, 427-437.
Nishiyama, A., Shimizu, T., Sherafat, A., and Richardson, W.D. (2021). Life-long oligodendrocyte development and plasticity. Semin Cell Dev Biol *116*, 25-37.
Nolbrant, S., Heuer, A., Parmar, M., and Kirkeby, A. (2017). Generation of high-purity human ventral midbrain dopaminergic progenitors for in vitro maturation and intracerebral transplantation. Nat Protoc *12*, 1962-1979.
Nowoshilow, S., Fei, J.F., Voss, S.R., Tanaka, E.M., and Murawala, P. (2022). Gene and transgenics nomenclature for the laboratory axolotl-Ambystoma mexicanum. Dev Dyn *251*, 913-921.
Nunes, I., Tovmasian, L.T., Silva, R.M., Burke, R.E., and Goff, S.P. (2003). Pitx3 is required for development of substantia nigra dopaminergic neurons. Proc Natl Acad Sci U S A *100*, 4245-4250.
Oh, M.S., Hong, S.J., Huh, Y., and Kim, K.S. (2009). Expression of transgenes in midbrain dopamine neurons using the tyrosine hydroxylase promoter. Gene Ther *16*, 437-440.
Oliveira, C.R., Knapp, D., Elewa, A., Gerber, T., Gonzalez Malagon, S.G., Gates, P.B., Walters, H.E., Petzold, A., Arce, H., Cordoba, R.C*., et al.* (2022). Tig1 regulates proximo-distal identity during salamander limb regeneration. Nat Commun *13*, 1141.
Omega, C. (2023).
Paasila, P.J., Davies, D.S., Kril, J.J., Goldsbury, C., and Sutherland, G.T. (2019). The relationship between the morphological subtypes of microglia and Alzheimer's disease neuropathology. Brain Pathol *29*, 726-740.

Panman, L., Papathanou, M., Laguna, A., Oosterveen, T., Volakakis, N., Acampora, D., Kurtsdotter, I., Yoshitake, T., Kehr, J., Joodmardi, E.*, et al.* (2014). Sox6 and Otx2 control the specification of substantia nigra and ventral tegmental area dopamine neurons. Cell Rep *8*, 1018-1025.
Parish, C.L., Beljajeva, A., Arenas, E., and Simon, A. (2007). Midbrain dopaminergic neurogenesis and behavioural recovery in a salamander lesion-induced regeneration model. Development *134*, 2881-2887.
Parmar, M., Grealish, S., and Henchcliffe, C. (2020). The future of stem cell therapies for Parkinson disease. Nat Rev Neurosci *21*, 103-115.
Parmar, M., Paul-Visse, G., Widner, H., Bjartmarz, H., Kirkeby, A., Barker, R., Piccini, P., Hansson, O., Smith, R., theme, C.C.t.u.N.*, et al.* (2023). First patient receives milestone stem cell-based transplant for Parkinson's Disease.
Pasini, D., Cloos, P.A., Walfridsson, J., Olsson, L., Bukowski, J.P., Johansen, J.V., Bak, M., Tommerup, N., Rappsilber, J., and Helin, K. (2010). JARID2 regulates binding of the Polycomb repressive complex 2 to target genes in ES cells. Nature *464*, 306-310.
Peferoen, L., Kipp, M., van der Valk, P., van Noort, J.M., and Amor, S. (2014). Oligodendrocyte-microglia cross-talk in the central nervous system. Immunology *141*, 302-313.
Penn, A.A., and Shatz, C.J. (1999). Brain waves and brain wiring: the role of endogenous and sensory-driven neural activity in development. Pediatr Res *45*, 447-458.
Pereira Luppi, M., Azcorra, M., Caronia-Brown, G., Poulin, J.F., Gaertner, Z., Gatica, S., Moreno-Ramos, O.A., Nouri, N., Dubois, M., Ma, Y.C.*, et al.* (2021). Sox6 expression distinguishes dorsally and ventrally biased dopamine neurons in the substantia nigra with distinctive properties and embryonic origins. Cell Rep *37*, 109975.
Pilz, G.A., Bottes, S., Betizeau, M., Jörg, D.J., Carta, S., April, S., Simons, B.D., Helmchen, F., and Jessberger, S. (2018). Live imaging of neurogenesis in the adult mouse hippocampus. Science *359*, 658-662.
Poulin, J.F., Caronia, G., Hofer, C., Cui, Q., Helm, B., Ramakrishnan, C., Chan, C.S., Dombeck, D.A., Deisseroth, K., and Awatramani, R. (2018). Mapping projections of molecularly defined dopamine neuron subtypes using intersectional genetic approaches. Nat Neurosci *21*, 1260-1271.
Poulin, J.F., Gaertner, Z., Moreno-Ramos, O.A., and Awatramani, R. (2020). Classification of Midbrain Dopamine Neurons Using Single-Cell Gene Expression Profiling Approaches. Trends Neurosci *43*, 155-169.
Poulin, J.F., Zou, J., Drouin-Ouellet, J., Kim, K.Y., Cicchetti, F., and Awatramani, R.B. (2014). Defining midbrain dopaminergic neuron diversity by single-cell gene expression profiling. Cell Rep *9*, 930-943.
Puelles, E., Acampora, D., Gogoi, R., Tuorto, F., Papalia, A., Guillemot, F., Ang, S.L., and Simeone, A. (2006). Otx2 controls identity and fate of glutamatergic progenitors of the thalamus by repressing GABAergic differentiation. J Neurosci *26*, 5955-5964.
Puelles, E., Annino, A., Tuorto, F., Usiello, A., Acampora, D., Czerny, T., Brodski, C., Ang, S.L., Wurst, W., and Simeone, A. (2004). Otx2 regulates the extent, identity and fate of neuronal progenitor domains in the ventral midbrain. Development *131*, 2037-2048.
Qian, H., Kang, X., Hu, J., Zhang, D., Liang, Z., Meng, F., Zhang, X., Xue, Y., Maimon, R., Dowdy, S.F.*, et al.* (2020). Reversing a model of Parkinson's disease with in situ converted nigral neurons. Nature *582*, 550-556.

Raudvere, U., Kolberg, L., Kuzmin, I., Arak, T., Adler, P., Peterson, H., and Vilo, J. (2019). g:Profiler: a web server for functional enrichment analysis and conversions of gene lists (2019 update). Nucleic Acids Res *47*, W191-w198.
Reich, S.G., and Savitt, J.M. (2019). Parkinson's Disease. Med Clin North Am *103*, 337-350.
Ren, G., Li, S., Zhong, H., and Lin, S. (2013). Zebrafish tyrosine hydroxylase 2 gene encodes tryptophan hydroxylase. J Biol Chem *288*, 22451-22459.
Richter, F., Meurers, B.H., Zhu, C., Medvedeva, V.P., and Chesselet, M.F. (2009). Neurons express hemoglobin alpha- and beta-chains in rat and human brains. J Comp Neurol *515*, 538-547.
Rink, E., and Wullimann, M.F. (2001). The teleostean (zebrafish) dopaminergic system ascending to the subpallium (striatum) is located in the basal diencephalon (posterior tuberculum). Brain Res *889*, 316-330.
Rivetti di Val Cervo, P., Romanov, R.A., Spigolon, G., Masini, D., Martin-Montanez, E., Toledo, E.M., La Manno, G., Feyder, M., Pifl, C., Ng, Y.H.*, et al.* (2017). Induction of functional dopamine neurons from human astrocytes in vitro and mouse astrocytes in a Parkinson's disease model. Nat Biotechnol *35*, 444-452.
Rostovskaya, M., Fu, J., Obst, M., Baer, I., Weidlich, S., Wang, H., Smith, A.J., Anastassiadis, K., and Stewart, A.F. (2012). Transposon-mediated BAC transgenesis in human ES cells. Nucleic Acids Res *40*, e150.
Salic, A., and Mitchison, T.J. (2008). A chemical method for fast and sensitive detection of DNA synthesis in vivo. Proc Natl Acad Sci U S A *105*, 2415-2420.
Salmani, B.Y., Lahti, L., Gillberg, L., Jacobsen, J.K., Mantas, I., Svenningsson, P., and Perlmann, T. (2023). Transcriptomic atlas of midbrain dopamine neurons uncovers differential vulnerability in a Parkinsonism lesion model. bioRxiv, 2023.2006.2005.543445.
Sandoval-Guzman, T., Wang, H., Khattak, S., Schuez, M., Roensch, K., Nacu, E., Tazaki, A., Joven, A., Tanaka, E.M., and Simon, A. (2014). Fundamental differences in dedifferentiation and stem cell recruitment during skeletal muscle regeneration in two salamander species. Cell Stem Cell *14*, 174-187.
Saunders, A., Macosko, E.Z., Wysoker, A., Goldman, M., Krienen, F.M., de Rivera, H., Bien, E., Baum, M., Bortolin, L., Wang, S.*, et al.* (2018). Molecular Diversity and Specializations among the Cells of the Adult Mouse Brain. Cell *174*, 1015-1030 e1016.
Schnapp, E., and Tanaka, E.M. (2005). Quantitative evaluation of morpholino-mediated protein knockdown of GFP, MSX1, and PAX7 during tail regeneration in Ambystoma mexicanum. Dev Dyn *232*, 162-170.
Shi, D.L., and Boucaut, J.C. (1995). The chronological development of the urodele amphibian Pleurodeles waltl (Michah). Int J Dev Biol *39*, 427-441.
Siletti, K., Hodge, R., Albiach, A.M., Hu, L., Lee, K.W., Lönnerberg, P., Bakken, T., Ding, S.-L., Clark, M., Casper, T.*, et al.* (2022). Transcriptomic diversity of cell types across the adult human brain. bioRxiv, 2022.2010.2012.511898.
Silver, J., Schwab, M.E., and Popovich, P.G. (2014). Central nervous system regenerative failure: role of oligodendrocytes, astrocytes, and microglia. Cold Spring Harb Perspect Biol *7*, a020602.
Simons, M., and Nave, K.A. (2015). Oligodendrocytes: Myelination and Axonal Support. Cold Spring Harb Perspect Biol *8*, a020479.
Smeets, W.J.A., and Reiner, A. (1994). Phylogeny and Development of Catecholamine Systems in the CNS of Vertebrates.

Sobkow, L., Epperlein, H.H., Herklotz, S., Straube, W.L., and Tanaka, E.M. (2006). A germline GFP transgenic axolotl and its use to track cell fate: dual origin of the fin mesenchyme during development and the fate of blood cells during regeneration. Dev Biol *290*, 386-397.
Song, S., Hasan, M.N., Yu, L., Paruchuri, S.S., Bielanin, J.P., Metwally, S., Oft, H.C.M., Fischer, S.G., Fiesler, V.M., Sen, T*., et al.* (2022). Microglial-oligodendrocyte interactions in myelination and neurological function recovery after traumatic brain injury. J Neuroinflammation *19*, 246.
Sorrells, S.F., Paredes, M.F., Cebrian-Silla, A., Sandoval, K., Qi, D., Kelley, K.W., James, D., Mayer, S., Chang, J., Auguste, K.I*., et al.* (2018). Human hippocampal neurogenesis drops sharply in children to undetectable levels in adults. Nature *555*, 377-381.
Sousounis, K., Bryant, D.M., Martinez Fernandez, J., Eddy, S.S., Tsai, S.L., Gundberg, G.C., Han, J., Courtemanche, K., Levin, M., and Whited, J.L. (2020). Eya2 promotes cell cycle progression by regulating DNA damage response during vertebrate limb regeneration. Elife *9*.
Spalding, K.L., Bergmann, O., Alkass, K., Bernard, S., Salehpour, M., Huttner, H.B., Bostrom, E., Westerlund, I., Vial, C., Buchholz, B.A*., et al.* (2013). Dynamics of hippocampal neurogenesis in adult humans. Cell *153*, 1219-1227.
Ståhl, P.L., Salmén, F., Vickovic, S., Lundmark, A., Navarro, J.F., Magnusson, J., Giacomello, S., Asp, M., Westholm, J.O., Huss, M*., et al.* (2016). Visualization and analysis of gene expression in tissue sections by spatial transcriptomics. Science *353*, 78-82.
Stolt, C.C., Schlierf, A., Lommes, P., Hillgartner, S., Werner, T., Kosian, T., Sock, E., Kessaris, N., Richardson, W.D., Lefebvre, V*., et al.* (2006). SoxD proteins influence multiple stages of oligodendrocyte development and modulate SoxE protein function. Dev Cell *11*, 697-709.
Subramanian, E., Elewa, A., Brito, G., Kumar, A., Segerstolpe, A., Karampelias, C., Bjorklund, A., Sandberg, R., Echeverri, K., Lui, W.O*., et al.* (2023). A small noncoding RNA links ribosome recovery and translation control to dedifferentiation during salamander limb regeneration. Dev Cell *58*, 450-460 e456.
Suster, M.L., Sumiyama, K., and Kawakami, K. (2009). Transposon-mediated BAC transgenesis in zebrafish and mice. BMC Genomics *10*, 477.
Suzuki, M., Hayashi, T., Inoue, T., Agata, K., Hirayama, M., Suzuki, M., Shigenobu, S., Takeuchi, T., Yamamoto, T., and Suzuki, K.T. (2018). Cas9 ribonucleoprotein complex allows direct and rapid analysis of coding and noncoding regions of target genes in Pleurodeles waltl development and regeneration. Dev Biol *443*, 127-136.
Ta, A.C., Huang, L.C., McKeown, C.R., Bestman, J.E., Van Keuren-Jensen, K., and Cline, H.T. (2022). Temporal and spatial transcriptomic dynamics across brain development in Xenopus laevis tadpoles. G3 (Bethesda) *12*.
Takahashi, J. (2019). Preparing for first human trial of induced pluripotent stem cell-derived cells for Parkinson's disease: an interview with Jun Takahashi. Regen Med *14*, 93-95.
Takeuchi, T., Matsubara, H., Minamitani, F., Satoh, Y., Tozawa, S., Moriyama, T., Maruyama, K., Suzuki, K.T., Shigenobu, S., Inoue, T*., et al.* (2022). Newt Hoxa13 has an essential and predominant role in digit formation during development and regeneration. Development *149*.
Tiklova, K., Bjorklund, A.K., Lahti, L., Fiorenzano, A., Nolbrant, S., Gillberg, L., Volakakis, N., Yokota, C., Hilscher, M.M., Hauling, T*., et al.* (2019). Single-cell RNA sequencing reveals midbrain dopamine neuron diversity emerging during mouse brain development. Nat Commun *10*, 581.
Tilley, L., Papadopoulos, S.C., Pende, M., Fei, J.F., and Murawala, P. (2022). The use of transgenics in the laboratory axolotl. Dev Dyn *251*, 942-956.

Tobin, M.K., Musaraca, K., Disouky, A., Shetti, A., Bheri, A., Honer, W.G., Kim, N., Dawe, R.J., Bennett, D.A., Arfanakis, K.*, et al.* (2019). Human Hippocampal Neurogenesis Persists in Aged Adults and Alzheimer's Disease Patients. Cell Stem Cell *24*, 974-982 e973.
Torper, O., Ottosson, D.R., Pereira, M., Lau, S., Cardoso, T., Grealish, S., and Parmar, M. (2015). In Vivo Reprogramming of Striatal NG2 Glia into Functional Neurons that Integrate into Local Host Circuitry. Cell Rep *12*, 474-481.
Tsissios, G., Sallese, A., Perez-Estrada, J.R., Tangeman, J.A., Chen, W., Smucker, B., Ratvasky, S.C., Grajales-Esquivel, E., Martinez, A., Visser, K.J.*, et al.* (2023). Macrophages modulate fibrosis during newt lens regeneration. bioRxiv, 2023.2006.2004.543633.
Tsonis, P.A., Haynes, T., Maki, N., Nakamura, K., Casco-Robles, M.M., Yamada, S., Miura, T., Chiba, C., and Del Rio-Tsonis, K. (2011). Controlling gene loss of function in newts with emphasis on lens regeneration. Nat Protoc *6*, 593-599.
UniProt (2023). UniProt database.
Urasaki, A., Morvan, G., and Kawakami, K. (2006). Functional dissection of the Tol2 transposable element identified the minimal cis-sequence and a highly repetitive sequence in the subterminal region essential for transposition. Genetics *174*, 639-649.
Urban, N., Blomfield, I.M., and Guillemot, F. (2019). Quiescence of Adult Mammalian Neural Stem Cells: A Highly Regulated Rest. Neuron *104*, 834-848.
Utz, S.G., See, P., Mildenberger, W., Thion, M.S., Silvin, A., Lutz, M., Ingelfinger, F., Rayan, N.A., Lelios, I., Buttgereit, A.*, et al.* (2020). Early Fate Defines Microglia and Non-parenchymal Brain Macrophage Development. Cell *181*, 557-573.e518.
van den Munckhof, P., Luk, K.C., Ste-Marie, L., Montgomery, J., Blanchet, P.J., Sadikot, A.F., and Drouin, J. (2003). Pitx3 is required for motor activity and for survival of a subset of midbrain dopaminergic neurons. Development *130*, 2535-2542.
Vanlandewijck, M., He, L., Mae, M.A., Andrae, J., Ando, K., Del Gaudio, F., Nahar, K., Lebouvier, T., Lavina, B., Gouveia, L.*, et al.* (2018). A molecular atlas of cell types and zonation in the brain vasculature. Nature *554*, 475-480.
Wakeman, D.R., Hiller, B.M., Marmion, D.J., McMahon, C.W., Corbett, G.T., Mangan, K.P., Ma, J., Little, L.E., Xie, Z., Perez-Rosello, T.*, et al.* (2017). Cryopreservation Maintains Functionality of Human iPSC Dopamine Neurons and Rescues Parkinsonian Phenotypes In Vivo. Stem Cell Reports *9*, 149-161.
Wallis, S.S., Ventimiglia, L.N., Otigbah, E., Infante, E., Cuesta-Geijo, M.A., Kidiyoor, G.R., Carbajal, M.A., Fleck, R.A., Foiani, M., Garcia-Manyes, S.*, et al.* (2021). The ESCRT machinery counteracts Nesprin-2G-mediated mechanical forces during nuclear envelope repair. Dev Cell *56*, 3192-3202 e3198.
Wang, D., Zhao, M., Tang, X., Gao, M., Liu, W., Xiang, M., Ruan, J., Chen, J., Long, B., and Li, J. (2023). Transcriptomic analysis of spinal cord regeneration after injury in Cynops orientalis. Neural Regeneration Research *18*, 2743-2750.
Wang, F., Flanagan, J., Su, N., Wang, L.C., Bui, S., Nielson, A., Wu, X., Vo, H.T., Ma, X.J., and Luo, Y. (2012). RNAscope: a novel in situ RNA analysis platform for formalin-fixed, paraffin-embedded tissues. J Mol Diagn *14*, 22-29.
Wang, L.L., Serrano, C., Zhong, X., Ma, S., Zou, Y., and Zhang, C.L. (2021). Revisiting astrocyte to neuron conversion with lineage tracing in vivo. Cell *184*, 5465-5481 e5416.
Wang, L.L., and Zhang, C.L. (2022). In vivo glia-to-neuron conversion: pitfalls and solutions. Dev Neurobiol *82*, 367-374.

Wang, L.L., and Zhang, C.L. (2023). Therapeutic Potential of PTBP1 Inhibition, If Any, Is Not Attributed to Glia-to-Neuron Conversion. Annu Rev Neurosci.
Wang, Y.K., Zhu, W.W., Wu, M.H., Wu, Y.H., Liu, Z.X., Liang, L.M., Sheng, C., Hao, J., Wang, L., Li, W.*, et al.* (2018). Human Clinical-Grade Parthenogenetic ESC-Derived Dopaminergic Neurons Recover Locomotive Defects of Nonhuman Primate Models of Parkinson's Disease. Stem Cell Reports *11*, 171-182.
Wei, C., Liu, J., Yu, Z., Zhang, B., Gao, G., and Jiao, R. (2013). TALEN or Cas9 - rapid, efficient and specific choices for genome modifications. J Genet Genomics *40*, 281-289.
Wei, X., Fu, S., Li, H., Liu, Y., Wang, S., Feng, W., Yang, Y., Liu, X., Zeng, Y.Y., Cheng, M.*, et al.* (2022). Single-cell Stereo-seq reveals induced progenitor cells involved in axolotl brain regeneration. Science *377*, eabp9444.
Wilhelm, J., Pingoud, A., and Hahn, M. (2003). Real-time PCR-based method for the estimation of genome sizes. Nucleic Acids Res *31*, e56.
Wittstatt, J., Reiprich, S., and Kuspert, M. (2019). Crazy Little Thing Called Sox-New Insights in Oligodendroglial Sox Protein Function. Int J Mol Sci *20*.
Woodcock, M.R., Vaughn-Wolfe, J., Elias, A., Kump, D.K., Kendall, K.D., Timoshevskaya, N., Timoshevskiy, V., Perry, D.W., Smith, J.J., Spiewak, J.E.*, et al.* (2017). Identification of Mutant Genes and Introgressed Tiger Salamander DNA in the Laboratory Axolotl, Ambystoma mexicanum. Sci Rep *7*, 6.
Woych, J., Ortega Gurrola, A., Deryckere, A., Jaeger, E.C.B., Gumnit, E., Merello, G., Gu, J., Joven Araus, A., Leigh, N.D., Yun, M.*, et al.* (2022). Cell-type profiling in salamanders identifies innovations in vertebrate forebrain evolution. Science *377*, eabp9186.
Xi, Y., Yu, M., Godoy, R., Hatch, G., Poitras, L., and Ekker, M. (2011). Transgenic zebrafish expressing green fluorescent protein in dopaminergic neurons of the ventral diencephalon. Dev Dyn *240*, 2539-2547.
Xie, Y., Zhou, J., and Chen, B. (2022). Critical examination of Ptbp1-mediated glia-to-neuron conversion in the mouse retina. Cell Rep *39*, 110960.
Xiong, M., Tao, Y., Gao, Q., Feng, B., Yan, W., Zhou, Y., Kotsonis, T.A., Yuan, T., You, Z., Wu, Z.*, et al.* (2021). Human Stem Cell-Derived Neurons Repair Circuits and Restore Neural Function. Cell Stem Cell *28*, 112-126 e116.
Yadav, A., Matson, K.J.E., Li, L., Hua, I., Petrescu, J., Kang, K., Alkaslasi, M.R., Lee, D.I., Hasan, S., Galuta, A.*, et al.* (2023). A cellular taxonomy of the adult human spinal cord. Neuron *111*, 328-344.e327.
Yamamoto, K., Ruuskanen, J.O., Wullimann, M.F., and Vernier, P. (2010). Two tyrosine hydroxylase genes in vertebrates New dopaminergic territories revealed in the zebrafish brain. Mol Cell Neurosci *43*, 394-402.
Yamamoto, K., and Vernier, P. (2011). The evolution of dopamine systems in chordates. Front Neuroanat *5*, 21.
Yan, C.H., Levesque, M., Claxton, S., Johnson, R.L., and Ang, S.L. (2011). Lmx1a and lmx1b function cooperatively to regulate proliferation, specification, and differentiation of midbrain dopaminergic progenitors. J Neurosci *31*, 12413-12425.
Yang, G., Yan, Z., Wu, X., Zhang, M., Xu, C., Shi, L., Yang, H., and Fang, K. (2023a). Ptbp1 knockdown failed to induce astrocytes to neurons in vivo. Gene Ther.
Yang, H.J., Vainshtein, A., Maik-Rachline, G., and Peles, E. (2016). G protein-coupled receptor 37 is a negative regulator of oligodendrocyte differentiation and myelination. Nat Commun *7*, 10884.

Yang, R.Y., Chai, R., Pan, J.Y., Bao, J.Y., Xia, P.H., Wang, Y.K., Chen, Y., Li, Y., Wu, J., and Chen, G. (2023b). Knockdown of polypyrimidine tract binding protein facilitates motor function recovery after spinal cord injury. Neural Regen Res *18*, 396-403.
Yao, X., Wang, X., Hu, X., Liu, Z., Liu, J., Zhou, H., Shen, X., Wei, Y., Huang, Z., Ying, W*., et al.* (2017). Homology-mediated end joining-based targeted integration using CRISPR/Cas9. Cell Res *27*, 801-814.
Yu, Y., Tang, J., Su, J., Cui, J., Xie, X., and Chen, F. (2019). Integrative Analysis of MicroRNAome, Transcriptome, and Proteome during the Limb Regeneration of Cynops orientalis. J Proteome Res *18*, 1088-1098.
Yu, Z.Y., Shiga, S., Casco-Robles, M.M., Takeshima, K., Maruo, F., and Chiba, C. (2022). The latent dedifferentiation capacity of newt limb muscles is unleashed by a combination of metamorphosis and body growth. Sci Rep *12*, 11653.
Yun, M.H., Hayashi, T., and Simon, A. (2022). Standardized gene and genetic nomenclature for the newt Pleurodeles waltl. Dev Dyn *251*, 911-912.
Zhao, X., and Moore, D.L. (2018). Neural stem cells: developmental mechanisms and disease modeling. Cell Tissue Res *371*, 1-6.
Zhou, H., Su, J., Hu, X., Zhou, C., Li, H., Chen, Z., Xiao, Q., Wang, B., Wu, W., Sun, Y*., et al.* (2020). Glia-to-Neuron Conversion by CRISPR-CasRx Alleviates Symptoms of Neurological Disease in Mice. Cell *181*, 590-603 e516.

8. SUPPLEMENTARY MATERIALS

Supplementary Table. 1 | Primers and gRNA sequences

Primer	Sequence
Vglut2 genotyping F1	GGTGCTACTACAGACCAAGC
Vglut2 genotyping R1	GGGGTATACTTGATTGGAGATGA
Lmx1b genotype F1	TGCAAACCAGGCTCGCAG
Lmx1b genotype R1	GCGGGTGGTCCTCAAGTTTA
Lmx1b genotype F2	ACCTCCTTAACGAGCCTCAG
Lmx1b genotype R2	AAGAACAAGGATGCGGGTTG
GFP F1	CAAGCTGGAGTACAACTACAACA
GFP R1	GAACTCCAGCAGGACCATGT
Cre F1	AATGCTTCTGTCCGTTTGCC
Cre R1	CATTGCTGTCACTTGGTCGT

gRNA / crRNA	Sequence
Lmx1b gRNA10	CAGCCCCTGAGTCTCTGGAG
Lmx1b gRNA11	ATCACACATGGGGGGTCGGT
Lmx1b gRNA12	CTCCTGACATTCGGACCCGA
Vglut2 gRNA1	ATACCATTATAGGGAAGGAG
Vglut2 gRNA2	GAACCATACCATTATAGGGA
Vglut2 gRNA3	ACAAGAACCATACCATTATA

Supplementary Table. 2 | Primary antibodies used in the thesis

Antibody	Catalog number and Producer	Clonality	Host	Antigen retrieval	dilution
Human Otx2 Antibody	AF1979, R&D/Novus	Polyclonal	Goat	Yes	1:200
Anti-Otx1 + Otx2 antibody	Ab21990, Abcam	Polyclonal	Rabbit	Yes	1:200
OTX2 Recombinant Rabbit Monoclonal Antibody (14H14L5)	701948, Thermo Fisher Scientific	Monoclonal	Rabbit	Yes	1:200
Anti-SOX2 antibody	ab97959, abcam	neural stem/ progenitor cell, neruon	Rabbit	Yes	1:200
AIF-1/Iba1 Antibody	NB100-1028, R&D/Novus	Polyclonal	Goat	No	1:200
Anti Iba1, Rabbit	019-19741, Wako	Polyclonal	Rabbit	No	1:500
Tyrosine Hydroxylase Antibody	NB300-110, R&D/Novus	Polyclonal	Sheep	No	1:500
Tyrosine Hydroxylase Antibody	NB300-109, R&D/Novus	Polyclonal	Rabbit	No	1:500
Anti-Tyrosine Hydroxylase Antibody, clone LNC1	MAB318, MERCK	Monoclonal	Mouse	No	1:500
Anti-Tyrosine Hydroxylase Antibody	AB152, MERCK	Polyclonal	Rabbit	No	1:500
GFAP Antibody	NBP1-05198, R&D/Novus	Polyclonal	Chicken	No	1:200
Anti-Glial Fibrillary Acidic Protein (GFAP)−Cy3 ™ antibody, Mouse monoclonal	C9205, MERCK	Monoclonal	Mouse	No	1:500
Anti-Vimentin Antibody	AB5733, MERCK	Polyclonal	Chicken	No	1:200

Antibody	Catalog number and Producer	Clonality	Host	Antigen retrieval	dilution
Human/Mouse /Rat Vimentin Alexa Fluor® 647-conjugated Antibody	IC2105R, R&D/Novus	Monoclonal	Rat	No	1:200
SOX6 Polyclonal Antibody	PA5-34616, Thermo Fisher Scientific	Polyclonal	Rabbit	Yes	1:200
SOX6 Antibody	NBP1-86149, Novus	Polyclonal	Rabbit	Yes	1:500
Human/Mouse Nurr1/NGFI-B beta /NR4A2 Antibody	AF2156, R&D/Novus	Polyclonal	Goat	Yes	1:200
Nurr1/Nur77 Antibody (E-20)	sc-990, Santa Cruz	Polyclonal	Rabbit	Yes	1:200
Nurr1 Polyclonal Antibody	PA5-22830, Thermo Fisher Scientific	Polyclonal	Rabbit	Yes	1:200
GPR37-3	#GPR37-3, MABTechnologies	Polyclonal	Rabbit	No	1:200
Human GPR37 Antibody	MAB44502, R&D/Novus	Monoclonal	Mouse	No	1:200
Human/Mouse Aldehyde Dehydrogenase 1-A1/ ALDH1A1 Antibody	AF5869-SP, R&D/Novus	Polyclonal	Goat	No	1:200
Anti-ALDH1A1 antibody	ab9883, Abcam	Polyclonal	Goat	No	1:200
Anti-LMX1b antibody	ab129306, Abcam	Polyclonal	Goat	Yes	1:100
LMX1B Polyclonal Antibody	PA5-34471, Thermo Fisher Scientific	Polyclonal	Rabbit	Yes	1:100

Antibody	Catalog number and Producer	Clonality	Host	Antigen retrieval	dilution
LMX1A Polyclonal Antibody	PA5-34470, Thermo Fisher Scientific	Polyclonal	Rabbit	Yes	1:100
c-Fos (E-8) Antibody	sc-166940, Santa Cruz	Monoclonal	Mouse	Yes	1:500
Calbindin D-28k	300, Swant	Monoclonal	Mouse	Yes	1:1000
Calretinin	7697, Swant	Polyclonal	Rabbit	Yes	1:1000
NFIA Antibody	PCRP-NFIA-2C6, DSHB	Monoclonal	Mouse	Yes	1:10
Monoclonal Anti-NFIX antibody	SAB1401263, MERCK	Monoclonal	Mouse	Yes	1:200
PTBP1 Rabbit pAb	A6107, Abclonal	Polyclonal	Rabbit	Yes	1:200
Human HNF-3 beta /FoxA2 Antibody	AF2400, R&D/Novus	Polyclonal	Goat	Yes	1:200
FOXA2 Polyclonal Antibody	PA518169, Thermo Fisher Scientific	Polyclonal	Goat	Yes	1:200
FOXA2 Antibody	PCRP-FOXA2-3A2, DSHB	Monoclonal	Mouse	Yes	1:50
HNF-3β Antibody (M-20)	sc-6554, Santa Cruz	Polyclonal	Goat	Yes	1:100
Human/Mouse /Rat MBP Antibody	MAB42282, R&D/Novus	Monoclonal	Mouse	Yes	1:200
MBP Antibody (12)	NB600-717, R&D/Novus	Monoclonal	Rat	Yes	1:500
MOG Antibody (CL2858)	NBP2-46634, R&D/Novus	Monoclonal	Mouse	Yes	1:100
Human/Mouse /Rat Olig2 Antibody	AF2418, R&D/Novus	Polyclonal	Goat	Yes	1:100
Human/Rat SOX10 Antibody	MAB2864, R&D/Novus	Monoclonal	Mouse	Yes	1:100

Antibody	Catalog number and Producer	Clonality	Host	Antigen retrieval	dilution
Human SOX10 Antibody	AF2864, R&D/Novus	Polyclonal	Goat	Yes	1:100
FoxO1/FKHR Antibody (83N7F8) - BSA Free	NBP2-31376, R&D/Novus	Monoclonal	Mouse	Yes	1:200
Human EGR1 Antibody	MAB2818, R&D/Novus	Monoclonal	Rat	Yes	1:200
Stat1 (D1K9Y) Rabbit mAb	14994, Cell Signaling Technology	Monoclonal	Rabbit	Yes	1:200
Human LYPD1 Antibody	AF6855, R&D/Novus	Polyclonal	Sheep	No	1:200
VIP Antibody (576721)	MAB6079, R&D/Novus	Monoclonal	Mouse	No	1:200
Mouse/Rat Wnt-5a Antibody	AF645, R&D/Novus	Polyclonal	Goat	No	1:200
GFP Antibody	600-101-215, Rockland	Polyclonal	Goat	No	1:500
Cre Recombinase	C7920, US Biological	Monoclonal	Mouse	No	1:500

Supplementary Table. 3 | mRNA orthologues of the newt used to design *in situ* probes

mRNA	**Identities to the human mRNA orthologue in conserved region (%)**	**Study**	**Technique**
GFAP	72	brain	digoxigenin-labelled ISH
LMX1A	70	brain	digoxigenin-labelled ISH
LMX1B	79	brain	digoxigenin-labelled ISH
DDC	72	brain	digoxigenin-labelled ISH
ALDH1A1	75	brain	digoxigenin-labelled ISH
DRD1A	75	brain	digoxigenin-labelled ISH
DRD1B (DRD5)	75	brain	digoxigenin-labelled ISH
DRD1C	not found in mammals	brain	digoxigenin-labelled ISH
DRD2	75	brain	digoxigenin-labelled ISH
DRD3	79	brain	digoxigenin-labelled ISH
DRD4	70	brain	digoxigenin-labelled ISH
FOXA2	78	brain	digoxigenin-labelled ISH
GPR37	79	brain	digoxigenin-labelled ISH
GPR37L1	71	brain	digoxigenin-labelled ISH
*SHH**	75	brain and limb	digoxigenin-labelled ISH and RNAscope
*IHH**	74	limb	RNAscope
*GLI1**	70	limb	RNAscope
*PTH**	no significant similarity	limb	RNAscope
*PTHRP**	71	limb	RNAscope

*(Kaucka et al., 2022)

Supplementary Table. 4. | Probes (antisense) designed and tested for ISH

Probe	Sequence (antisense)
Gfap	TCCTCGAAGTGCCTCCATTTCACTGTTGAGGCTCTGGAGCTGGCGCCGGTACTCGTTGGCTTCTTGCTTAGCCTGCCGCAAAGCTTC ATTGTTACGCGCTGCTGCATCGGTCATCTCAGCAAACTTGGATTTATACCATTCCTCAGTTTCCTGTAGATTGGAGGACGCCAGAGA CTCGTACTGAACACGAATCTCCCGCAGCGCAGCGGTCAGGTCAGGCTTCACCAAGTCTTTTTCGATGTGAACCTGTTGATGGGTCAG CTGGTCATGCAGCTCTCGCAGCTCCTCGTCGTGGACTTTCTTCAGAAAGTTGATCTCATCCTGTAAAGATTCAATTTTCCTCTCCAG ATCTACACGGATCAGGGATGCGTCATCCACATCCTGTCTGTATGAAGACAAATTGTTTTCAGCTTCCGAGCGAAGATTAATCTCGTC TTGTAACCTACGCCTCAGCTTCTCTACATCCTCTGCTAAGTTGTCTCTCTCGATCTCTGTCCGGGCCTTGGCATTGGCCAGCTGGTC CAGCTGTCGCCTCAGATCCCTCAGCTCCTCCTGGTAGATGTCACCCAGGTGGGTGGGCTCCTTCTCCCGGATCTGGTTGAGCTCGGT CACCAGCACCTTGTTTTGCTGCTCCAG
Lmx1a	CCTCCAAGCCATGAACACTGGCCCCATCTTCACTGTCATCATTGCTCTGTCGGCTGTTCCTGCTGGCCCCGCGTCCAGACCCCAGGC GTGGGTTGCCAAGTTGGTCTTGCTCCTGCTGCTGTTGCTGCTGCTGCTGCCTTCGTGCAATCTTTTTCATCTTGGCTCTTTGATTCT GGAACCAAACCTGGACCACACGGACAGTGAGGCCGGTCTCAGCAGCCAATGTCTCTCTCACCTTTCGGCAGGGCTTGGAGGACACCT CGAATGACGCTTTGAAGGCCCGCCGCTGCTGCGTGGTCAGGATGGTCCGCGGCCTCTTTGAACGCTTATGGTCTTTACTGTCATCGC CCCCTTTACCTTGTGAGTGGCTGCCATCCTCATCTTCACTTTTAACTGATTCTGTGGGGGTGGGGCTGATGGCCGACAGCATCTCCT TTTCTTTTTCATAGTCACTCCGACAGAGGAGCTGGCCTTCCTTCAGCACAAACTCGTCCCCCCGCTGTAATCGGCGCTCGCACTCGC AGCAGTAGAAACAGTTCACATGGTAGACATTGTCCAGGACTCGCATGATGAACTCAGATGGGTTGATCACCTTCAGACAGCTGCTGC ACTTTGTTGCAAAAAGTTTTTCATAGTCGTGCTTGCAGTACAGCTGTCGGTTGCGGCAGAAGCAGGTGCCGGAGAGCTGCTGGAGGC AGGCAGCACACTTCACACAGGCCTCATGCCAGGATCGTTCATTGACTCGCAGGAG
Lmx1b	CTTCGCTCTCTGGTTCTGGAACCAAACTTGAACAACGCGTACACTGAGCCCCGTTTCTGCTGCTAATGTCTCCCTAACCTTCCTGCA GGGCTTGGAGGACACCTCGAAGGACGCTTTGAAGGCGCGCCTCTGTTGTGTTGTGAGGATTGTTCTAGGCCGCTTGGGCCTTCTTGG GTCCTTCCCATCGTCGCTGCCTTTCCCTGGGGTGGGCTGTCCTTTGCACGGTTTGATGTCGCCATCCTCGTCATCGCTCTTAACTGA GTCGGAGTCGTCGGGGCTGACGGAGCTGAGGAGATCTTTCTCCTTCTCATAGTCACTTTTGCACAGCAACTGTCCTTCCTTCAGCAC AAACTCGTCGCCTTTCCTCAGCTGTCTCTCGCAGACGCAGCAGCAGAAGCAGCTTAGGTGGTAGACG
Ddc	TGAGGCCAGCAGCTTTATCTTCTTCCATAGCTTTCCTCAGGGCCGGTCCACGAGCCGCAAACTTTTCATCAGAAGGGATTACTTTCA TTTTTACACCACCAATCAAACCAGCCCTCTCCACCGATGAGTGGGCCTGGTCTGAAGAATATCCCACAAGCTTGTCCATGATTTCGG CTTTCGACAGTTCAGGGTGTTTAAGCTGTAATTGTTGTAACACTTTTGTTCTGGCAGCAAGCAGCACCATTAAGGACGCCTCACTAG CAGTGCCCTGAATTACTCCGCCACCTTCTCCGTCATTTCCAGCTAAAAACTCTTTGGGTAAATTGATCATTTTCCCCAGCCAGTCCA ACATGACTGTCTCGAGCTCTGTGCAAGCCGGACTGGCAGTCCAGGAAAAGCCAATACATCCAATAGCACCACACAGCATGTCTGCTA GTAAAGATGGATATGACTGTCCGGCAGGGAAATAGGCAAAGAAGTAGGGGCTGTGCCAGTGAGTCACTCCAGGCATAATAACCCTTT CTACATCTTTCATGACATCTTCAAATGTCTCAGGATCCTCGGGTGCAGATTCGGGAAGCATAGGTCTTAGATACCCAGGATTCAGGT CAGG
Aldh1a1	AATTGGGCTCTTTCCTCCGAGTTCTAGAGTCACCCTCTTCAGGTTACTTTTTCCAGCAGCTTCTTTGATCATTTTGCCAACCTCTGT TGATCCAGTGAAAGCCACTTTGTCAACATCCATGTGGTGAGAAATAGCTGCTCCTGCTGTTGGTCCGTATCCTGGCACGATGTTTAC AACACCTGGTGGAATTCCAGCCTCTTGGATCAATGATCCCATGTAGAGAGCAGAAAGTGGCGTTTGCTCTGCTGGTTTAATTACAAC GGTGTTCCCACAGCAGAGAGCAGGTGCGAGCTTCCAAGCAAACATCACCAAAGGGAAGTTCCATGGAATAATTTGACCGCATACACC AACAGGCTCGTGTCTTGTAAATGTAAAGAAGTCTCCATCTGAGGGAATAGTGCGTCCATGATTTTTATCAGCCCAGCCTGCACAGTA CCGCAATGATTTAATGGCACCAGGCACATCAGCGTAGTAGGCAGCAGAAA
Drd1a	TCCCCATCCTCCTCTTTCTTCAGATCATCCTCCTCTGGACAGATGATGGCGTGAGGAATCAGGTAGACCAGGTTGCAGTCATTTGGG ATGGACCCCTTGGGCTCATGTTGACAAGAGAAAAGGACTGCCCCATTGTTGTTGATACTCACTGTCTCAATGGCATTACTAGAGCTG GGGCAGAGCCTGTAGCAGCCGAGAAGAGTTGAGAAGGCCTTGCGGAAGTCAGCATTGAAGGCGTAGATGATCGGGTTAAGAGAGGAG TTGGCCCAGCCGAACCAAACAAATACATCAAAGGTAGTGGAGCTGATGCAGAAGGGCTCTGCCCCACCAGAAGTGTAGCTGGGGTCG CAGAAGGGCACCATGCAGTTTAATATAAAAAAAGGTAGCCAGCAGCAGACAAACACCCCCATTATAACAGATAAGGTCTTAAGGACC TTGGTCTCCCGCTTGAAGGACATTTTGAACGAACTTTCTGGTTGCTGGCAGTCCATGCTGCTGCCATTGCCTGTGCTGCTCTGGCAG TTCTTGGCATGCACCGCTGCCCTTTCTAGGGCAGAGATGCGCCTAATCTGCTTTGCTGCAATCCT
Drd1b (Drd5)	GCAGTTCAGGACGAAGAAGGGAAGCCAGCAGAAGACGAAGACGCCCATGATGACAGACAGCGTCTTCAGCACCTTGGTCTCCTTGCG GAGAGAGTGGCGCAGTCTCTTGTGGTGCTGCTGGCAGTCCAGTCGTGCGGTCCGGCAGCTTTGGGCGTGCTCGGCCGCCCTCTCCAG AATGGAGATGCGCCGTATCTGCACCTGGGCGATGCGGTAGATGCGGGTGTAGGTGACTATCATAATAGCCACAGGAATGTAGAAGCT GATGAGGGAGGAGGAGATGGCATATGTCCGGTTAAGGCTAGAGTCGCAGTCCTGACTGATGGTGTGGTTGCTGCGGGGACTCTCGGC TCCACTGCGGTGCCAGTCCAGTTGCACGGGGATGAAGGAGATAAGCACAGAGAGTGTCCATGCTGTGCCGATCATCACCAGGGCCGC GCGCGGGGTCATCTTGCGCTCGTACCTGAAGGGGTTGGAGATGGCCCAGTAGCGGTCCACGCTGATCATGCAGAGGTTCAGGATGGA GGCCGTGGAGCACATGATGTCAAAGGCTATCCAGATGTTGCAGAAGGCTCCAAAGGGCCAATGACCAGCTACTTCAGCCACAGCCTT CCAGGGCATAACCAACAGCGCCACCAGCAGGTCGGACACGGCCAGAGAAATAA
Drd1c	AGCGGTTGCAGCCTAGAATAGTGGAGAAGGCCTTCCGGAAGTCCGCGTTAAAGGCATAGATGACTGGGTTAAGTGAGGAGTTAGCCC AGCCAAACCACACAAAGATGTTGAAGGTAGTCTCACTGACACATGGTGGCTCGGCCTCCCCTTCCAGAGACATGCTGATGTCACAAA AGGGCACCAGACAGTTAAGTACAAAGAAGGGTAGCCAGCAGAAGACAAACACTCCCATGATGATGGAGAGAGTTTTGAGTACCTTGG TTTCCTTCTTAAAGGAAGTCTTGAGTGAATTCTCATGTGGGCAGTCTGGTTGGCAGCTCTGGGCATGCTCCACTGCACGCTCCAGGG AGGAGATCCTGCGGATTTGTGTCTGTGCAATACGATAAATGCGGGTATAGGTGCCAATCATGATAGCGACTGGGATGTAGAAGCTGA TGAGGGAGGAAGAGATGGCATAGGTGCGGCTCAAGCTTGAGTCACAATTAATGCTTTGATTGGTGGCATTCAAGGCCATGTCAGATT CTGGGGCCTTGTGCCAATTAAGTTGCACTGGAATGAAGGAGATTAGGATGGACAGTGTCCAGGCCACGCCAATCATGATGAAGGCCA CTCTCTGTGTCATTTTCCTTTCATATCGGAAGGGACTGGCGATGGCCCAGTAACGGTCCAGGCTGATAATGCAGAGGTTGAGGATGG AAGCAGTGGAGCACATGATATCAAAAGCCACCCAGATGTCAC
Drd2	GGGTGAGTGCATTTGTCCTTCAGTGGGCCGTCGTGCTCTAGACCATGGCCATTTCGCTTGGTGTTCACCCTTTTCCGGCGCTTCCGG AGGACGATATAAATCTGCACATACACCAGCAGCGTGACAATGAAGGGGGCGTAGAAGGAGACAATGGAGGAATAGACAACAAAAGTG GGATTTTCAATGAGGCATTCATTGTCCGCTGTGTTATTGAATCCAAATAAAATTGGACAGGAGATGGCAAAGGAGAGTACCCATACC ACCGAAATCATAACAGTTACTCTTCGCTTTGAACTGTATCTAGTGTTATAAAGCATTGGCATGGCTACAGCAGTATACCTGTCAATG CTGATGGCGCAGAGATTGAGAATGCTAGCAGTGCACATCATGACATCCAGGGTGACAAAGATATCACAGTGGATTCGGCTGAACCGC CACTCACCAACCACCTCAAGATAGACCACCCATGGCATGACTAGTGTGGCCACCAGAAGATCTGCCACTGCCAGACTGACTATCAAG TAGTTGGTGGTGGTCTGAAGCGCTTTTTC
Drd3	CTGGTCAACACCTTCTCGCTGCTTTCCACTCTTCCATTAGCTTCAGGCAGCGGTGCTCTGTCCCGGACCAAGAAGCGCTTGATGCGA GTGAGCTGCAGGCTGGTGCCTTTGGCTCCGATGGCCTTGACCTGCGCGAGTCTCAGGCTCTCCCCCCTCCGCTTAGTGCCAATTATA CGCTTTCTTCTGCTCCGTAGCGCGAAGTAAATCCGGATGTAAACCAGCAGCGTCACCACAAACGGCAAGTAGAAGGAGACCACGGAG

	GAGTAGATGACAAAGTCAGGGTTTGATATGGAGCAGATCTCGGGGTCTCCTGTGGTGTTGAAGCCAAACAGTAATGGGCAGGAGACT GCGAACGACAAAACCCAGACAGTCAGAATCATGAGGGAGACGCGCCTGCAGGAGCTCTCTCCCGTGTTGTATTGCACTGGCATGACC ACTGCGGTGTACCTGTCGATGCTGATGGCACAGAGGTTTAAAATGCTGGCTGTGCACATCATGACATCCATTGTCACAAAAACATCA CAGGAGGTACGGCTGAAGTTCCAGACCCCACCAGTCACCTCCAGATACACCACCCAGGGCATCACCAGCGTGGCCACCAGCAGGTCC GCCACCGCCAAGCTGACCACCAAGTAGTTGGTCATGGTCTGCAAGGACCTCTCCCTCAGCACCGCCAGACAGACCAATGCGTTTCCA AACACAATGGCGAAAATAAGGAGGCAGTAGAGCAGGGAGTAGTAGCTATGGGGGTGCGGCAGACTGTGCACAGTAAAGTTCTCCTGC CCGCAG
Drd4	ACAGGTAGCACCTTCATCGCCTTCCTCTCCCGGCCACAGATTTTGGCTTGCTTCCTTTGCGGTACAGGGTGGGGTGTATACTTCAGT TCGGGGTATGCCACTGTCTGTATGCCATGGCCATTTTCCACATAAGCCCGGGGGAATGGGCATTCTGAATGACTGTAGATACTTAAG TCCTCCAGTCTACTGTCACTTGGGCTCCTATCGAAGAGCAACGGTGGGCATGGCGGCTTCCCTTCTGGGTTCATGTGACTCCTTAAC TTAGCCTTTCTAGCCTCTTCCCAGCGCCTCAGGCCATTGAACATGGCACAATAGAGTACCAACATGATGGGGCAAGGAATGAAGAAG GAACAAATGGAAGAGTAGATAACAAAATTGTCATCCTCCAGTTTGCATATAGTAGGGTCCCGGTTTGGGACATTGTTGAGTCCAAAG ATGACAGGCGATGCAACAGCAAATGAAAATATCCAAGTGGTGGAAAGGAGAAAGAGCTGGCGGTTGTCAACTTGGCGGCGGTTGTAA TTTAGTGGAATGGAGACAGCTATGAACCGGTCAACGCTGATTGCACAG
Foxa2	AGGAAGCAGTCGTTGAAGGAGAGCGAGTGGCGGATGGAGTTCTGCCAGCGCTGCTGGTTCTGCCGGTAGAAGGGGAAGAGGTCCATG ATCCACTGGTAGATCTCGCTCAGCGTCAGCATCTTGTTGGGCGACTGCTGGATGGCCATGGTGATGAGCGAGATGTAGGAGTAGGGC GGCTTGGCGTGCGTGTAGCTGCGCCGGTAGCTCTTGGGGTCCCGCGAGCGGTTGATGGCCGACTGGCCGTAGAGGGGGCTCATGGAG CTCATGCTGGGGTAGGGCGCCAGGCCGTTCATGGCGGGGGCCTGGGCGCTCATCGGGCTCAGGCTGGGGCTCAGGTGGCTGCCCATT CCGGCGCCCATGCCGCCCATGGTGCCCGGGGACATGCCGGCCAGCGACGGGCTCATGGCCGTGTTCACGTAGGACATGTTCATGGGG GCGGCGGACATGTTGGCGCTGGAGCTCATGGCGGACATGCCCATGTAGGTGTTCATGCTGTTCATGCTCAGGCCGGCGTTCATGTTG CCCACGGAGGGGTAGGTCTCGGGCTCGGCATAGTAGCTGCTCCAGTCGTTGTGCTCGTGTCCTTCCATCTTCACGGCT
Gpr37	CAGGGGCAGACAGAAGAAGATGATCAGGAAGTCCCAGAAGGCGAGGTTGGCCAGCAGCGAGTTTGAGATGCTCCGCATGTAGTAGTT GTGGCAGACAATGCACATGATGGCCATGTTGCCCATGATTCCGATGACAAAGATGACTACCGCAAGGCACATGATCCCGTAGGCCCC ATAGGACTCCTCGGTCAGTGGGTAGAAGGGGTTCTTCAGGCGGGGCCTCTTGTTGCTGGTGTTTCTGGGGAACAGACCCTGGTTTAT TTCCAAGTCATCCGGCACTGTTTGCAGAATGTAGGAGTCATTGAGAGCTAGGTATTGCGGTACTGGTGGAGCCGTGGGAGTCTGATG AGACTCATTCATGTGCCCTTTAAGGGAACTTTCGTTCCTTGGGTTCTTGTTTTTCCCTCTGCTTTTTCTCTCTTGGGAGCCACCGGA TGCTCTTTTGCTTCTATAGTGAAGACCCTCTGCAGC
Gpr37l1	ATGGACAGGTTGCCGATGATGCCCACGGCGAAGACGATCAGTGAGAGCAGCATCACGGCGTAGGCGCTATATGAGTTCTCCGTCATG GGGTACAGTGGGTTCTGGACCTGGGGGCGCTTCTGGCCGGTCGCGGTTTTGTTCCCCAGAGGTCCCCTCTCAGCCTTGTCGGTCCCC GAGGCCCCTCCATGTCCACCTTTGGAAGGGTCTGTGCTTGAAGGAAGCAGGGGCTTGGTAGGCCTCAGGTGGGCCGGGTCAATGAGT CGAGGGTACTCGGCGATTACTCTTGGCTCATACTGCTGCACAGCCTTGGCATCATCGTCCTCTGCACCTCTGCGGGCTCGCAACAAG GTCCCAGGGGTGTCCGGGGCACTCCGCCGTCGCCCCCTGCTCATTCGAAGCCAATATTGCCCAGGTGTTTCCACTGACGGGTTCCCC GTCCCTCGGTTTTCCGAAAACATCTCTTCCGCA

Supplementary Table. 5 | Sample information of scRNAseq and snRNAseq

Sample name	Treatment	Number	Age	Sample type	Cell/Nucleus number after FACS	[DNA] cDNA (ng/µl) by qubit assay	[DNA] Library (ng/µl) qubit assay	Sequencing type	Cutoff of knee_plot	Nuclues number recovered after knee_plot	Doublets estimation	Number after removing doublets
P27159_1003	6-OHDA brain injury	2	young adult	Nucleus	74290	4,8	22,4	NovaSeq S1 100 cycles	400	4473	0.076	4133
P27159_1004	6-OHDA brain injury	2	young adult	Nucleus	74290	6,2	43,4	NovaSeq S1 100 cycles	400	4031	0.076	3725
P27160_1004	6-OHDA brain injury	3	young adult	Nucleus	64289	2,98	20,8	NovaSeq SP 100 cycles	300	5949	0.076	5497
P28512_1010	Sham brain injury	2	young adult	Nucleus	160670	9,5	50,2	NovaSeq6000 S2-100	800	4628	0.076	4276
P27160_1003	Sham brain injury	5	young adult	Nucleus	81944	2,5	20	NovaSeq SP 100 cycles	1200	3775	0.076	3488
P28512_1014	Uninjured VMb	3	old adult	Nucleus	300719	3,22	20,4	NovaSeq6000 S2-100	300	5669	0.076	5238
P28512_1015	Uninjured VMb	3	old adult	Nucleus	300719	3,38	20,8	NovaSeq6000 S2-100	300	4804	0.076	4439
P28512_1011	Uninjured VMb	2	young adult	Nucleus	56247	5,1	24,2	NovaSeq6000 S2-100	300	4763	0.076	4401
P27160_1002	Uninjured VMb	5	young adult	Nucleus	124000	3,7	28,6	NovaSeq SP 100 cycles	500	8379	0.076	7742
P18856_1003	Uninjured VMb	3	young adult	cell	6488	not available	not available	NovaSeq S1, 100 cycles	1000	301	0.01	298
P20861_1003	Uninjured VMb	8	young adult	cell	19200	not available	not available	NovaSeq SP, 100 cycles	1000	2363	0.031	2290
P28512_1012	Uninjured VMb	8	larvae st.54	Nucleus	161443	2,08	13,4	NovaSeq6000 S2-100	400	886	0.008	879
P28512_1013	Uninjured VMb	8	larvae st.54	Nucleus	161443	2,7	20,8	NovaSeq6000 S2-100	400	1946	0.008	1930
P27160_1001	Uninjured VMb	7	larvae st.54	Nucleus	4118	0,7	19,1	NovaSeq SP 100 cycles	200	806	0.008	800
P23151_9015	Uninjured VMb	6	larvae st.54	cell	51247	not available	not available	NovaSeq S2, 100 cycles	1000	1205	0.031	1168

Supplementary Figures

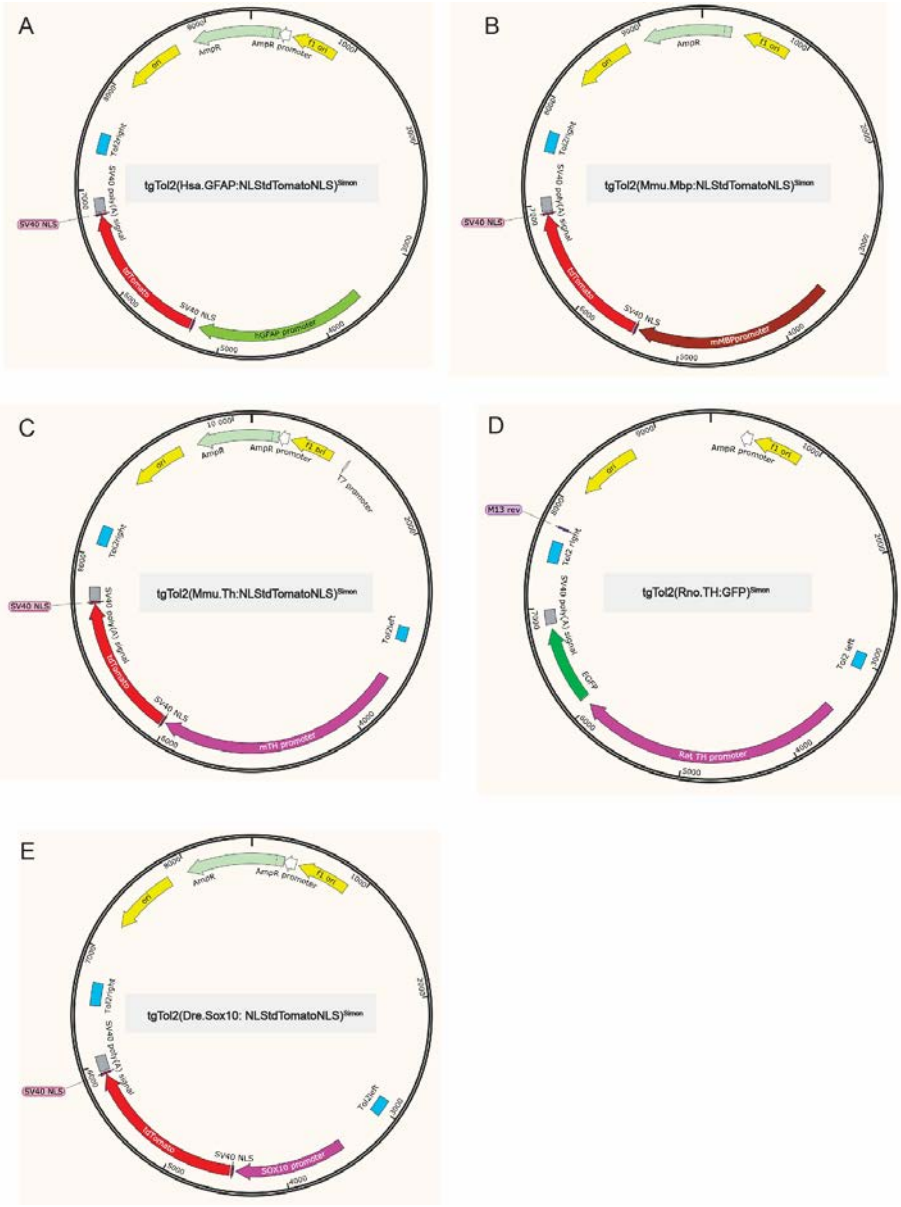

Supplementary Fig. S1 | Maps of plasmids used to label specific cell types in Tol2-mediated transgenic newts. tgTol2(Hsa.*GFAP:NLStdTomatoNLS*)^{Simon} **(A)** for ependymoglia, tgTol2(Mmu.*Mbp:NLStdTomatoNLS*)^{Simon} **(B)** and tgTol2(Dre.Sox10*: NLStdTomatoNLS*)^{Simon} **(E)** for oligodendrocytes, tgTol2(Mmu.*Th:NLStdTomatoNLS*)^{Simon} **(C)** and tgTol2(Rno.*TH:GFP*)^{Simon} **(D)** for dopaminergic neurons.

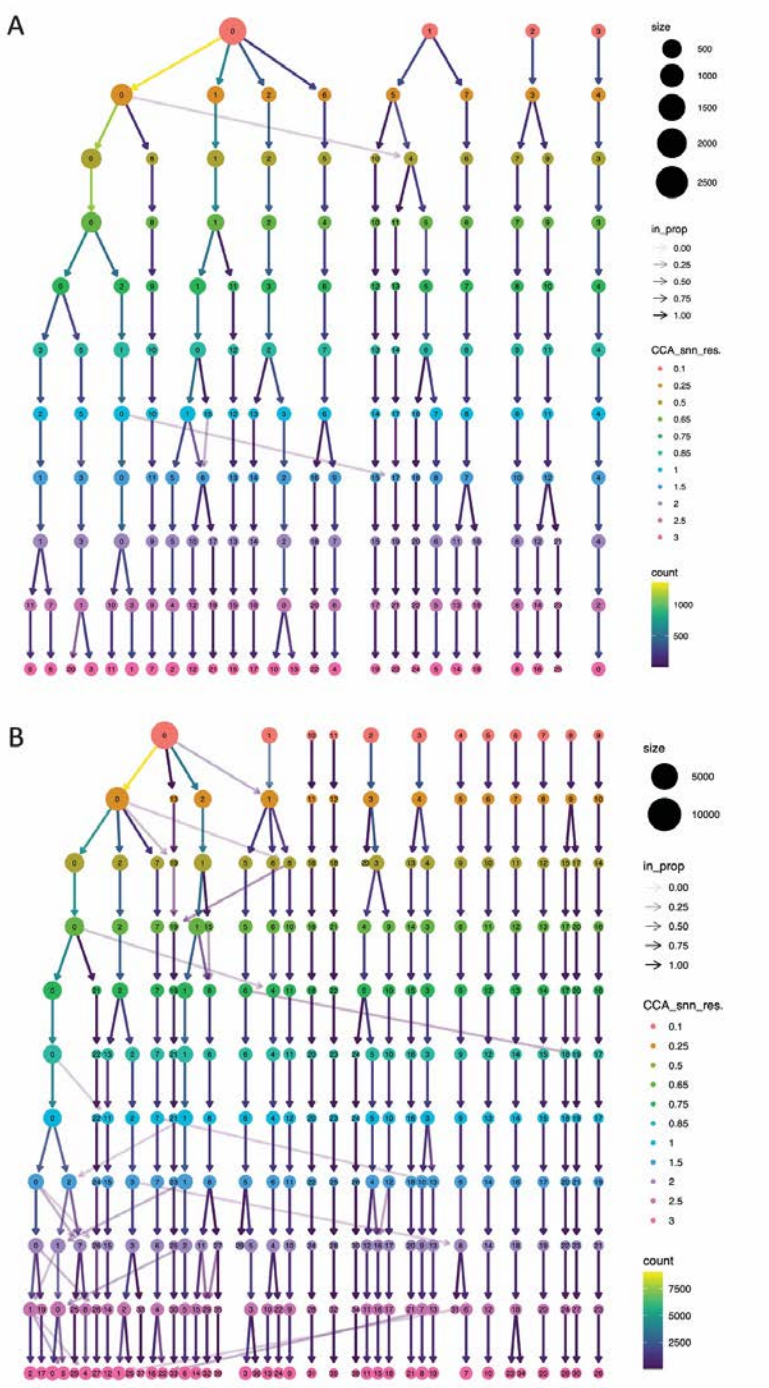

Supplementary Fig. S2 | Unsupervised clustering classified the events from scRNAseq (A) in less clusters than the events from snRNAseq (B)

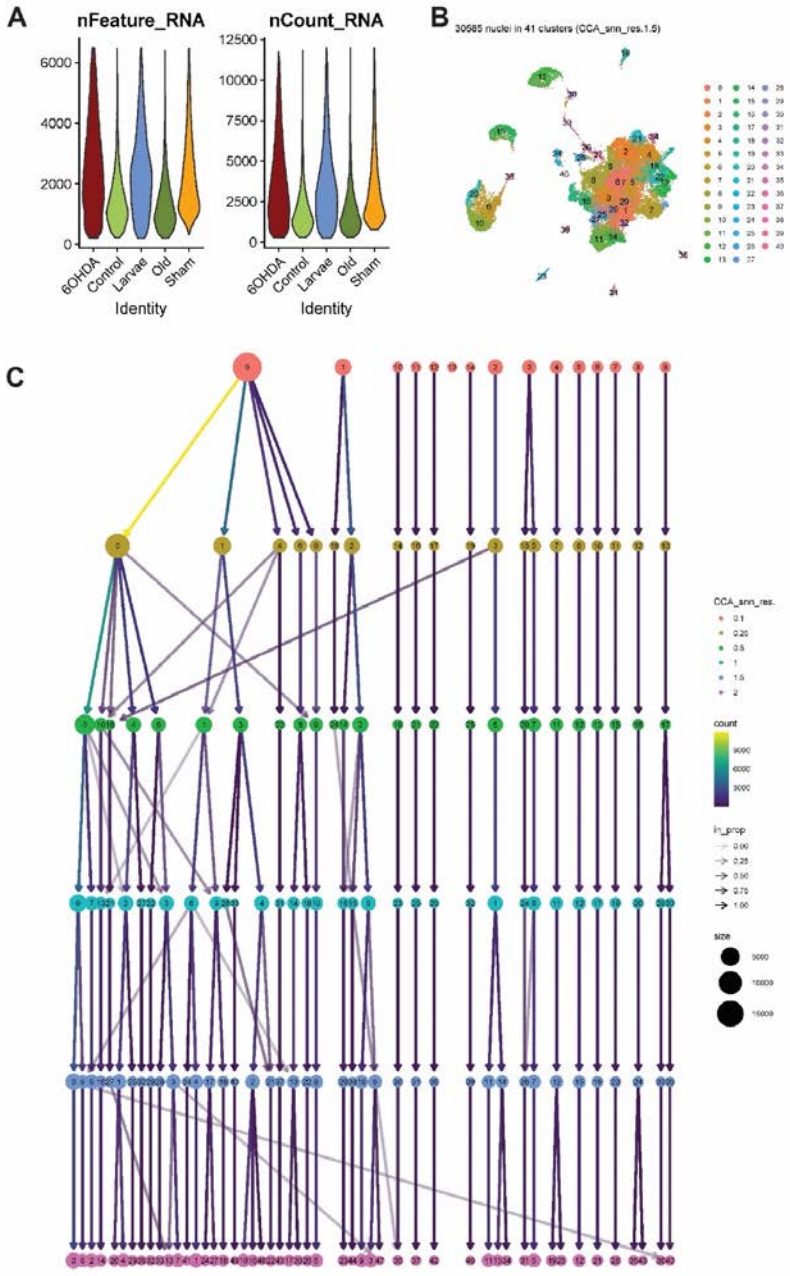

Supplementary Fig. S3 (previous page) | QC and louvain clustering on the single-nulceus RNAseq dataset from the young adult newts in conditions of 6OHDA, sham and control. (A) QC on the dataset based on the treatment conditions. **(B)** UMAP of louvain clustering at CCA_snn_res.1.5 on the dataset. **(C)** Louvain hierarchical clustering of the dataset.

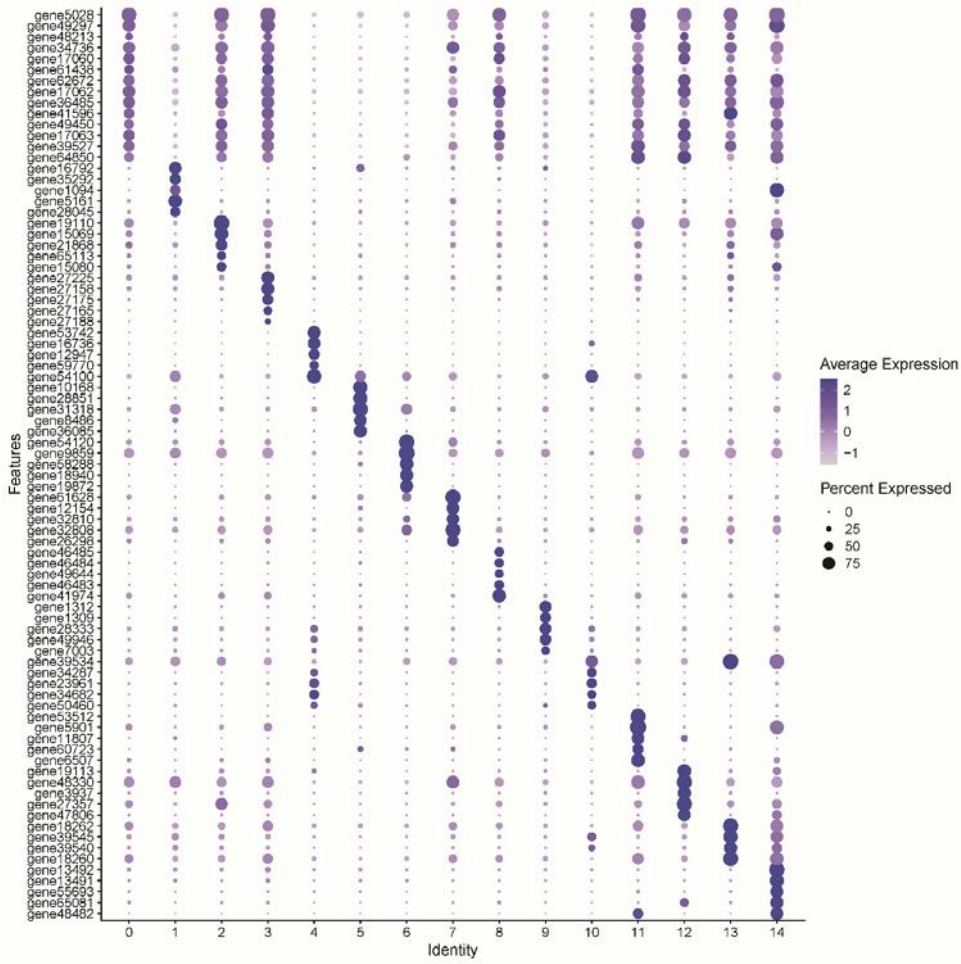

Supplementary Fig. S4 | Dotplot showing the key marker genes of each cluster at CCA_snn_res.0.1 in the single-nucleus RNAseq dataset containing ventral midbrains of young adults from 6OHDA, sham, and control.

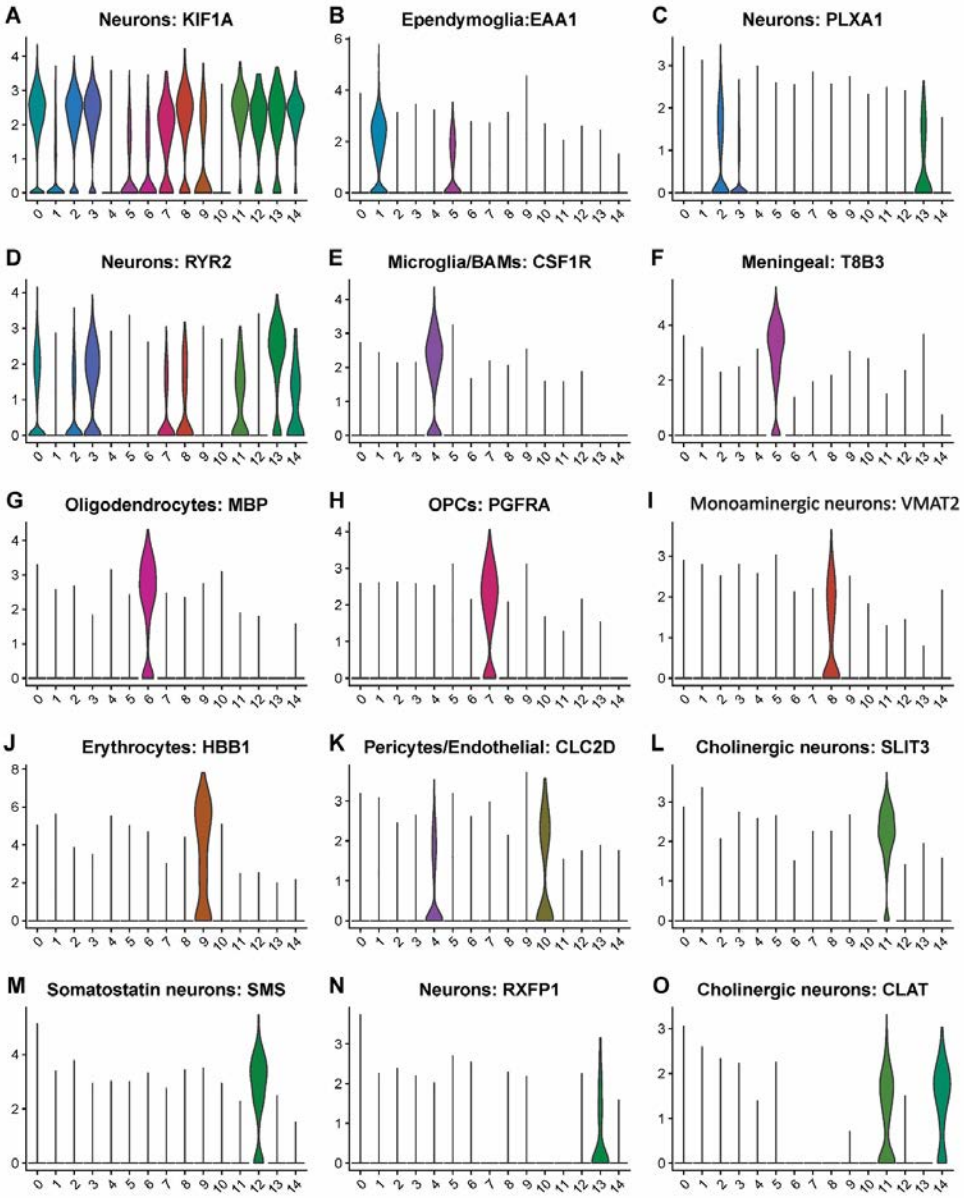

Supplementary Fig. S5 | Violin plot showing the expression of a selection of one of the top expressed genes for each cluster. **(A)** Cluster 0. Neurons. **(B)** Cluster 1. Ependymoglia. **(C)** Cluster 2. Neurons. **(D)** Cluster 3. Neurons. **(E)** Cluster 4. Neurons. **(F)** Cluster 5. Microglia/BAMs. **(G)** Cluster 6. Oligodendrocytes **(H)** Cluster 7. OPC. **(I)** Cluster 8. Monoaminergic. **(J)** Cluster 9. Erythrocytes. **(K)** Cluster 10. Pericytes/Endothelial cells. **(L)** Cluster 11. Cholinergic neurons. **(M)** Cluster 12. Somatostain neurons. **(N)** Cluster 13. Neurons. **(O)** Cluster 14. Cholinergic neurons.

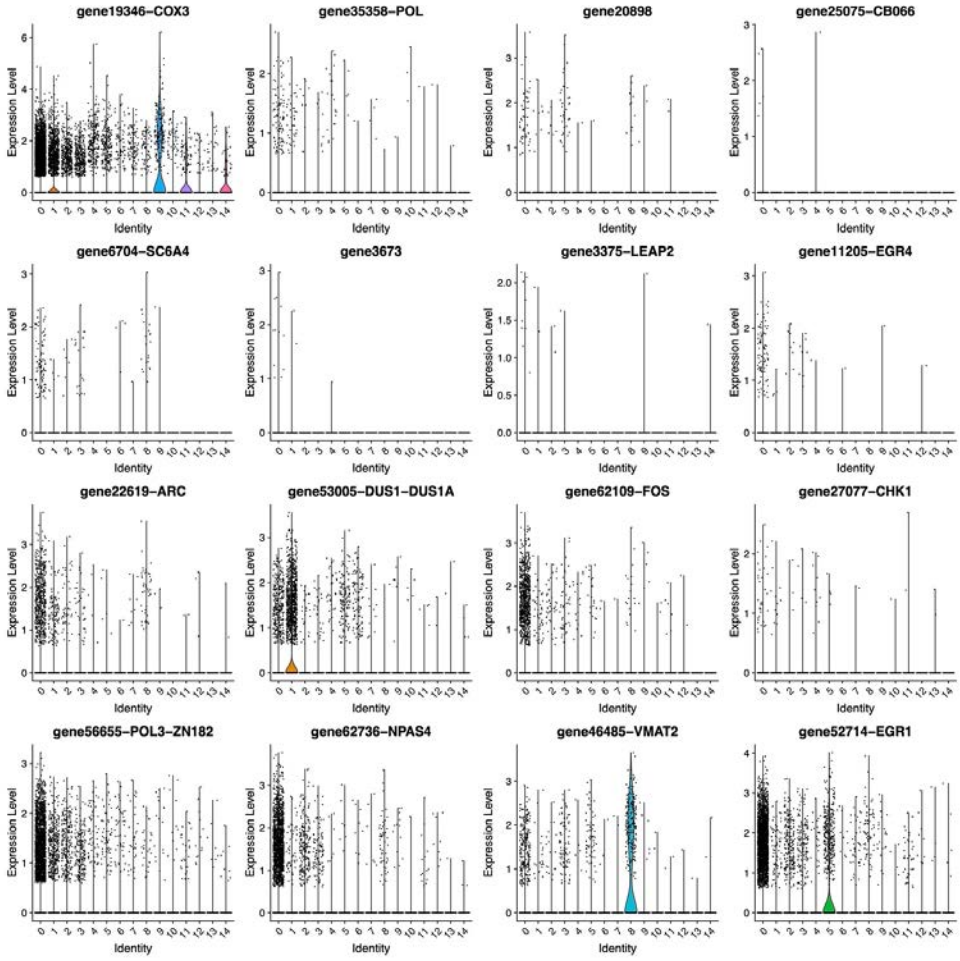

Supplementary Fig. S6 | RNA counts of genes putatively downregulated in 6-OHDA compared to sham conditions (detected by previous bulkRNAseq experiment) in the whole snRNAseq plotted by cell cluster.

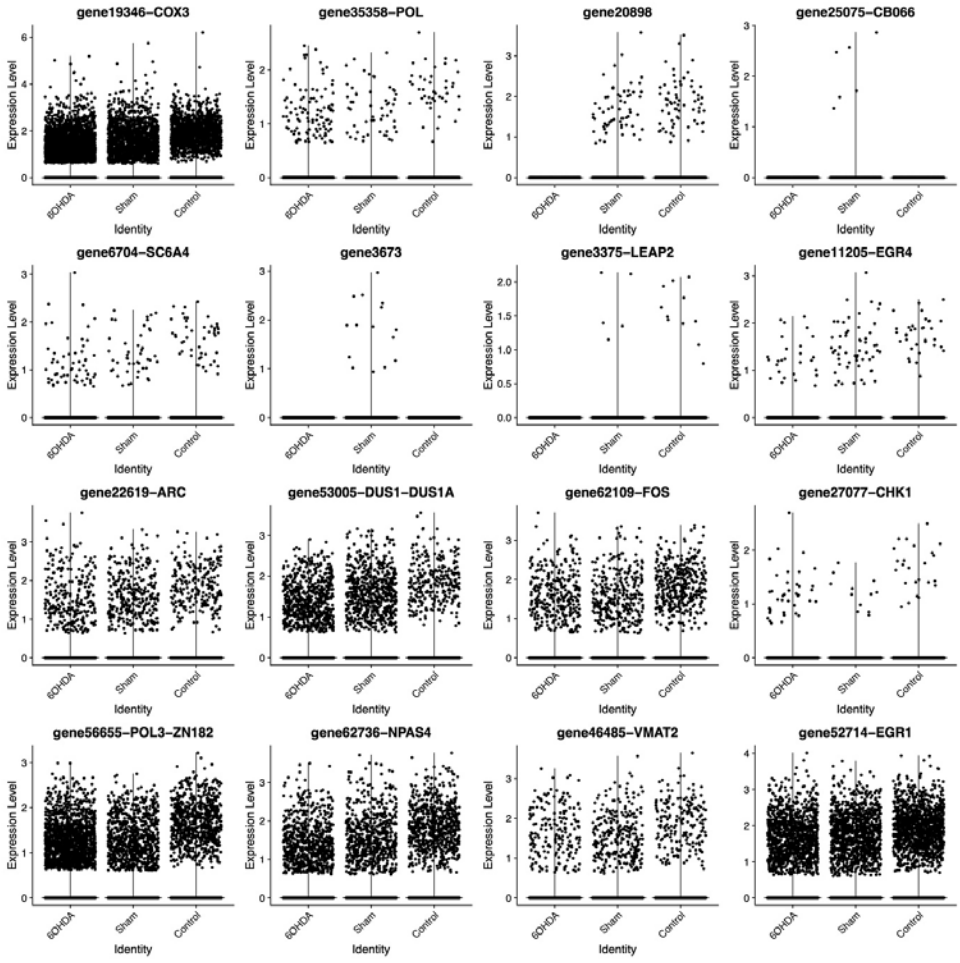

Supplementary Fig. S7 | RNA counts of genes putatively downregulated in 6-OHDA compared to sham conditions (detected by previous bulkRNAseq experiment) in the whole snRNAseq plotted by experimental condition.

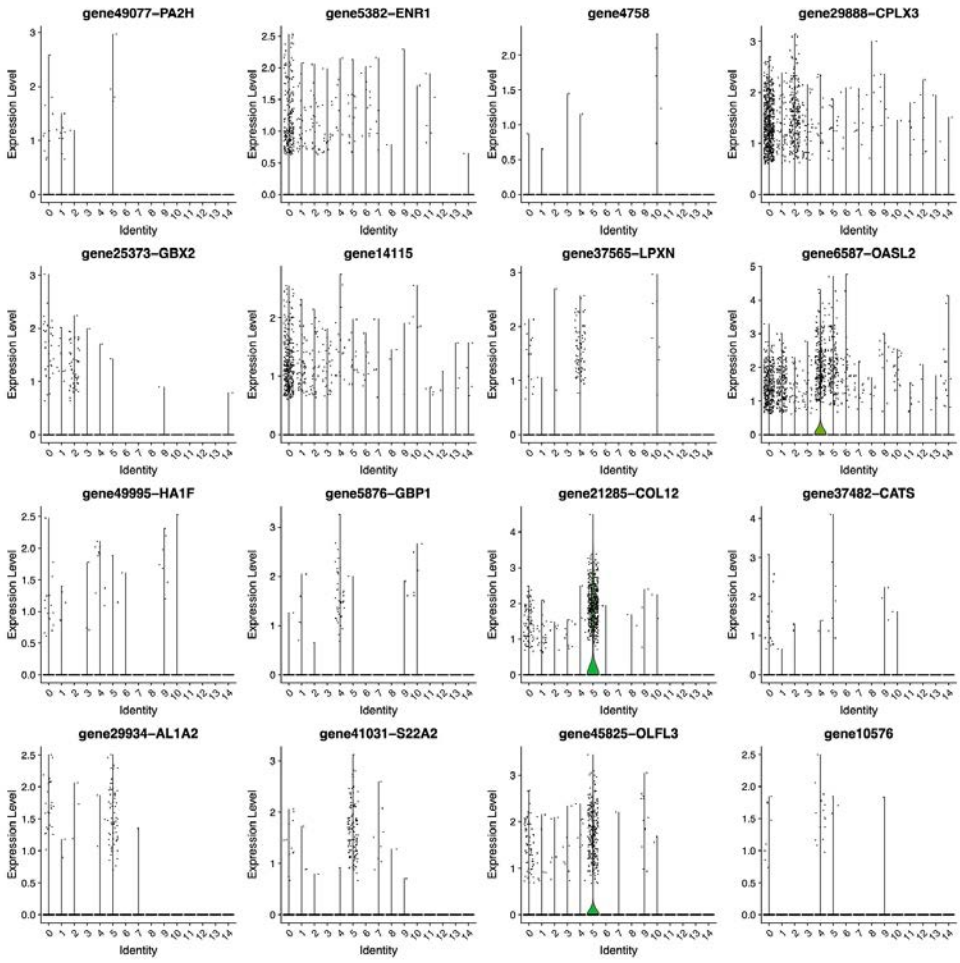

Supplementary Fig. S8 | RNA counts of genes putatively upregulated in 6-OHDA compared to sham conditions (detected by previous bulkRNAseq experiment) in the whole snRNAseq plotted by cell cluster.

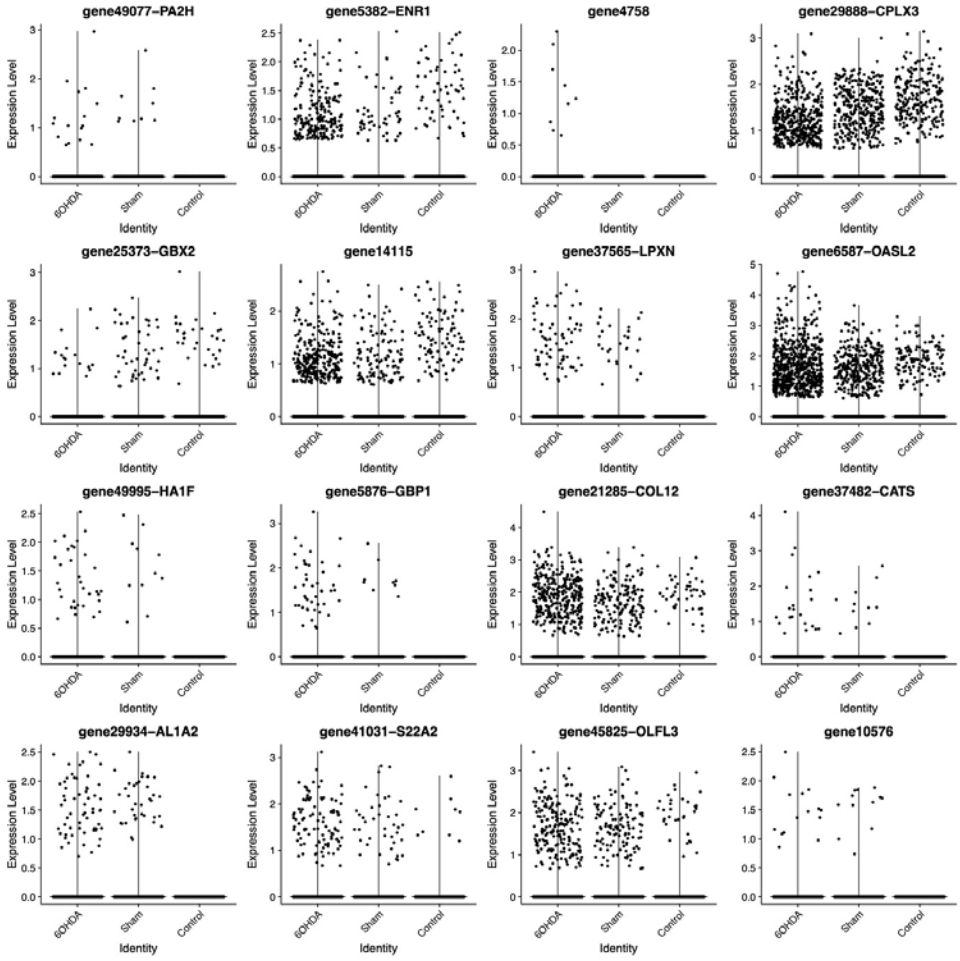

Supplementary Fig. S9 | RNA counts of genes putatively upregulated in 6-OHDA compared to sham conditions (detected by previous bulkRNAseq experiment) in the whole snRNAseq plotted by experimental condition.

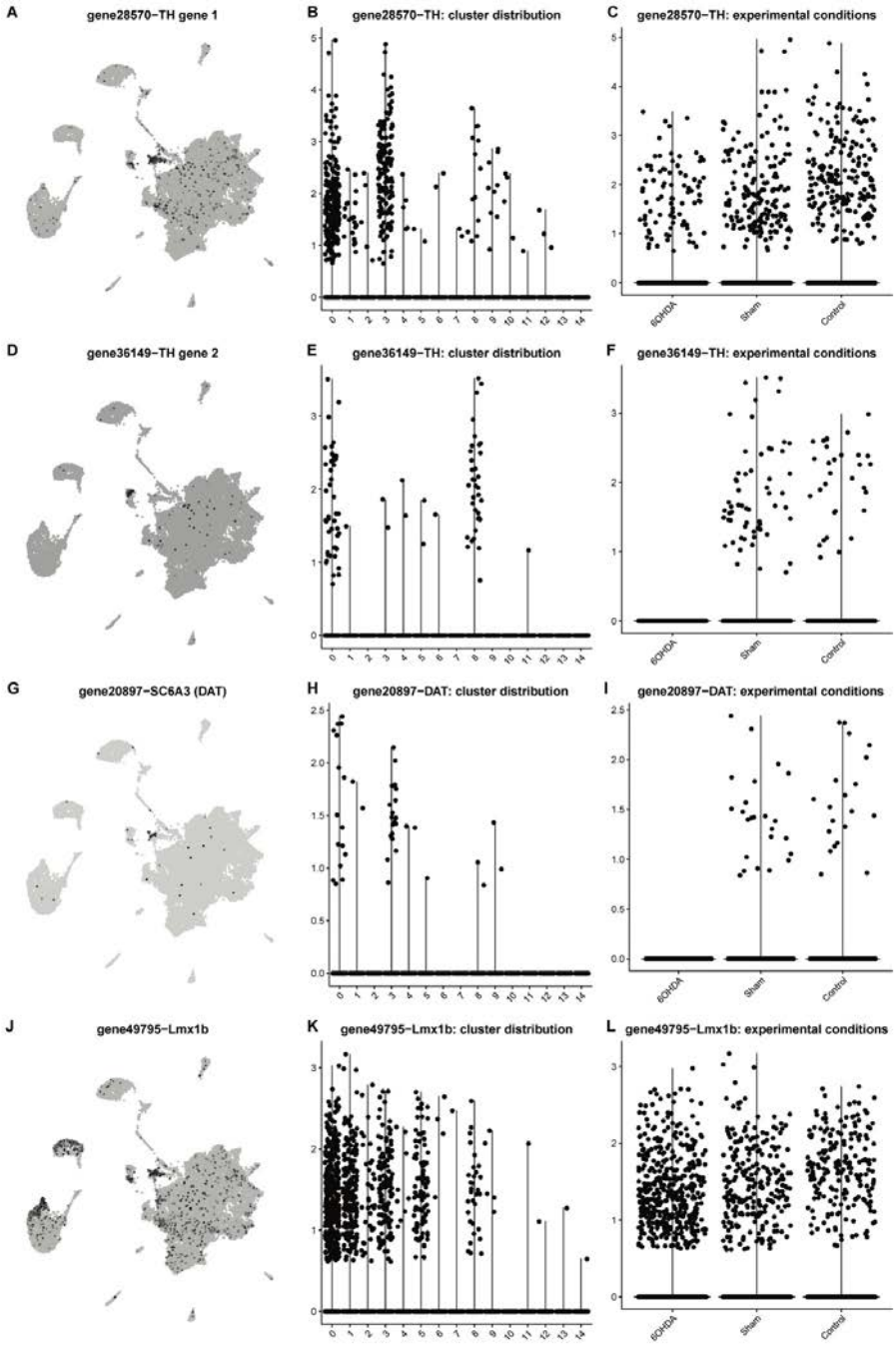

Supplementary Fig. S10 | The expressions of dopaminergic-related genes *gene28570-TH* (A-C), *gene36149-TH* (D-F), *gene20897-SC6A3* (G-I), and *gene49795-lmx1b* (J-L) upon 6-OHDA-mediated lesion in the whole snRNAseq dataset.

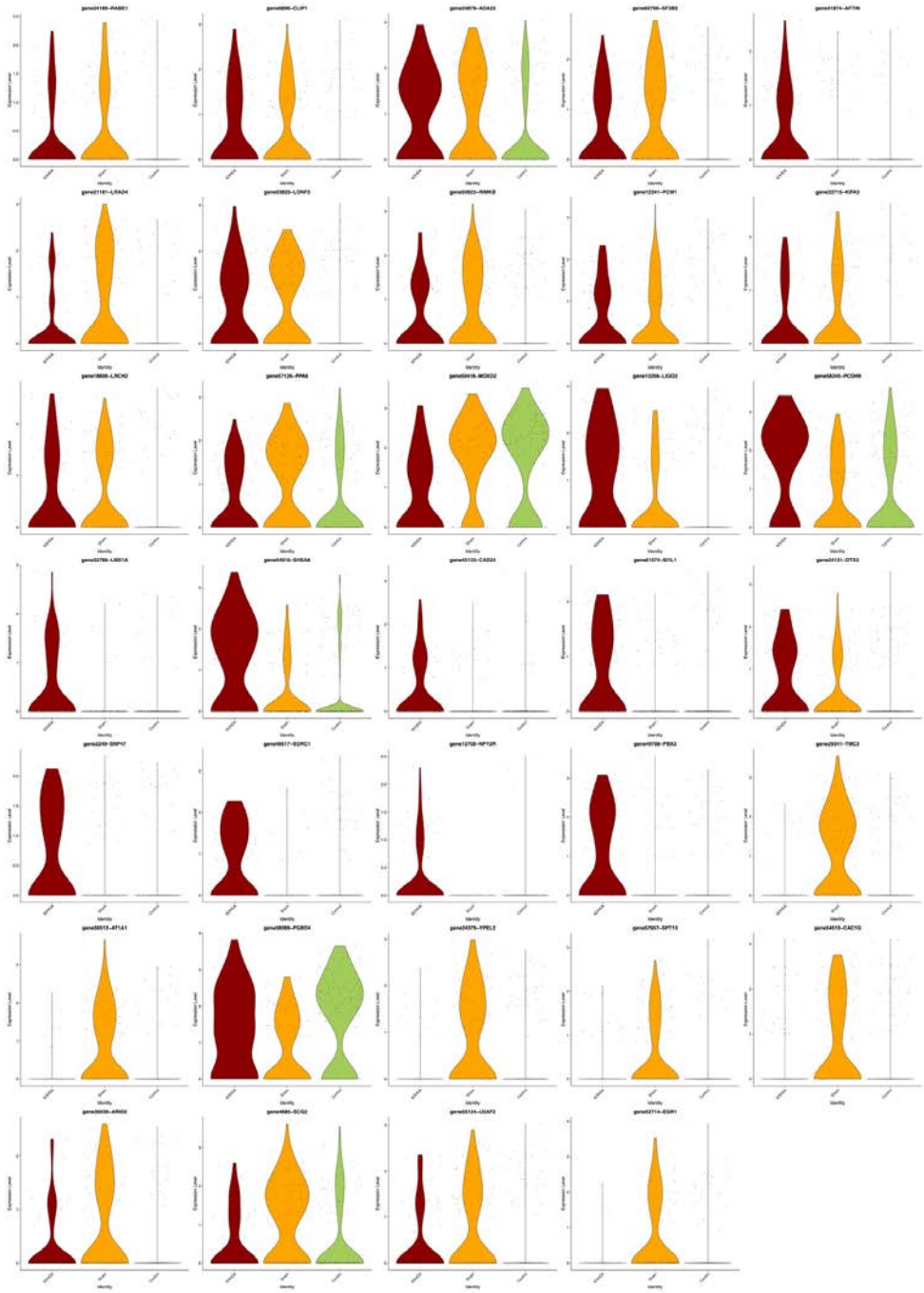

Supplementary Fig. S11 | Unbiased analysis of DEG genes for monoaminergic neurons cluster in the snRNAseq plotted by experimental condition.

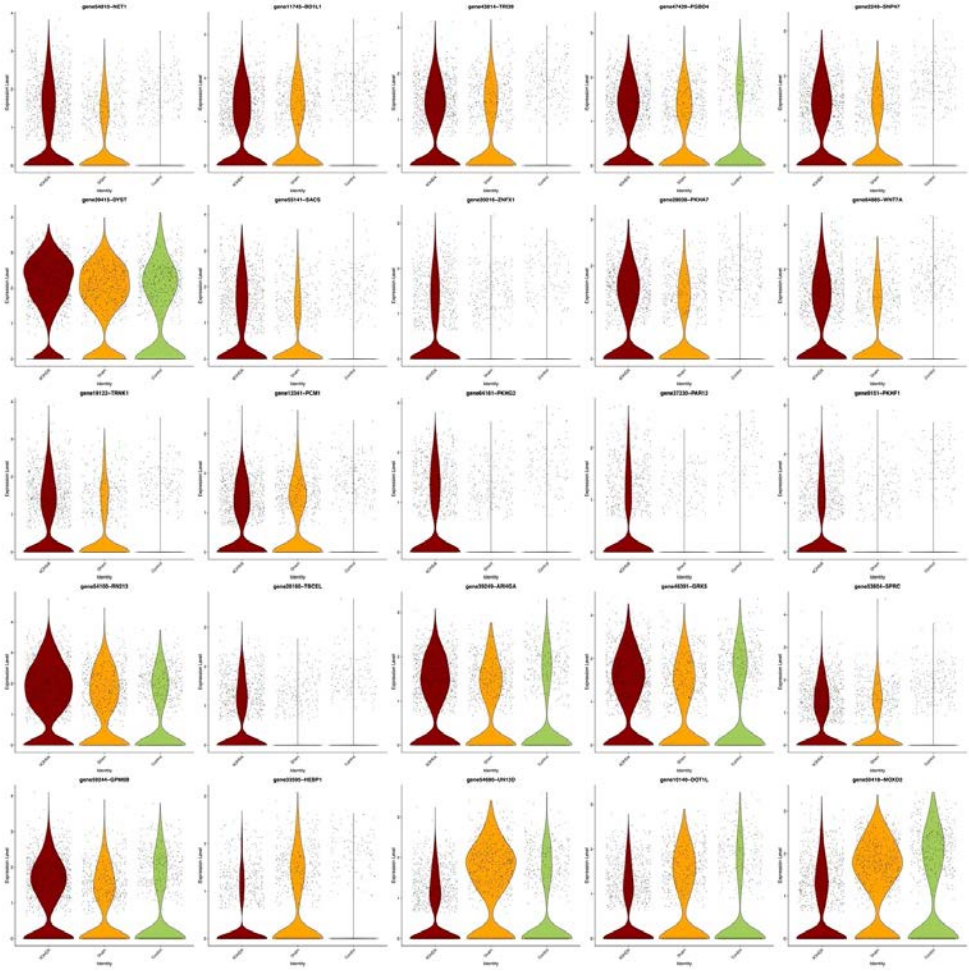

Supplementary Fig. S12 | Unbiased analysis of DEG genes for ependymoglia cluster in the snRNAseq plotted by experimental condition.